frontiers | Research Topics

Dynamic functioning of resting state networks in physiological and pathological conditions, volume II

Edited by
Roberto Esposito, Filippo Cieri, Nicoletta Cera and Fernando Barbosa

Published in
Frontiers in Neuroscience
Frontiers in Neuroimaging

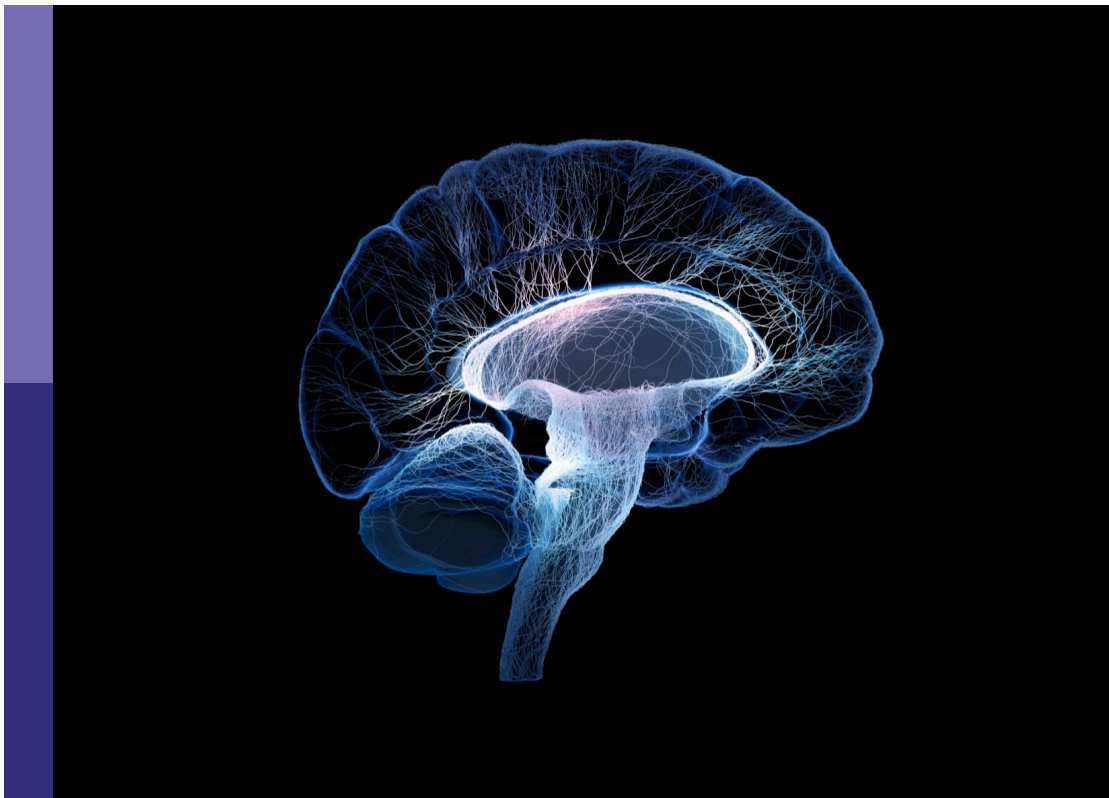

ISSN 1664-8714
ISBN 978-2-83251-535-8
DOI 10.3389/978-2-83251-535-8

About Frontiers

Frontiers is more than just an open access publisher of scholarly articles: it is a pioneering approach to the world of academia, radically improving the way scholarly research is managed. The grand vision of Frontiers is a world where all people have an equal opportunity to seek, share and generate knowledge. Frontiers provides immediate and permanent online open access to all its publications, but this alone is not enough to realize our grand goals.

Frontiers journal series

The Frontiers journal series is a multi-tier and interdisciplinary set of open-access, online journals, promising a paradigm shift from the current review, selection and dissemination processes in academic publishing. All Frontiers journals are driven by researchers for researchers; therefore, they constitute a service to the scholarly community. At the same time, the *Frontiers journal series* operates on a revolutionary invention, the tiered publishing system, initially addressing specific communities of scholars, and gradually climbing up to broader public understanding, thus serving the interests of the lay society, too.

Dedication to quality

Each Frontiers article is a landmark of the highest quality, thanks to genuinely collaborative interactions between authors and review editors, who include some of the world's best academicians. Research must be certified by peers before entering a stream of knowledge that may eventually reach the public - and shape society; therefore, Frontiers only applies the most rigorous and unbiased reviews. Frontiers revolutionizes research publishing by freely delivering the most outstanding research, evaluated with no bias from both the academic and social point of view. By applying the most advanced information technologies, Frontiers is catapulting scholarly publishing into a new generation.

What are Frontiers Research Topics?

Frontiers Research Topics are very popular trademarks of the *Frontiers journals series*: they are collections of at least ten articles, all centered on a particular subject. With their unique mix of varied contributions from Original Research to Review Articles, Frontiers Research Topics unify the most influential researchers, the latest key findings and historical advances in a hot research area.

Find out more on how to host your own Frontiers Research Topic or contribute to one as an author by contacting the Frontiers editorial office: frontiersin.org/about/contact

Dynamic functioning of resting state networks in physiological and pathological conditions, volume II

Topic editors

Roberto Esposito — ASUR Marche, Italy

Filippo Cieri — Lou Ruvo Center for Brain Health, Neurological Institute, Cleveland Clinic, United States

Nicoletta Cera — University of Porto, Portugal

Fernando Barbosa — University of Porto, Portugal

Citation

Esposito, R., Cieri, F., Cera, N., Barbosa, F., eds. (2023). *Dynamic functioning of resting state networks in physiological and pathological conditions, volume II*. Lausanne: Frontiers Media SA. doi: 10.3389/978-2-83251-535-8

Table of contents

frontiers | Frontiers in Neuroscience

TYPE Editorial
PUBLISHED 18 January 2023
DOI 10.3389/fnins.2022.1134113

OPEN ACCESS

EDITED AND REVIEWED BY
Vince D. Calhoun,
Georgia State University, United States

*CORRESPONDENCE
Roberto Esposito
✉ resposito1979@gmail.com

SPECIALTY SECTION
This article was submitted to Brain Imaging Methods, a section of the journal Frontiers in Neuroscience

RECEIVED 29 December 2022
ACCEPTED 30 December 2022
PUBLISHED 18 January 2023

CITATION
Esposito R, Cera N, Barbosa F and Cieri F (2023) Editorial: Dynamic functioning of resting state networks in physiological and pathological conditions, volume II.
Front. Neurosci. 16:1134113.
doi: 10.3389/fnins.2022.1134113

Editorial: Dynamic functioning of resting state networks in physiological and pathological conditions, volume II

Roberto Esposito[1,2]*, Nicoletta Cera[3,4], Fernando Barbosa[3] and Filippo Cieri[5]

[1]Titano Diagnostic Clinic, Falciano, San Marino, [2]Azienda Sanitaria Territoriale (AST), Pesaro-Urbino (PU), Marche, Italy, [3]Faculty of Psychology and Education Sciences, University of Porto, Porto, Portugal, [4]Coimbra Institute for Biomedical Imaging and Translational Research (CIBIT), Coimbra, Portugal, [5]Department of Neurology, Cleveland Clinic Lou Ruvo Center for Brain Health, Las Vegas, NV, United States

KEYWORDS

resting state networks, dynamic brain activity, default network, advanced neuroimaging techniques, neuropsychiatric diseases

Editorial on the Research Topic
Dynamic functioning of resting state networks in physiological and pathological conditions, volume II

1. Introduction

Advanced neuroimaging techniques represent a valid tool to study brain physiology and neural mechanisms in several pathological conditions such as neuropsychiatric disorders (Spinosa et al., 2022), allowing to examine brain structural and functional changes (Cieri and Esposito, 2018; Esposito et al., 2018; Cieri et al., 2020). This Research Topic is a second volume of a previous Research Topic, now convening nine research articles based on the current understanding of brain neuroimaging technique addressing theoretical and methodological questions.

2. Neurodegenerative diseases: Mild cognitive impairment and Alzheimer's disease

Wang et al. explored the clinical role of structural and functional MRI in early diagnose of Alzheimer's Disease (AD) and amnestic MCI (aMCI), where fMRI can identify brain functional abnormalities in the early stages of the disease. Combining the textural features of the amplitude of low frequency fluctuation (ALFF) in the slow-frequency band and structural images in the hippocampus, the authors investigated diagnostic performance of their approach for AD and aMCI, using multimodal radiomics technique. Radiomics models based on structural images in the hippocampus had a better diagnostic performance for AD compared with the models using ALFF, while the latest model exhibited better discriminant performance for aMCI than the structural approach.

3. Emotional disturbances and psychiatric diseases

Allen et al. examined whether psychopathic traits are associated with aberrant inter-network connectivity, intra-network connectivity, and amplitude of fluctuations across limbic and surrounding paralimbic regions among incarcerated women. PCL-R Factor 1 scores (interpersonal/affective psychopathic traits) were associated with increased low-frequency fluctuations in executive control and attentional networks, decreased high-frequency fluctuations in executive control and visual networks, and decreased intra-network functional connectivity in default network (DN). PCL-R Factor 2 scores (lifestyle/antisocial psychopathic traits) were associated with decreased high-frequency fluctuations and DN, and both increased and decreased intra-network functional connectivity in visual networks.

Zhang et al. explored neuropathological mechanisms of postpartum depression (PPD) through voxel-based degree centrality (DC) analysis to explore intrinsic dysconnectivity pattern of whole-brain functional networks in this clinical condition. DC image, clinical symptom correlation, and seed-based functional connectivity (FC) analyses were performed to reveal the abnormalities of the whole-brain functional network in PPD. Compared with healthy controls (HCs), patients exhibited significantly increased DC in the right hippocampus and left inferior orbitofrontal gyrus. In the seed-based FC analyses, the PPD showed significantly decreased FC between the right hippocampus and right middle frontal gyrus, between the right hippocampus and left median cingulate and paracingulate gyri, and between the left inferior orbitofrontal gyrus and the left fusiform (FFG.L) compared with HCs. The authors provided evidence of aberrant voxel-based FC within brain regions in PDD, potentially helpful to better understand neural circuitry dysfunction in these patients.

4. Other clinical conditions

4.1. Epilepsy

Qin et al. explored idiopathic generalized epilepsy and particularly the dynamics and the causal relationship among 3–6 Hz generalized spike-wave discharges and extensive altered interactions in subcortical-cortical circuit, using rs-fMRI. Their results showed that thalamus and precuneus were key regions representing abnormal FC in subcortical-cortical circuit. Moreover, the connectivity between precuneus and adjacent regions had causal effect on the widespread dysfunction of the thalamocortical circuit, and the connection between the striatum and thalamus indicated the modulation role on the cortical connection in epilepsy.

Li et al. focused their attention on neural mechanisms underlying the alterations of thalamus in children with generalized tonic-clonic seizures. They explored the temporal properties of functional pathways connecting thalamus in these patients. The findings of both increased and decreased connectivity variability in the thalamo-cortical network imply a dynamic restructuring of the functional pathways connecting the thalamus in children with generalized tonic-clonic seizures. These results contribute to extend the understanding of the neural mechanism underlying this disorder in children.

4.2. Rheumatoid arthritis

Fanton et al. explored time-varying changes in brain network integration and segregation during pain over a disease-affected area (joint) compared to a neutral site (thumbnail) in patients with rheumatoid arthritis (RA). The authors quantified measures of integration and segregation at multiple spatial scales, both at the level of single nodes and communities (clusters of nodes), finding that Participation Coefficient (PC) at the community level was generally higher in patients compared to HCs during and after painful pressure over the inflamed joint and corresponding site in controls. This shows that all brain communities integrate more in patients than in HCs for time points following painful stimulation to a disease-relevant body site. Moreover, there was no specific nodal contribution to brain network integration or segregation. Altogether, this evidence suggests widespread and persistent changes in network interaction in RA patients compared to HCs in response to painful stimulation.

4.3. Kallmann syndrome

Di Nardo et al. investigated the dynamic spectral changes of the sensorimotor network FC in Kallmann syndrome (KS) patients with and without mirror movement (MM) symptom. Compared to KS patients without MM and HCs, the sensorimotor brain network (SMN) of patients with MM displayed significantly larger spectral power changes in the slow 3 canonical sub-band and significantly fewer transitions between state 1 (less recurrent) and state 2 (more recurrent). This study shows that the presence of mirror movement in this syndrome is associated with reduced spontaneous transitions of the SMN between dynamic FC states and a higher recurrence and an increased spectral power change of the high-frequency state.

4.4. Pathological fatigue

Skau et al. recruited individuals suffering from pathological fatigue after mild traumatic brain injury (mTBI). They used functional near-infrared spectroscopy to assess hemodynamic changes in the frontal cortex. The participants underwent to a session before and after an experiment involving cognitive tasks, including the Digit Symbol Coding test. The authors have shown a Group vs. Time interaction with a *post-hoc* test revealing that patients developed higher modularity toward the end of the cognitive test session. This work helps to identify how functional networks differ under pathological fatigue compared to HCs.

5. Brain physiology and methodological approaches

Vazquez-Trejo et al. have used connectotyping, which efficiently models functional brain connectivity to reveal the progression of temporal brain connectivity patterns in task fMRI. They found significantly different dynamic connectivity patterns during word vs. pseudoword processing between the Fronto-Parietal and Cingulo-Parietal Systems, that are involved in cognitive task control, memory retrieval, and semantic processing. The findings support the presence of dynamic changes in functional connectivity during task execution and that such changes can be characterized using connectotyping.

Author contributions

RE, FC, NC, and FB conceived and developed the Research Topic. RE and FC wrote the editorial. All authors contributed to the article and approved the submitted version.

Conflict of interest

The authors declare that the research was conducted in the absence of any commercial or financial relationships that could be construed as a potential conflict of interest.

Publisher's note

All claims expressed in this article are solely those of the authors and do not necessarily represent those of their affiliated organizations, or those of the publisher, the editors and the reviewers. Any product that may be evaluated in this article, or claim that may be made by its manufacturer, is not guaranteed or endorsed by the publisher.

References

Cieri, F., Cera, N., Griffa, A., Mantini, D., and Esposito, R. (2020). Dynamic functioning of resting state networks in physiological and pathological conditions. *Front. Neurosci.* 14, 624401. doi: 10.3389/fnins.2020.624401

Cieri, F., and Esposito, R. (2018). Neuroaging through the lens of the resting state networks. *Biomed. Res. Int.* 2018, 5080981. doi: 10.1155/2018/5080981

Esposito, R., Cieri, F., Chiacchiaretta, P., Cera N., Lauriola M., Di Giannantonio, M., et al. (2018). Modifications in resting state functional anticorrelation between default mode network and dorsal attention network: comparison among young adults, healthy elders and mild cognitive impairment patients. *Brain Imag Behav.* 12, 127–141. doi: 10.1007/s11682-017-9686-y

Spinosa, V., Brattico, E., Campo, F., and Logroscino, G. (2022). A systematic review on resting state functional connectivity in patients with neurodegenerative disease and hallucinations. *Neuroimage Clin.* 35, 103112. doi: 10.1016/j.nicl.2022.103112

frontiers | Frontiers in Neuroscience

ORIGINAL RESEARCH
published: 30 June 2022
doi: 10.3389/fnins.2022.925968

Causality Analysis to the Abnormal Subcortical–Cortical Connections in Idiopathic-Generalized Epilepsy

Yun Qin[1,2†], Sipei Li[3†], Dezhong Yao[1,2] and Cheng Luo[1]*

[1] Sichuan Provincial People's Hospital, MOE Key Lab for Neuroinformation, School of Life Science and Technology, University of Electronic Science and Technology of China, Chengdu, China, [2] Sichuan Institute for Brain Science and Brain-Inspired Intelligence, Chengdu, China, [3] Glasgow College, University of Electronic Science and Technology of China, Chengdu, China

Idiopathic generalized epilepsy (IGE) was characterized by 3–6 Hz generalized spike-wave discharges (GSWDs), and extensive altered interactions in subcortical-cortical circuit. However, the dynamics and the causal relationship among these interactions were less studied. Using resting-state functional magnetic resonance imaging (fMRI) data, the abnormal connections in the subcortical-cortical pathway in IGE were examined. Then, we proposed a novel method of granger causal analysis based on the dynamic functional connectivity, and the predictive effects among these abnormal connections were calculated. The results showed that the thalamus, and precuneus were key regions representing abnormal functional network connectivity (FNC) in the subcortical-cortical circuit. Moreover, the connectivity between precuneus and adjacent regions had a causal effect on the widespread dysfunction of the thalamocortical circuit. In addition, the connection between the striatum and thalamus indicated the modulation role on the cortical connection in epilepsy. These results described the causality of the widespread abnormality of the subcortical-cortical circuit in IGE in terms of the dynamics of functional connections, which provided additional evidence for understanding the potential modulation pattern of the abnormal epileptic pathway.

Keywords: idiopathic generalized epilepsy, dynamic functional networks, causal relationship, subcortical-cortical circuit, modulation

OPEN ACCESS

Edited by:
Roberto Esposito, ASUR Marche, Italy

Reviewed by:
Denggui Fan, University of Science and Technology Beijing, China
Fei Li, Zhejiang University of Technology, China

***Correspondence:**
Cheng Luo
chengluo@uestc.edu.cn

† These authors have contributed equally to this work and share first authorship

Specialty section:
This article was submitted to Brain Imaging Methods, a section of the journal Frontiers in Neuroscience

Received: *22 April 2022*
Accepted: *06 June 2022*
Published: *30 June 2022*

Citation:
Qin Y, Li S, Yao D and Luo C (2022) Causality Analysis to the Abnormal Subcortical–Cortical Connections in Idiopathic-Generalized Epilepsy. Front. Neurosci. 16:925968. doi: 10.3389/fnins.2022.925968

INTRODUCTION

Idiopathic generalized epilepsy (IGE) was typically characterized by 3–6 Hz generalized spike-wave discharges (GSWDs). The mainstream concept believed that the burst of GSWD was related to the inter-regional interactions in the subcortical-cortical circuit (Blumenfeld, 2003, 2005), involving the abnormal connectivity between the thalamus and cortex, and also the altered connectivity among the prefrontal and sensorimotor area (Szaflarski et al., 2010; Qin et al., 2019). Invasive animal studies have found that there was a large-scale burst of rhythmic oscillations in the thalamus during epileptic discharge (Avanzini et al., 2000; Timofeev and Steriade, 2004). Moreover, it was found that GSWDs were time-locked with BOLD activation of the thalamus and cortical deactivation, especially in the frontal cortex (Salek-Haddadi et al., 2003). In addition, even in the resting-state without GSWD, extensive abnormal functional networks and connections between networks were found in IGE, such as the default mode network (DMN), basal ganglia, and sensorimotor

network (SMN) (Luo et al., 2011, 2012; Jiang et al., 2020; Parsons et al., 2020). However, the causal relationship among these abnormal connections was less studied, which may provide evidence for understanding the modulation mechanism within the epileptic pathway.

Regarding the origin of generalized epileptic discharge, previous studies have proposed some different discharge model hypotheses, with two representative concepts of the cortical focus theory and the thalamic pacemaker theory. The hypothesis of cortical focus theory assumed that epileptic discharges originated in a certain local area of the cortex and then spread through the interaction of subcortical structures with the cortex, thus recruiting specific neuronal networks into typical oscillatory behavior (Meeren et al., 2005; Stefan and Lopes da Silva, 2013). Under this concept, a general comment about the thalamus burst, was that a sustained flow of GSWD signals propagated from cortex to thalamus in a couple of hundreds of milliseconds, and triggered the oscillation entrainment in the cortical-thalamus-cortical loop. On other hand, the hypothesis of thalamic pacemaker suggested the reticular thalamic nucleus contained the pacemaker cells for the thalamic clock, imposing its rhythm to the cortex, then resulting to the spread of discharge activity in the cortex (Buzsaki, 1991; Avanzini et al., 1992). Moreover, studies have shown that interference with thalamus activity through stimulation can promote the termination of epileptic discharge (Berenyi et al., 2012; Paz et al., 2013; Burdette et al., 2020), indicating that the thalamus not only played an important role in epileptic seizures and transmission, but also modulated the termination of epileptic discharge. Besides the animal and model analysis, we think investigating the predictive relationship among the abnormal connections based on the dynamic functioning in the resting-state in thalamocortical circuit can provide additional evidence for understanding the origin and propagation the epileptic activity.

Other structures under the cortex, such as the striatum and cerebellum, also played an important role in regulating epilepsy. Some animal studies have shown that the striatum, whose fibers connected to the substantia nigra reticulum, was involved in the regulation of epileptic discharges (Turski et al., 1989; Deransart et al., 2000). Previous EEG–functional magnetic resonance imaging (fMRI) studies have shown that the putamen and caudate nucleus was closely related to epileptic discharges, and that the increase of epileptic discharges was accompanied by the enhancement of the internal connectivity within the basal ganglia network (BGN) (Luo et al., 2012; Moeller et al., 2013; Bartolini et al., 2014). It was generally assumed that the regulation of the GSWD of epilepsy by the striatum was achieved through its contribution to the thalamocortical circuit. On the other hand, the cerebellum was considered to be a potential regulator of epileptic discharge activity. It has been found that direct stimulation of the cerebellar cortex could effectively destroy the thalamus-cortex oscillations and thereby inhibit the activity of GSWD (Berenyi et al., 2012). Therefore, probing how these subcortical regions, i.e., striatum and cerebellum interacted with the epileptic circuit would be helpful for the modulation strategy of the potential clinical intervene.

In this study, we investigated the altered subcortical-cortical pathway of IGE, and the causality relationship among these abnormal connections was examined using the dynamic functional of the resting-state network. The dynamic interactions within the abnormal epileptic networks may provide evidence for the origin and modulation of epileptic activity.

MATERIALS AND METHODS

Participants

In total, seventy-eight patients with IGE (40 women; mean age: 23.8 years) including 32 patients with juvenile myoclonic epilepsy (JME) and 46 patients with generalized tonic–clonic seizures (GTCSs) were recruited in this study. Diagnosis and classification was made by neurologists in accordance with the International League Against Epilepsy (ILAE) guidelines (Fisher et al., 2017; Scheffer et al., 2017). Routine CT and MRI examinations were conducted and no structural abnormality was found in all the epilepsy patients. Clinical information was showed in **Table 1**. In total, 60 healthy controls (29 women; mean age: 25.7 years) with no history of psychiatric or neurologic disorders participated in the study. Written informed consent according to the Declaration of Helsinki was obtained from all the participants. This study was approved by the Ethics Committee of the University of Electronic Science and Technology of China (UESTC).

Magnetic Resonance Imaging Acquisition

In this study, the MRI data of all the participants were recorded from the 3T MRI scanner (Discovery MR750, GE) with an eight channel-phased array head coil in UESTC. Resting-state fMRI data were acquired using a gradient-echo echo planar imaging sequences (FOV = 24 cm × 24 cm, FA = 90°, TR / TE = 2,000 ms/30 ms, matrix = 64 × 64, slice thickness/gap = 4 mm/0.4 mm). A total of 255 volumes were collected in the resting-state scan for each participant. During fMRI scanning, all the participants were instructed to keep still and close their eyes without sleeping. In addition, high-resolution T1-weighted images were also acquired using a 3D fast spoiled gradient echo (T1-3D FSPGR) sequence (FOV = 25.6 cm × 25.6 cm, FA = 9°, matrix = 256 × 256, TR / TE = 5.936 ms/1.956 ms, slice thickness = 1 mm, no gap, 152 slices).

TABLE 1 | Summary demographic of patients and healthy controls.

	HC *n*=60		Patients *n*=78		χ^2 t-test *p value*	
Gender (Male/Female)	31/29		38/40		0.12	
Seizure type (JME/GTCS)	–		32/46		–	
	Mean	**Std**	**Mean**	**Std**		
Age(year)	23.8	2.6	25.7	9.6	0.474	
Seizure duration	–	–	6.75	6.45	–	–
Age at seizure onset	–	–	18.95	10.4	–	–

Functional Magnetic Resonance Imaging Data Pre-processing

fMRI data were pre-processed using SPM12[1] and NIT toolboxes[2] (Dong et al., 2018). The first five volumes were discarded from all fMRI scans for the magnetization equilibrium. The remaining volumes were slice-timing corrected using the first slice as reference, and spatially realigned to the mean of volumes within subject to correct head motion. We checked the head motion parameters after processing, the head motion of all participants was less than 2 mm translation and less than 2°rotation in any direction. Individual T1 images were co-registered to the functional images, and segmented into gray matter, white matter, and cerebrospinal fluid, and then normalized to the Montreal Neurologic Institute (MNI) space. Then, the functional images were spatial normalized based on T1 transformation matrix, resampled to 3 mm × 3 mm × 3 mm voxels, and spatially smoothed using a 6 mm full-width half maximum (FWHM) Gaussian kernel. Nuisance signals (12 motion parameters, linear drift signal, and also mean white matter and cerebrospinal fluid signals) were regressed out for the fMRI data to reduce the effect of potential artifacts.

Causality Analysis to the Subcortical–Cortical Pathways in Idiopathic Generalized Epilepsy

This study aimed to investigate the alteration of subcortical–cortical pathways in IGE and the causality among these alterations. The main diagrams of this study was showed in **Figure 1**, including the following parts: (1) the regions of interest (ROIs) were extracted using ICA to the fMRI data, with the independent spatial patterns and the temporal courses being obtained; (2) we constructed the static and dynamic functional network connectivity (FNC) among ROIs; (3) according to the abnormal static FNC in IGE and their dynamic courses across the slide time windows, granger causality analysis (GCA) was performed to examine the causal relationship among these abnormal connections.

Extraction of Regions of Interest in Subcortical–Cortical Pathways

Spatial ICA was performed to the group fMRI, and the functional networks identified by the ICs were obtained. Here, the number of ICs was 100 and determined according to the previous studies. In ICASSO,[3] the infomax algorithm was repeated 30 times to estimate the ICs. Then, dual regression approach was used in the back reconstruction to get the individual spatial maps and time courses. In this study, we focused on the subcortical and some frontal regions according to the previous studies, therefore, we selected the components of DMN, SMN, BGN, the salience network (SN), and also cerebellum network, each of network consisting of a few components, that is the ROIs. The MNI coordinates for the selected ROIs were shown in **Supplementary Table 1**. Then, the temporal coursed was band-pass filtered (0.01–0.1 Hz).

Static and Dynamic Functional Network Connectivity Analysis

The static FNC and dynamic FNC was constructed among ROIs. Static FNC was computed by the Pearson's correlation of the time courses between any two selected components. Based on the static FNC, we calculated the degree of FNC nodes by summarizing the weights of the connections of each node. Dynamic FNC was also computed using correlations between windowed time-courses of different ROIs. Here, the length of the slide window was 50TR, with the sliding step width 1TR. The selection of the window length was constrained by the minimum frequency of the BOLD signal (f_{min} = 0.01 Hz). Then, the variation of the weights for the dynamic FNC in the time course was calculated, representing the dynamics of the connections in the subcortical–cortical circuit.

Causality Analysis of Functional Network Connectivitys

To detect the abnormal connections in IGE, two-sample *t*-test of the static FNC was performed. Based on the dynamic FNC weights, GCA was conducted to examine the causal relationship among these abnormal connections. Here, we used the residual-based bivariate GCA, and the main calculations were as follows:

First, autoregression models were constructed for two time series X and Y, which were the dynamic FNC weights of two abnormal connections in IGE.

$$X_t = \sum_{k=1}^{p} b_k X_{(t-k)} + \varepsilon_t \; Y_t = \sum_{k=1}^{p} b'_k Y_{(t-k)} + \varepsilon'_t \quad (1)$$

Here, ε_t and ε'_t were the residual of the autoregressive model, p was the order of model. The variance of the two models can be expressed as:

$$R1 = var(\varepsilon_t) \qquad T1 = var(\varepsilon'_t) \quad (2)$$

Then, the regression models of X and Y were combined, that is:

$$X_t = \sum_{k=1}^{p} A_k X_{(t-k)} + \sum_{k=1}^{p} B_k Y_{(t-k)} + u_t$$

$$Y_t = \sum_{k=1}^{p} A'_k Y_{(t-k)} + \sum_{k=1}^{p} B'_k X_{(t-k)} + u'_t \quad (3)$$

Here, u_t and u'_t is the residual of the combined regression model, and their variance can be expressed as:

$$R2 = var(u_t) \qquad T2 = var(u'_t) \quad (4)$$

The influence of X on Y can be described as $F_{x\to y} = ln\frac{R1}{R2}$ and $F_{y\to x} = ln\frac{T1}{T2}$. Therefore, when the past values of X has a predictive effect on the current value of Y, $F_{x\to y}$ will be significantly larger than zero, that is, the directed connection from X to Y. Considering the non-normality of the distribution

[1] http://www.fil.ion.ucl.ac.uk/spm/

[2] http://www.neuro.uestc.edu.cn/NIT.html

[3] http://research.ics.tkk.fi/ica/icasso

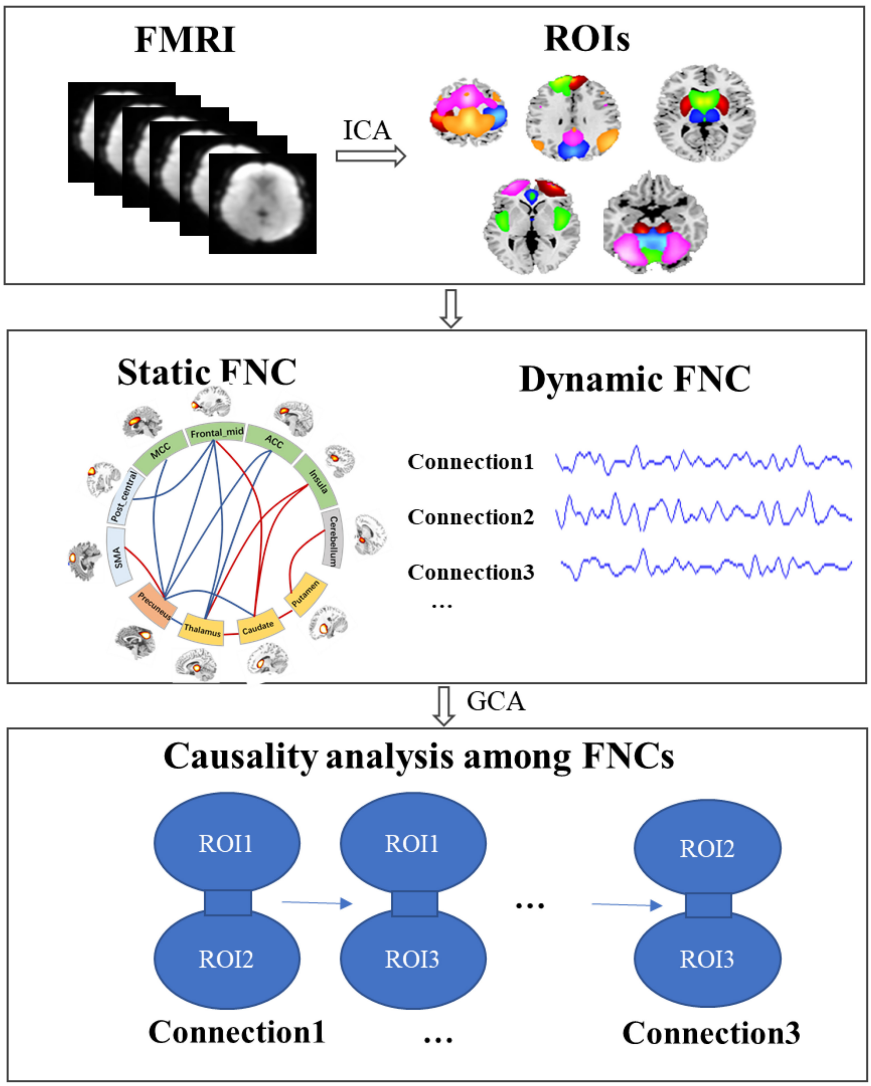

FIGURE 1 | The diagram of this study to the detect the causality in subcortical–cortical pathways in IGE. First, the regions of interest (ROIs) were extracted using ICA, and then we constructed the static and dynamic functional network connectivity (FNC) among ROIs; furthermore, according to the abnormal static FNC in IGE and their dynamic courses across the slide time windows, granger causality analysis (GCA) was performed to examine the causal relationship among these abnormal connections.

of $F_{x\to y}$, we used the transformed $F'_{x\to y}$, as the alternative $F'_{x\to y}$ and $F'_{y\to x}$ representing an approximate normal distribution according to the previous studies, and the order p here was selected as 1 (Zang et al., 2012).

$$F'_{x\to y} = \left[\frac{(t-p)\,F_{x\to y} - (p-1)}{3}\right]^{1/2}$$

$$F'_{y\to x} = \left[\frac{(t-p)F_{y\to x} - (p-1)}{3}\right]^{1/2} \quad (5)$$

Finally, $F'_{x\to y}$ and $F'_{y\to x}$ was z-scored at the individual level and then statistically analyzed using one-sample t-test (statistical threshold $P < 0.01$).

RESULTS

Alteration of Functional Network Connectivity in Idiopathic Generalized Epilepsy

According to the previous studies, we selected the components in DMN, SMN, BGN, SN, and cerebellum from 100 ICs obtained in ICA analysis. Thus, each network was constituted of a few components, i.e., the ROIs. Here, DMN included the frontal_sup_medial area, the angular, cingulum_post (PCC), and two precuneus components. SMN included bilateral post-central areas, pre-central, paracentral_lobule, and supp_motor_area (SMA). BGN was comprised of the thalamus, putamen, and caudate. SN involved the left and right frontal_mid area, the

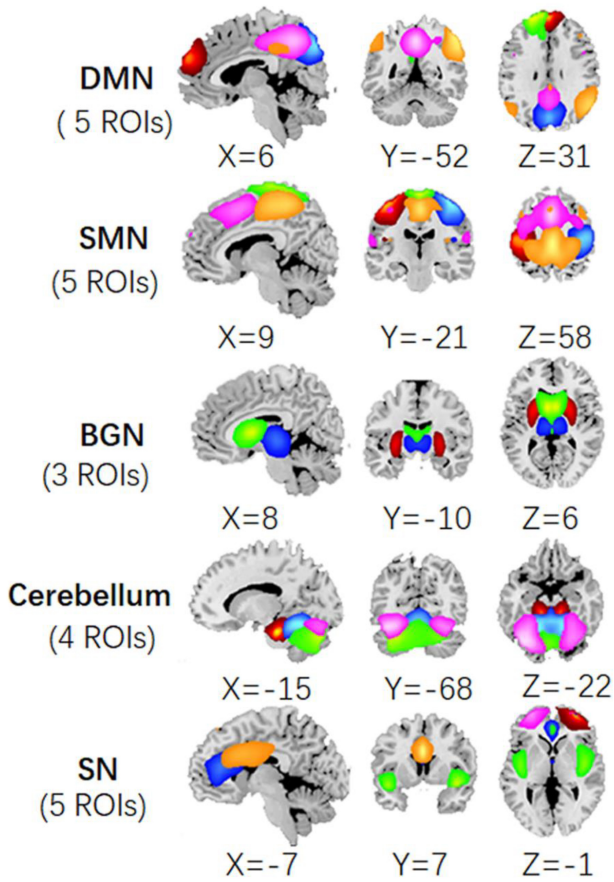

FIGURE 2 | The ROIs extracted from the ICA processing of fMRI data, including precuneus, angular, PCC, frontal_sup_medial areas in DMN; bilateral post_central, pre_central, paracentral_lobule, and SMA in SMN; thalamus, putamen, and caudate in BGN; frontal_mid, ACC, MCC, and insula in SN; and cerebellum regions.

cingulum_ant (ACC), cingulum_mid (MCC), and insula. The cerebellum network included the cerebellum posterior lobe and the declive. The maps of these five networks were illustrated in **Figure 2**. The central coordinates of the ROIs were shown in **Supplementary Table 1**.

After the ROIs of the five networks were selected, the static FNC and dynamic FNC was constructed among ROIs. Then, two-sample *t*-test was conducted to the static FNC, and the difference of FNC between IGE and HC was shown in **Figure 3** ($P < 0.001$). In between-group comparisons, age and gender were regressed out as the covariates. The results showed that thalamus, precuneus were the key nodes representing significant alteration in the subcortical–cortical circuit in epilepsy. Increased connectivity between thalamus and striatum, as well as the insula, and increased connectivity between precuneus and motor area was found in IGE comparing to HC. Decreased connectivity between the thalamus and frontal area, between precuneus and the frontal area, and also the thalamus/striatum was found in IGE. In addition, striatum showed increased connectivity with insula and cerebellum in epilepsy brain. Moreover, we compared the degree of FNC nodes between IGE and HC, and the thalamus, precuneus, ACC and post-central areas had decreased static FNC in IGE ($P < 0.05$) (**Figure 3B**).

Besides, comparison of static FNC was also performed between two epilepsy groups, i.e., JME and GTCS. Comparing to GTCS, JME showed decreased connectivity in thalamus-precuneus, and thalamus-frontal connections. The results may be related to the longer epilepsy duration of these patients with JME in this study.

Causality Among the Abnormal Functional Network Connectivitys in Idiopathic Generalized Epilepsy

After the abnormal connections of static FNC in the epilepsy group were labeled, the dynamic changes of these connections were extracted according to the weights of the dynamic FNC matrices. The variation of the dynamic FNC showed that the connections of thalamus-frontal_mid, thalamus-precuneus, precuneus-frontal_mid, and frontal_mid-post_central had increased dynamics in IGE ($P < 0.05$) (**Figure 3C**). Then, the weights of the dynamic FNC were taken into the GCA processing. The directed GCA connections with statistical significance at the group level ($P < 0.01$) were shown in **Figure 4**. Hierarchical causal relationship was demonstrated between the connections. The connections between precuneus and nearby cortex, i.e., SMA and MCC, had predictive effects on the widespread connections between thalamus and frontal regions. Moreover, these decreased connections between thalamus and multiple cortexes also had predictive effects on the connectivity between frontal and other cortex, such as the precuneus and post-central area. The increased connectivity between thalamus and caudate had bidirectional causal relationship with the decreased frontal-precuneus connection.

To sum up, patients with epilepsy had increased cerebellum-striatal-thalamic connections and widespread decrease in thalamocortical circuits. The causal relationship between these abnormal connections was summarized in **Figure 5**. Particularly, connectivity between precuneus and adjacent regions can predict the widespread dis-coupling in thalamocortical circuit. Moreover, the coupling between thalamus and the striatum had a two-way causal effect on the inter-cortical connectivity.

DISCUSSION

This study investigated the subcortical–cortical pathway in IGE, and showed that thalamus, precuneus were key nodes representing abnormal functional connectivity in subcortical–cortical circuit. Furthermore, the causality relationship among these abnormal connections in IGE was examined. It was shown that the increased connections between precuneus and the adjacent regions had the causal effect on the widespread decreased connections in thalamocortical circuit. In addition, the two-way causal effect of the connection between the thalamus and the striatum on the cortical connection indicated the modulation role of subcortical circuit in epilepsy.

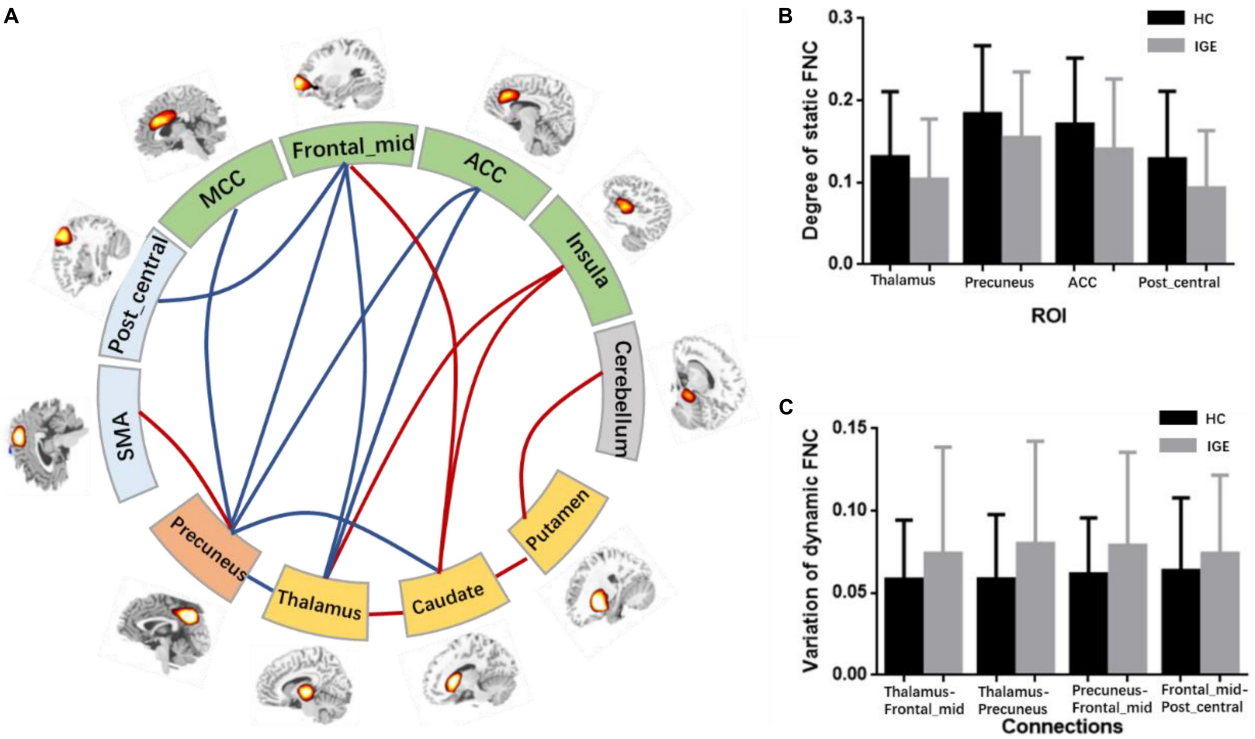

FIGURE 3 | (A) Abnormal FNCs in IGE. This figure contained regions with significant alteration of FNC. The red lines represented the enhancement of connections in IGE and the blue lines represented the decrease of FNCs in IGE. **(B)** The degree of the static FNC nodes in IGE and HC, and significant decreased degree of thalamus, precuneus, ACC and post_central area was found in IGE. **(C)** The variation of dynamic FNCs in IGE and HC, and increased variation was found in thalamocortical and cortical–cortical circuit.

Numerous studies have shown that there were abnormalities in a wide range of functional connections in IGE (Moeller et al., 2008; Vollmar et al., 2011; Jiang et al., 2018). Altered interactions in the subcortical–cortical and corticocortical circuit were thought to play an important role in the origin and propagation of epileptic activity (Luo et al., 2011; Benuzzi et al., 2012; Conradsen et al., 2013). The present study provided further evidence that the thalamus and precuneus were the key nodes of the abnormal subcortical–cortical circuit in IGE. A lot of decreased connections were found between thalamus and the cortical areas, involving the frontal and precuneus area. Meanwhile the connectivity between the frontal and precuneus area was also impaired. Moreover, the node degree of FNCs gave further evidence that thalamus and precuneus were important areas showing decreased connectivity in epilepsy. Furthermore, in the temporal dimension, the time-varying dynamics of the connections in thalamus-frontal_mid, thalamus-precuneus, precuneus-frontal_mid, and also the frontal_mid-post_central were significantly increased in IGE. The spatial dysconnectivity and the altered FNC dynamics in thalamocortical circuit in epileptic brain have been reported in many studies (O'Muircheartaigh et al., 2012; Kim et al., 2014; Zhang et al., 2018; Qin et al., 2020b). Previous studies have demonstrated the role of thalamus in leading in initiating and maintaining the epileptic activity, which may be involved early or late in the discharge (Tyvaert et al., 2009; Martin-Lopez et al., 2017). In addition, the striatum-thalamic-cortical circuit was considered to be the key circuit in the modulation of epileptic discharges (Paz et al., 2013). In the current study, intensive connectivity was found within BGN network, as well as between BGN nuclei and other brain regions, which implied the basal ganglia providing an endogenous control of thalamocortical SWDs.

According to the hypothesis of generalized epileptic discharges (Meeren et al., 2005), the epileptic discharge may originate from the focal area and the propagation involved abnormal cortical and subcortical interactions. In this study, the predictive relationship among these abnormal connections in epileptic brain was investigated using the mode-free granger causal analysis, which did not depend on the assumptions about the directions of the processes. The connections between precuneus and nearby cortex, i.e., SMA and MCC, had predictive effects on the widespread connections between thalamus and frontal regions. The precuneus has been reported to be involved in epileptic discharge network, with distinct activity changing within seconds before the discharge onset (Vaudano et al., 2009; Bai et al., 2010). Causal analysis showed that the precuneus gated the discharge activity in thalamocortical network, and was the region with the most occurrence of initial spikes and slow waves comparing to the thalamus and

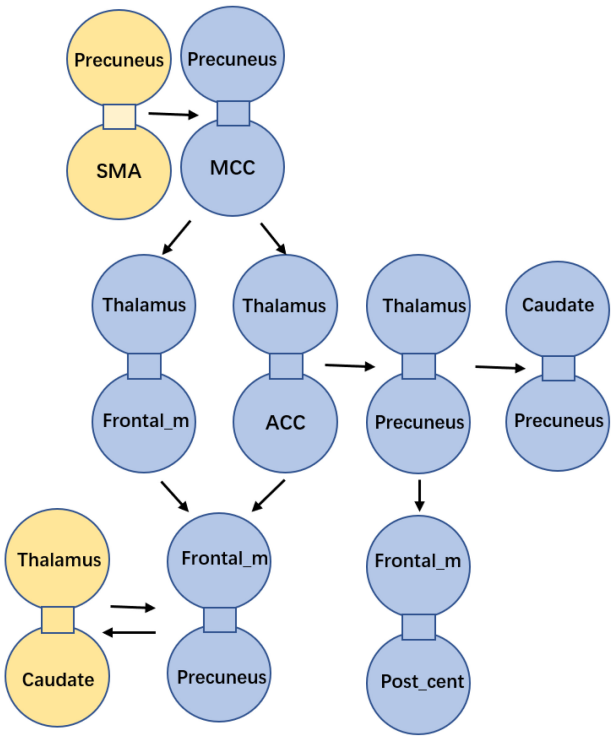

FIGURE 4 | Causality among the abnormal FNCs in IGE. Each bounded sub-graph in the figure is one abnormal connection in IGE, with the yellow sub-graph denoting the increased connection, and the blue sub-graph denoting the decreased connection in IGE. The arrows denoted the predictive directions among the connections.

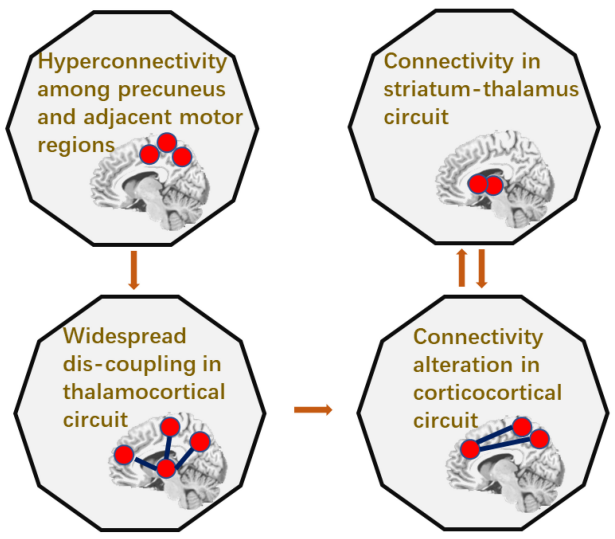

FIGURE 5 | The summarization of the causality in epileptic circuit.

frontal area (Lee et al., 2014). Also, precuneus has been shown the strongest connectivity strength before epileptic discharges, and the increased connectivity between precuneus and the nearby cortex was found before discharges (Qin et al., 2020a). Therefore, this study demonstrated the contribution of the connectivity between precuneus and the motor-related area to the widespread dysfunction of thalamocortical circuit, which implied that the hyperexcitability and hyperconnectivity of precuneus may be one important trigger of epileptic discharges, thus, resulting to the wide dysconnectivity in thalamocortical circuit and the following altered connectivity between cortical areas.

In one of our previous study, we detected the synchronous network during the stage of epileptic discharges, and found the connectivity within frontal areas and between frontal–parietal areas was the main network pattern after the discharge onset (Qin et al., 2020a). Also, extensive signal enhancement in bilateral frontal regions was found both at discharge initiation and after discharge in IGE (Bai et al., 2010). In this study, the frontal areas were directly involved in the dysconnectivity of thalamocortical circuit and corticocortical interaction, which indicated the role of thalamus and frontal areas in propagation of epileptic discharges. In addition, it was interesting that the increased connectivity between thalamus and caudate had bidirectional causal effect on the decreased frontal–precuneus connection. Previous studies have shown that the circuit of striatum-thalamus modulated the cortical interactions in epileptic brain (Deransart et al., 2000). It was suggested that the modulation of BGN may be associated with the enhanced integration within BGN regions, i.e., the connectivity between striatum and thalamus, and this modulation effect on the inter-cortical connectivity may uncover the potential intervene mechanism of the deep brain stimulation in epileptic brain.

To re-test the stability of the causal analysis, we also conducted the multivariate GCA to describe the directed causal effect from this seed connection to the other connections, as well as the reverse impact intensities from other connections to this seed connection. The results showed similar directed patterns with the bivariate GCA, including the predictive effect from precuneus-related connections to the thalamocortical connections, and then to the cortical–cortical connections. Moreover, much extensive effects were found from the striatum-thalamus to both the thalamocortical and the cortical–cortical connections. The results were shown in **Supplementary Figure 1**.

To sum up the results, we concluded the causal relationship among the abnormal functional connectivity in epileptic brain, which described the trigger role of precuneus with its extensive hyperconnectivity, and the widely distributed dysconnectivity of thalamocortical circuit, and also the following alteration of frontal and motor-related connectivity. This causality in epileptic circuit provided additional evidence for the theory of epileptic origin and propagation on the level of macro functional connectivity. However, the main limitation of this study is that the causal relationship of the abnormal connectivity was based on the resting-state data rather than the discharging state. Therefore, the result provided the potential modulation pattern in terms of the epileptic activity, and the inference of the epileptic propagation circuit in this study was urgently needed to test by the physical stimulation and clinical evaluation.

CONCLUSION

This study investigated the subcortical–cortical pathway in IGE, and showed that thalamus, precuneus were key regions of the abnormal FNC in epileptic brain. Furthermore, the causality analysis among these abnormal connections demonstrated the predictive effect of precuneus on the widely distributed thalamocortical dysconnectivity. In addition, the increased connectivity between thalamus and the striatum indicated the modulation role of subcortical circuit on the cortical connection in epilepsy. These results provided additional evidence for the widespread abnormality in epilepsy brain based on the dynamics of functional connections, and the predictive relationship in the subcortical–cortical circuit enlightened the theory of epileptic origin and propagation.

DATA AVAILABILITY STATEMENT

The raw data supporting the conclusions of this article will be made available by the authors, without undue reservation.

ETHICS STATEMENT

The studies involving human participants were reviewed and approved by the Ethics Committee of the University of Electronic Science and Technology of China. The patients/participants provided their written informed consent to participate in this study.

AUTHOR CONTRIBUTIONS

YQ, DY, and CL conceived and designed the work. YQ and SL acquired the data. YQ analyzed the data. YQ and CL wrote the manuscript. All authors revised the work for important intellectual content and read, and approved the manuscript.

FUNDING

This work was supported by grants from the National Nature Science Foundation of China (grant number: 82102175), National Key Research and Development Project (2021YFF1200605), Project of Science and Technology Department of Sichuan Province (grant number: 2020YJ0456), and Scientific Research Foundation of Sichuan Provincial People's Hospital (2021LY21).

ACKNOWLEDGMENTS

We thank the two radiologists for the neuroimaging evaluation.

SUPPLEMENTARY MATERIAL

The Supplementary Material for this article can be found online at: https://www.frontiersin.org/articles/10.3389/fnins.2022.925968/full#supplementary-material

REFERENCES

Avanzini, G., de Curtis, M., Marescaux, C., Panzica, F., Spreafico, R., and Vergnes, M. (1992). Role of the thalamic reticular nucleus in the generation of rhythmic thalamo-cortical activities subserving spike and waves. *J. Neural Transm. Suppl.* 35, 85–95. doi: 10.1007/978-3-7091-9206-1_6

Avanzini, G., Panzica, F., and de Curtis, M. (2000). The role of the thalamus in vigilance and epileptogenic mechanisms. *Clin. Neurophysiol.* 111, S19–S26. doi: 10.1016/S1388-2457(00)00398-9

Bai, X., Vestal, M., Berman, R., Negishi, M., Spann, M., Vega, C., et al. (2010). Dynamic time course of typical childhood absence seizures: EEG, behavior, and functional magnetic resonance imaging. *J. Neurosci.* 30, 5884–5893. doi: 10.1523/JNEUROSCI.5101-09.2010

Bartolini, E., Pesaresi, I., Fabbri, S., Cecchi, P., Giorgi, F. S., Sartucci, F., et al. (2014). Abnormal response to photic stimulation in juvenile myoclonic epilepsy: an EEG-fMRI study. *Epilepsia* 55, 1038–1047. doi: 10.1111/epi.12634

Benuzzi, F., Mirandola, L., Pugnaghi, M., Farinelli, V., Tassinari, C. A., Capovilla, G., et al. (2012). Increased cortical BOLD signal anticipates generalized spike and wave discharges in adolescents and adults with idiopathic generalized epilepsies. *Epilepsia* 53, 622–630. doi: 10.1111/j.1528-1167.2011.03385.x

Berenyi, A., Belluscio, M., Mao, D., and Buzsaki, G. (2012). Closed-loop control of epilepsy by transcranial electrical stimulation. *Science* 337, 735–737. doi: 10.1126/science.1223154

Blumenfeld, H. (2003). From molecules to networks: cortical/subcortical interactions in the pathophysiology of idiopathic generalized epilepsy. *Epilepsia* 44, 7–15. doi: 10.1046/j.1528-1157.44.s.2.2.x

Blumenfeld, H. (2005). Cellular and network mechanisms of spike-wave seizures. *Epilepsia* 46, 21–33. doi: 10.1111/j.1528-1167.2005.00311.x

Burdette, D. E., Haykal, M. A., Jarosiewicz, B., Fabris, R. R., Heredia, G., Elisevich, K., et al. (2020). Brain-responsive corticothalamic stimulation in the centromedian nucleus for the treatment of regional neocortical epilepsy. *Epilepsy Behav.* 112:107354.

Buzsaki, G. (1991). The thalamic clock: emergent network properties. *Neuroscience* 41, 351–364. doi: 10.1016/0306-4522(91)90332-i

Conradsen, I., Moldovan, M., Jennum, P., Wolf, P., Farina, D., and Beniczky, S. (2013). Dynamics of muscle activation during tonic-clonic seizures. *Epilepsy Res.* 104, 84–93. doi: 10.1016/j.eplepsyres.2012.09.004

Deransart, C., Riban, V., Le, B., Marescaux, C., and Depaulis, A. (2000). Dopamine in the striatum modulates seizures in a genetic model of absence epilepsy in the rat. *Neuroscience* 100, 335–344. doi: 10.1016/s0306-4522(00)00266-9

Dong, L., Luo, C., Liu, X. B., Jiang, S. S., Li, F. L., Feng, H. S., et al. (2018). Neuroscience information toolbox: an open source toolbox for EEG-fMRI multimodal fusion analysis. *Front. Neuroinf.* 12:56. doi: 10.3389/Fninf.2018.00056

Fisher, R. S., Cross, J. H., French, J. A., Higurashi, N., Hirsch, E., Jansen, F. E., et al. (2017). Operational classification of seizure types by the international league against epilepsy: position paper of the ILAE commission for classification and terminology. *Epilepsia* 58, 522–530. doi: 10.1111/epi.13670

Jiang, S., Luo, C., Gong, J., Peng, R., Ma, S., Tan, S., et al. (2018). Aberrant thalamocortical connectivity in juvenile myoclonic epilepsy. *Int. J. Neural Syst.* 28:17500344. doi: 10.1142/S0129065717500344

Jiang, S., Pei, H., Huang, Y., Chen, Y., Liu, L., Li, J., et al. (2020). Dynamic temporospatial patterns of functional connectivity and alterations in idiopathic generalized epilepsy. *Int. J. Neural Syst.* 30:2050065.

Kim, J. B., Suh, S. I., Seo, W. K., Oh, K., Koh, S. B., and Kim, J. H. (2014). Altered thalamocortical functional connectivity in idiopathic generalized epilepsy. *Epilepsia* 55, 592–600. doi: 10.1111/epi.12580

Lee, C., Kim, S. M., Jung, Y. J., Im, C. H., Kim, D. W., and Jung, K. Y. (2014). Causal influence of epileptic network during spike-and-wave discharge in juvenile myoclonic epilepsy. *Epilepsy Res.* 108, 257–266. doi: 10.1016/j.eplepsyres.2013.11.005

Luo, C., Li, Q., Lai, Y., Xia, Y., Qin, Y., Liao, W., et al. (2011). Altered functional connectivity in default mode network in absence epilepsy: a resting-state fMRI study. *Hum. Brain Mapp.* 32, 438–449. doi: 10.1002/hbm.21034

Luo, C., Li, Q. F., Xia, Y., Lei, X., Xue, K. Q., Yao, Z. P., et al. (2012). Resting state basal ganglia network in idiopathic generalized epilepsy. *Hum. Brain Mapp.* 33, 1279–1294. doi: 10.1002/hbm.21286

Martin-Lopez, D., Jimenez-Jimenez, D., Cabanes-Martinez, L., Selway, R. P., Valentin, A., and Alarcon, G. (2017). The role of thalamus versus cortex in epilepsy: evidence from human ictal centromedian recordings in patients assessed for deep brain stimulation. *Int. J. Neural Syst.* 27:1750010. doi: 10.1142/S0129065717500101

Meeren, H., van Luijtelaar, G., Lopes da Silva, F., and Coenen, A. (2005). Evolving concepts on the pathophysiology of absence seizures: the cortical focus theory. *Arch. Neurol.* 62, 371–376. doi: 10.1001/archneur.62.3.371

Moeller, F., Siebner, H. R., Wolff, S., Muhle, H., Boor, R., Granert, O., et al. (2008). Changes in activity of striato-thalamo-cortical network precede generalized spike wave discharges. *Neuroimage* 39, 1839–1849. doi: 10.1016/j.neuroimage.2007.10.058

Moeller, F., Stephani, U., and Siniatchkin, M. (2013). Simultaneous EEG and fMRI recordings (EEG-fMRI) in children with epilepsy. *Epilepsia* 54, 971–982. doi: 10.1111/epi.12197

O'Muircheartaigh, J., Vollmar, C., Barker, G. J., Kumari, V., Symms, M. R., Thompson, P., et al. (2012). Abnormal thalamocortical structural and functional connectivity in juvenile myoclonic epilepsy. *Brain* 135(Pt 12), 3635–3644. doi: 10.1093/brain/aws296

Parsons, N., Bowden, S. C., Vogrin, S., and D'Souza, W. J. (2020). Default mode network dysfunction in idiopathic generalised epilepsy. *Epilepsy Res.* 159:106254.

Paz, J. T., Davidson, T. J., Frechette, E. S., Delord, B., Parada, I., Peng, K., et al. (2013). Closed-loop optogenetic control of thalamus as a tool for interrupting seizures after cortical injury. *Nat. Neurosci.* 16, 64–70. doi: 10.1038/nn.3269

Qin, Y., Jiang, S., Zhang, Q., Dong, L., Jia, X., He, H., et al. (2019). BOLD-fMRI activity informed by network variation of scalp EEG in juvenile myoclonic epilepsy. *Neuroimage Clin.* 22:101759. doi: 10.1016/j.nicl.2019.101759

Qin, Y., Zhang, N., Chen, Y., Zuo, X., Jiang, S., Zhao, X., et al. (2020b). Rhythmic network modulation to thalamocortical couplings in epilepsy. *Int. J. Neural Syst.* 30:2050014. doi: 10.1142/S0129065720500148

Qin, Y., Zhang, N., Chen, Y., Tan, Y., Dong, L., Xu, P., et al. (2020a). How Alpha rhythm spatiotemporally acts upon the thalamus-default mode circuit in idiopathic generalized epilepsy. *IEEE Trans. Biomed. Eng.* 68, 1282–1292.

Salek-Haddadi, A., Lemieux, L., Merschhemke, M., Friston, K. J., Duncan, J. S., and Fish, D. R. (2003). Functional magnetic resonance imaging of human absence seizures. *Ann. Neurol.* 53, 663–667. doi: 10.1002/ana.10586

Scheffer, I. E., Berkovic, S., Capovilla, G., Connolly, M. B., French, J., Guilhoto, L., et al. (2017). ILAE classification of the epilepsies: position paper of the ILAE Commission for classification and terminology. *Epilepsia* 58, 512–521. doi: 10.1111/epi.13709

Stefan, H., and Lopes da Silva, F. H. (2013). Epileptic neuronal networks: methods of identification and clinical relevance. *Front. Neurol.* 4:8. doi: 10.3389/fneur.2013.00008

Szaflarski, J. P., DiFrancesco, M., Hirschauer, T., Banks, C., Privitera, M. D., Gotman, J., et al. (2010). Cortical and subcortical contributions to absence seizure onset examined with EEG/fMRI. *Epilepsy Behav.* 18, 404–413. doi: 10.1016/j.yebeh.2010.05.009

Timofeev, I., and Steriade, M. (2004). Neocortical seizures: initiation, development and cessation. *Neuroscience* 123, 299–336. doi: 10.1016/j.neuroscience.2003.08.051

Turski, L., Cavalheiro, E. A., Calderazzo-Filho, L. S., Bortolotto, Z. A., Klockgether, T., Ikonomidou, C., et al. (1989). The basal ganglia, the deep prepyriform cortex, and seizure spread: bicuculline is anticonvulsant in the rat striatum. *Proc. Natl. Acad. Sci. U.S.A.* 86, 1694–1697. doi: 10.1073/pnas.86.5.1694

Tyvaert, L., Chassagnon, S., Sadikot, A., LeVan, P., Dubeau, F., and Gotman, J. (2009). Thalamic nuclei activity in idiopathic generalized epilepsy: an EEG-fMRI study. *Neurology* 73, 2018–2022. doi: 10.1212/WNL.0b013e3181c55d02

Vaudano, A. E., Laufs, H., Kiebel, S. J., Carmichael, D. W., Hamandi, K., Guye, M., et al. (2009). Causal hierarchy within the thalamo-cortical network in spike and wave discharges. *PLoS One* 4:e6475. doi: 10.1371/journal.pone.0006475

Vollmar, C., O'Muircheartaigh, J., Barker, G. J., Symms, M. R., Thompson, P., Kumari, V., et al. (2011). Motor system hyperconnectivity in juvenile myoclonic epilepsy: a cognitive functional magnetic resonance imaging study. *Brain* 134, 1710–1719. doi: 10.1093/brain/awr098

Zang, Z. X., Yan, C. G., Dong, Z. Y., Huang, J., and Zang, Y. F. (2012). Granger causality analysis implementation on MATLAB: a graphic user interface toolkit for fMRI data processing. *J. Neurosci. Methods* 203, 418–426. doi: 10.1016/j.jneumeth.2011.10.006

Zhang, Z., Liu, G., Yao, Z., Zheng, W., Xie, Y., Hu, T., et al. (2018). Changes in dynamics within and between resting-state subnetworks in juvenile myoclonic epilepsy occur at multiple frequency bands. *Front. Neurol.* 9:448. doi: 10.3389/fneur.2018.00448

Conflict of Interest: The authors declare that the research was conducted in the absence of any commercial or financial relationships that could be construed as a potential conflict of interest.

Publisher's Note: All claims expressed in this article are solely those of the authors and do not necessarily represent those of their affiliated organizations, or those of the publisher, the editors and the reviewers. Any product that may be evaluated in this article, or claim that may be made by its manufacturer, is not guaranteed or endorsed by the publisher.

frontiers | Frontiers in Neuroscience

ORIGINAL RESEARCH
published: 30 June 2022
doi: 10.3389/fnins.2022.914894

Abnormal Voxel-Based Degree Centrality in Patients With Postpartum Depression: A Resting-State Functional Magnetic Resonance Imaging Study

Shufen Zhang[1†], Bo Li[2†], Kai Liu[2], Xiaoming Hou[3] and Ping Zhang[4*]*

[1] Department of Obstetrics, Shandong Second Provincial General Hospital, Jinan, China, [2] Department of Radiology, The 960th Hospital of the PLA Joint Logistics Support Force, Jinan, China, [3] Department of Pediatrics, Provincial Hospital Affiliated to Shandong First Medical University, Jinan, China, [4] Department of Neurosurgery, Qi Lu Hospital, Shandong University, Jinan, China

OPEN ACCESS

Edited by:
Nicoletta Cera,
University of Porto, Portugal

Reviewed by:
Bochao Cheng,
Sichuan University, China
Zhao Qing,
Nanjing Drum Tower Hospital, China
Xuhong Liao,
Beijing Normal University, China

***Correspondence:**
Xiaoming Hou
houxiaoming11111@hotmail.com
Ping Zhang
pz.qlh@hotmail.com

[†] These authors have contributed equally to this work and share first authorship

Specialty section:
This article was submitted to Brain Imaging Methods, a section of the journal Frontiers in Neuroscience

Received: 07 April 2022
Accepted: 03 June 2022
Published: 30 June 2022

Citation:
Zhang S, Li B, Liu K, Hou X and Zhang P (2022) Abnormal Voxel-Based Degree Centrality in Patients With Postpartum Depression: A Resting-State Functional Magnetic Resonance Imaging Study. Front. Neurosci. 16:914894. doi: 10.3389/fnins.2022.914894

Postpartum depression (PPD) is a major public health concern with significant consequences for mothers, their children, and their families. However, less is known about its underlying neuropathological mechanisms. The voxel-based degree centrality (DC) analysis approach provides a new perspective for exploring the intrinsic dysconnectivity pattern of whole-brain functional networks of PPD. Twenty-nine patients with PPD and thirty healthy postpartum women were enrolled and received resting-state functional magnetic resonance imaging (fMRI) scans in the fourth week after delivery. DC image, clinical symptom correlation, and seed-based functional connectivity (FC) analyses were performed to reveal the abnormalities of the whole-brain functional network in PPD. Compared with healthy controls (HCs), patients with PPD exhibited significantly increased DC in the right hippocampus (HIP.R) and left inferior frontal orbital gyrus (ORBinf.L). The receiver operating characteristic (ROC) curve analysis showed that the area under the curve (AUC) of the above two brain regions is all over 0.7. In the seed-based FC analyses, the PPD showed significantly decreased FC between the HIP.R and right middle frontal gyrus (MFG.R), between the HIP.R and left median cingulate and paracingulate gyri (DCG.L), and between the ORBinf.L and the left fusiform (FFG.L) compared with HCs. The PPD showed significantly increased FC between the ORBinf.L and the right superior frontal gyrus, medial (SFGmed.R) compared with HCs. Mean FC between the HIP.R and DCG.L positively correlated with EDPS scores in the PPD group. This study provided evidence of aberrant DC and FC within brain regions in patients with PPD, which was associated with the default mode network (DMN) and limbic system (LIN). Identification of these above-altered brain areas may help physicians to better understand neural circuitry dysfunction in PPD.

Keywords: postpartum depression, voxel-based degree centrality, seed-based functional connectivity, fMRI, receiver operating characteristic (ROC) curve analysis

INTRODUCTION

Postpartum depression (PPD) is a common but complex condition that affects approximately 10–20% of new mothers and has detrimental effects on mothers, infants, and their families (Nguyen et al., 2019). The risk of maternal suicide, infant abuse, and infanticide are all elevated among mothers with PPD (Lee and Chung, 2007). PPD further has a long-term negative impact on the cognitive, emotional, and behavioral development of children (Halligan et al., 2007). Due to the risks posed to the mother and the infant, the mother with PPD needs early diagnosis and treatment. Understanding the changes of PPD in brain structure, function and metabolism will help us to develop early screening, diagnosis, and targeted treatment techniques.

Resting-state functional magnetic resonance imaging (rs-fMRI) has been used to detect spontaneous neural brain activity in PPD using the amplitude of low-frequency fluctuation (ALFF) analysis (Deligiannidis et al., 2013, 2019; Chase et al., 2014) or dynamic ALFF (Cheng et al., 2022b), regional homogeneity (ReHo) analysis (Xiao-juan et al., 2011), voxel-mirrored homotopic connectivity (Zhang et al., 2020), dynamic or static functional connectivity (FC) (Cheng et al., 2022b), functional connectivity density (FCD) (Cheng et al., 2021), and functional connectivity strength (FCS) (Cheng et al., 2022a). Compared with healthy controls (HCs), mothers with PPD showed significantly increased ReHo in the posterior cingulate and medial frontal gyrus and decreased ReHo in the temporal gyrus (Xiao-juan et al., 2011). The depressed mothers also showed reduced connectivity among the anterior cingulate cortex (ACC), amygdala, hippocampus, and dorsolateral prefrontal cortex, between the corticocortical and corticolimbic regions (Deligiannidis et al., 2013), between the posterior cingulate cortex (PCC) and amygdala (Chase et al., 2014), and between the dorsomedial prefrontal cortex (dmPFC) and the precuneus, posterior cingulate cortex, and supramarginal gyrus/angular gyrus regions (Deligiannidis et al., 2019). However, they showed increased connectivity between dmPFC and the rest of the default mode network (DMN) (Deligiannidis et al., 2019). Decreased voxel-mirrored homotopic connectivity values in the bilateral dmPFC, dorsal anterior cingulate cortex (dACC), and orbitofrontal cortex were observed in patients with PPD (Zhang et al., 2020). Mothers with PPD exhibited increased static FC (sFC) between the subgenual anterior cingulate cortex (sgACC) and ventral anterior insula and disrupted sFC between the sgACC and middle temporal gyrus. The changes in dynamic FC between the sgACC and superior temporal gyrus could differentiate PPD and HCs (Cheng et al., 2022b). Patients with PPD showed specifically weaker long-range FCD in the right lingual gyrus (LG.R), functional couplings between LG.R and dmPFC, and left precentral gyrus, and specifically stronger functional coupling between LG.R and right angular. Moreover, the altered FCD and resting-state FC were closely associated with depression and anxiety symptoms load (Cheng et al., 2021). The PPD group showed specifically higher FCS in right parahippocampus, and perceived social support mediated the influence of FCS in the right cerebellum posterior lobe on depression and anxiety symptoms (Cheng et al., 2022a). These studies can help clarify how PPD may affect a mother's baseline brain activity at rest and provide a more comprehensive understanding of neural circuitry dysfunction in mothers with PPD.

The above studies focus on regional functional connectivity or analyze neural networks between selected brain regions based on a prior assumption (Deligiannidis et al., 2013, 2019). To better understand the changes in neural circuitry in PPD, we employed degree centrality (DC) to measure the global connectivity at the voxel level. DC is a new emerging reliable and compelling graph-based analysis method (Xia and He, 2017), which can identify that the voxels showed altered direct connections to all other voxels with high sensitivity, specificity, and reproducibility. It does not depend on the selection of brain regions based on prior assumptions (Bullmore and Sporns, 2009). Degree centrality (DC) has been applied to brain network research, and its abnormalities have been found in various mental disorders, such as schizophrenia (Li X. et al., 2019), major depressive disorder (Sheng et al., 2018), bipolar disorder (Deng et al., 2019), multiple sclerosis (Eijlers et al., 2017), Alzheimer's disease (AD) (Guo et al., 2016), epilepsy (Ren et al., 2019), and Parkinson's disease (Li M. et al., 2019). However, the DC analysis cannot provide detailed information regarding the connectivity between a voxel and the particular regions that were changed. In this study, we further conducted a seed-based FC analysis using the regions with high DC values as seeds to comprehensively explore the intrinsic abnormal connectivity of the whole-brain functional network. We tested the following hypotheses: (1) the PPD group showed abnormal DC in several brain regions compared with HCs; (2) the alterations of DC would be related to clinical symptoms; and (3) the brain regions with abnormal DC showed the aberrant FC with other brain regions.

MATERIALS AND METHODS

Participants

The ethics committee of the Shandong Second Provincial General Hospital approved this study, and all participants provided written informed consent. Twenty-nine right-handed patients with PPD were recruited from the Department of Obstetrics of Shandong Second Provincial General Hospital and the Department of Obstetrics of the 960th Hospital of the PLA Joint Logistics Support Force. Two experienced senior associate chief physicians of neurology confirmed their diagnoses using the Structured Clinical Interview for Diagnostic and Statistical Manual of Mental Disorders, Fifth Edition (DSM-V) and Chinese Classification and Diagnostic Criteria of Mental Disorders, 3rd edition (CCMD-3). Inclusion criteria for patients were as follows: (a) their age ranged from 21 to 38 years, in the fourth week after delivery; (b) they were current first-episode, treatment-naive patients with PPD; (c) they had an Edinburgh postpartum depression scale (EPDS) score $\geqq$12; (d) they had no other medical or mental illness history, (e) they were not substance abusers or substance dependent; (f) there were no contraindications of an MR examination; and (g) there were no organic abnormalities for MRI routine series. The EPDS scale was assessed in 1 h before the image acquisition.

A total of thirty right-handed, age-matched healthy postpartum women were recruited from the department of obstetrics. Inclusion criteria for the healthy postpartum group were as follows: (a) they were aged from 21 to 38 years and in the fourth week after delivery; (b) they did not have a current or previous history of depressive episodes; (c) their EDPS score was<3; (d) they had no other medical or mental illness history; (e) there were no substance abusers or substance dependent; (f) there were no contraindications of the MR examination; and (g) there were no organic abnormalities for the MRI routine series.

Image Acquisition

All brain imaging data were acquired on a 3.0 T MR system (Discovery MR750, General Electric, Milwaukee, WI, United States) with a standard eight-channel head coil. During scanning, all subjects were instructed to lie still and awake, close their eyes, and breathe steadily. Special nonmagnetic foam pads were used to fix the head and minimize head movement.

High-resolution structural T1-weighted scan (Three-dimensional Brain Volume, 3D BRAVO) was performed with the following parameters: time repetition (TR) = 8.2 ms, time echo (TE) = 3.2 ms, flip angle = 12°, field of view (FOV) = 240 mm × 240 mm, slices = 115, voxel size = 1 mm, and thickness = 1.0 mm. Resting-state BOLD MR images were acquired with the following parameters: TR = 2,000 ms, TE = 30 ms, flip angle = 90°, FOV = 240 mm × 240 mm, resolution = 64 × 64, thickness = 4.0 mm, no interspace, slices = 41, gradient echo-planar volumes = 200, and duration was 6 min 40 s. In addition, T1 and T2-weighted images were collected to exclude anatomic abnormality and brain diseases for each subject.

Functional Image Preprocessing

The fMRI data preprocessing was conducted using the Data Processing Assistant for Resting-State fMRI (DPARSF) and RESTing-state fMRI data analysis toolkit (REST)[1], which is based on Statistical Parametric Mapping (SPM12).[2] First, the first 10 time points of resting-state image data were discarded to ensure steady-state longitudinal magnetization. Second, the slice-time corrected images were realigned to the first volume for head motion correction. Then, T1 images were coregistered to the realigned functional images and segmented to gray matter, white matter, and cerebrospinal fluid. We normalized the resulting images to a standard Montreal Neurological Institute (MNI) template in the Montreal Neurological Institute space by applying the parameters of structural image normalization and resampling the normalized images to 3 mm isotropic voxels. After linear trend removal, the data were band-pass filtered (0.01–0.08 Hz) to eliminate physiological noise. Several sources of spurious covariates along with their temporal derivatives, including the six head motion parameters, global mean, white matter, and cerebrospinal fluid, were removed. Then, the time series of each subject was used to compute the DC.

Degree Centrality Calculation

We computed voxel-wise DC using Pearson correlations with the REST 1.8 toolbox. The time course of each voxel in the gray matter (GM) mask was extracted and correlated with every other voxel within the mask to generate a correlation matrix (**Supplementary Figure 1** and **Table 1**). The threshold for the Pearson's correlation coefficient was set at $r > 0.25$ (**Supplementary Figure 2**). DC was computed as the sum of the weights of connections (weighted) for each voxel (**Supplementary Figure 3**). The resulting DC maps were spatially smoothed with a 4 mm × 4 mm × 4 mm FWHM Gaussian kernel and were improved in normality using the Fisher-z transformation. To validate the main results that did not depend on the selection of correlation thresholds, we also computed the DC maps using other different correlation thresholds (i.e., 0.1, 0.2, 0.3, and 0.4) and then reperformed statistical analysis. We found that the choice of these thresholds did not have a significant impact on the main results.

[1]http://www.restfmri.net

[2]http://www.fil.ion.ucl.ac.uk/spm

TABLE 1 | Demographic and clinical characteristics of participants.

	Healthy control (HC, *n* = 30)		Postpartum depressed (PPD, *n* = 29)		
Characteristic	**Mean (SD)**	**Percent (%)**	**Mean (SD)**	**Percent (%)**	***P*-value**
Age (years)	27.33 (4.10)		27.24 (3.55)		0.99[a]
Primipara	26	86.66	25	86.21	0.96[b]
Caesarean	9	30.0	11	37.93	0.52[b]
Breastfeeding	30	100	29	100	
Socioeconomic status					
(Thousand RMB)	133.0 (2.47)		144.48 (2.20)		0.06[a]
Education (years)	12.23 (2.58)		13.00 (2.15)		0.68[a]
Neuropsychological tests					
EPDS	0.50 (0.73)		15.79 (1.86)		0.00[a]
PSQI	6.52 (3.02)		15.17 (2.96)		0.00[a]

SD, standard deviation; RMB, Renminbi; EPDS, Edinburgh postpartum depression scale; PSQI, Pittsburgh sleep quality index.
[a]Unpaired t-test, b$\chi 2$.

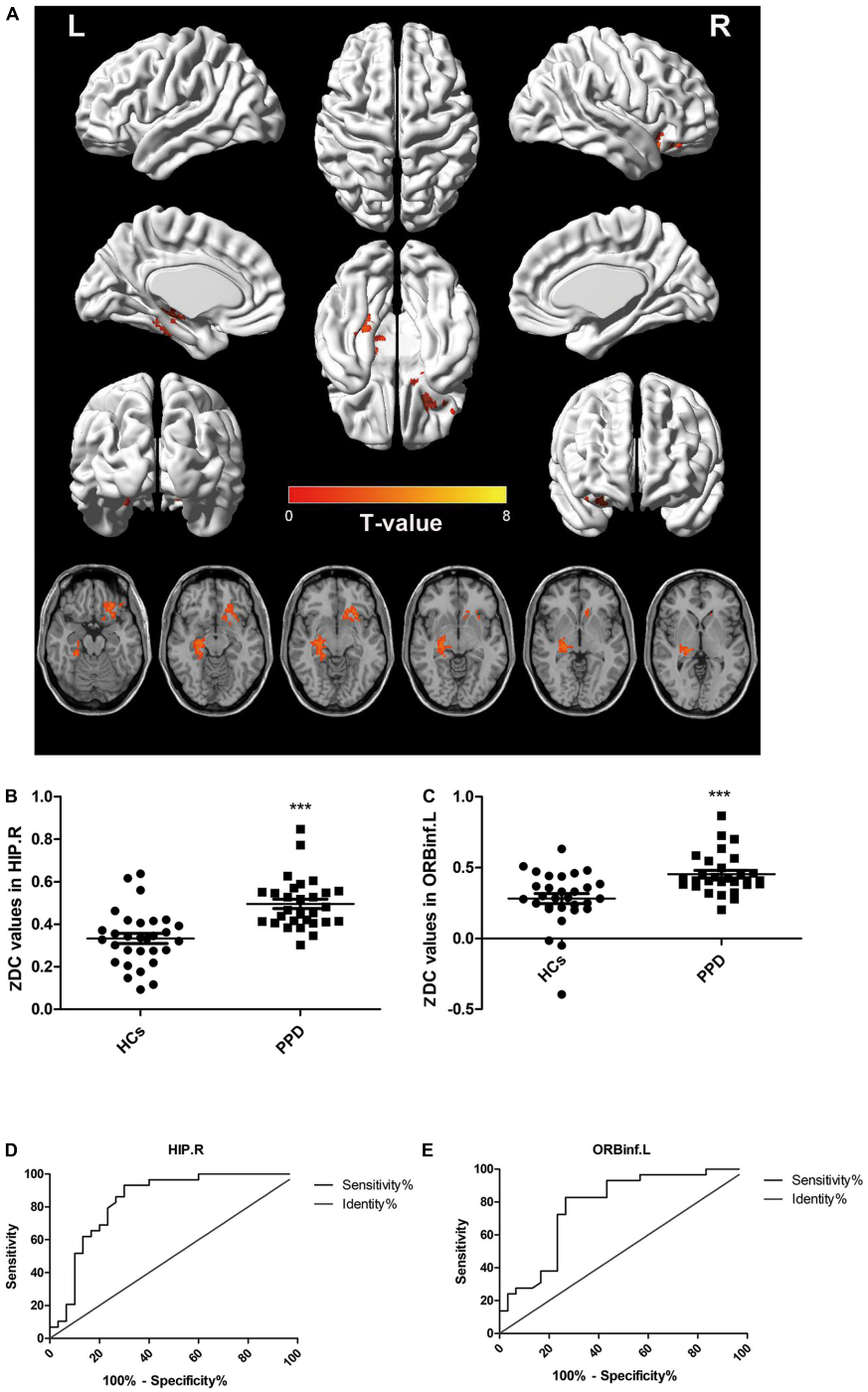

FIGURE 1 | Comparisons of degree centrality between patients with postpartum depression (PPD) and healthy controls (HCs). **(A)** Brain regions with different degree centrality (DC) values between groups: HIP.R and ORBinf.L. **(B,C)** The distribution and comparison of DC values of brain regions in the PPD and HCs. **(D,E)** The ROC curve evaluates the diagnostic value of the DC value of different brain regions to distinguish patients with PPD from healthy mothers. HIP.R, right hippocampus; ORBinf.L, left inferior frontal orbital gyrus.

Functional Connectivity Analysis

The whole-brain cluster with significant abnormal DC in patients with PDD (compared with control subjects) was selected as seeds. We obtained FC maps by calculating the correlation coefficient (r score) between the mean time series of each seed region and the rest of the brain. Finally, FC maps were converted to z-score maps using Fisher's z transformation to improve the normality. Correction for between-group FC comparisons was conducted

TABLE 2 | Brain regions showing significant differences in the degree centrality between postpartum depression (PPD) and healthy controls (HCs).

Brain region	Peak MNI coordinates			Cluster size	Peak *T* value
	x	y	z	(mm^3)	
Right hippocampus	27	−21	−6	208	3.74
Frontal_Inf_Orb_L	−24	27	−18	146	3.19

MNI, Montreal Neurological Institute.

using REST1.8 software *via* the Gaussian random field (GRF) theory correction program (voxel $p < 0.05$, cluster $p < 0.05$, 2-tailed).

Statistical Analysis

The variables, including age and clinical symptom scores between the PPD and control group, were analyzed using the Mann–Whitney *U* test using SPSS 18.0 (SPSS Inc., Chicago, IL, United States). The differences in delivery method and time were determined using chi-square tests. The threshold was set at $p < 0.05$ (two-tailed). With age as covariates, two sample *t*-tests were performed in REST1.8 software to determine significant voxel-based differences in the DC value between the two groups. Correction for multiple comparisons was conducted using REST1.8 software *via* the GRF theory correction program within the whole brain (voxel $p < 0.001$, cluster $p < 0.05$, 2-tailed). Since DC calculation is very important in this study, we increased the *p*-value ($p < 0.001$) when doing GRF correction.

In addition, we performed Pearson correlation analyses between the DC and neuropsychological test scores of patients with PPD. We used the receiver operating characteristic (ROC) curve analysis of DC values of brain regions showing differences between the two groups to determine the brain regions' diagnostic significance for PPD. The threshold was set at $p < 0.05$. The peak voxel coordinates with the highest significance within the brain areas of altered FC were described in terms of standard Montreal Neurological Institute coordinates. The software "BrainNet Viewer" in REST[3] was used to draw a 3D brain figure.

RESULTS

Demographic and Clinical Characteristics

The demographic and clinical characteristics of all subjects are listed in **Table 1**. There were no significant differences in age, delivery time, delivery method, feed options, socioeconomic status, or education level between PPDs and controls ($p > 0.05$). PPD groups had higher EPDS and PSQI scores ($p < 0.001$) than the HCs.

[3]http://www.nitrc.org/projects/bnv/

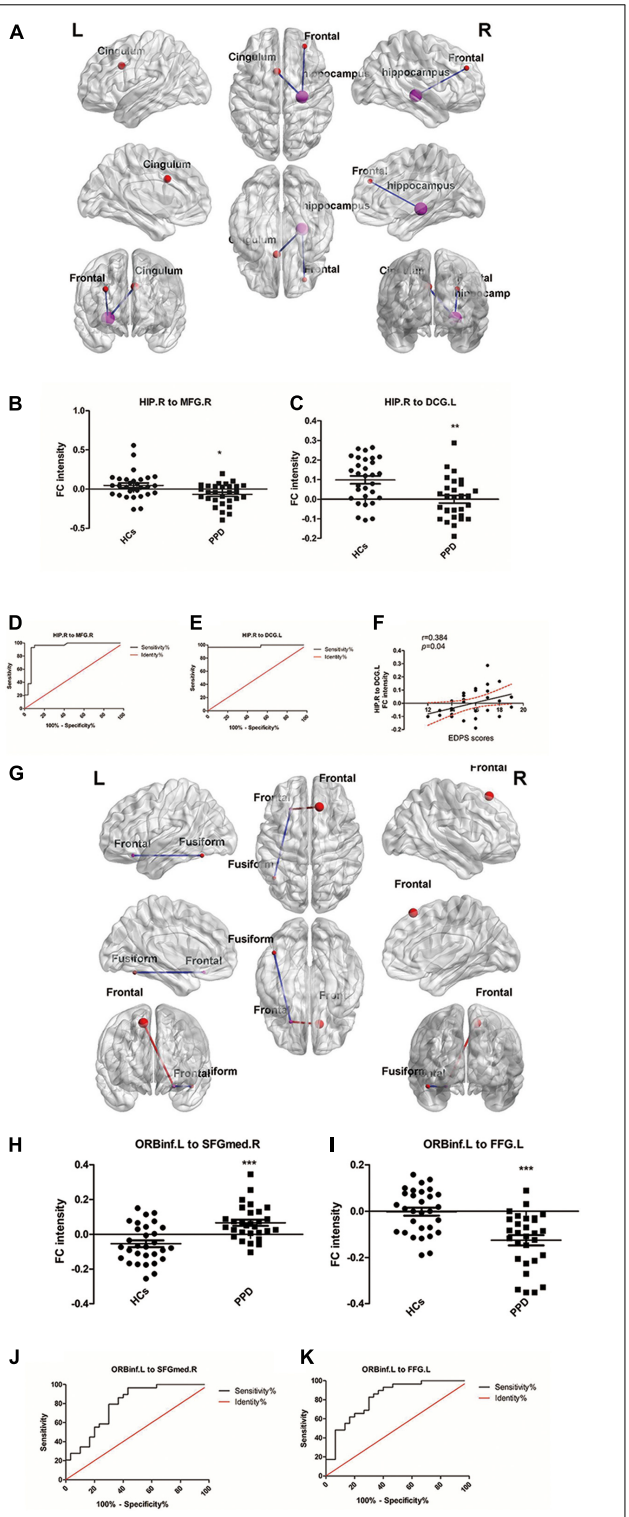

FIGURE 2 | (A) Brain regions showing aberrant functional connectivity (FC) with HIP.R (seed region) in the PPD group compared with the HCs. Cool color represents significantly decreased FC. **(B,C)** Mean values of the abnormal functional connectivity in these groups. **(D,E)** The ROC curve evaluates the diagnostic value of the FC value of different brain regions to distinguish patients with PPD from healthy mothers, in which HIP.R was as seeds.

(Continued)

FIGURE 2 | (F) Scatter plots depicting a partial correlation between the HIP.R-related functional connectivity in the DCG.L and the EDPS scores for patients with PPD. **(G)** Brain regions showing aberrant FC with ORBinf.L (seed region) in the PPD group compared with the HCs. Warm color represents significantly increased FC, and cool color represents significantly decreased FC. **(H,I)** Mean values of the abnormal functional connectivity in these groups. **(J,K)** The ROC curve evaluates the diagnostic value of the FC value of different brain regions to distinguish patients with PPD from healthy mothers, in which ORBinf.L was as seeds. HIP.R, right hippocampus; ORBinf.L, left inferior frontal orbital gyrus; MFG.R, right middle frontal gyrus; DCG.L, left median cingulate and paracingulate gyri; FFG.L, left fusiform; SFGmed.R, right superior frontal gyrus, medial. ***Significant at 0.001 level and *significant at 0.05 level.

TABLE 3 | Significant differences in functional connectivity between postpartum depression (PPD) and healthy controls (HCs).

Seed area	Area with altered FC	Peak MNI coordinates			Cluster size	Peak *T* value
		x	y	z	(mm^3)	
Right	Frontal_Mid_R	30	45	30	91	−2.98
hippocampus	Cingulum_Mid_L	−6	12	33	148	−3.17
Frontal_	Fusiform_L	−45	−60	−18	172	−3.44
Inf_Orb_L	Frontal_Sup_Medial_R	12	30	57	590	3.46

MNI, Montreal Neurological Institute.

Degree Centrality Analysis

Compared with the HCs, the PPD group showed increased DC in the right hippocampus (HIP.R) and left inferior frontal orbital gyrus (ORBinf.L) (**Figures 1A–C** and **Table 2**). The brain areas with decreased DC were not found in PPDs compared with the HCs.

The ROC curve analysis was used to test the diagnostic value of two brain regions (cluster1: HIP.R; cluster 2: ORBinf.L) with significantly altered DC between groups. The area under the curve (AUC) includes the HIP.R 0.8374 and ORBinf.L 0.7764 (**Figures 1D,E**).

There were no significant correlations between the DC values in the two brain regions (HIP.R and ORBinf.L) and any scores (EPDS and PSQI) in the PPD group.

Seed-Based Functional Connectivity Analysis

We used HIP.R and ORBinf.L as seeds in the functional connectivity analysis of the whole brain. In the PDD group, the HIP.R showed significantly decreased FC with the right middle frontal gyrus (MFG.R) and the left median cingulate and paracingulate gyri (DCG.L) compared with HCs. Furthermore, in the PPD group, the ORBinf.L showed increased FC with the right superior frontal gyrus, medial (SFGmed.R), while decreased FC with the left fusiform (FFG.L) compared with HCs (**Figures 2A–C,G–I** and **Table 3**).

The ROC curve analysis was used to test the diagnostic value of the four significant different FCs (HIP.R to MFG.R; HIP.R to DCG.L; ORBinf.L to SFGMED.R; and ORBinf.L to FFG.L) between groups. The area under the curve (AUC) includes the HIP.R to MFG.R: 0.9397; HIP.R to DCG.L: 0.9816; ORBinf.L to SFGMED.R:0.7920; and ORBinf.L to FFG.L:0.8241 (**Figures 2D,E,J,K**).

Correlation analysis revealed that FC intensity between HIP.R and the DCG.L positively correlated with the score of EDPS in patients with PPD ($r = 0.384$, $p = 0.04$; **Figure 2F**). There were no significant correlations among the FC intensity among any other regions and any other scores (EPDS and PSQI) in the PPD group.

DISCUSSION

This study observed voxel-level whole-brain FC abnormalities in patients with PPD using both DC and seed-based FC approaches. In this study, we found the following: (1) compared with the HCs, the PDD group showed increased DC in HIP.R and the ORBinf.L; the ROC curve analysis showed that the AUCs of the above two brain regions are all over 0.7. (2) In the seed-based FC analyses, the PPD showed significantly decreased FC between the HIP.R and MFG.R, between the HIP.R and DCG.L, and between the ORBinf.L and FFG.L compared with HCs. The PPD showed significantly increased FC between the ORBinf.L and SFGmed.R compared with HCs. (3) In particular, the HIP.R-related FC abnormalities in the DCG.L of patients with PPD were associated with EDPS scores.

The hippocampus is the core region in the limbic system (LIN) and plays a very important role in memory and cognitive function as well as the regulation of motivation, stress, and emotion (Eichenbaum, 2013). The hippocampus is highly sensitive to stress (Thomas et al., 2007). Both normal sadness and depressive illness were reported to be linked to increases in limbic areas including the hippocampus (Fitzgerald et al., 2008; Delaveau et al., 2011). It has been reported that MDD leads to an increased nodal centrality (both degree and strength) for the right hippocampus (Chu et al., 2018); patients with MDD have impaired functional connections of the hippocampus (Gray et al., 2020). In this study, we found that higher DC in the right hippocampus in PPD, which means that the right hippocampus had the increased centrality in PPD's brain network. However, the seed-based FC analysis showed that the right hippocampus presented weaker connectivity with the MFG.R and the DCG.L compared with HCs. It had already been observed the attenuation of connectivity between the dlPFC and hippocampus in PPD subjects (Deligiannidis et al., 2013). The results suggested that a higher DC value is not necessarily better; too high may indicate wrong connectivity or invalid connectivity. The appearance of invalid connectivity or wrong connectivity will lead to a decrease in brain function. The abnormal DC and FC of the hippocampus might explain memory deficits and the depression experienced by patients with PDD.

The MFG plays an essential role in a variety of cognitive functions, such as working memory, motor control, and attentional reorientation (Japee et al., 2015). Decreased structural and FC of MFG have been frequently reported in depressed individuals (Korgaonkar et al., 2014; Sheng et al., 2018).

DCG.L is the part of the cingulate gyrus and is involved in behavior, motor, and somatosensory function, especially in emotion, information transmission, and cognitive processing (Oane et al., 2020). Aberrant activity of this brain region is associated with negative emotions (Jiang et al., 2020), episodic memory, and rumination processing of depressive symptoms (Huang et al., 2021). We found that FC intensity between HIP.R and DCG.L positively correlated with the score of EDPS in patients with PPD. We used the original FC value when doing the correlation analysis. There were 15 negative values of FC between HIP.R and the DCG.L. The negative values mean that the stronger the FC, the smaller the value, so it was positively correlated with the score. This result highlighted the importance of HIP.R and DCG.L in PPD, and the abnormal FC between them might be a distinct feature in the neurobiology of PPD. Integrative dysfunctions of these regions may contribute to disturbances in mood, cognition, and memory in PPD.

The ORBinf.L refers to one of the three parts of the inferior frontal gyrus that plays an important role in the regulation of emotion and attention (Cha et al., 2016). It is involved in behaviors related to emotion and empathy and shows increased functional activity when individuals experience subjective feelings of guilt (Briggs et al., 2019). In disease, the orbital part of the inferior frontal gyrus exhibits abnormal functional connectivity in patients with depression (Rolls et al., 2020) and anxiety (Cha et al., 2016). In this study, we found that the PPD group showed increased DC in ORBinf.L that showed increased FC with the SFGmed.R, while decreased FC with the FFG.L compared with HCs. The medial superior frontal gyrus, as an important part of the superior prefrontal gyrus, is associated with self-consciousness, self-referential processing, emotion regulation, and cognitive processing (Yan et al., 2021). It played a partial mediating role in the relationship between perceived stress and depression (Wang et al., 2019). The fusiform gyrus is involved in many aspects of cognition, especially emotion recognition in social-cognitive processes (Jung et al., 2021). The abnormal neural activity in the fusiform gyrus may be associated with the severity of depression or susceptibility to depression (Huang et al., 2021). The abnormal FC among these above regions might explain depression, anxiety, stress, and social impairments among patients with PPD.

In this study, we demonstrated that PPD-related integrative disturbances were most commonly located in the DMN and LIN. The HIP.R, MFG.R, DCG.L, ORBinf.L, and SFGmed.R were suggested as key nodes of DMN. DMN is engaged in a diverse array of functions, such as episodic memory, self-referential activity, and monitoring the self and surrounding environment (Raichle, 2015). LIN is mainly involved in memory, regulation of negative cognition, and emotion (Rolls, 2015). DMN and LIN exhibited abnormal neuro-activity and were involved in the physiopathology of depression (Sheng et al., 2018). Our results supported the preferential involvement of hubs and the DMN/LIN in PPD and developed models of network alterations in the disease, which might help better understand the underlying neurobiology of PPD. The ROC curve analysis showed that the AUC of the HIP.R and the ORBinf.L and their altered FCs were all over 0.7. The range of AUC between 0.7 and 0.9 indicates the ideal diagnostic value. The brain regions with high DC values and the abnormal FCs in PPD had appropriate diagnosis accuracy and could be used as the imaging biomarkers of patients with PPD for diagnosis.

However, this study has several limitations. First, the sample size was relatively small, which may affect statistical power. Second, DC can only identify brain regions with abnormal functional connectivity and is unable to provide a clear causal relationship. Third, this study lacks the comparison between the pretreatment and posttreatment of patients with PPD and could not provide the imaging change of the above brain areas after treatment. Fourth, it is controversial about the time of onset of PPD. We chose the fourth week, the time of the new mother's first postpartum follow-up in the hospital, to do the EPDS scale and acquire the fMRI images. We will follow up with the mothers and do the EPDS scale and acquire the fMRI images within the first 6 weeks and 1 year after delivery in our following research to further verify our results. Fifth, the cognitive functions of the new mothers were not assessed in detail. In our following research, we will use Beck's Anxiety Inventory (BAI), Pittsburgh Sleep Quality Index (PSQI), and SymptomChecklist90 (SCL-90) to assess the new mothers thoroughly. There is still no complete consensus on the orders between the temporal filtering and the nuisance regression during data preprocessing. In this study, linear regression was conducted after band-pass filtering the data (0.01–0.08 Hz) according to the processing procedure of similar studies (Zhang et al., 2020; Li et al., 2021; Wang et al., 2021) and the default order DPARSF and REST software. We will explore two data processing pipelines for PPD disease in future studies. In conclusion, we found abnormal DC values and FCs in a variety of brain regions in the PPD groups, which might demonstrate the reorganization of the brain network in PPD and provide imaging biomarkers for early screening and accurate diagnosis of PPD.

DATA AVAILABILITY STATEMENT

The original contributions presented in this study are included in the article/ **Supplementary Material**, further inquiries can be directed to the corresponding authors.

ETHICS STATEMENT

The studies involving human participants were reviewed and approved by the Shandong Second Provincial General Hospital. The patients/participants provided their written informed consent to participate in this study.

AUTHOR CONTRIBUTIONS

PZ and XH: conception, study design, interpretation of the results, drafting the manuscript work, or revising it critically for

important intellectual content. SZ, BL, and KL: data collection or acquisition. SZ and BL: statistical analysis. All authors approved the final version to be published and agreement to be accountable for the integrity and accuracy of all aspects of the work.

FUNDING

This study was supported by the National Natural Science Foundation for Young Scholars of China (grant number 81902540), the Shandong Provincial Medical and Health Science and Technology Development Plan Project (grant number 20210520733), the Clinical Medical Science and Technology Innovation Program (grant numbers 202019112 and 202019022), and the President's Foundation of the 960th Hospital of the Chinese People's Liberation Army Joint Service Support Force (grant number 2021MS04).

ACKNOWLEDGMENTS

This research was conducted in accordance with the Code of Ethics of the World Medical Association (Declaration of Helsinki) for experiments involving humans. The manuscript was in line with the Recommendations for the Conduct, Reporting, Editing, and Publication of Scholarly Work in Medical Journal. Informed consent was obtained from all individual participants included in the study.

SUPPLEMENTARY MATERIAL

The Supplementary Material for this article can be found online at: https://www.frontiersin.org/articles/10.3389/fnins.2022.914894/full#supplementary-material

REFERENCES

Briggs, R. G., Chakraborty, A. R., Anderson, C. D., Abraham, C. J., Palejwala, A. H., Conner, A. K., et al. (2019). Anatomy and white matter connections of the inferior frontal gyrus. *Clin. Anat.* 32, 546–556. doi: 10.1002/ca.23349

Bullmore, E., and Sporns, O. (2009). Complex brain networks: graph theoretical analysis of structural and functional systems. *Nat. Rev. Neurosci.* 10, 186–198. doi: 10.1038/nrn2575

Cha, J., DeDora, D., Nedic, S., Ide, J., Greenberg, T., Hajcak, G., et al. (2016). Clinically anxious individuals show disrupted feedback between inferior frontal gyrus and prefrontal-limbic control circuit. *J. Neurosci.* 36, 4708–4718. doi: 10.1523/JNEUROSCI.1092-15.2016

Chase, H. W., Moses-Kolko, E. L., Zevallos, C., Wisner, K. L., and Phillips, M. L. (2014). Disrupted posterior cingulate-amygdala connectivity in postpartum depressed women as measured with resting BOLD fMRI. *Soc. Cogn. Affect. Neurosci.* 9, 1069–1075. doi: 10.1093/scan/nst083

Cheng, B., Roberts, N., Zhou, Y., Wang, X., Li, Y., Chen, Y., et al. (2022a). Social support mediates the influence of cerebellum functional connectivity strength on postpartum depression and postpartum depression with anxiety. *Trans. Psychiatry* 12, 54–60. doi: 10.1038/s41398-022-01781-9

Cheng, B., Wang, X., Roberts, N., Zhou, Y., Wang, S., Deng, P., et al. (2022b). Abnormal dynamics of resting-state functional activity and couplings in postpartum depression with and without anxiety. *Cereb Cortex*. 00, 1–12. doi: 10.1093/cercor/bhac038

Cheng, B., Zhou, Y., Kwok, V. P. Y., Li, Y., Wang, S., Zhao, Y., et al. (2021). Altered functional connectivity density and couplings in postpartum depression with and without anxiety. *Soc. Cogn. Affect. Neurosci.* doi: 10.1093/scan/nsab127

Chu, S. H., Lenglet, C., Schreiner, M. W., Klimes-Dougan, B., Cullen, K., and Parhi, K. K. (2018). Biomarkers for adolescent MDD from anatomical connectivity and network topology using diffusion MRI. *Ann. Int. Conf. IEEE Eng. Med. Biol. Soc.* 2018, 1152–1155. doi: 10.1109/EMBC.2018.8512505

Delaveau, P., Jabourian, M., Lemogne, C., Guionnet, S., Bergouignan, L., and Fossati, P. (2011). Brain effects of antidepressants in major depression: a meta-analysis of emotional processing studies. *J. Affect. Dis.* 130, 66–74. doi: 10.1016/j.jad.2010.09.032

Deligiannidis, K. M., Fales, C. L., Kroll-Desrosiers, A. R., Shaffer, S. A., Villamarin, V., Tan, Y., et al. (2019). Resting-state functional connectivity, cortical GABA, and neuroactive steroids in peripartum and peripartum depressed women: a functional magnetic resonance imaging and spectroscopy study. *Neuropsychopharmacology* 44, 546–554. doi: 10.1038/s41386-018-0242-2

Deligiannidis, K. M., Sikoglu, E. M., Shaffer, S. A., Frederick, B., Svenson, A. E., Kopoyan, A., et al. (2013). GABAergic neuroactive steroids and resting-state functional connectivity in postpartum depression: a preliminary study. *J. Psychiatr Res.* 47, 816–828. doi: 10.1016/j.jpsychires.2013.02.010

Deng, W., Zhang, B., Zou, W., Zhang, X., Cheng, X., Guan, L., et al. (2019). Abnormal degree centrality associated with cognitive dysfunctions in early bipolar disorder. *Front. Psychiatry* 10:140. doi: 10.3389/fpsyt.2019.00140

Eichenbaum, H. (2013). Hippocampus: remembering the choices. *Neuron* 77, 999–1001. doi: 10.1016/j.neuron.2013.02.034

Eijlers, A. J., Meijer, K. A., Wassenaar, T. M., Steenwijk, M. D., Uitdehaag, B. M., Barkhof, F., et al. (2017). Increased default-mode network centrality in cognitively impaired multiple sclerosis patients. *Neurology* 88, 952–960. doi: 10.1212/WNL.0000000000003689

Fitzgerald, P. B., Laird, A. R., Maller, J., and Daskalakis, Z. J. (2008). A meta-analytic study of changes in brain activation in depression. *Hum. Brain Mapp.* 29, 683–695. doi: 10.1002/hbm.20426

Gray, J. P., Muller, V. I., Eickhoff, S. B., and Fox, P. T. (2020). Multimodal abnormalities of brain structure and function in major depressive disorder: a meta-analysis of neuroimaging studies. *Am. J. Psychiatry* 177, 422–434. doi: 10.1176/appi.ajp.2019.19050560

Guo, Z., Liu, X., Hou, H., Wei, F., Liu, J., and Chen, X. (2016). Abnormal degree centrality in Alzheimer's disease patients with depression: a resting-state functional magnetic resonance imaging study. *Exp. Gerontol.* 79, 61–66. doi: 10.1016/j.exger.2016.03.017

Halligan, S. L., Murray, L., Martins, C., and Cooper, P. J. (2007). Maternal depression and psychiatric outcomes in adolescent offspring: a 13-year longitudinal study. *J. Affect. Dis.* 97, 145–154. doi: 10.1016/j.jad.2006.06.010

Huang, Q., Xiao, M., Ai, M., Chen, J., Wang, W., Hu, L., et al. (2021). Disruption of neural activity and functional connectivity in adolescents with major depressive disorder who engage in non-suicidal self-injury: a resting-state fMRI study. *Front. Psychiatry* 12:571532. doi: 10.3389/fpsyt.2021.571532

Japee, S., Holiday, K., Satyshur, M. D., Mukai, I., and Ungerleider, L. G. (2015). A role of right middle frontal gyrus in reorienting of attention: a case study. *Front. Syst. Neurosci.* 9:23. doi: 10.3389/fnsys.2015.00023

Jiang, B., He, D., Guo, Z., and Gao, Z. (2020). Effect-size seed-based d mapping of resting-state fMRI for persistent insomnia disorder. *Sleep Breath* 24, 653–659. doi: 10.1007/s11325-019-02001-3

Jung, S., Kim, J. H., Kang, N. O., Sung, G., Ko, Y. G., Bang, M., et al. (2021). Fusiform gyrus volume reduction associated with impaired facial expressed emotion recognition and emotional intensity recognition in patients with schizophrenia spectrum psychosis. *Psychiatry Res. Neuroimaging* 307:111226. doi: 10.1016/j.pscychresns.2020.111226

Korgaonkar, M. S., Fornito, A., Williams, L. M., and Grieve, S. M. (2014). Abnormal structural networks characterize major depressive disorder: a connectome analysis. *Biol. Psychiatry* 76, 567–574. doi: 10.1016/j.biopsych.2014.02.018

Lee, D. T., and Chung, T. K. (2007). Postnatal depression: an update. *Best Pract. Res. Clin. Obstet Gynaecol.* 21, 183–191. doi: 10.1016/j.bpobgyn.2006.10.003

Li, J., He, P., Lu, X., Guo, Y., Liu, M., Li, G., et al. (2021). A resting-state functional magnetic resonance imaging study of whole-brain functional connectivity

of voxel levels in patients with irritable bowel syndrome with depressive symptoms. *J. Neurogastr. Motil.* 27, 248–256. doi: 10.5056/jnm20209

Li, M., Liu, Y., Chen, H., Hu, G., Yu, S., Ruan, X., et al. (2019). Altered global synchronizations in patients with parkinson's disease: a resting-state fMRI study. *Front. Aging Neurosci.* 11:139. doi: 10.3389/fnagi.2019.00139

Li, X., Wu, K., Zhang, Y., Kong, L., Bertisch, H., and DeLisi, L. E. (2019). Altered topological characteristics of morphological brain network relate to language impairment in high genetic risk subjects and schizophrenia patients. *Schizophr Res.* 208, 338–343. doi: 10.1016/j.schres.2019.01.025

Nguyen, A. J., Hoyer, E., Rajhans, P., Strathearn, L., and Kim, S. (2019). A tumultuous transition to motherhood: altered brain and hormonal responses in mothers with postpartum depression. *J. Neuroendocrinol.* 31:e12794. doi: 10.1111/jne.12794

Oane, I., Barborica, A., Chetan, F., Donos, C., Maliia, M. D., Arbune, A. A., et al. (2020). Cingulate cortex function and multi-modal connectivity mapped using intracranial stimulation. *Neuroimage* 220:117059. doi: 10.1016/j.neuroimage.2020.117059

Raichle, M. E. (2015). The brain's default mode network. *Ann. Rev. Neurosci.* 38, 433–447. doi: 10.1146/annurev-neuro-071013-014030

Ren, Y., Cong, F., Ristaniemi, T., Wang, Y., Li, X., and Zhang, R. (2019). Transient seizure onset network for localization of epileptogenic zone: effective connectivity and graph theory-based analyses of ECoG data in temporal lobe epilepsy. *J. Neurol.* 266, 844–859. doi: 10.1007/s00415-019-09204-4

Rolls, E. T. (2015). Limbic systems for emotion and for memory, but no single limbic system. *Cortex* 62, 119–157. doi: 10.1016/j.cortex.2013.12.005

Rolls, E. T., Cheng, W., Du, J., Wei, D., Qiu, J., Dai, D., et al. (2020). Functional connectivity of the right inferior frontal gyrus and orbitofrontal cortex in depression. *Soc. Cogn. Affect. Neurosci.* 15, 75–86. doi: 10.1093/scan/nsaa014

Sheng, J., Shen, Y., Qin, Y., Zhang, L., Jiang, B., Li, Y., et al. (2018). Spatiotemporal, metabolic, and therapeutic characterization of altered functional connectivity in major depressive disorder. *Hum. Brain Mapp.* 39, 1957–1971. doi: 10.1002/hbm.23976

Thomas, R. M., Hotsenpiller, G., and Peterson, D. A. (2007). Acute psychosocial stress reduces cell survival in adult hippocampal neurogenesis without altering proliferation. *J. Neurosci.* 27, 2734–2743. doi: 10.1523/JNEUROSCI.3849-06.2007

Wang, L., Hu, F., Wang, W., Li, Q., Li, Y., Zhu, J., et al. (2021). Altered brain intrinsic functional hubs and connectivity associated with relapse risk in heroin dependents undergoing methadone maintenance treatment: a resting-state fMRI study. *Drug Alcohol Depend.* 219:108503. doi: 10.1016/j.drugalcdep.2020.108503

Wang, S., Zhao, Y., Zhang, L., Wang, X., Wang, X., Cheng, B., et al. (2019). Stress and the brain: perceived stress mediates the impact of the superior frontal gyrus spontaneous activity on depressive symptoms in late adolescence. *Hum. Brain Mapp.* 40, 4982–4993. doi: 10.1002/hbm.24752

Xia, M., and He, Y. (2017). Functional connectomics from a "big data" perspective. *Neuroimage* 160, 152–167. doi: 10.1016/j.neuroimage.2017.02.031

Xiao-juan, W., Jian, W., Zhi-hong, L., Yan, M., and Shi-wei, Z. (2011). Increased posterior cingulate, medial frontal and decreased temporal regional homogeneity in depressed mothers. a resting-state functional magnetic resonance study. *Proc. Environ. Sci.* 8, 737–743. doi: 10.1016/j.proenv.2011.10.112

Yan, M., Cui, X., Liu, F., Li, H., Huang, R., Tang, Y., et al. (2021). Abnormal default-mode network homogeneity in melancholic and nonmelancholic major depressive disorder at rest. *Neural Plast.* 2021:6653309. doi: 10.1155/2021/6653309

Zhang, S., Wang, W., Wang, G., Li, B., Chai, L., Guo, J., et al. (2020). Aberrant resting-state interhemispheric functional connectivity in patients with postpartum depression. *Behav. Brain Res.* 382:112483. doi: 10.1016/j.bbr.2020.112483

Conflict of Interest: The authors declare that the research was conducted in the absence of any commercial or financial relationships that could be construed as a potential conflict of interest.

frontiers | Frontiers in Neuroscience

TYPE Original Research
PUBLISHED 22 July 2022
DOI 10.3389/fnins.2022.953356

OPEN ACCESS

EDITED BY
Roberto Esposito,
ASUR Marche, Italy

REVIEWED BY
Jintao Sun,
Nanjing Brain Hospital Affiliated to Nanjing Medical University, China
Chayanin Tangwiriyasakul,
King's College London, United Kingdom

*CORRESPONDENCE
Yongxin Li
yxin-li@163.com

†These authors have contributed equally to this work

SPECIALTY SECTION
This article was submitted to Brain Imaging Methods, a section of the journal Frontiers in Neuroscience

RECEIVED 26 May 2022
ACCEPTED 24 June 2022
PUBLISHED 22 July 2022

CITATION
Li Y, Wang J, Wang X, Chen Q, Qin B and Chen J (2022) Reconfiguration of static and dynamic thalamo-cortical network functional connectivity of epileptic children with generalized tonic-clonic seizures.
Front. Neurosci. 16:953356.
doi: 10.3389/fnins.2022.953356

Reconfiguration of static and dynamic thalamo-cortical network functional connectivity of epileptic children with generalized tonic-clonic seizures

Yongxin Li[1]*†, Jianping Wang[2]†, Xiao Wang[3], Qian Chen[4], Bing Qin[3] and Jiaxu Chen[1]

[1]Guangzhou Key Laboratory of Formula-Pattern of Traditional Chinese Medicine, Formula-pattern Research Center, School of Traditional Chinese Medicine, Jinan University, Guangzhou, China, [2]The Second Affiliated Hospital of Guangzhou Medical University, Guangzhou, China, [3]Epilepsy Center and Department of Neurosurgery, The First Affiliated Hospital, Jinan University, Guangzhou, China, [4]Department of Pediatric Neurosurgery, Shenzhen Children's Hospital, Shenzhen, China

Objective: A number of studies in adults and children with generalized tonic-clonic seizure (GTCS) have reported the alterations in morphometry, functional activity, and functional connectivity (FC) in the thalamus. However, the neural mechanisms underlying the alterations in the thalamus of patients with GTCS are not well understood, particularly in children. The aim of the current study was to explore the temporal properties of functional pathways connecting thalamus in children with GTCS.

Methods: Here, we recruited 24 children with GTCS and 36 age-matched healthy controls. Static and dynamic FC approaches were used to evaluate alterations in the temporal variability of thalamo-cortical networks in children with GTCS. The dynamic effective connectivity (dEC) method was also used to evaluate the directions of the fluctuations in effective connectivity. In addition, the relationships between the dynamic properties and clinical features were assessed.

Results: The static FC analysis presented significantly decreased connectivity patterns between the bilateral thalamus and between the thalamus and right inferior temporal gyrus. The dynamic connectivity analysis found decreased FC variability in the thalamo-cortical network of children with epilepsy. Dynamic EC analyses identified increased connectivity variability from the frontal gyrus to the bilateral thalamus, and decreased connectivity variability from the right thalamus to the left thalamus and from the right thalamus to the right superior parietal lobe. In addition, correlation analysis revealed that both static FC and connectivity temporal variability in the thalamo-cortical network related to the clinical features (epilepsy duration and epilepsy onset time).

Significance: Our findings of both increased and decreased connectivity variability in the thalamo-cortical network imply a dynamic restructuring of

the functional pathways connecting the thalamus in children with GTCS. These alterations in static and temporal dynamic pathways connecting the bilateral thalamus may extend our understanding of the neural mechanisms underlying the GTCS in children.

KEYWORDS

generalized tonic-clonic seizure, epileptic children, resting-state fMRI, thalamus, temporal variability, dynamic functional connectivity, dynamic effective connectivity

Introduction

Generalized tonic-clonic seizure (GTCS) is a subgroup of idiopathic generalized epilepsy that is typically characterized by generalized spike-wave discharges (2.5-5 Hz) (Ji et al., 2014). The clinical symptoms of GTCS mainly include muscle contraction of the body and complete loss of consciousness. Patients with GTCS showed cognitive impairments in their attention, memory, and executive function (Hommet et al., 2006). One of the hallmarks of GTCS is the absence of visible abnormalities on routine magnetic resonance imaging (MRI). Based on the connectome view, the GTCS has been hypothesized as a disorder of brain connectivity (Kim et al., 2014; Li et al., 2020a; Royer et al., 2022). It has been widely accepted that generalized spike-wave discharges might be caused by the imbalance of local excitation and inhibition through thalamo-cortical network (Wang et al., 2012; Lüttjohann and van Luijtelaar, 2022). As a result, abnormal activity was detected in wide brain regions in patients with epilepsy (Assenza et al., 2020).

As we know, the thalamus is globally connected with distributed cortical regions. Previous studies have found that the thalamus is a critical hub region that is involved in the integration of information across the cortical networks (Hwang et al., 2017; Elvsåshagen et al., 2021). The thalamus plays a central role in ongoing cortical functioning, which is performed by the thalamo-cortical network. Neuroimaging studies in epilepsy have found that low volume of the thalamus is a common pattern across epilepsy syndromes (Whelan et al., 2018; Xu et al., 2021). Thalamic atrophy may be the effect of seizure activity, such as thalamo-cortical network remodeling or thalamic disconnection (Bernhardt et al., 2009; Li et al., 2017b; Chen et al., 2019). Previous studies have also detected that atrophy of the thalamic nuclei and resting-state functional hyperconnectivity between the thalamus and cerebral cortex can be considered as imaging markers in generalized patients with refractory epilepsy (Wang et al., 2018; Chen et al., 2021). Specific changes in the thalamus imply that this region plays an important role in epilepsy. A recent study has detected that abnormal functional and structural integration in the cerebellum, basal ganglia, and thalamus could result in an imbalance of inhibition and excitability in the brain system of idiopathic generalized epilepsy (Gong et al., 2021). Patients with GTCS showed a more constrained network embedding of the thalamus and an increased functional diversity of the frontocentral neocortical regions (Wang et al., 2019a). Graph theory analysis of the structural covariance network of the gray matter found that children with GTCS also showed significant alterations in the nodal betweenness in the right thalamus, bilateral temporal pole, and some regions of DMN (Li et al., 2020b). These previous neuroimaging studies have provided converging evidence for both intrinsic functional connectivity (FC) and structural connectivity abnormalities of the thalamo-cortical network in patients with GTCS (Kim et al., 2014; Lee et al., 2014; Ji et al., 2015; Li et al., 2016; Wang et al., 2019a; Gong et al., 2021). Focus on the functional and structural changes of thalamo-cortical network would provide additional information to understand the neural mechanism of GTCS.

Although these basic connectivity approaches are widely used in previous epilepsy studies and improved our understanding of GTCS, these methods may not be sufficient to fully characterize the specific role of the thalamus in patients with GTCS. How the organization of thalamo-cortical network was interfered by the seizure and the temporality and causality between the epilepsy-related regions were not fully understood. Currently, there are two directions of studies trying to solve the above concerns. One direction is based on the deep brain stimulation that aims to verify the functional role of the thalamus during the treatment process. Recent studies have confirmed the satisfactory results of thalamic nucleus deep brain stimulation in drug-resistant generalized epilepsy (Fasano et al., 2021; Vetkas et al., 2022). This approach is effective in clinical practice but is invasive. Another direction is based on the dynamic connectivity methods that aim to explore the spontaneous fluctuations in the activity and connectivity with the thalamus in epilepsy. The conventional FC analysis assumes that the communication between regions is relatively stable during the entire scan. This method may not capture the dynamic nature of communication. The human brain is a complex dynamic system (Fox et al., 2005). Recently, a dynamic FC (dFC) method was developed by measuring the variability in the strength or spatial dynamic organization of brain connectivity (Preti et al., 2017; Rolls et al., 2021).

Previous studies in neurological disorders have proved that this approach can sensitively capture the time-varying changes of the ongoing activity over the whole scan time (Liao et al., 2018; Kottaram et al., 2019; Guo et al., 2020). In epilepsy, compared to the conventional FC analysis, dynamic techniques can be used to identify additionally activated brain regions during the course of interictal epileptic discharges (Kowalczyk et al., 2020). Dynamic FC analyses have demonstrated that state transitions and modular function of dissociable hippocampal networks were altered in temporal lobe epilepsy, which can reflect different memory phenotypes (Li et al., 2022a). Disruption of this dynamic organization may be the neuroimaging expression of the cognitive dysfunction in epilepsy patients. For adults with GTCS, state-specific dFC disruptions and the majority of aberrant functional connectivity were observed in DMN (Liu et al., 2017). Recently, dFC approaches were also used to evaluate alterations in the temporal variability of FC in patients with GTCS at the region and network levels (Jia et al., 2020; Li et al., 2022c). Patients with GTCS showed a dynamic restructuring of the large-scale brain networks. Although these previous studies offered evidence for the dynamic interaction among whole-brain functional networks in adults with GTCS, no study regarding GTCS has been performed to investigate the temporal variability of FC with the thalamus and their connectivity direction in thalamo-cortical network. Investigation of brain dynamic FC network and dynamic effective connectivity (dEC) in thalamo-cortical network could allow us to understand the dynamic roles of the thalamus in the brain with GTCS.

Additionally, most of these previous studies were performed in adults with GTCS (Wang et al., 2011; Ji et al., 2014; Li et al., 2016; Liu et al., 2017; Jia et al., 2020). Children with GTCS have not received enough attention. Up to now, only a few neuroimaging studies were conducted in children with GTCS (Wang et al., 2018; Li et al., 2020a,b, 2022b). In these previous studies in children with GTCS, brain activity, gray matter volume, and the topological properties of the brain network were analyzed. The consistent results among these studies demonstrate that children with GTCS showed both functional and structural abnormalities in the thalamus and DMN. Although these previous studies indicate that the thalamus also plays an important role in children with GTCS, the dynamic exchange of information in the thalamo-cortical network remains largely unknown. Recently, the temporal variability in FC and EC has attracted increasing attention in epilepsy to understand the dynamic role of the regions in the brain system (Jia et al., 2020; Kowalczyk et al., 2020). Thus, examining the temporal properties of the thalamo-cortical network in children with GTCS would provide further information for understanding this disease.

In the present study, we aim to explore the temporal variability of the thalamo-cortical network connectivity in children with GTCS. We first used the static FC based on the bilateral thalamus to obtain the specific connectivity changes in children with GTCS. Then, we conducted dFC and dEC analysis to investigate the between-group differences in temporal variability and connectivity direction in thalamo-cortical network. Finally, the correlation between altered connectivity and clinical variables was measured in children with GTCS. On the basis of the previous studies in GTCS, we hypothesized that dynamic FC and dynamic EC of the thalamo-cortical network would be reconfigured in children with GTCS compared with the healthy controls. Variability of the connectivity in the thalamo-cortical networks should be responsible for the clinical characteristics.

Methods

Subjects

This study recruited 24 children with GTCS (9 female, mean age: 69.94 ± 46.36 months) from the Shenzhen Children's Hospital. All human procedures were approved by the Ethical Committee of the Shenzhen Children's Hospital. All participants' parents or their guardians provided written informed assent and consent. Based on their clinical and seizure semiology information, all patients were diagnosed to have genetic associated epilepsy with GTCS by two experienced neurologists (Fisher et al., 2017). The inclusion criteria for patients were as follows: (1) symmetrical tonic and clonic seizure, and loss of consciousness during seizure without any other focal features; (2) typically showed generalized spike-wave or poly-spike-wave without any other focal discharge on EEG; (3) no focal abnormality was detected in all patients on routine MRI; and (4) no other developmental disability. The exclusion criteria included the following: (1) pathologic abnormality on conventional MRI; (2) history of addition or neurological diseases besides epilepsy; (3) subjects with MRI contraindications; (4) age older than 13 years; and (5) head motion exceeding 3 mm in translation or 3° in rotation. All patients took at least one antiepileptic drug (AED: topiramate, valproic acid, levetiracetam, or oxcarbazepine) to control seizures before the image scanning. Eleven patients took one AED, 10 patients took two AEDs, and 3 patients took three AEDs. All patients were maintained seizure-free for at least 2 days prior to the MRI scanning. Thirty-six healthy controls (HCs, 11 female, mean age: 71.89 ± 31.13 months) were enrolled. All control children did not have a history of neurological disorders or psychiatric illnesses or gross abnormalities on brain MRI. In order to reduce the head movement during the MRI scanning, 18 children (9 controls and 9 patients) under the age of 4 years were sedated with 10% chloral hydrate (dosage: 50 mg/kg, the maximum dose was 1 g). The demographic and clinical information of the two groups is listed in **Table 1**.

Scan acquisition

All MRI data were acquired with a 3.0T German Siemens Trio Tim scanner (MAGNETOM, Germany, 8-channel prototype quadrature birdcage head coil) at the Shenzhen Children's Hospital, Shenzhen, China. During the imaging scanning, the head of all the participants was fixed with foam padding to minimize head movements. Earplugs were also used to reduce the impact of machine noise. All participants were lying quietly, as motionless as possible. During the imaging scanning, the participants over the age of 4 years were instructed to keep still with their eyes closed, remain awake, and instructed not to think about anything. We observed them throughout the whole scanning process, and enquired about their conditions after the test. They were asked whether they fell asleep or moved their head during the scanning process. The acquisition parameters for the resting-state fMRI data of all subjects were as follows: repetition time (TR) = 2,000 ms, echo time (TE) = 30 ms, flip angle = 90°, field of view (FOV) = 220 × 220 mm^2, 94 × 94 matrix, slice thickness = 3 mm, and 36 interleaved axial slices. A total of 130 volumes were obtained in each run. High-resolution 3D T1-weighted anatomical images were acquired for all the subjects in the sagittal orientation using a MPRAGE sequence: TR = 2,300 ms, TE = 2.26 ms, flip angle = 8°, FOV = 200 × 256 mm^2, 200 × 256 matrix, slice thickness = 1 mm, and 160 sagittal slices.

Image data preprocessing

Functional images were preprocessed using the data assistant software DPABI (Yan et al., 2016). The following steps were performed in preprocessing stage: (1) The first 10 scans were discarded to allow for magnetization equilibrium. (2) We performed slice timing and motion correction for the remaining images. The translations in each direction and the rotations in angular motions were estimated in this step. The participants with a head motion of >3 mm in maximum displacement or >3° rotation during data acquisition were excluded from the study. (4) The mean frame-wise displacement (FD) was computed by averaging the FD of each participant across the time points, which can determine the comparability of head movement across groups. No significant differences were found between the two groups (HCs: mean FD = 0.145 ± 0.113 mm, children with GTCS: mean FD = 0.131 ± 0.087 mm). (5) Individual 3D T1-weighted images were co-registered to the mean functional images by rigid body transformation after the motion correction. The transformed structural images were then segmented into gray matter, white matter, and cerebrospinal fluid by using a unified segmentation algorithm. (6) The segmented images were normalized to the Montreal Neurological Institute (MNI) space by using a 12-parameter non-linear transformation. The obtained transformation parameters were then applied to the functional images, and these functional images were normalized to the MNI space. (7) The normalized images were resampled into a voxel size of 3 mm × 3 mm × 3 mm and spatially smoothed with a half-maximum Gaussian kernel of 6 mm full width. (8) Linear regression analysis was used to control for confounding factors, including Friston-24 motion parameters, white matter signals, and cerebrospinal fluid signals. (9) Finally, band-pass temporal filtering (0.01–0.08 Hz) was used to remove the effects of very-low-frequency drift and high-frequency noise (Biswal et al., 1995; Lowe et al., 1998).

Static functional connectivity analysis

The FC maps were obtained using the voxel-wise approach by computing FC between the region of interest (ROI) and each voxel within the brain. The bilateral thalamus was used as the seed ROIs, which were obtained from the Anatomical Automatic Labeling atlas. The time series of the voxel in each ROI was extracted and averaged, followed by a correlation with the time series of each other voxel across the entire brain. The correlation value was z-transformed for each sample. The *z*-transformed FC maps were compared between the two groups by a two-sample *t*-test (AlphaSim corrected for multiple comparisons; $p < 0.005$)[1]. In this step, age and sex were regressed as confounding covariates.

Dynamic functional network connectivity

To identify the dFC variability of the thalamo-cortical network, we used a sliding window dFC approach in the Dynamic BC toolbox (Liao et al., 2014) [2]. Currently, window length is an open area of research in the sliding window-based dFC analysis. This parameter is important for capturing the rapidly shifting relationship between the windows. Here, a rectangle window with a size of 60 s (30 TRs) was selected to segment the resting-state time series by sliding across the whole scan with a step of 1 TR, resulting in 90 overlapping windows per subject. We chose the window length of 60 s because previous studies have proven that the window size of around 30-60 s could optimize the balance between the temporal resolution and the quality of the functional network connectivity estimate (Allen et al., 2014). We also tried other window lengths (20 TRs) to further examine the possible effects on dFC results. In each sliding window, we computed the temporal correlation coefficient between the truncated time course of the thalamus

1 https://afni.nimh.nih.gov/pub/dist/doc/manual/AlphaSim.pdf
2 www.restfmri.net/forum/DynamicBC

seeds and those of all the other voxels. After this step, a set of sliding window correlation maps were created for each participant. All the correlation maps were transformed by a Fisher's *r*-to-*z* transformation to improve the normality of the correlation distribution. The variance in the time series of the correlation coefficient was computed by calculating the standard deviation of *z*-values at each voxel to assess the dFC variability.

To examine the difference in dFC variability patterns between the two groups, a two-sample *t*-test analysis was performed on the standard deviation in *z*-values at each voxel. In this step, age and sex were regressed as confounding covariates. The statistical significance level for the comparison analysis was thresholded at $p < 0.005$, after AlphaSim correction.

Dynamic effective network connectivity

Seed-based dEC analysis was obtained using time-varying dynamic Granger causality. The time-varying strength and direction of the connections were calculated between the thalamus and each voxel within the brain. We used a sliding window dEC approach in the Dynamic BC toolbox. Here, a rectangle window with a size of 60 s (30 TRs) was selected to segment the resting-state time series by sliding across the whole scan with a step of 1 TR, resulting in 90 overlapping windows per subject. We also tried other window lengths (20 TRs) to further examine the possible effects on dEC results. In each sliding window, we computed the strength and direction of the connections between the truncated time course of the thalamus seeds and those of all the other voxels. After this step, two sets of sliding window correlation maps were created for each participant: one represents the input directions and the other represents the output directions. All the correlation maps were transformed by a Fisher's r-to-z transformation to improve the normality of the correlation distribution. The variance in the time series of the correlation coefficient was computed by calculating the standard deviation of *z*-values at each voxel to assess the dEC variability.

To examine the difference in dEC variability patterns between the two groups, a two-sample *t*-test analysis was performed on the standard deviation in *z*-values at each voxel. In this step, age and sex were regressed as confounding covariates. The statistical significance level for the comparison analysis was thresholded at $p < 0.005$, after AlphaSim correction.

Clinical correlation analysis

We then further explored the potential relationship between the brain static FC and clinical characteristics (epilepsy duration and epilepsy onset age) in children with GTCS. Partial correlation analyses between the connectivity variability (dFC variability and dEC variability) and clinical characteristics (epilepsy duration and epilepsy onset age) were conducted in children with GTCS after controlling for age and sex. The statistical significance level for the correlation analysis was set at $p < 0.05$.

Results

Demographic characteristics

The demographic and clinic characteristics of the children with GTCS and controls are listed in Table 1. No significant differences were found ($p > 0.05$) in age or sex distribution between the two groups. The mean epilepsy duration (32.58 ± 31.20 months) and disease onset age (37.35 ± 46.22) of the children with GTCS were also collected and listed in Table 1.

Differences in functional connectivity analysis

Compared to controls, children with GTCS showed a significant decrease in FC connecting the bilateral thalamus. The connectivity pattern of the left thalamus was centered on the right inferior temporal gyrus (ITG), right thalamus, bilateral middle temporal gyrus (MTG), right orbital inferior frontal gyrus (IFG), and right precuneus (Figure 1A). The connectivity pattern of the right thalamus was centered on the right ITG and left thalamus (Figure 1B). The details showing significant differences between the groups are listed in Table 2.

Dynamic functional connectivity variability results

Figure 2 and Table 3 illustrate the significant differences in dFC variability between the two groups for the bilateral thalamus seeds. Compared with the HCs, the patient group exhibited a significantly less dFC variability between the left

TABLE 1 Demographic and clinical information data of the subjects.

Characteristics	Patient group (Mean ± SD)	Control group (Mean ± SD)	Comparisons
Sex (female/male)	9/15	11/25	$X^2 = 0.31$ ($p = 0.58$)
Age (month)	69.94 ± 46.36	71.89 ± 31.13	$t = 0.20$ ($p = 0.85$)
Disease onset age (month)	37.35 ± 46.22	\	
Epilepsy duration (month)	32.58 ± 31.20	\	

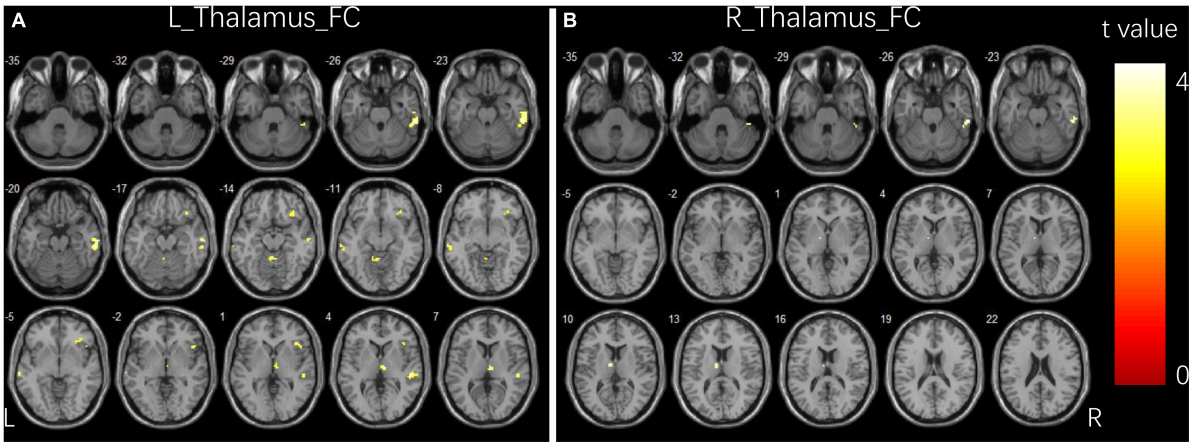

FIGURE 1
Group differences in functional connectivity for bilateral thalamus seeds between two groups. **(A)** Brain regions showing significant differences in FC for left thalamus seed. **(B)** Brain regions showing significant differences in FC for right thalamus seed. The comparison analysis was thresholded at $p < 0.005$, AlphaSim corrected. R, right hemisphere; L, left hemisphere; FC, functional connectivity.

thalamus seed and regions of bilateral IFG, right middle frontal gyrus (MFG), right angular gyrus, right inferior parietal lobule (IPL), right fusiform, right ITG, right cerebellum, left precentral gyrus, left supplementary motor area (SMA), left superior parietal lobule (SPL), left precuneus, and left paracentral gyrus (Figure 2A). Compared with the HCs, the patient group exhibited significant less dFC variability between the right thalamus seed and regions of bilateral MFG, bilateral IPL, right superior frontal gyrus (SFG), right angular gyrus, right SMA, right SPL, right fusiform, right ITG, right MTG, right cerebellum, left precuneus, and left paracentral gyrus (Figure 2B). No significant excessive dFC variability was found in the patient group with the bilateral thalamus seeds.

TABLE 2 Significant group differences in FC analysis.

Cluster location	Statistical values		Peak (MNI)		
	Cluster size	*t-value*	*x*	*y*	*z*
Seed L thalamus Control > Patient					
R inferior temporal gyrus	87	3.86	60	−33	−27
R middle temporal gyrus		3.46	66	−18	−21
R superior temporal gyrus	21	3.73	54	−27	3
L middle temporal gyrus	21	3.34	−66	−24	−6
R thalamus	23	3.28	6	−18	6
R orbital inferior frontal gyrus	25	3.25	36	30	−15
R precuneus[#]	11	3.2	6	−51	21
Seed R thalamus Control > Patient					
R inferior temporal gyrus	22	3.28	60	−33	−27
L thalamus	15	3.35	−6	−9	12

The MNI coordinates and *t*-values for the FC results. Threshold for significant clusters reported here was set at $p < 0.005$ (AlphaSim correction) and cluster size of 14.
[#]The result was uncorrected; MNI, Montreal Neurological Institute.

Dynamic effective connectivity variability results

Figure 3 and Table 4 show the significant dEC variability differences between the two groups for the bilateral thalamus seeds. Compared with the HCs, the patient group exhibited significantly excessive dEC variability from right MFG, right triangular part of IFG, and right precentral gyrus to the seed of the left thalamus (Figure 3A). Compared with the HCs, the patient group exhibited significantly excessive dEC variability from bilateral MFG and bilateral medial part of SFG to the seed of the right thalamus (Figure 3B). It is interesting that we observed a significantly low dEC variability from the seed of the right thalamus to the left thalamus and right SPL (Figure 3C).

Partial correlation analysis between connectivity properties and clinical characteristics

We then further explored the potential relationship between the connectivity properties and clinical characteristics in children with GTCS. After controlling for age and sex, partial correlation analyses showed that FC between the left thalamus and right precuneus was positively correlated with the epilepsy duration ($r = 0.553$, $p = 0.008$, Figure 4A). FC between the left thalamus and the right orbital part of IFG was positively correlated with the epilepsy duration ($r = 0.547$, $p = 0.008$, Figure 4B).

The epilepsy duration of children with GTCS was positively correlated with the dFC variability between the left thalamus and left medial IFG ($r = 0.585$, $p = 0.004$, Figure 5A). The epilepsy duration of children with GTCS was also positively

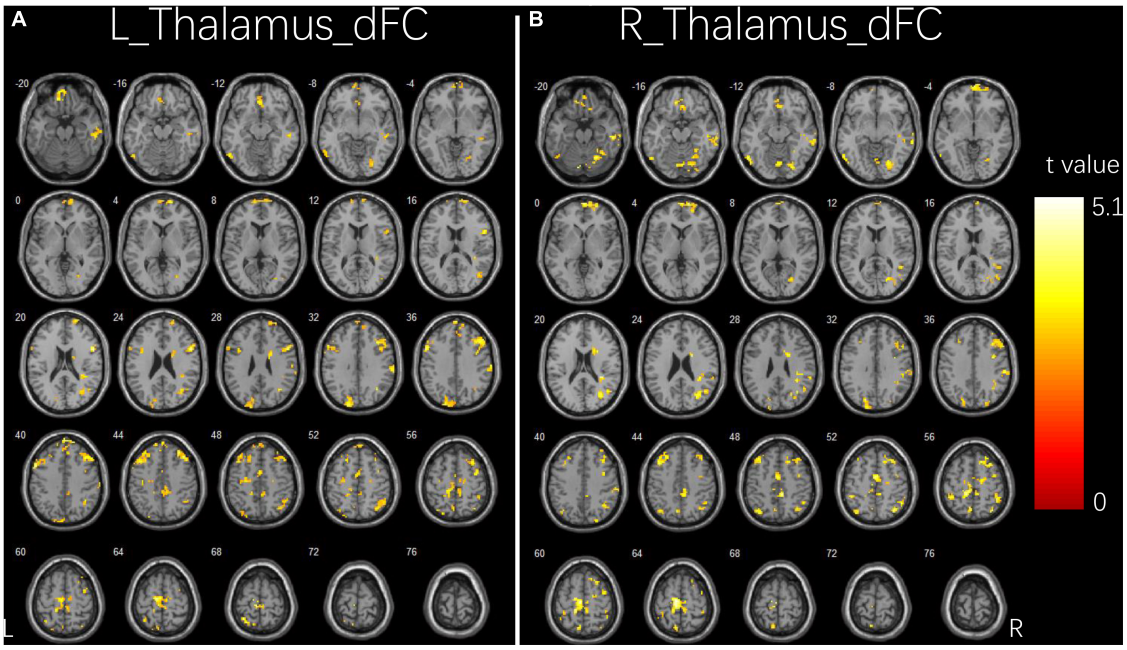

FIGURE 2
Group differences in dFC variability for bilateral thalamus seeds between two groups. **(A)** Brain regions showing significant differences in dFC variability for left thalamus seed. **(B)** Brain regions showing significant differences in dFC variability for right thalamus seed. The comparison analysis was thresholded at $p < 0.005$, AlphaSim corrected. R, right hemisphere; L, left hemisphere; dFC, dynamic functional connectivity.

correlated with the dFC variability between the left thalamus and left precuneus ($r = 0.627$, $p = 0.002$, Figure 5B). Furthermore, the age of epilepsy onset in children with GTCS was positively correlated with the dFC variability between the left thalamus and right MFG ($r = 0.436$, $p = 0.042$, Figure 5C).

Discussion

Using a seed-based connectivity approach, the current study provides a unique investigation of the static and dynamic FC of thalamo-cortical network in children with GTCS. We observed a significant decrease in static FC between bilateral thalamus and between thalamus and right inferior temporal gyrus. Dynamic FC analysis found that children with epilepsy showed decreased FC variability in the thalamo-cortical network, mostly correlated with the cortices of the frontal, motor, cerebellum, and default mode network. We also characterized the causal effect between the thalamus and the whole brain. We found increased connectivity variability from frontal gyrus to bilateral thalamus, and decreased connectivity variability from right thalamus to left thalamus and from right thalamus to right superior parietal lobe. Importantly, both static FC and connectivity temporal variability in the thalamo-cortical network showed significant correlations to the clinical features (epilepsy duration and epilepsy onset time). These alterations in static and temporal dynamic pathways connecting the bilateral thalamus exhibited the dynamic exchange of information in the thalamo-cortical network. The present findings characterize the specific role of the thalamus in children with GTCS and extend our understanding of the neural mechanism underlying the GTCS in children.

Children with generalized tonic-clonic seizure presented decreased connection between bilateral thalamus compared with the controls

Functional connectivity is suggested to describe the relationship between the neuronal activation patterns of anatomically separated brain regions. The analysis result of this method is believed to reflect functional communication between brain regions (van den Heuvel and Hulshoff Pol, 2010). Our results indicated that children with GTCS showed a significant decrease in FC between the bilateral thalamus. The neural connection between the bilateral thalamus may also be disrupted. This view is supported by the previous neuroimaging studies in epilepsy. Patients with generalized epilepsy showed a widespread functional disruption throughout the resting state (Kim et al., 2014; McGill et al., 2014). Multiple interconnected brain systems were involved in this process, resulting in functional impairments (McGill et al., 2014; Wei et al., 2015). Previous studies in patients with

TABLE 3 Significant group differences in dFC analysis.

Cluster location	Statistical values		Peak (MNI)		
	Cluster size	*t*-value	*x*	*y*	*z*
Seed L thalamus Control > Patient					
R opercular inferior frontal gyurs	270	5.1	54	12	21
R middle frontal gyrus		4.37	33	39	45
L paracentral lobe	261	4.93	−12	−15	66
L precentral gyrus	188	4.69	−54	12	39
L middle frontal gyrus		4.03	−39	21	45
L superior frontal gyrus	117	4.62	−15	54	42
R superior frontal gyrus		4	15	57	39
L superior parietal lobule	35	4.27	−24	−60	69
L orbital inferior frontal gyrus	71	4.17	−12	42	−21
L superior occipital gyrus	116	4.1	−18	−90	33
R superior frontal gyrus	155	4.04	15	69	3
L medial superior frontal gyrus		3.76	−6	63	−6
R inferior temporal gyrus	77	3.94	54	−24	−18
R middle temporal gyrus		3.54	66	−24	−18
R middle frontal gyrus	23	3.87	39	−3	57
supplementary motor area	28	3.74	0	−6	54
L superior parietal lobule	27	3.71	−33	−69	54
R angular	137	3.69	36	−66	51
R inferior parietal lobule		3.48	39	−51	39
R supramarginal gyrus	34	3.57	63	−24	33
L precuneus	28	3.48	−3	−66	54
R fusiform	35	3.44	27	−81	−9
Seed R thalamus Control > Patient					
L paracentral lobule	249	5.04	−12	−15	66
R supplementary motor area	78	4.44	9	−9	54
R superior frontal gyrus	119	4.42	15	69	3
R superior parietal gyrus	213	4.29	36	−66	54
R inferior parietal lobule		4.15	48	−54	51
R middle temporal gyrus	89	4.27	69	−36	−9
L cerebellum	39	4.2	−9	−81	−21
R middle frontal gyrus	172	4.14	30	18	57
R superior frontal gyrus		4.04	15	24	54
L middle frontal gyrus	81	4.11	−36	30	48
R cerebellum	156	4.11	24	−63	−21
R fusiform		3.8	24	−72	−9
L inferior temporal gyrus	42	4.07	−57	−63	−12
L cuneus	44	3.99	−18	−78	33
R middle occipital gyrus	87	3.92	33	−69	21
R middle frontal gyrus	35	3.86	39	3	36
R precentral gyrus		2.95	39	−3	48
L precuneus	48	3.8	−9	−66	69

The MNI coordinates and *t*-values for the FC results. Threshold for significant clusters reported here was set at $p < 0.005$ (AlphaSim correction) and cluster size of 14.
MNI, Montreal Neurological Institute.

GTCS found aberrant interhemispheric functional connectivity (Wang et al., 2011; Ji et al., 2014; Li et al., 2022c). In line with these findings, we observed decreased FC between the bilateral thalamus, which may indicate functional disruption between the two hemispheres. This result can reflect brain network reorganization under frequent abnormal discharges in children with GTCS.

Our study also extended results from static FC analysis to a more subtle time scale. Using the dynamic Granger causality method, we identified the flow direction and magnitude of the connection between the bilateral thalamus. This method can characterize the positive causality and negative causality between the brain regions. Given that epilepsy is a neurological disease caused by an imbalance between excitation and inhibition in the central nervous system (Goodman and Szaflarski, 2021), the causality results based on the Granger causality method may represent inhibitory and excitatory effects in physiology, which can further provide a special advantage for investigating the neural mechanism of epilepsy. Previous studies have used the Granger causality method to investigate the causal effect in epilepsy (Ji et al., 2013; Wu et al., 2015). Compared with the controls, children with GTCS showed a significant decrease in the temporal variability of the connectivity from the right thalamus to the left thalamus. The abnormal causal effect between the bilateral thalamus is unidirectional. This result is consistent with our previous studies that children with GTCS showed significant changes in spontaneous activity and gray matter volume in the right thalamus (Wang et al., 2018; Li et al., 2020b). These previous studies also found that significant correlations between the neuroimaging index and the epilepsy duration were detected in the right thalamus but not in the left thalamus. Combined with these previous studies and our present results, decreased dEC variability from the right thalamus to the left thalamus reflects the chronic damaging effect of GTCS in children. The chronic variability changes and the decreased FC between the bilateral thalamus are associated with the dysfunction of thalamo-cortical circuits in epilepsy. The specific role of the right thalamus in children with GTCS needs to be paid more attention in future studies.

Children with generalized tonic-clonic seizure presented significant alterations in thalamo-cortical networks compared with the controls

As we know, the human brain is a complex, interconnected system with an optimal balance between functional specialization and integration. In addition, the thalamus is a cortical hub region that could integrate diverse information that is being processed throughout the cerebral cortex

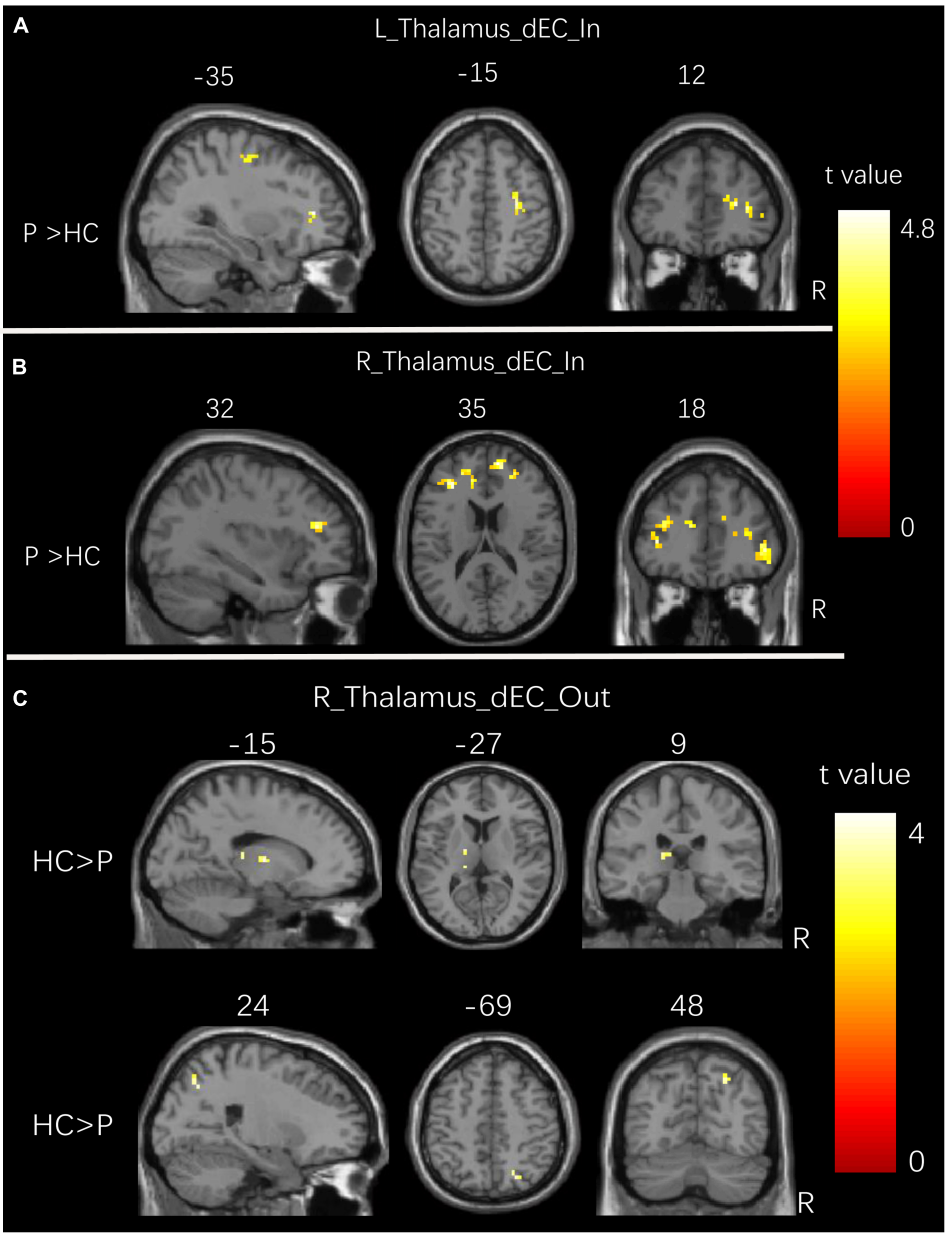

FIGURE 3
Group differences in dEC variability for bilateral thalamus seeds between two groups. **(A)** Brain regions showing significant differences in dEC variability from the whole brain to the seed of the left thalamus. **(B)** Brain regions showing significant differences in dEC variability from the whole brain to the seed of the right thalamus. **(C)** Brain regions showing significant differences in dEC variability from the seed of the right thalamus to the whole brain. The comparison analysis was thresholded at $p < 0.005$, AlphaSim corrected. R, right hemisphere; L, left hemisphere. dEC, dynamic effective connectivity; HC, healthy controls; P, patients with generalized tonic-clonic seizures.

(Hwang et al., 2017). There is no doubt regarding the participation of the thalamus in generalized epilepsy (Lüttjohann and van Luijtelaar, 2022). Based on this prior view, we selected the bilateral thalamus as a seed to build the functional network in children with GTCS. Static and dynamic functional connectivity methods were combined in the present study. One main finding of our present study is the detection of significant alteration in the static and dynamic connections of thalamo-cortical networks in children with GTCS. As expected, decreased static FC between the thalamus and cortex (frontal and temporal cortex) was observed. This result was consistent with a previous study that showed a decreased correlation in thalamo-temporopolar connection (Bernhardt et al., 2009; Gong et al., 2021). A recent review study showed that there were overlapping findings in patients with GTCS regarding deactivation in the middle/inferior temporal

gyrus (Parsons et al., 2020). Decreased thalamo-cortical connectivity was also detected between the left thalamus and right frontal pole in patients with idiopathic generalized epilepsy (Chen et al., 2021). Decreased FC between the thalamus and cognitive-related cortex in children with GTCS may render these networks less capacity to function and communicate efficiently. In clinical settings, the phenomenon of cognitive impairment in children with GTCS can be explained by these disrupted connections.

The right precuneus belongs to the DMN and is regarded as a pivotal node of the human brain network. Adults with GTCS showed a disrupted FC related to DMN (Wang et al., 2011; Kim et al., 2014). Graph theory studies showed that patients with GTCS had aberrant core hub role of regions, including precuneus and orbital frontal cortex (Li et al., 2016; Li et al., 2020b). The present study showed a significant decrease in FC between the thalamus and precuneus, which was consistent with these previous studies. The reduced FC between regions in resting-state networks may be a result of seizures in children with GTCS. Extensive FC changes in children with GTCS again verify the previous study results that seizure signal in generalized epilepsy transmit through the regions of thalamus and the bilaterally distributed brain network (Berg et al., 2010). Thus, the decreased FC between the thalamus and cortex (inferior/middle temporal gyrus, orbital IFG, and precuneus) in the present study may result from disruptions in neural connections and reflects the functional impairments of the thalamo-cortical network associated with GTCS in children.

In addition, it is worth noting that significantly different connections were found in dFC between the two groups. The decreased FC temporal variability connecting the thalamus in patients was found not only in the inferior/middle temporal gyrus, IFG, and precuneus, but also in SMA, angular gyrus, IPL, SPL, paracentral gyrus, and cerebellum. We can see that most of these regions belong to the DMN, attention, and motor network. The DMN is considered as a key network in integrating information from cognition networks (Raichle et al., 2001). Decreased static FC and dFC between the thalamus and the regions of DMN may be associated with impaired consciousness in GTCS. In addition, previous studies have detected both increased and decreased connections between the DMN and cognitive control network, which implied that deficits in self-process are correlated with cognitive function impairment in patients with generalized epilepsy (Li et al., 2017a). Despite the clear reductions in FC and significant deactivation within DMN, significantly decreased connections between DMN and sensorimotor network were observed in adults with GTCS (Liu et al., 2017; Li et al., 2022b). The findings of these previous studies implied that functional abnormality of these interconnections may influence information communication and impair functional integrations. In the present study, significant changes in the temporal variability between the thalamus and cortical regions were also detected. This result may imply that the interconnections of the brain network are disrupted in children with GTCS. As a result, the function and information communication efficiency in the thalamo-cortical network was affected, leading to cognitive impairment in patients with epilepsy.

However, the dFC results of the present study are not entirely consistent with one previous study in adults with GTCS using a similar method (Jia et al., 2020). In this previous study, significantly increased temporal variability of FC was observed both at the region level and at the between-network level. No significant changes in the dFC results were detected based on the thalamus at the region level or network level in this previous study. In the present study, we used a seed-based approach in children with GTCS to analyze the dFC and dEC of the thalamus. A significantly decreased temporal variability of FC in the thalamo-cortical network was detected in children with GTCS. Although no significantly increased temporal variability of FC was detected by the dFC method, both increased and decreased temporal variability of causal connectivity was detected by the dEC method. The temporal variability of causal connectivity from the frontal cortex to thalamus showed a significant increase in children with GTCS. Moreover, the temporal variability of causal connectivity from the right thalamus to the right SPL showed a significant decrease in children with GTCS. One explanation for the inconsistent results may be that the research subjects were different: the

TABLE 4 Significant group differences in dEC analysis.

Cluster location	Statistical values		Peak (MNI)		
	Cluster size	*t*-value	*x*	*y*	*z*
Seed L thalamus_in Patient > Control					
R middle frontal gyrus	21	4.43	27	45	12
R inferior frontal gyrus	25	4.35	45	39	3
R precentral gyrus	34	3.94	30	−15	51
Seed R thalamus_in Patient > Control					
R medial superior frontal gryus	41	4.8	12	54	18
L medial superior frontal gryus	30	3.9	−12	39	18
L middle frontal gyrus		3.85	−21	45	18
R middle frontal gyrus	42	3.68	27	45	18
L middle frontal gyrus	69	4.51	−30	36	18
L inferior frontal gyrus		4.51	−39	39	6
Seed R thalamus_out Control > Patient					
L thalamus	14	3.84	−15	−9	6
R superior parietal lobule	16	3.49	24	−69	48
L thalamus [#]	8	3.23	−15	−27	9

The MNI coordinates and *t*-values for the FC results. Threshold for significant clusters reported here was set at $p < 0.005$ (AlphaSim correction) and cluster size of 14.
[#]The result was uncorrected; MNI, Montreal Neurological Institute.

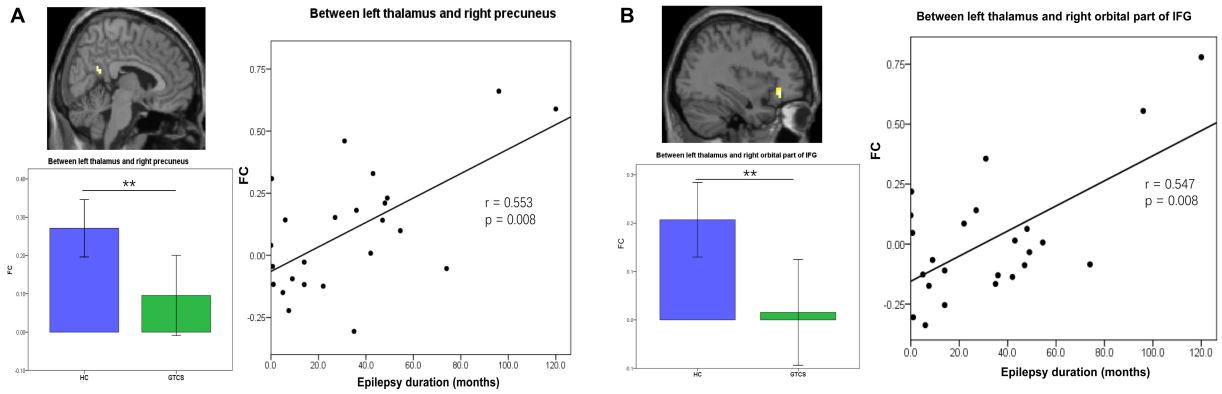

FIGURE 4
Partial correlation between static FC and the epilepsy duration in children with GTCS. **(A)** The FC values between the left thalamus and right precuneus showed a significant correlation with the epilepsy duration (r = 0.553, p = 0.008). **(B)** The FC values between the left thalamus and right orbital part of IFG showed a significant correlation with the epilepsy duration (r = 0.547, p = 0.008). FC, functional connectivity; IFG, inferior frontal gyrus.

subjects of Jia et al. (2020) comprise adults with GTCS, while the subjects of the present study are children with GTCS. Previous studies have found that adults and children with GTCS showed a different brain organization (Li et al., 2016; Wang et al., 2018; Li et al., 2020a,b). A recent study considering the role of thalamo-cortical interaction has shown that the normal aging process can affect the interconnections between the thalamus and other brain networks (Das et al., 2021). The connection strength and direction of the thalamo-cortical networks were different between the young and old groups. The difference in the view of brain organization could also be approved by a previous study that investigated the normal development of brain white matter between healthy children and adults (Oyefiade et al., 2018). In this previous study, the participants showed significant age-related differences in diffusion index across the frontal, parietal, and temporal lobes. These age-related changes reflect continued myelination and axonal organization of short-range white matter with increasing age. Thus, the age factor may affect the connection architecture. Children with GTCS showed specific changes in the temporal properties of the thalamo-cortical network. Another explanation for this inconsistency may be the combined effect of brain development and AED in children with GTCS. Once a child has been diagnosed, AED treatment is the first choice in most cases. Then, the influence of AED on the brain is initiated. The generalized spike-wave discharge burden is moderated by AED, and the effect of the disease on normal brain development is suppressed. The combined effects of these factors resulted in this inconsistency between the children and adults with GTCS. Future studies should include both children and adults with GTCS simultaneously to verify the above explanation.

Besides, both increased and decreased temporal variabilities of causal connectivity in children with GTCS were considered to be of great interest and importance. The compensatory mechanism can explain this result. We know that the MFG and SPL belong to the central executive network (Uddin et al., 2019). A previous study in normal individuals has detected that the thalamus acts as a causal outflow hub (Das et al., 2021). The frontal cortex and superior parietal cortex were driven by the thalamus in normal individuals. In the present study, we detected increased temporal variability of connectivity from MFG to the thalamus. The increased temporal variability of connectivity implicated hyper-integration of information in the thalamus and over-interaction between the thalamus and frontal gyrus. The original balance between inhibition and excitation information through the thalamus was broken. In order to maintain the balance in the transmission of information through the thalamus, temporal variability of connectivity from the right thalamus to the right SPL was suppressed. Consistent with a previous study in idiopathic generalized epilepsy, a decreased FC between the thalamus and SPL was observed (Gong et al., 2021). Increased inhibition of this pathway may help to produce a new balance. This dynamic balance between the thalamus and regions of the central executive network can also help to maintain the critical integrative hub of thalamus. The abnormal connectivity temporal variability of thalamo-cortical network might be associated with cognitive dysfunction in children with GTCS.

Clinical relevance of the connectivity properties in thalamus

Moreover, we observed that static FC values and dynamic FC temporal properties were significantly correlated with epilepsy duration. As shown in **Figures 4**, **5**, epilepsy duration positively correlated with the connectivity properties of the left thalamus. Correlation analysis between the neuroimaging index

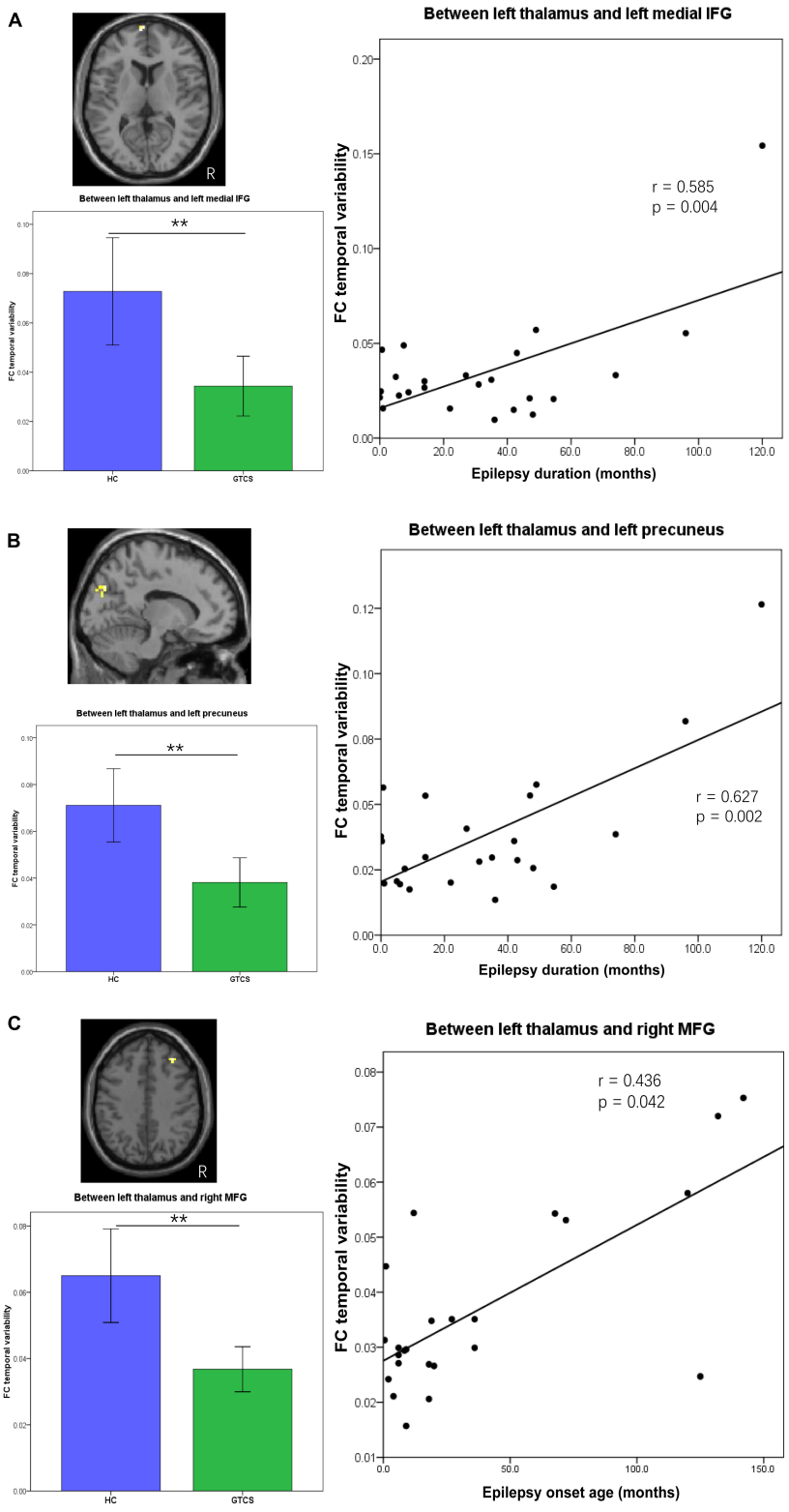

FIGURE 5
Partial correlation between connectivity temporal variability and clinical characteristics (epilepsy duration or epilepsy onset age) in children with GTCS. **(A)** The dFC temporal variability between left thalamus and left medial IFG showed significant correlation with the epilepsy duration (r = 0.585, p = 0.004). **(B)** The dFC temporal variability between left thalamus and left precuneus showed significant correlation with the epilepsy duration (r = 0.627, p = 0.002). **(C)** The dFC temporal variability between left thalamus and right MFG showed significant correlation with the epilepsy onset age (r = 0.436, p = 0.042). dFC, dynamic functional connectivity; IFG, inferior frontal gyrus; MFG, medial frontal gyrus.

and disease duration is the most popularly used method in epilepsy. Previous studies have found that disease duration was positively correlated with resting-state network abnormalities in idiopathic generalized epilepsy (Luo et al., 2012; Parsons et al., 2020; Gong et al., 2021). That is, the longer the patient had the condition, the more abnormal connections between brain regions were detected. Epilepsy duration presented negative effects on the brain connectivity in patients with generalized epilepsy (Li et al., 2016; Wang et al., 2019b; Jia et al., 2020; Xu et al., 2021). In this study, we demonstrated decreased static FC and dFC between the thalamus and brain cortex (IFG and precuneus). In the children with long epilepsy duration, their thalamo-cortical network (thalamus-IFG and thalamus-precuneus) showed a high FC or high temporal variability. That means the longer the children had the condition, the more functional connections between the thalamus and cortex regions were enhanced. This correlation result in the present study may be inconsistent with the results reported by the above previous studies. The reason for this inconsistency might be that the patient's screening criteria were different. In the present study, all patients were diagnosed with GTCS, and the subjects with focal epilepsy generalizing secondary GTCS were excluded. Previous studies have found that these two groups of patients with GTCS demonstrated different relationships between the thalamo-cortical network connection and the epilepsy duration (Xu et al., 2021; Hsieh et al., 2022). FC between the somatosensory cortex and thalamus was negatively correlated with the epilepsy duration of focal epilepsy patients with bilateral tonic-clonic seizure, while it was positively correlated with the epilepsy duration in genetic generalized epilepsy patients (Hsieh et al., 2022). Our correlation results were consistent with this previous study. The positive correlations in the present study suggest that in the patients with the longer conditions, the alteration of connectivity between the thalamus and cortex may further serve to affect synchrony. Another reason for this inconsistency may be that the subjects of the present study were children. The combined effects of brain development and AED would help the children with GTCS to control seizures. The depressed pathways or decreased temporal variability of connections were enhanced by the effective drug treatment and normal brain development.

The relationship between the epilepsy onset age and functional properties was also calculated, as the epilepsy onset age is another factor that is known to affect the brain connectivity in epilepsy (Doucet et al., 2015). For children with GTCS, the epilepsy onset age showed a positive correlation with the dFC variability between the left thalamus and right MFG. The relationship direction is consistent with a previous study that the FC between the insular and thalamic projections was significantly correlated with the onset of illness (Gong et al., 2021). The relationship in this previous study showed that the later the onset, the lower the abnormal FC changes. A recent study also showed that the interhemispheric connectivity values within the DMN were positively correlated with the onset age of the children with GTCS (Li et al., 2022c). The brain of children with long period for normal developing would have great tolerate to the disease effect. In the present study, the dFC variability between the left thalamus and right MFG was decreased significantly. A significant correlation may imply that the children with later onset of illness would show a less decrease in the temporal variability between the left thalamus and right MFG. However, this observation needs further verification in the future.

Limitations

Several limitations in this work should be noted, which lay the groundwork for additional important future studies. First, although information about antiepileptic medications was collected, the long-term treatment effects could not be obtained for some patients. The contact information was no longer valid. Hence, we could not combine the actual treatment effects to verify our results. Second, the sample size was relatively small, and the scanning time was short. In the future, a larger number of subjects should be recruited. In addition, more communication work with the subjects should be executed to increase the scanning time and the imaging quality.

Conclusion

In this work, we used a combination of static and dynamic functional analyses to explore the functional properties of the thalamo-cortical network in children with GTCS. Importantly, we have shown that static FC strength and FC variability in the thalamo-cortical circuitry were decreased significantly in children with GTCS. Both increased and decreased temporal variability of causal connectivity in the thalamo-cortical circuitry was also detected in children with GTCS. In addition, the functional properties of some functional pathways showed a significant correlation with the clinical characteristics. Both increased and decreased connectivity variability in the thalamo-cortical circuitry implies a dynamic restructuring of the thalamo-cortical networks in children with GTCS. These alterations in static and temporal dynamic pathways connecting the thalamus may extend our understanding of the neural mechanism underlying the GTCS in children.

Data availability statement

The original contributions presented in the study are included in the article/supplementary material. Further inquiries can be directed to the corresponding author.

Ethics statement

The studies involving human participants were reviewed and approved by the Ethical Committee of the Shenzhen Children's Hospital. Written informed consent to participate in this study was provided by the participants' legal guardian/next of kin.

Author contributions

YL and QC conceived and designed the experiments. QC performed the experiments. YL and XW analyzed the image data and sorted the results. QC, BQ, and JC were responsible for patient management and conceptualized the study. YL and JW wrote and reviewed the manuscript. All authors contributed to the article and approved the submitted version.

Funding

This study was supported by the National Natural Science Foundation of China (No. 81601483) and the Medical Science and Technology Research Foundation of Guangdong Province (A2021076). This work was also supported by the Administration of Traditional Chinese Medicine of Guangdong Province (20221099), the Key-Ares Research and Development Program of Guangdong Province (No. 2020B1111100001), Guangzhou Key Laboratory of Formula-Pattern of Traditional Chinese Medicine (No. 202102010014), and China Scholarship Council (No. 201906785005). This work was also supported by the Guang Zhou Science and Technology Project (202201011812).

Acknowledgments

We thank all participants in the present study for their cooperation. We would also like to thank the radiographers at the Department of Pediatric Radiology of Shenzhen Children's Hospital for their support during the imaging data collection.

Conflict of interest

The authors declare that the research was conducted in the absence of any commercial or financial relationships that could be construed as a potential conflict of interest.

Publisher's note

References

Allen, E. A., Damaraju, E., Plis, S. M., Erhardt, E. B., Eichele, T., and Calhoun, V. D. (2014). Tracking whole-brain connectivity dynamics in the resting state. *Cereb. cortex* 24, 663–676. doi: 10.1093/cercor/bhs352

Assenza, G., Lanzone, J., Dubbioso, R., Coppola, A., Boscarino, M., Ricci, L., et al. (2020). Thalamic and cortical hyperexcitability in juvenile myoclonic epilepsy. *Clin. Neurophys.* 131, 2041–2046. doi: 10.1016/j.clinph.2020.04.164

Berg, A. T., Berkovic, S. F., Brodie, M. J., Buchhalter, J., Cross, J. H., Van Emde Boas, W., et al. (2010). Revised terminology and concepts for organization of seizures and epilepsies: report of the ILAE commission on classification and terminology, 2005–2009. *Epilepsia* 51, 676–685. doi: 10.1111/j.1528-1167.2010.02522.x

Bernhardt, B. C., Rozen, D. A., Worsley, K. J., Evans, A. C., Bernasconi, N., and Bernasconi, A. (2009). Thalamo–cortical network pathology in idiopathic generalized epilepsy: insights from MRI-based morphometric correlation analysis. *NeuroImage* 46, 373–381. doi: 10.1016/j.neuroimage.2009.01.055

Biswal, B., Zerrin Yetkin, F., Haughton, V. M., and Hyde, J. S. (1995). Functional connectivity in the motor cortex of resting human brain using echo-planar MRI. *Magn. Reson. Med.* 34, 537–541. doi: 10.1002/mrm.1910340409

Chen, C., Li, H., Ding, F., Yang, L., Huang, P., Wang, S., et al. (2019). Alterations in the hippocampal-thalamic pathway underlying secondarily generalized tonic–clonic seizures in mesial temporal lobe epilepsy: a diffusion tensor imaging study. *Epilepsia* 60, 121–130. doi: 10.1111/epi.14614

Chen, Y., Fallon, N., Kreilkamp, B. A. K., Denby, C., Bracewell, M., Das, K., et al. (2021). Probabilistic mapping of thalamic nuclei and thalamocortical functional connectivity in idiopathic generalised epilepsy. *Hum. Brain Mapp.* 42, 5648–5664. doi: 10.1002/hbm.25644

Das, M., Singh, V., Uddin, L. Q., Banerjee, A., and Roy, D. (2021). Reconfiguration of Directed Functional Connectivity Among Neurocognitive Networks with Aging: Considering the Role of Thalamo-Cortical Interactions. *Cereb. cortex* 31, 1970–1986. doi: 10.1093/cercor/bhaa334

Doucet, G. E., Sharan, A., Pustina, D., Skidmore, C., Sperling, M. R., and Tracy, J. I. (2015). Early and late age of seizure onset have a differential impact on brain resting-state organization in temporal lobe epilepsy. *Brain Topogr.* 28, 113–126. doi: 10.1007/s10548-014-0366-6

Elvsåshagen, T., Shadrin, A., Frei, O., van der Meer, D., Bahrami, S., Kumar, V. J., et al. (2021). The genetic architecture of the human thalamus and its overlap with ten common brain disorders. *Nat. Commun.* 12:2909. doi: 10.1038/s41467-021-23175-z

Fasano, A., Eliashiv, D., Herman, S. T., Lundstrom, B. N., Polnerow, D., Henderson, J. M., et al. (2021). Experience and consensus on stimulation of the anterior nucleus of thalamus for epilepsy. *Epilepsia* 62, 2883–2898. doi: 10.1111/epi.17094

Fisher, R. S., Cross, J. H., D'Souza, C., French, J. A., Haut, S. R., Higurashi, N., et al. (2017). Instruction manual for the ILAE 2017 operational classification of seizure types. *Epilepsia* 58, 531–542. doi: 10.1111/epi.13671

Fox, M. D., Snyder, A. Z., Vincent, J. L., Corbetta, M., Van Essen, D. C., and Raichle, M. E. (2005). The human brain is intrinsically organized into dynamic,

anticorrelated functional networks. *Proc. Natl. Acad. Sci. U.S.A.* 102, 9673–9678. doi: 10.1073/pnas.0504136102

Gong, J., Jiang, S., Li, Z., Pei, H., Li, Q., Yao, D., et al. (2021). Distinct effects of the basal ganglia and cerebellum on the thalamocortical pathway in idiopathic generalized epilepsy. *Hum. Brain Mapp.* 42, 3440–3449. doi: 10.1002/hbm.25444

Goodman, A. M., and Szaflarski, J. P. (2021). Recent advances in neuroimaging of epilepsy. *Neurotherapeutics* 18, 811–826. doi: 10.1007/s13311-021-01049-y

Guo, X., Duan, X., Chen, H., He, C., Xiao, J., Han, S., et al. (2020). Altered inter- and intrahemispheric functional connectivity dynamics in autistic children. *Hum. Brain Mapp.* 41, 419–428. doi: 10.1002/hbm.24812

Hommet, C., Sauerwein, H. C., De Toffol, B., and Lassonde, M. (2006). Idiopathic epileptic syndromes and cognition. *Neurosci. Biobehav. Rev.* 30, 85–96. doi: 10.1016/j.neubiorev.2005.06.004

Hsieh, H., Xu, Q., Yang, F., Zhang, Q., Hao, J., Liu, G., et al. (2022). Distinct functional cortico-striato-thalamo-cerebellar networks in genetic generalized and focal epilepsies with generalized tonic-clonic seizures. *J. Clin. Med.* 11:1612. doi: 10.3390/jcm11061612

Hwang, K., Bertolero, M. A., Liu, W. B., and D'Esposito, M. (2017). The human thalamus is an integrative hub for functional brain networks. *J. Neurosci.* 37, 5594–5607. doi: 10.1523/JNEUROSCI.0067-17.2017

Ji, G. J., Zhang, Z., Xu, Q., Wang, Z., Wang, J., Jiao, Q., et al. (2015). Identifying Corticothalamic Network Epicenters in Patients with Idiopathic Generalized Epilepsy. *AJNR Am. J. Neuroradiol.* 36, 1494–1500. doi: 10.3174/ajnr.A4308

Ji, G.-J., Zhang, Z., Xu, Q., Zang, Y.-F., Liao, W., and Lu, G. (2014). Generalized tonic-clonic seizures: aberrant interhemispheric functional and anatomical connectivity. *Radiology* 271, 839–847. doi: 10.1148/radiol.13131638

Ji, G. J., Zhang, Z. Q., Zhang, H., Wang, J., Liu, D. Q., Zang, Y. F., et al. (2013). Disrupted causal connectivity in mesial temporal lobe epilepsy. *PLos One* 8:10. doi: 10.1371/journal.pone.0063183

Jia, X., Xie, Y., Dong, D., Pei, H., Jiang, S., Ma, S., et al. (2020). Reconfiguration of dynamic large-scale brain network functional connectivity in generalized tonic-clonic seizures. *Hum. Brain Mapp.* 41, 67–79. doi: 10.1002/hbm.24787

Kim, J. B., Suh, S.i, Seo, W. K., Oh, K., Koh, S. B., and Kim, J. H. (2014). Altered thalamocortical functional connectivity in idiopathic generalized epilepsy. *Epilepsia* 55, 592–600. doi: 10.1111/epi.12580

Kottaram, A., Johnston, L. A., Cocchi, L., Ganella, E. P., Everall, I., Pantelis, C., et al. (2019). Brain network dynamics in schizophrenia: Reduced dynamism of the default mode network. *Hum. Brain Mapp.* 40, 2212–2228. doi: 10.1002/hbm.24519

Kowalczyk, M. A., Omidvarnia, A., Dhollander, T., and Jackson, G. D. (2020). Dynamic analysis of fMRI activation during epileptic spikes can help identify the seizure origin. *Epilepsia* 61, 2558–2571. doi: 10.1111/epi.16695

Lee, C. Y., Tabesh, A., Spampinato, M. V., Helpern, J. A., Jensen, J. H., and Bonilha, L. (2014). Diffusional kurtosis imaging reveals a distinctive pattern of microstructural alternations in idiopathic generalized epilepsy. *Acta Neurol. Scand.* 130, 148–155. doi: 10.1111/ane.12257

Li, Y., Qin, B., Chen, Q., and Chen, J. (2022c). impaired functional homotopy and topological properties within the default mode network of children with generalized tonic-clonic seizures: a resting-state fMRI study. *Front. Neurosci.* 16:833837. doi: 10.3389/fnins.2022.833837

Li, H., Ding, F., Chen, C., Huang, P., Xu, J., Chen, Z., et al. (2022a). Dynamic functional connectivity in modular organization of the hippocampal network marks memory phenotypes in temporal lobe epilepsy. *Hum. Brain Mapp.* 43, 1917–1929. doi: 10.1002/hbm.25763

Li, Y., Qin, B., Chen, Q., and Chen, J. (2022b). Altered dynamic functional network connectivity within default mode network of epileptic children with generalized tonic-clonic seizures. *Epilepsy Res.* 184:106969. doi: 10.1016/j.eplepsyres.2022.106969

Li, R., Liao, W., Li, Y., Yu, Y., Zhang, Z., Lu, G., et al. (2016). Disrupted structural and functional rich club organization of the brain connectome in patients with generalized tonic-clonic seizure. *Hum. Brain Mapp.* 37, 4487–4499.

Li, Y., Tan, Z., Wang, J., Wang, Y., Gan, Y., Wen, F., et al. (2017b). Alterations in spontaneous brain activity and functional network reorganization following surgery in children with medically refractory epilepsy: a resting-state functional magnetic resonance imaging study. *Front. Neurol.* 8:374. doi: 10.3389/fneur.2017.00374

Li, R., Yu, Y., Liao, W., Zhang, Z., Lu, G., and Chen, H. (2017a). Disrupted architecture of large-scale brain functional connectivity networks in patients with generalized tonic–clonic seizure. *Appl. Inf.* 4:15.

Li, Y., Chen, Q., and Huang, W. (2020a). Disrupted topological properties of functional networks in epileptic children with generalized tonic-clonic seizures. *Brain Behav.* 10:e01890. doi: 10.1002/brb3.1890

Li, Y., Wang, Y., Wang, Y., Wang, H., Li, D., Chen, Q., et al. (2020b). Impaired topological properties of gray matter structural covariance network in epilepsy children with generalized tonic-clonic seizures: a graph theoretical analysis. *Front. Neurol.* 11:253. doi: 10.3389/fneur.2020.00253

Liao, W., Li, J., Duan, X., Cui, Q., Chen, H., and Chen, H. (2018). Static and dynamic connectomics differentiate between depressed patients with and without suicidal ideation. *Hum. Brain Mapp.* 39, 4105–4118. doi: 10.1002/hbm.24235

Liao, W., Wu, G. R., Xu, Q., Ji, G. J., Zhang, Z., Zang, Y. F., et al. (2014). DynamicBC: a MATLAB toolbox for dynamic brain connectome analysis. *Brain Connect* 4, 780–790. doi: 10.1089/brain.2014.0253

Liu, F., Wang, Y., Li, M., Wang, W., Li, R., Zhang, Z., et al. (2017). Dynamic functional network connectivity in idiopathic generalized epilepsy with generalized tonic–clonic seizure. *Hum. Brain Mapp.* 38, 957–973. doi: 10.1002/hbm.23430

Lowe, M., Mock, B., and Sorenson, J. (1998). Functional connectivity in single and multislice echoplanar imaging using resting-state fluctuations. *NeuroImage* 7, 119–132. doi: 10.1006/nimg.1997.0315

Luo, C., Li, Q., Xia, Y., Lei, X., Xue, K., Yao, Z., et al. (2012). Resting state basal ganglia network in idiopathic generalized epilepsy. *Hum. Brain Mapp.* 33, 1279–1294. doi: 10.1002/hbm.21286

Lüttjohann, A., and van Luijtelaar, G. (2022). The role of thalamic nuclei in genetic generalized epilepsies. *Epilepsy Res.* 182:106918. doi: 10.1016/j.eplepsyres.2022.106918

McGill, M. L., Devinsky, O., Wang, X., Quinn, B. T., Pardoe, H., Carlson, C., et al. (2014). Functional neuroimaging abnormalities in idiopathic generalized epilepsy. *NeuroImage Clin.* 6, 455–462. doi: 10.1016/j.nicl.2014.10.008

Oyefiade, A. A., Ameis, S., Lerch, J. P., Rockel, C., Szulc, K. U., Scantlebury, N., et al. (2018). Development of short-range white matter in healthy children and adolescents. *Hum. Brain Mapp.* 39, 204–217. doi: 10.1002/hbm.23836

Parsons, N., Bowden, S. C., Vogrin, S., and D'Souza, W. J. (2020). Default mode network dysfunction in idiopathic generalised epilepsy. *Epilepsy Res.* 159:106254. doi: 10.1016/j.eplepsyres.2019.106254

Preti, M. G., Bolton, T. A. W., and Van De Ville, D. (2017). The dynamic functional connectome: State-of-the-art and perspectives. *NeuroImage* 160, 41–54. doi: 10.1016/j.neuroimage.2016.12.061

Raichle, M. E., MacLeod, A. M., Snyder, A. Z., Powers, W. J., Gusnard, D. A., and Shulman, G. L. (2001). A default mode of brain function. *Proc. Natl. Acad. Sci. U.S.A.* 98, 676–682. doi: 10.1073/pnas.98.2.676

Rolls, E. T., Cheng, W., and Feng, J. (2021). Brain dynamics: synchronous peaks, functional connectivity, and its temporal variability. *Hum. Brain Mapp.* 42, 2790–2801. doi: 10.1002/hbm.25404

Royer, J., Bernhardt, B. C., Larivière, S., Gleichgerrcht, E., Vorderwülbecke, B. J., Vulliémoz, S., et al. (2022). Epilepsy and brain network hubs. *Epilepsia* 63, 537–550. doi: 10.1111/epi.17171

Uddin, L. Q., Yeo, B. T. T., and Spreng, R. N. (2019). Towards a universal taxonomy of macro-scale functional human brain networks. *Brain Topogr.* 32, 926–942. doi: 10.1007/s10548-019-00744-6

van den Heuvel, M. P., and Hulshoff Pol, H. E. (2010). Exploring the brain network: a review on resting-state fMRI functional connectivity. *Eur. Neuropsychopharmacol.* 20, 519–534. doi: 10.1016/j.euroneuro.2010.03.008

Vetkas, A., Fomenko, A., Germann, J., Sarica, C., Iorio-Morin, C., Samuel, N., et al. (2022). Deep brain stimulation targets in epilepsy: systematic review and meta-analysis of anterior and centromedian thalamic nuclei and hippocampus. *Epilepsia* 63, 513–524. doi: 10.1111/epi.17157

Wang, J., Li, Y., Wang, Y., and Huang, W. (2018). Multimodal data and machine learning for detecting specific biomarkers in pediatric epilepsy patients with generalized tonic-clonic seizures. *Front. Neurol.* 9:1038. doi: 10.3389/fneur.2018.01038

Wang, Z., Larivière, S., Xu, Q., Vos de Wael, R., Hong, S.-J., Wang, Z., et al. (2019a). Community-informed connectomics of the thalamocortical system in generalized epilepsy. *Neurology* 93, 1112–1122. doi: 10.1212/WNL.0000000000008096

Wang, Z., Wang, X., Rong, R., Xu, Y., Zhang, B., and Wang, Z. (2019b). Impaired hippocampal functional connectivity in patients with drug resistant, generalized tonic-clonic seizures. *Neuroreport* 30, 700–706. doi: 10.1097/WNR.0000000000001262

Wang, Z., Lu, G., Zhang, Z., Zhong, Y., Jiao, Q., Zhang, Z., et al. (2011). Altered resting state networks in epileptic patients with generalized tonic–clonic seizures. *Brain Res.* 1374, 134–141. doi: 10.1016/j.brainres.2010.12.034

Wang, Z., Zhang, Z., Jiao, Q., Liao, W., Chen, G., Sun, K., et al. (2012). Impairments of thalamic nuclei in idiopathic generalized epilepsy revealed by a study combining morphological and functional connectivity MRI. *PLoS One* 7:e39701. doi: 10.1371/journal.pone.0039701

Wei, H. L., An, J., Zeng, L. L., Shen, H., Qiu, S. J., and Hu, D. W. (2015). Altered functional connectivity among default, attention, and control networks in idiopathic generalized epilepsy. *Epilepsy Behav.* 46, 118–125. doi: 10.1016/j.yebeh.2015.03.031

Whelan, C. D., Altmann, A., Botía, J. A., Jahanshad, N., Hibar, D. P., Absil, J., et al. (2018). Structural brain abnormalities in the common epilepsies assessed in a worldwide ENIGMA study. *Brain* 141, 391–408. doi: 10.1093/brain/awx341

Wu, Y., Ji, G. J., Zang, Y. F., Liao, W., Jin, Z., Liu, Y. L., et al. (2015). Local activity and causal connectivity in children with benign epilepsy with centrotemporal spikes. *PLoS One* 10:e0134361. doi: 10.1371/journal.pone.0134361I

Xu, Q., Zhang, Q., Yang, F., Weng, Y., Xie, X., Hao, J., et al. (2021). Cortico-striato-thalamo-cerebellar networks of structural covariance underlying different epilepsy syndromes associated with generalized tonic-clonic seizures. *Hum. Brain Mapp.* 42, 1102–1115. doi: 10.1002/hbm.25279

Yan, C. G., Wang, X. D., Zuo, X. N., and Zang, Y. F. (2016). DPABI: data processing & analysis for (resting-state) brain imaging. *Neuroinformatics* 14, 339–351. doi: 10.1007/s12021-016-9299-4

frontiers | Frontiers in Neuroscience

TYPE Original Research
PUBLISHED 08 August 2022
DOI 10.3389/fnins.2022.970245

OPEN ACCESS

EDITED BY
Nicoletta Cera,
University of Porto, Portugal

REVIEWED BY
Kun Zhao,
Beihang University, China
Weizhao Lu,
Shandong First Medical University, China
Matteo Bruno Lodi,
University of Cagliari, Italy

*CORRESPONDENCE
Yating Lv
lvyating198247@gmail.com
Zhongxiang Ding
hangzhoudzx73@126.com

†These authors have contributed equally to this work and share first authorship

SPECIALTY SECTION
This article was submitted to Brain Imaging Methods, a section of the journal Frontiers in Neuroscience

RECEIVED 15 June 2022
ACCEPTED 19 July 2022
PUBLISHED 08 August 2022

CITATION
Wang L, Feng Q, Ge X, Chen F, Yu B, Chen B, Liao Z, Lin B, Lv Y and Ding Z (2022) Textural features reflecting local activity of the hippocampus improve the diagnosis of Alzheimer's disease and amnestic mild cognitive impairment: A radiomics study based on functional magnetic resonance imaging.
Front. Neurosci. 16:970245.
doi: 10.3389/fnins.2022.970245

Textural features reflecting local activity of the hippocampus improve the diagnosis of Alzheimer's disease and amnestic mild cognitive impairment: A radiomics study based on functional magnetic resonance imaging

Luoyu Wang[1,2†], Qi Feng[1†], Xiuhong Ge[1], Fenyang Chen[3], Bo Yu[4], Bing Chen[5], Zhengluan Liao[6], Biying Lin[1], Yating Lv[7*] and Zhongxiang Ding[1*]

[1]Key Laboratory of Clinical Cancer Pharmacology and Toxicology Research of Zhejiang Province, Department of Radiology, Affiliated Hangzhou First People's Hospital, Zhejiang University School of Medicine, Hangzhou, China, [2]The Center for Integrated Oncology and Precision Medicine, Affiliated Hangzhou First People's Hospital, Zhejiang University School of Medicine, Hangzhou, China, [3]The Fourth School of Medical, Zhejiang Chinese Medical University, Hangzhou, China, [4]School of Medical Imaging, Hangzhou Medical College, Hangzhou, China, [5]Jing Hengyi School of Education, Hangzhou Normal University, Hangzhou, China, [6]Center for Rehabilitation Medicine, Department of Geriatric VIP No. 3, Department of Clinical Psychology, Zhejiang Provincial People's Hospital, Hangzhou, China, [7]Center for Cognition and Brain Disorders, The Affiliated Hospital of Hangzhou Normal University, Hangzhou, China

Background: Textural features of the hippocampus in structural magnetic resonance imaging (sMRI) images can serve as potential diagnostic biomarkers for Alzheimer's disease (AD), while exhibiting a relatively poor discriminant performance in detecting early AD, such as amnestic mild cognitive impairment (aMCI). In contrast to sMRI, functional magnetic resonance imaging (fMRI) can identify brain functional abnormalities in the early stages of cerebral disorders. However, whether the textural features reflecting local functional activity in the hippocampus can improve the diagnostic performance for AD and aMCI remains unclear. In this study, we combined the textural features of the amplitude of low frequency fluctuation (ALFF) in the slow-5 frequency band and structural images in the hippocampus to investigate their diagnostic performance for AD and aMCI using multimodal radiomics technique.

Methods: Totally, 84 AD, 50 aMCI, and 44 normal controls (NCs) were included in the current study. After feature extraction and feature selection, the radiomics models incorporating sMRI images, ALFF values and their combinations in the bilateral hippocampus were established for the diagnosis

of AD and aMCI. The effectiveness of these models was evaluated by receiver operating characteristic (ROC) analysis. The radiomics models were further validated using the external data from the Alzheimer's Disease Neuroimaging Initiative (ADNI) database.

Results: The results of ROC analysis showed that the radiomics models based on structural images in the hippocampus had a better diagnostic performance for AD compared with the models using ALFF, while the ALFF-based model exhibited better discriminant performance for aMCI than the models with structural images. The radiomics models based on the combinations of structural images and ALFF were found to exhibit the highest accuracy for distinguishing AD from NCs and aMCI from NCs.

Conclusion: In this study, we found that the textural features reflecting local functional activity could improve the diagnostic performance of traditional structural models for both AD and aMCI. These findings may deepen our understanding of the pathogenesis of AD, contributing to the early diagnosis of AD.

KEYWORDS

Alzheimer's disease, amnestic mild cognitive impairment, resting-state functional magnetic resonance imaging, the amplitude of low frequency fluctuation, radiomics

Introduction

Alzheimer's disease (AD) is an aging-related central nervous system disease characterized by impaired memory function, which severely affects the quality of life of the elderly (Masters et al., 2015; Soria Lopez et al., 2019). Recent projection data suggests that, by 2050, the prevalence of dementia will double in Europe and triple globally, and the estimated number of new dementia cases would be three times higher based on the biological rather than clinical definition of Alzheimer's disease (Knopman et al., 2021; Scheltens et al., 2021). AD is still incurable due to incomplete understanding of its etiology and underlying neurological mechanisms (Sun et al., 2018). However, recent studies have indicated that certain necessary interventions such as statins in the early stages of the disease may slow the progression of AD, prolonging the lifespan of patients (Sperling et al., 2011; McDade and Bateman, 2017). Amnestic Mild Cognitive Impairment (aMCI), characterized by some degree of cognitive decline and memory impairment, is generally considered an early AD (Bradfield et al., 2018). Dietary intervention and alleviation of neuropsychiatric symptoms may reduce the risk of conversion to dementia (Cooper et al., 2015). However, the medical diagnosis of aMCI, which mainly relies on neuropsychological tests, remains challenging due to the lack of objective biological approaches (Murayama et al., 2013; Alves et al., 2021). Therefore, our current research focused on the identification of brain-imaging surrogate markers sensitive to early disease that could distinguish AD from normal cognition in the elderly, thus enabling an efficient effective diagnosis of aMCI.

The hippocampus plays a crucial role in human cognition, especially memory, and it is considered to be the most vulnerable region during AD pathogenesis (Braak and Braak, 1997). Both amyloid-β and Tau proteins have been noted to be selectively deposited in the hippocampal cortical layers of AD patients (Braak and Braak, 1997). In addition, hippocampal gray matter atrophy is an important indicator for assessing the severity of dementia (Pini et al., 2016). Using structural MRI, a previous study showed that a reduction in bilateral hippocampal gray matter volume was associated with cognitive decline in AD and aMCI patients (Feng F. et al., 2021). However, the volumetric measures may overlook some specific morphological features, such as the textural features of the hippocampus (Dachena et al., 2019; Curado et al., 2020).

Radiomics, originally developed for tumor diagnosis, is a computer-aided diagnostic approach used to mine and analyze quantitative image characteristics such as intensity and textural features (Feng Q. et al., 2021; Iancu et al., 2021). Radiomics have been well-validated in the classification of AD and NC based on textural features of the structural hippocampus in previous studies (Rajeesh et al., 2017; Zhao et al., 2020). For example, a previous study has indicated that the accuracy of discrimination of Alzheimer's disease patients is 93.6% using textural features of the structural hippocampus (Rajeesh et al., 2017). In addition,

the hippocampal texture was superior to volume reduction as a predictor of MCI-to-AD conversion (Sørensen et al., 2016; Zhao et al., 2020), though it has been reported that textural features of the structural hippocampus are unsatisfactory in diagnosing aMCI (Feng et al., 2019; Park et al., 2021). This may be because the structural images could not capture all the changes in the hippocampus in aMCI (Cai et al., 2017).

As an advanced non-invasive neuroimaging technique, resting-state functional magnetic resonance imaging (fMRI) is an important imaging modality to understand the neurodegenerative course of aMCI and early AD (Wu et al., 2022), because the memory dysfunction may occur before the structural degeneration (Jin et al., 2012). The amplitude of low frequency fluctuation (ALFF) is proposed to characterize the local properties of rs-fMRI signals (Zang et al., 2007), showing frequency-dependent pattern (Zuo et al., 2010) and temporal variability (dynamics) (Liao et al., 2019), and thus has been widely used to detect functional abnormalities in brain disorders (Li et al., 2020; Wang et al., 2021). As for AD and aMCI patients, previous studies have consistently observed the alterations of ALFF value in the hippocampus (Liu et al., 2014; Cha et al., 2015; Yang et al., 2018; Yuan et al., 2021). For example, Liu and colleagues have demonstrated increased ALFF values in the bilateral hippocampus of AD patients compared with healthy controls (Liu et al., 2014). Meta-analyses have also shown significant alterations of ALFF in the left hippocampus/parahippocampal gyrus in AD and aMCI patients (Cha et al., 2015; Yuan et al., 2021). More importantly, these ALFF changes were found to exhibit a frequency-dependent pattern (Han et al., 2011; Liu et al., 2014). In our previous study, we observed the difference in ALFF in the slow-5 frequency band between groups, mainly corresponding to the bilateral hippocampus as well as regions within the default mode network, with the highest accuracy in discriminating the three groups (Wang et al., 2021). Our findings indicated that ALFF in the slow-5 frequency band might serve as a promising functional indicator to aid the diagnosis of AD and aMCI (Wang et al., 2021). Recently, ALFF combined with structural features has been investigated for the diagnosis of AD and aMCI (Khatri and Kwon, 2022; Liu et al., 2022). Yet ALFF has not been used in the analysis of radiomics and it is unclear whether incorporating functional measures into radiomics analysis can improve the effectiveness of traditional hippocampal structural models for the diagnosis of AD and aMCI.

In this study, we combined the ALFF textural feature of the hippocampus in the slow-5 frequency band with structural MRI images to investigate their discriminative performance for AD and aMCI using radiomics analysis. We hypothesized that the inclusion of hippocampal functional metrics in radiomics could improve the effectiveness of traditional hippocampal structural models in distinguishing AD and aMCI patients from healthy elderly, especially for the diagnosis of aMCI.

Materials and methods

Participants

From September 2016 to August 2020, 98 AD and 53 aMCI patients at Zhejiang Provincial Hospital and 50 normal controls (NCs) at the hospital's health promotion center were recruited. All participants signed the written informed consent. This study was approved by the local Ethics Committee of Zhejiang Provincial People's Hospital (No. 2012KY002) and was conducted according to the Declaration of Helsinki. The inclusion and exclusion criteria have been described at our previous study (Wang et al., 2021). All participants underwent medical history collection, physical examinations, laboratory examinations, routine brain magnetic resonance scans and the Mini-Mental State Test (MMSE). AD patients were diagnosed based on the criteria of the revised NINCDS-ADRDA (National Institute of Neurological and Communicative Disorders and Stroke and the Alzheimer's Disease and Related Disorders Association) and the DSM-IV-R (revised Diagnostic and Statistical Manual of Mental Disorders, Fourth Edition) with MMSE score $\leq$ 24. The aMCI patients were selected according to the following criteria: (1) complaint of memory impairment; (2) normal clinical manifestations; (3) 24 $<$ MMSE score $\leq$ 27; and (4) failure to meet the criteria for dementia according to DSM-IV-R. The inclusion criteria for NCs was as follows: (1) absence of neurological impairment, such as visual loss or hearing and (2) MMSE score $\geq$ 28. Patients and participants with stroke, brain trauma, epilepsy, Parkinson's disease, hypertension, serious anemia, diabetes, brain tumor, history of mental illness and signal alterations in the medial temporal cortex caused by infectious or vascular factors on MRI FLAIR and T2-weighted images were excluded. The summary of subjects was illustrated in **Table 1** and the flow chart of the radiomic analysis was shown in **Figure 1**.

Image acquisition

MRI data were obtained using a 3.0T magnetic resonance scanner (Discovery MR750; GE Healthcare, Waukesha, WI, United States) at Zhejiang People's Hospital and an 8-channel phased array coil was used for all the subjects. Raw structural images were acquired using a high-resolution 3D T1-weighted magnetization-prepared rapid gradient echo (MPRAGE) sagittal sequence with predefined direct MR acquisition parameters [repetition time (TR) = 6.7 ms, echo time (TE) = 2.9 ms, slice thickness = 1 mm, field of view (FOV) = 256 $\times$ 256 mm^2, flip angle = 12°, resolution = 256 $\times$ 256, and 192 slices]. Rs-fMRI images were acquired using an echo-planar imaging sequence (TR = 2,000 ms, TE = 30 ms, slice thickness = 3.2 mm,

TABLE 1 Demographic data and clinical characteristics of the participants.

Sample size	AD ($N = 84$)	aMCI ($N = 50$)	NC ($N = 44$)	Statistic	*P*-value
Gender (male: female)	37:47	27:23	21:23	1.244	0.537[a]
Age (years, mean ± SD)	69.226 ± 9.303	65.840 ± 11.171	65.477 ± 9.690	2.847	0.061[b]
Education (years, mean ± SD)	7.167 ± 4.412	7.120 ± 4.059	7.114 ± 3.356	0.003	0.997[b]
MMSE	17.512 ± 5.084	26.200 ± 0.881	29.023 ± 0.902	182.686	<0.001[b]

[a]*p*-values for sex distribution obtained by the chi-square test; [b]*p*-value obtained by analysis of variance. AD, Alzheimer's disease; aMCI, amnestic mild cognitive impairment; NCs, normal controls.

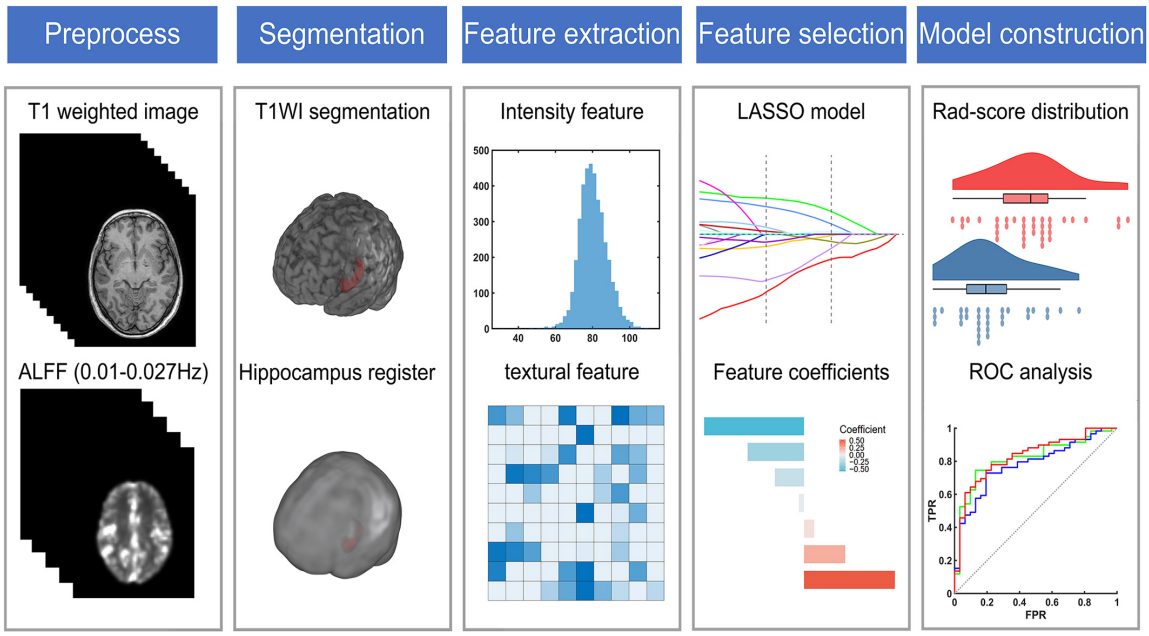

FIGURE 1
The flow chart of radiomic analysis. ALFF, the amplitude of low frequency fluctuation; LASSO, the least absolute shrinkage and selection operator; ROC, receiver operating characteristic.

FOV = 220 × 220 mm^2, flip angle = 90°, resolution = 64 × 64, and 210 volumes and 44 slices).

Amplitude of low frequency fluctuation calculation

Rs-fMRI data were mainly processed using SPM[1] (Penny et al., 2011) and DPABI (Yan et al., 2016) in the following steps: (1) Due to the magnetic field inhomogeneity of the MR machine during the initial scan, the first 10 time points which recommended in DPABI (Chao-Gan and Yu-Feng, 2010) were discarded to reduce the impact on data quality. (2) A temporal layer correction was performed to rectify the differences in interlayer acquisition time using the middle slice as the reference slice. The correction was performed by lagging (shifting forward) the time series on each slice using sinc interpolation. (3) A head motion correction was performed to reduce the effect of the subject's head motion on data quality (Friston et al., 1995; Whitfield-Gabrieli and Nieto-Castanon, 2012). (4) Linear trend of the time series was regressed. (5) Regression of covariates including white matter, cerebrospinal fluid and Friston 24 parameters was performed (Friston et al., 1996). (6) According to our previous studies (Wang et al., 2021), the ALFF in the slow-5 frequency band (0.01–0.027 Hz) was calculated for each participant. The flow chart for calculating the ALFF in the slow-5 frequency band was shown in **Supplementary Figure 1**.

In this study, we first excluded patients with the criteria of displacement > 3 mm and rotation > 3°. To improve the reliability of fMRI-based radiomics, we further removed the

1 http://fil.ion.ucl.ac.uk/spm

patients with FD > 0.5 (Power et al., 2015). A 25 subjects were excluded, leaving 84 AD patients, 50 aMCI patients and 44 NCs healthy controls in the follow-up analysis.

Hippocampus segment

To improve the segmentation efficiency while ensuring the stability of the results, a deep learning-based hippocampal segmentation toolkit hippodeep[2] was used to automatically segment the bilateral hippocampus (Thyreau et al., 2018). Structural MRI was performed on all patients to obtain bilateral structural image masks of the hippocampus. We randomly selected five cases to compare the segmentation mask of the algorithm and that of a highly qualified head and neck radiologist using the dice coefficient. The mean dice coefficient of the left hippocampus is 0.935 and that of the right hippocampus is 0.967. The results showed the good consistency and validity of the automatic segmentation adopted in our study. Then the bilateral hippocampal masks for assessment of ALFF were obtained by aligning the structural images with the functional images.

Features extraction

Based on the segmentation results, radiomics features of bilateral hippocampus extracted from two modalities (sMRI and ALFF images) were compared to quantify tissue spatial heterogeneity. The features were analyzed using an open-source radiomics analysis package[3] based on the radiomics toolbox[4], conforming to the Imaging Biomarker Standardization Initiative (IBSI) (Xu et al., 2020; Zwanenburg et al., 2020). In the current study, 101 features were extracted from sMRI or ALFF images within each region of the bilateral hippocampus, including 13 intensity features and 88 textural features for each modality (Xu et al., 2020). The names of the 101 radiomic features were shown in **Supplementary Table 1**.

Feature selection and radiomic signature building

Before data processing, the createDataPartition function from the caret package was used to randomly split the data of 84 AD patients and 44 NCs, of which 70% of the data were classified as the training set and 30% of the data were classified as the test set and make the ratio of positive samples to negative samples the same between the training and test set. To avoid sample bias of grouping and get a steady result, 10 times repetition of the validation in the present study was adopted. To remove the unit limit of each feature before applying it to the machine learning model for classification, z-normalization was performed on the training set and applied to the test set and the external validation set. Due to sample imbalance, the synthetic minority over-sampling (SMOTE) algorithm (Chawla et al., 2002) was used to balance the minority group in the training set.

Two feature selection methods, including the minimum redundancy maximum relevance (mRMR) (Ding and Peng, 2005) and the least absolute shrinkage and selection operator (LASSO) (Tibshirani, 2011), were used to select the most valuable predictive features in the training cohort. Firstly, using the mRMR method, the features were ranked by their relevance-redundancy index, and the top 20 features with the highest relevance were selected (Ding and Peng, 2005). Then, LASSO regression was conducted on the training cohort using 10-fold cross-validation to choose the optimized subset of features and build a radiomic signature (Tibshirani, 2011). The corresponding coeficients were evaluated. As a simple score developed to classify the patients and NCs using radiomics, the radiomics score (radscore) was calculated by summing selected textural features weighted by their respective coeficients (plus a constant term) (Zheng et al., 2018). All rad-scores between the AD and NCs groups were compared on the training and validation sets, respectively.

The above process was carried out six times in total. Using the same train-test split, six radiomics signatures were created based on sMRI and ALFF in the slow-5 band and their combination in the left and right hippocampus, respectively. Then images from 50 aMCI patients and 44 NCs were similarly processed. The following 12 radiomics signatures were constructed: AD diagnosis model based on left hippocampal structural image, AD diagnosis model based on left hippocampal ALFF, AD diagnosis model based on left hippocampal structural and ALFF image, AD diagnosis model based on right hippocampal structural image, AD diagnosis model based on right hippocampal ALFF, AD diagnosis model based on right hippocampal structural and ALFF images, aMCI diagnosis model based on left hippocampal structural image, aMCI diagnosis model based on left hippocampal ALFF, aMCI diagnosis model based on left hippocampal structural and ALFF images, aMCI diagnosis model based on right hippocampal structural image, aMCI diagnosis model based on right hippocampal ALFF, and aMCI diagnosis model based on right hippocampal structural and ALFF images.

Statistical analysis

Wilcoxon test was performed on the rad-score for detecting AD and aMCI in the train and test sets, respectively. As recommended in previous study (Ge et al., 2022), $P < 0.05$ was considered to be statistically significant in accordance with

2 https://github.com/bthyreau/hippodeep_pytorch

3 https://github.com/WenbingLv/Subregional-Radiomics

4 https://github.com/mvallieres/radiomics

statistical conventions. The area under the curve (AUC) of the training and test set was used to assess the discriminative accuracy of the Rad-score. This process was repeated 10 times and the average AUC value was obtained as the final metric for this study. Receiver operating characteristic (ROC) curves were analyzed and visualized using the Matlab-based classification model effectiveness analysis tool ROCA.[5] To further assess the classification effects of different models, this study used the Delong test (DeLong et al., 1988) to compare the differences in the AUCs of each classification model.

Correlation analyses were performed on the features retained for AD and aMCI diagnosis. The textural features selected in unimodality and retained in the combined model were correlated with MMSE by the Spearman correlation coefficient, and an α level of less than 0.05 was considered statistically significant. The correlation coefficient was calculated using the following formula:

$$\rho = \frac{\sum_i \left(R(x_i) - R(\overline{x})\right)\left(R(y_i) - R(\overline{y})\right)}{\sqrt{\sum_{i(R(x_i)-R(\overline{x}))^2}}\sqrt{\sum_{i\left(R(y_i)-R(\overline{y})\right)^2}}}$$

Where, R(x) and R(y) are the rank order of x and y, respectively.

External validation

The external validation dataset including 33 AD, 34 MCI patients and 38 NCs was downloaded from the ADNI database.[6] The searching criteria were as follows: (1) data containing 3.0 T Philips MRI scans; (2) scan sequences containing high-definition T1 structural images; (3) scan sequences containing resting-state functional MRI data (TR = 3.0 s, layer thickness = 3.3 mm, resolution = 64 × 64, and 140 time points); and (4) the baseline data were collected from the initial visit. ADNI was reviewed and approved by the institutional review boards of all participating institutions[7], and written informed consent was obtained from all participants or their guardians in accordance with the Declaration of Helsinki (Petersen et al., 2010; Trojanowski et al., 2010; Weiner et al., 2010). A total of 6 subjects with a maximum head movement displacement > 3 mm, a rotation > 3° and an FD > 0.5 during resting-state functional MRI scanning were excluded, and 32 AD, 32 MCI, and 35 NCs subjects were finally included in the validation analyses. The summary of ADNI subjects were shown in **Supplementary Table 2**.

The radiomics models obtained from the train set of our data were applied to the ADNI dataset to validate the robustness of the models in clinical practice. In addition, to further validate our results, we performed a classification analysis with a combination of the bilateral hippocampus.

5 https://github.com/Luoyu-Wang/ROCA

6 https://adni.loni.usc.edu

7 http://www.adni-info.org

Results

Demographic data and neuropsychological tests

No significant differences in demographic information (i.e., sex, age, education) were noted ($P > 0.05$). A significant difference in MMSE score was shown among the three groups. *Post hoc* analyses were performed and the results indicated that the NCs had the highest neuropsychological performance, aMCI patients had intermediate performance, AD patients had the worst performance ($P < 0.001$). **Table 1** summarizes the detailed demographic characteristics and MMSE scores of all subjects.

Receiver operating characteristic analysis and delong tests

The processes of feature selection and rad-score calculation for all 12 models are shown in **Supplementary Figures 2–7**. The results of the ROC analyses are shown in **Figure 2** and **Tables 2, 3**.

When differentiating the AD from NCs, the AUC of the left hippocampal structural model was 0.864, while that of the model based on left hippocampal ALFF in the slow-5 frequency band was 0.828. Delong test reflected the significant difference in AUC between these two models ($z = 3.087$, $P = 0.002$). The combined model based on the left hippocampal structural and ALFF images exhibited the highest accuracy (AUC = 0.873). And the AUC of the combined model was significantly higher than that of the structural image model ($z = 3.003$, $P = 0.003$). In addition, similar results were obtained for assessing the right hippocampus. The AUC of the right hippocampal structural model was 0.818, while that of the model based on right hippocampal ALFF in the slow-5 frequency band was 0.780. Delong test reflected the significant AUC difference between these two models ($z = 2.898$, $P = 0.004$). The combined model based on the right hippocampal structural and ALFF images exhibited the highest accuracy (AUC = 0.830). Additionally, the AUC of the combined model was significantly higher than that of the structural image model ($z = 2.361$, $P = 0.018$).

Unlike AD, the model based on left hippocampal ALFF in the slow-5 frequency (AUC = 0.764) showed better discriminative performance than the left hippocampal structural model (AUC = 0.729) when distinguishing aMCI from NCs. There was a marginally significant difference in AUC between these two models ($z = 1.805$, $P < 0.071$). The combined model based on the left hippocampal structural and ALFF image (AUC = 0.804) had better performance than the left hippocampal structural model ($z = 6.629$, $P < 0.001$). The combined model based on the right hippocampal structural and ALFF images (AUC = 0.810) also had better performance

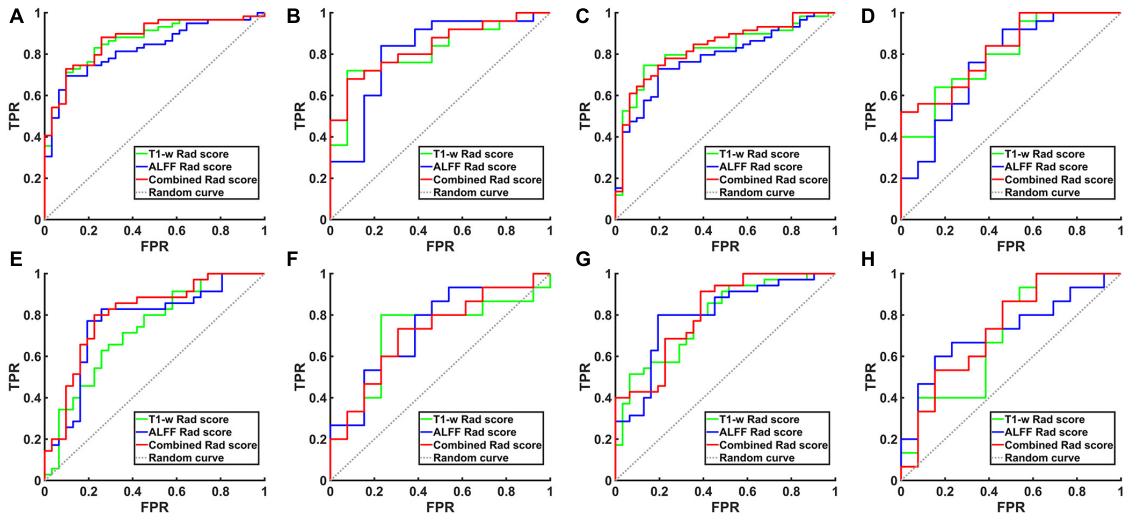

FIGURE 2
The ROC curve of the hippocampal structural image, hippocampal ALFF in slow-5 frequency band and their combined model. **(A)** ROC curves for AD and NCs in the training set based on left hippocampal images. **(B)** ROC curves for aMCI and NCs in the training set based on left hippocampal images. **(C)** ROC curves for AD and NCs in the training set based on right hippocampal images. **(D)** ROC curves for aMCI and NCs in the training set based on right hippocampal images. **(E)** ROC curves for AD and NCs in the test set based on left hippocampal images. **(F)** ROC curves for aMCI and NCs in the test set based on left hippocampal images. **(G)** ROC curves for AD and NCs in the test set based on right hippocampal images. **(H)** ROC curves for aMCI and NCs in the test set based on right hippocampal images. TPR, true positive rate; FPR, false positive rate; AD, Alzheimer's disease; aMCI, amnestic mild cognitive impairment; NCs, normal controls; ROC, receiver operating characteristic; ALFF, the amplitude of low frequency fluctuation.

(z = 1.763, P = 0.078) than the right hippocampal structural model (AUC = 0.790).

The results of external validation suggested a consistent trend between the validation and the train sets, as shown in Table 4. In addition, we performed a classification analysis with a combination of the bilateral hippocampus. The results were consistent with the findings based on the unilateral hippocampus and were shown in the Supplementary Table 3.

Correlation analysis

The features subjected to unimodal selection and retained in the combined model were correlated with the MMSE scores in AD and aMCI diagnostic models, respectively, and the results were shown in Figure 3. In the diagnostic model for AD, the features significantly associated with MMSE score were T1-w_GLRLM (gray-level run-length matrix) _RLN

TABLE 2 The ROC curve of left hippocampal structural images, ALFF in slow-5 frequency band and their combined model.

Classifier	Model	Data set	AUC	95% CI	Accuracy
AD vs. NCs	T1	Training	0.864	0.841–0.887	0.778
		Test	0.818	0.767–0.858	0.790
	ALFF	Training	0.828	0.801–0.853	0.767
		Test	0.809	0.758–0.856	0.816
	T1+ALFF	Training	0.873	0.849–0.895	0.789
		Test	0.837	0.792–0.872	0.763
aMCI vs. NCs	T1	Training	0.729	0.689–0.766	0.682
		Test	0.713	0.650–0.772	0.786
	ALFF	Training	0.764	0.725–0.800	0.788
		Test	0.738	0.678–0.796	0.714
	T1+ALFF	Training	0.804	0.763–0.834	0.788
		Test	0.718	0.657–0.774	0.714

AD, Alzheimer's disease; aMCI, amnestic mild cognitive impairment; NCs, normal controls; ROC, area under the curve; ALFF, the amplitude of low frequency fluctuation.

TABLE 3 The ROC curve of right hippocampal structural images, ALFF in slow-5 frequency band and their combined model.

Classifier	Model	Data set	AUC	95% CI	Accuracy
AD vs. NCs	T1	Training	0.818	0.789–0.844	0.788
		Test	0.797	0.750–0.838	0.710
	ALFF	Training	0.780	0.746–0.806	0.756
		Test	0.763	0.708–0.816	0.789
	T1+ALFF	Training	0.830	0.802–0.856	0.778
		Test	0.822	0.772–0.857	0.684
aMCI vs. NCs	T1	Train	0.790	0.756–0.825	0.712
		Test	0.708	0.643–0.772	0.714
	ALFF	Training	0.798	0757–0.830	0.803
		Test	0.723	0.659–0.780	0.714
	T1+ALFF	Training	0.810	0.778–0.840	0.722
		Test	0.733	0.666–0.793	0.714

AD, Alzheimer's disease; aMCI, amnestic mild cognitive impairment; NCs, normal controls; ROC, area under the curve; ALFF, the amplitude of low frequency fluctuation.

TABLE 4 External validation.

Classifier	Model	Hippocampus	AUC	95% CI	Accuracy
AD vs. NCs	T1	left	0.829	0.794–0.859	0.791
		right	0.738	0.700–0.773	0.731
	ALFF	left	0.757	0.719–0.790	0.731
		right	0.678	0.638–0.717	0.657
	T1+ALFF	left	0.830	0.795–0.862	0.791
		right	0.746	0.706–0.781	0.701
MCI vs. NCs	T1	left	0.554	0.511–0.600	0.627
		right	0.529	0.487–0.574	0.582
	ALFF	left	0.598	0.552–0.639	0.642
		right	0.563	0.520–0.611	0.597
	T1+ALFF	left	0.634	0.589–0.676	0.642
		right	0.558	0.512–0.603	0.582

AD, Alzheimer's disease; aMCI, amnestic mild cognitive impairment; NCs, normal controls; ROC, area under the curve; ALFF, the amplitude of low frequency fluctuation.

(run-length non-uniformity) (r = 0.381, P < 0.001), T1-w_GLRLM_RLV (run-length variance) (r = −0.281, P = 0.012), ALFF_GLCM (gray level concurrence matrix)_Correlation (r = 0.305, P = 0.005) from the left hippocampus and T1-w_GLCM_Entropy (r = 0.245, P < 0.025), and ALFF_GLSZM (gray-level size zone matrix)_GLN (gray-level non-uniformity) from the right hippocampus (r = 0.274, P = 0.010). In the diagnostic model for aMCI, significant MMSE-correlated features included ALFF_GLCM_Correlation from the left hippocampus (r = 0.445, P = 0.001).

Discussion

To the best of our knowledge, this was the first study to explore the functional indicator ALFF calculated from rs-fMRI as textural features. In the present study, the textural features of the hippocampus in both ALFF map in the slow-5 frequency band and structural MRI image were combined in the radiomics model to explore their discriminant performance for detecting AD and aMCI. We found that the radiomics model based on hippocampal structural image had a better performance than that based on ALFF in the slow-5 frequency band when distinguishing AD from NCs. When differentiating the aMCI from NCs, the model based on hippocampal ALFF in the slow-5 frequency band showed better diagnostic ability than that based on hippocampal structural images. More importantly, the combined model exhibited the best performance for the diagnosis of both AD and aMCI, which meant that the multimodal radiomics models based on hippocampal structural images and ALFF in the slow-5 frequency band had the potential to become a new diagnostic tool for AD.

Using the radiomics approach, we found that the model based on hippocampus structural images performed well in diagnosing AD. This was consistent with the results of previous radiomics studies on hippocampal structural MRI (Zhang et al., 2012; Rajeesh et al., 2017). Moreover, the above model showed better performance than the model based on hippocampal ALFF in the slow-5 frequency band. On the contrary, the model based on hippocampal ALFF in the slow-5 frequency band instead had better performance than the radiomics model based on radiomics studies of hippocampal structural MRI in diagnosing aMCI. The structural image may not fully reflect the changes in the hippocampus of aMCI patients, and ALFF is generally considered to represent the local activity of the brain (Zang et al., 2007). In the early stages of AD when structural damage is not yet evident, local brain functional changes may precede structural changes. The model based on hippocampal structural images and ALFF in the slow-5 frequency band showed better performance on AD (z = 3.003, P = 0.003, for left hippocampus; z = 2.361, P = 0.018, for right hippocampus) and aMCI (z = 6.629, P < 0.001, for left hippocampus; z = 1.763, P = 0.078, for right hippocampus) than the classical model based on structural images. The textural features of ALFF may provide additional spatial textural information about the local activity of the brain. In addition, consistent results were also obtained in the external validation set. These results together suggest that the textural features of hippocampal ALFF could improve the diagnosis of traditional structural hippocampus models for AD and aMCI. In contrast, the diagnostic power for aMCI in the validation set was relatively lower than in our data. There are differences in the inclusion criteria such as MMSE scores and symptoms[8] between the two datasets. In our data, the MMSE score for aMCI patients is between 24 and 27, while in the ADNI database, the MMSE score for aMCI is between 24 and 30. Moreover, aMCI patients from our dataset have a complaint of memory impairment and normal clinical manifestations, while aMCI patients in ADNI suffer a subjective memory concern, informant, or clinician and absence of significant levels of impairment in other cognitive domains. Thus, we speculate that the lower diagnostic power for aMCI in the validation set may be due to the differences in the inclusion criteria. Future studies to recruit the aMCI patients with the same inclusion criteria as our data could be attained to test the radiomics models in the current study.

The features retained in the combined model were correlated with the MMSE score. Our results were consistent with previous studies which showed significant correlations between the run-length non-uniformity (RLN) based on hippocampal structural images and MMSE score (Zhao et al., 2020). In addition, correlation analysis further revealed that the features that were significantly correlated with MMSE scores were T1-w_GLRLM_RLN from the left hippocampus, T1-w_GLRLM_RLV, ALFF_GLCM_Correlation and T1-w_GLCM_Entropy and ALFF_GLSZM_GLN from the right

8 https://adni.loni.usc.edu/methods/documents/

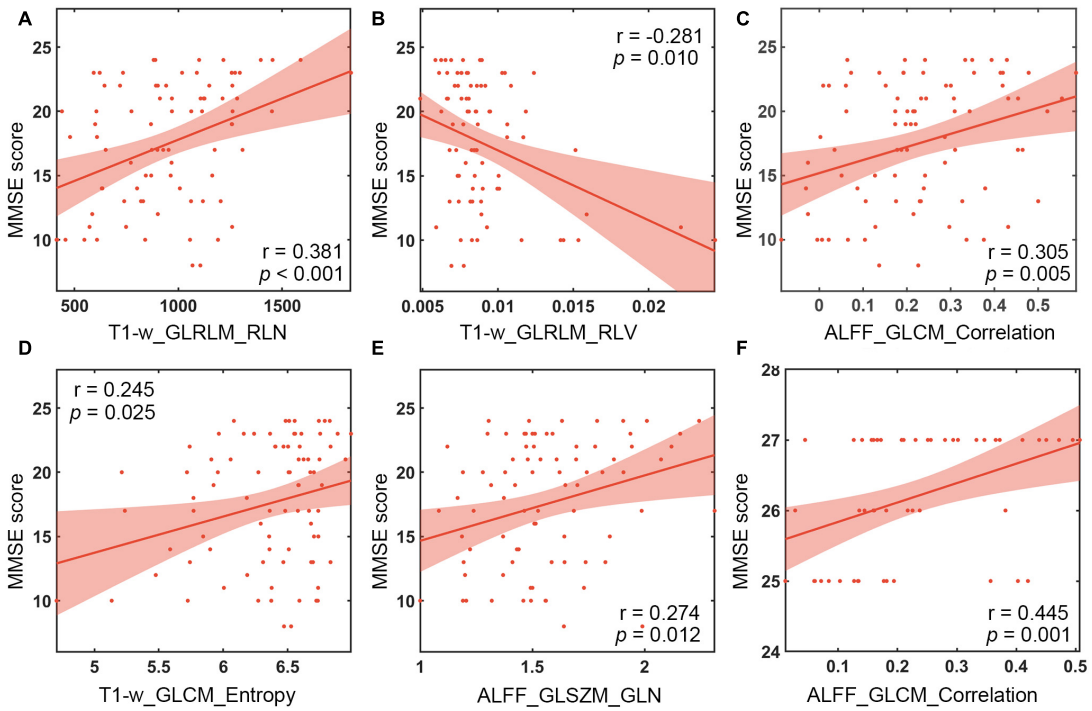

FIGURE 3
Correlation analysis between MMSE scales and textural features. **(A)** Correlation of T1-w_GLRLM_RLN in the left hippocampus with MMSE scores of AD patients. **(B)** Correlation of T1-w_GLRLM_RLV in the left hippocampus with MMSE scores of AD patients. **(C)** Correlation of ALFF_GLCM_Correlation in the left hippocampus with MMSE scores of AD patients. **(D)** Correlation between T1-w_GLCM_Entropy in the right hippocampus and MMSE scores of AD patients. **(E)** Correlation of ALFF_GLSZM_GLN in the right hippocampus with MMSE scores of AD patients. **(F)** Correlation of ALFF_GLCM_Correlation in the left hippocampus with MMSE scores of aMCI patients. MMSE, Mini Mental State Test; ALFF, the amplitude of low frequency fluctuation.

hippocampus in diagnosing AD. Moreover, the feature ALFF_GLCM_Correlation was significantly correlated with MMSE score in detecting aMCI. The features mentioned above may be associated with the cognitive decline of AD or aMCI patients. Among the textural features, ALFF_GLCM_Correlation preserved by feature selection in both diagnosing AD and aMCI was positively correlated with MMSE score (**Figure 3**). GLCM is generally defined as the joint probability occurrence of pixel or voxel pairs, and GLCM_Correlation is usually considered to reflect the consistency of the image texture (Haralick et al., 1973). The correlation is high if all matrix element values are consistent and low if the values of matrix elements are not consistent. The results of this study were obtained using the grayscale distribution in all 13 directions, reflecting the joint probability information of the image grayscale in the adjacent 26 voxels. GLCM_Correlation may reflect the local texture consistency in the image space (Haralick et al., 1973), and ALFF is generally considered to represent the local activity of the brain (Zang et al., 2007). Therefore, ALFF_GLCM_Correlation may reflect the local coherence of the brain's activity. This finding suggests that AD and aMCI patients may show cognitive decline as the local coherence decreases. The underlying mechanism is still currently unclear, probably because Tau protein and amyloid-β are selectively deposited in the hippocampal cortex of patients during early onset of AD (Braak and Braak, 1997), resulting in a coherent alteration in the local activity of brain function, which is consistent with previous Regional Homogeneity (ReHo) findings in AD and aMCI patients (Zang et al., 2004; Cha et al., 2015; Wang et al., 2015).

This study had certain shortcomings and limitations. First and foremost, we only used hippocampal ALFF in the slow-5 frequency band, ignoring the consistency within the hippocampus and the connectivity within the whole brain. Future studies should make full use of the advantages of multiple indicators from fMRI such as ALFF, Regional Homogeneity and degree centrality for a comprehensive analysis. Second, the patients with AD and aMCI suffered from cognitive impairments in multiple domains (Stogmann et al., 2016), which could not be fully evaluated by MMSE. However, we failed to collect other cognitive scales and behavior data. Future studies employing different cognitive and behavioral tests in AD patients can aid the validation of the results. Third, the altered hippocampal function may not be the most significant alteration in AD. In future studies, texture features of other brain regions with functional changes, such as the default network,

should be employed to further explore their diagnostic effect. Finally, recent studies which adopted a 3-class classification model and exhibited better discriminative performance usually included thousands of data samples (Elola et al., 2021; Katz et al., 2021). We only have 178 MRI data and failed to build a 3-class classification model in the current study. In future study, more data should be acquired to classify AD and MCI simultaneously by building a 3-class classification model.

Conclusion

In this study, we used the hippocampal radiomics technique to establish predictive models incorporating structural image, ALFF in slow-5 frequency band and their combinations for diagnosis of AD and aMCI. We found that the radiomics model based on hippocampal structural image had a better diagnostic power for detecting AD compared with the model using hippocampal ALFF in the slow-5 frequency band; while the model based on ALFF in the slow-5 frequency band had a higher diagnostic power for aMCI than that based on the hippocampal structural image. The textural features of hippocampal ALFF can improve the diagnostic accuracy of traditional structural image models for detecting AD and aMCI, which meant that multimodal radiomics models based on the hippocampal structural images and the ALFF in the slow-5 frequency band can better diagnose AD and aMCI compared with the traditional structural image model, having the potential to become a new AD diagnostic tool. In future studies, we would make full use of the advantages of multiple indicators from fMRI such as ALFF and functional connectivity, to further examine their diagnostic effect.

Data availability statement

The raw data supporting the conclusions of this article will be made available by the authors, without undue reservation.

Ethics statement

The studies involving human participants were reviewed and approved by the Local Ethics Committee of Zhejiang Provincial People's Hospital. The patients/participants provided their written informed consent to participate in this study.

Author contributions

ZD and YL: work concept or design and make important revisions to the manuscript. LW: draft manuscript and data processing. QF: collect data. XG, FC, BY, BC, ZL, and BL: provide the measurement devices and review the manuscript. All authors contributed to the article and approved the final manuscript for publication.

Funding

This work was supported by grants from National Natural Science Foundation of China (No. 81871337), Natural Science Foundation of Zhejiang Province (Nos. Y22H185692 and LGJ22H180001), and Zhejiang Medical and Health Science and Technology Project (No. 2021KY249).

Conflict of interest

The authors declare that the research was conducted in the absence of any commercial or financial relationships that could be construed as a potential conflict of interest.

Publisher's note

Supplementary material

The Supplementary Material for this article can be found online at: https://www.frontiersin.org/articles/10.3389/fnins.2022.970245/full#supplementary-material

References

Alves, L., Cardoso, S., Silva, D., Mendes, T., Marôco, J., Nogueira, J., et al. (2021). Neuropsychological profile of amyloid-positive versus amyloid-negative amnestic mild cognitive impairment. *J. Neuropsychol.* 15(Suppl. 1), 41–52.

Braak, H., and Braak, E. (1997). Frequency of stages of Alzheimer-related lesions in different age categories. *Neurobiol. Aging* 18, 351–357. doi: 10.1016/s0197-4580(97)00056-0

Bradfield, N. I., Ellis, K. A., Savage, G., Maruff, P., Burnham, S., Darby, D., et al. (2018). Baseline amnestic severity predicts progression from amnestic mild cognitive impairment to Alzheimer disease dementia at 3 years. *Alzheimer Dis. Assoc. Disord.* 32, 190–196. doi: 10.1097/WAD.0000000000000252

Cai, S., Chong, T., Peng, Y., Shen, W., Li, J., von Deneen, K. M., et al. (2017). Altered functional brain networks in amnestic mild cognitive impairment: A resting-state fMRI study. *Brain Imaging Behav.* 11, 619–631. doi: 10.1007/s11682-016-9539-0

Cha, J., Hwang, J. M., Jo, H. J., Seo, S. W., Na, D. L., and Lee, J. M. (2015). Assessment of functional characteristics of amnestic mild cognitive impairment and Alzheimer's Disease using various methods of resting-state FMRI analysis. *Biomed. Res. Int.* 2015:907464. doi: 10.1155/2015/907464

Chao-Gan, Y., and Yu-Feng, Z. (2010). DPARSF: A MATLAB TOOLBOX for "Pipeline" data analysis of resting-state fMRI. *Front. Syst. Neurosci.* 4:13. doi: 10.3389/fnsys.2010.00013

Chawla, N. V., Bowyer, K. W., Hall, L. O., and Kegelmeyer, W. P. (2002). Smote: Synthetic minority over-sampling technique. *J. Artif. Intell. Res.* 16, 321–357.

Cooper, C., Sommerlad, A., Lyketsos, C. G., and Livingston, G. (2015). Modifiable predictors of dementia in mild cognitive impairment: A systematic review and meta-analysis. *Am. J. Psychiatry* 172, 323–334. doi: 10.1176/appi.ajp.2014.14070878

Curado, M., Escolano, F., Lozano, M. A., and Hancock, E. R. (2020). Early detection of Alzheimer's Disease: Detecting asymmetries with a return random walk link predictor. *Entropy* 22:465. doi: 10.3390/e22040465

Dachena, C., Casu, S., Fanti, A., Lodi, M. B., and Mazzarella, G. (2019). Combined use of mri, fmriand cognitive data for Alzheimer's disease: Preliminary results. *Appl. Sci.* 9:3156.

DeLong, E. R., DeLong, D. M., and Clarke-Pearson, D. L. (1988). Comparing the areas under two or more correlated receiver operating characteristic curves: A nonparametric approach. *Biometrics* 44, 837–845.

Ding, C., and Peng, H. (2005). Minimum redundancy feature selection from microarray gene expression data. *J. Bioinform. Comput. Biol.* 3, 185–205. doi: 10.1142/s0219720005001004

Elola, A., Aramendi, E., Irusta, U., Berve, P. O., and Wik, L. (2021). Multimodal algorithms for the classification of circulation states during out-of-hospital cardiac arrest. *IEEE Trans. Biomed. Eng.* 68, 1913–1922. doi: 10.1109/TBME.2020.3030216

Feng, F., Huang, W., Meng, Q., Hao, W., Yao, H., Zhou, B., et al. (2021). Altered volume and structural connectivity of the hippocampus in Alzheimer's Disease and amnestic mild cognitive impairment. *Front. Aging Neurosci.* 13:705030. doi: 10.3389/fnagi.2021.705030

Feng, Q., Niu, J., Wang, L., Pang, P., Wang, M., Liao, Z., et al. (2021). Comprehensive classification models based on amygdala radiomic features for Alzheimer's disease and mild cognitive impairment. *Brain Imaging Behav.* 15, 2377–2386. doi: 10.1007/s11682-020-00434-z

Feng, Q., Song, Q., Wang, M., Pang, P., Liao, Z., Jiang, H., et al. (2019). Hippocampus radiomic biomarkers for the diagnosis of amnestic mild cognitive impairment: A machine learning method. *Front. Aging Neurosci.* 11:323. doi: 10.3389/fnagi.2019.00323

Friston, K. J., Frith, C. D., Frackowiak, R. S., and Turner, R. (1995). Characterizing dynamic brain responses with fMRI: A multivariate approach. *Neuroimage* 2, 166–172. doi: 10.1006/nimg.1995.1019

Friston, K. J., Williams, S., Howard, R., Frackowiak, R. S., and Turner, R. (1996). Movement-related effects in fMRI time-series. *Magn. Reson. Med.* 35, 346–355. doi: 10.1002/mrm.1910350312

Ge, X., Wang, L., Pan, L., Ye, H., Zhu, X., Feng, Q., et al. (2022). Risk factors for unilateral trigeminal neuralgia based on machine learning. *Front. Neurol.* 13:862973. doi: 10.3389/fneur.2022.862973

Han, Y., Wang, J., Zhao, Z., Min, B., Lu, J., Li, K., et al. (2011). Frequency-dependent changes in the amplitude of low-frequency fluctuations in amnestic mild cognitive impairment: A resting-state fMRI study. *Neuroimage* 55, 287–295. doi: 10.1016/j.neuroimage.2010.11.059

Haralick, R. M., Shanmugam, K., and Dinstein, I. (1973). Textural features for image classification. *Stud. Media Commun.* 3, 610–621.

Iancu, R. I., Zara, A. D., Mirestean, C. C., and Iancu, D. (2021). Radiomics in head and neck cancers radiotherapy. Promises and Challenges. *Maedica* 16, 482–488. doi: 10.26574/maedica.2020.16.3.482

Jin, M., Pelak, V. S., Curran, T., Nandy, R. R., and Cordes, D. (2012). A preliminary study of functional abnormalities in aMCI subjects during different episodic memory tasks. *Magn. Reson. Imaging* 30, 459–470. doi: 10.1016/j.mri.2011.12.014

Katz, I., O'Brien, B., Clark, S., Thompson, C. T., Schapiro, B., Azzi, A., et al. (2021). Assessment of a diagnostic classification system for management of lesions to exclude melanoma. *JAMA Netw. Open* 4:e2134614. doi: 10.1001/jamanetworkopen.2021.34614

Khatri, U., and Kwon, G. R. (2022). Alzheimer's disease diagnosis and biomarker analysis using resting-state functional MRI functional brain network with multi-measures features and hippocampal subfield and amygdala volume of structural MRI. *Front. Aging Neurosci.* 14:818871. doi: 10.3389/fnagi.2022.818871

Knopman, D. S., Amieva, H., Petersen, R. C., Chételat, G., Holtzman, D. M., Hyman, B. T., et al. (2021). Alzheimer disease. *Nat. Rev. Dis. Primers* 7:33. doi: 10.1038/s41572-021-00269-y

Li, Z., Li, K., Luo, X., Zeng, Q., Zhao, S., Zhang, B., et al. (2020). Distinct brain functional impairment patterns between suspected Non-Alzheimer disease pathophysiology and Alzheimer's Disease: A study combining static and dynamic functional magnetic resonance imaging. *Front. Aging Neurosci.* 12:550664. doi: 10.3389/fnagi.2020.550664

Liao, W., Li, J., Ji, G. J., Wu, G. R., Long, Z., Xu, Q., et al. (2019). Endless fluctuations: Temporal dynamics of the amplitude of low frequency fluctuations. *IEEE Trans. Med. Imaging* 38, 2523–2532. doi: 10.1109/TMI.2019.2904555

Liu, L., Wang, T., Du, X., Zhang, X., Xue, C., Ma, Y., et al. (2022). Concurrent structural and functional patterns in patients with amnestic mild cognitive impairment. *Front. Aging Neurosci.* 14:838161. doi: 10.3389/fnagi.2022.838161

Liu, X., Wang, S., Zhang, X., Wang, Z., Tian, X., and He, Y. (2014). Abnormal amplitude of low-frequency fluctuations of intrinsic brain activity in Alzheimer's disease. *J. Alzheimers Dis.* 40, 387–397. doi: 10.3233/JAD-131322

Masters, C. L., Bateman, R., Blennow, K., Rowe, C. C., Sperling, R. A., and Cummings, J. L. (2015). Alzheimer's disease. *Nat. Rev. Dis. Primers* 1:15056.

McDade, E., and Bateman, R. J. (2017). Stop Alzheimer's before it starts. *Nature* 547, 153–155. doi: 10.1038/547153a

Murayama, N., Tagaya, H., Ota, K., Fujishiro, H., Manabe, Y., Sato, K., et al. (2013). Neuropsychological detection of the early stage of amnestic mild cognitive impairment without objective memory impairment. *Dement. Geriatr. Cogn. Disord.* 35, 98–105. doi: 10.1159/000346286

Park, Y. W., Choi, D., Park, M., Ahn, S. J., Ahn, S. S., Suh, S. H., et al. (2021). Predicting amyloid pathology in mild cognitive impairment using radiomics analysis of magnetic resonance imaging. *J. Alzheimers Dis.* 79, 483–491. doi: 10.3233/JAD-200734

Penny, W. D., Friston, K. J., Ashburner, J. T., Kiebel, S. J., and Nichols, T. E. (2011). *Statistical Parametric Mapping: The Analysis of Functional Brain Images*. Amsterdam: Elsevier.

Petersen, R. C., Aisen, P. S., Beckett, L. A., Donohue, M. C., Gamst, A. C., Harvey, D. J., et al. (2010). Alzheimer's Disease Neuroimaging Initiative (ADNI): Clinical characterization. *Neurology* 74, 201–209. doi: 10.1212/WNL.0b013e3181cb3e25

Pini, L., Pievani, M., Bocchetta, M., Altomare, D., Bosco, P., Cavedo, E., et al. (2016). Brain atrophy in Alzheimer's Disease and aging. *Ageing Res. Rev.* 30, 25–48. doi: 10.1016/j.arr.2016.01.002

Power, J. D., Schlaggar, B. L., and Petersen, S. E. (2015). Recent progress and outstanding issues in motion correction in resting state fMRI. *Neuroimage* 105, 536–551. doi: 10.1016/j.neuroimage.2014.10.044

Rajeesh, J., Moni, R. S., and Gopalakrishnan, T. (2017). Discrimination of Alzheimer's disease using hippocampus texture features from MRI. *Asian Biomed.* 6, 87–94.

Scheltens, P., De Strooper, B., Kivipelto, M., Holstege, H., Chételat, G., Teunissen, C. E., et al. (2021). Alzheimer's disease. *Lancet* 397, 1577–1590. doi: 10.1016/S0140-6736(20)32205-4

Sørensen, L., Igel, C., Liv Hansen, N., Osler, M., Lauritzen, M., Rostrup, E., et al. (2016). Early detection of Alzheimer's disease using MRI hippocampal texture. *Hum. Brain Mapp.* 37, 1148–1161.

Soria Lopez, J. A., González, H. M., and Léger, G. C. (2019). Alzheimer's disease. *Handb. Clin. Neurol.* 167, 231–255. doi: 10.1016/B978-0-12-804766-8.00013-3

Sperling, R. A., Aisen, P. S., Beckett, L. A., Bennett, D. A., Craft, S., Fagan, A. M., et al. (2011). Toward defining the preclinical stages of Alzheimer's disease: Recommendations from the National Institute on Aging-Alzheimer's Association workgroups on diagnostic guidelines for Alzheimer's disease. *Alzheimers Dement.* 7, 280–292. doi: 10.1016/j.jalz.2011.03.003

Stogmann, E., Moser, D., Klug, S., Gleiss, A., Auff, E., Dal-Bianco, P., et al. (2016). Activities of daily living and depressive symptoms in patients with subjective cognitive decline, mild cognitive impairment, and Alzheimer's Disease. *J. Alzheimers Dis.* 49, 1043–1050.

Sun, B. L., Li, W. W., Zhu, C., Jin, W. S., Zeng, F., Liu, Y. H., et al. (2018). Clinical research on Alzheimer's Disease: Progress and perspectives. *Neurosci. Bull.* 34, 1111–1118. doi: 10.1007/s12264-018-0249-z

Thyreau, B., Sato, K., Fukuda, H., and Taki, Y. (2018). Segmentation of the hippocampus by transferring algorithmic knowledge for large cohort processing. *Med. Image Anal.* 43, 214–228. doi: 10.1016/j.media.2017.11.004

Tibshirani, R. (2011). Regression shrinkage and selection via the lasso: A retrospective. *J. R. Stat. Soc. Ser. B* 73, 267–288.

Trojanowski, J. Q., Vandeerstichele, H., Korecka, M., Clark, C. M., Aisen, P. S., Petersen, R. C., et al. (2010). Update on the biomarker core of the Alzheimer's Disease Neuroimaging Initiative subjects. *Alzheimers Dement.* 6, 230–238. doi: 10.1016/j.jalz.2010.03.008

Wang, L., Feng, Q., Wang, M., Zhu, T., Yu, E., Niu, J., et al. (2021). An effective brain imaging biomarker for AD and aMCI: ALFF in slow-5 frequency band. *Curr. Alzheimer Res.* 18, 45–55. doi: 10.2174/1567205018666210324130502

Wang, Y., Zhao, X., Xu, S., Yu, L., Wang, L., Song, M., et al. (2015). Using regional homogeneity to reveal altered spontaneous activity in patients with mild cognitive impairment. *Biomed. Res. Int.* 2015:807093. doi: 10.1155/2015/807093

Weiner, M. W., Aisen, P. S., Jack, C. R. Jr., Jagust, W. J., Trojanowski, J. Q., Shaw, L., et al. (2010). The Alzheimer's disease neuroimaging initiative: Progress report and future plans. *Alzheimers Dement.* 6, 202–211.e7. doi: 10.1016/j.jalz.2010.03.007

Whitfield-Gabrieli, S., and Nieto-Castanon, A. (2012). Conn: A functional connectivity toolbox for correlated and anticorrelated brain networks. *Brain Connect.* 2, 125–141. doi: 10.1089/brain.2012.0073

Wu, H., Song, Y., Chen, S., Ge, H., Yan, Z., Qi, W., et al. (2022). An activation likelihood estimation meta-analysis of specific functional alterations in dorsal attention network in mild cognitive impairment. *Front. Neurosci.* 16:876568. doi: 10.3389/fnins.2022.876568

Xu, H., Lv, W., Feng, H., Du, D., Yuan, Q., Wang, Q., et al. (2020). Subregional radiomics analysis of PET/CT imaging with intratumor partitioning: Application to prognosis for nasopharyngeal carcinoma. *Mol. Imaging Biol.* 22, 1414–1426. doi: 10.1007/s11307-019-01439-x

Yan, C. G., Wang, X. D., Zuo, X. N., and Zang, Y. F. (2016). DPABI: Data processing & analysis for (Resting-State) brain imaging. *Neuroinformatics* 14, 339–351. doi: 10.1007/s12021-016-9299-4

Yang, L., Yan, Y., Wang, Y., Hu, X., Lu, J., Chan, P., et al. (2018). Gradual disturbances of the Amplitude of Low-Frequency Fluctuations (ALFF) and fractional ALFF in alzheimer spectrum. *Front. Neurosci.* 12:975. doi: 10.3389/fnins.2018.00975

Yuan, Q., Qi, W., Xue, C., Ge, H., Hu, G., Chen, S., et al. (2021). Convergent functional changes of default mode network in mild cognitive impairment using activation likelihood estimation. *Front. Aging Neurosci.* 13:708687. doi: 10.3389/fnagi.2021.708687

Zang, Y. F., He, Y., Zhu, C. Z., Cao, Q. J., Sui, M. Q., Liang, M., et al. (2007). Altered baseline brain activity in children with ADHD revealed by resting-state functional MRI. *Brain Dev.* 29, 83–91. doi: 10.1016/j.braindev.2006.07.002

Zang, Y., Jiang, T., Lu, Y., He, Y., and Tian, L. (2004). Regional homogeneity approach to fmri data analysis. *Neuroimage* 22, 394–400.

Zhang, J., Yu, C., Jiang, G., Liu, W., and Tong, L. (2012). 3D texture analysis on MRI images of Alzheimer's disease. *Brain Imaging behav.* 6, 61–69. doi: 10.1007/s11682-011-9142-3

Zhao, K., Ding, Y., Han, Y., Fan, Y., Alexander-Bloch, A., Han, T., et al. (2020). Independent and reproducible hippocampal radiomic biomarkers for multisite Alzheimer's disease: Diagnosis, longitudinal progress and biological basis. *Sci. Bull.* 65, 1103–1113.

Zheng, B. H., Liu, L. Z., Zhang, Z. Z., Shi, J. Y., Dong, L. Q., Tian, L. Y., et al. (2018). Radiomics score: A potential prognostic imaging feature for postoperative survival of solitary HCC patients. *BMC Cancer* 18:1148. doi: 10.1186/s12885-018-5024-z

Zuo, X. N., Di Martino, A., Kelly, C., Shehzad, Z. E., Gee, D. G., Klein, D. F., et al. (2010). The oscillating brain: Complex and reliable. *Neuroimage* 49, 1432–1445. doi: 10.1016/j.neuroimage.2009.09.037

Zwanenburg, A., Vallières, M., Abdalah, M. A., Aerts, H., Andrearczyk, V., Apte, A., et al. (2020). The image biomarker standardization initiative: Standardized quantitative radiomics for high-throughput image-based phenotyping. *Radiology* 295, 328–338. doi: 10.1148/radiol.2020191145

frontiers | Frontiers in Neuroscience

TYPE Original Research
PUBLISHED 09 August 2022
DOI 10.3389/fnins.2022.942136

OPEN ACCESS

EDITED BY
Roberto Esposito,
ASUR Marche, Italy

REVIEWED BY
Dominik Kraft,
University Hospital Tübingen, Germany
Hsiao-ju Cheng,
ETH Zürich, Singapore

*CORRESPONDENCE
Silvia Fanton
silvia.fanton@ki.se

SPECIALTY SECTION
This article was submitted to Brain Imaging Methods, a section of the journal Frontiers in Neuroscience

RECEIVED 12 May 2022
ACCEPTED 06 July 2022
PUBLISHED 09 August 2022

CITATION
Fanton S, Altawil R, Ellerbrock I, Lampa J, Kosek E, Fransson P and Thompson WH (2022) Multiple spatial scale mapping of time-resolved brain network reconfiguration during evoked pain in patients with rheumatoid arthritis. *Front. Neurosci.* 16:942136. doi: 10.3389/fnins.2022.942136

Multiple spatial scale mapping of time-resolved brain network reconfiguration during evoked pain in patients with rheumatoid arthritis

Silvia Fanton[1,2]*, Reem Altawil[3], Isabel Ellerbrock[1,2], Jon Lampa[3], Eva Kosek[1,2,4], Peter Fransson[1,2] and William H. Thompson[1,5]

[1]Department of Clinical Neuroscience, Karolinska Institutet, Stockholm, Sweden, [2]Department of Neuroradiology, Karolinska University Hospital, Stockholm, Sweden, [3]Rheumatology Unit, Department of Medicine, Center for Molecular Medicine, Karolinska Institutet, Karolinska University Hospital, Stockholm, Sweden, [4]Department of Surgical Sciences, Uppsala University, Uppsala, Sweden, [5]Division of Cognition and Communication, Department of Applied IT, University of Gothenburg, Gothenburg, Sweden

Functional brain networks and the perception of pain can fluctuate over time. However, how the time-dependent reconfiguration of functional brain networks contributes to chronic pain remains largely unexplained. Here, we explored time-varying changes in brain network integration and segregation during pain over a disease-affected area (joint) compared to a neutral site (thumbnail) in 28 patients with rheumatoid arthritis (RA) in comparison with 22 healthy controls (HC). During functional magnetic resonance imaging, all subjects received individually calibrated pain pressures corresponding to visual analog scale 50 mm at joint and thumbnail. We implemented a novel approach to track changes of task-based network connectivity over time. Within this framework, we quantified measures of integration (participation coefficient, PC) and segregation (within-module degree *z*-score). Using these network measures at multiple spatial scales, both at the level of single nodes (brain regions) and communities (clusters of nodes), we found that PC at the community level was generally higher in RA patients compared to HC during and after painful pressure over the inflamed joint and corresponding site in HC. This shows that all brain communities integrate more in RA patients than in HC for time points following painful stimulation to a disease-relevant body site. However, the elevated community-related integration seen in patients appeared to not pertain uniquely to painful stimulation at the inflamed joint, but also at the neutral thumbnail, as integration and segregation at the community level did not differ across body sites in patients. Moreover, there was no

specific nodal contribution to brain network integration or segregation. Altogether, our findings indicate widespread and persistent changes in network interaction in RA patients compared to HC in response to painful stimulation.

KEYWORDS

fMRI, brain networks, time-varying functional connectivity, temporal network theory, chronic pain, rheumatoid arthritis

Introduction

Alterations in the functional connectivity between brain regions have been reported in patients with chronic pain (Napadow et al., 2010; Tagliazucchi et al., 2010; Hemington et al., 2016), bringing factual contribution to the consideration of chronic pain as a condition that can be studied and understood from a brain network modeling perspective (Apkarian et al., 2009; Mano et al., 2018).

Within this framework, recent advances have been made in the identification of an objective biomarker of chronic pain. Notably, a recent study provided evidence for a neuroimaging marker for tonic experimental pain predicting sustained clinical pain (Lee et al., 2021). An interesting feature of this biomarker signature is its largely distributed network-level representation of the sustained pain state (Lee et al., 2021). Yet recently, the organization of networks in the brain was proposed as potential biomarker and further investigated, specifically, as the assignment of nodes (brain regions) to different communities (clusters of nodes) in the whole-network (brain) (Larkin et al., 2021) and via the examination of brain hub topology (Kaplan et al., 2019). Interestingly, the hub topology was altered (Kaplan et al., 2019) and the allocation of nodes in communities more variable (Larkin et al., 2021) in chronic pain patients compared to healthy controls (HC), providing knowledge into both the local and global functional resting-state network architecture of chronic pain patients (Larkin et al., 2021).

Variables obtained from modeling functional magnetic resonance imaging (fMRI) data in the context of time-varying brain networks may act as more sensitive markers of acute and chronic pain, given the dynamic nature of pain and the brain itself. Specifically, there is evidence to suggest that the organization of brain networks fluctuates between states of integration and segregation (Shine et al., 2016) and, within a time-varying functional connectivity (TVC) framework, these measures have been proven to be critical in understanding cognition (Cohen and D'Esposito, 2016; Shine et al., 2016; Fransson et al., 2018).

However, the application of integration and segregation measures to the investigation of pain-related patterns of network reconfiguration is still in its infancy. Recent work from our group assessed TVC changes in network integration/segregation in HC during thermal pain, showing increased brain network integration with increased pain (Kastrati et al., 2022). To add specificity to the investigation of pain processing in chronic pain patients, we used TVC to explore changes in brain network integration and segregation that are time-locked to pressure pain stimulations over a disease-affected body site (i.e., inflamed joint) and a neutral body part (i.e., thumbnail) in chronic pain patients with rheumatoid arthritis (RA) compared to HC. Notably, pain pressure stimuli were individually calibrated across both groups and sites. When comparing the same cohort of RA patients and HC, previous work from our group showed: (1) increased intrinsic, static FC between bilateral sensorimotor and frontal midline brain regions in patients compared to HC (Flodin et al., 2016), (2) reduced activation in brain regions associated to the processing of pain and somatosensory information in patients compared to HC when painful stimulation is delivered to the joint, and not to the thumb (Sandström et al., 2019). When comparing body sites within patients, Sandström et al. (2019) showed that abnormalities in cerebral pain processing in patients were confined uniquely to the joint (i.e., the disease-affected site) and not generalizable to the thumb (i.e., the neutral area), with patients exhibiting a reduced activation in somatosensory and pain processing regions as well as in coupled right and left dorsolateral prefrontal cortex.

Based on these premises, the objective of the present work was to determine whether and how the degree of change in integration and segregation between network communities and nodes varies over time and is putatively influenced by pressure pain stimuli across groups and stimulation sites in patients. This might add more specificity to the understanding of cerebral pain processing mechanisms in patients with RA.

Materials and methods

Participants and study description

The dataset used in the current study has previously been described in Flodin et al. (2016) and in Sandström et al. (2019).

A detailed account of participants and information regarding exclusion and inclusion criteria can be found in Sandström et al. (2019). Participants underwent two testing sessions, on two consecutive days. Of relevance to the current study, on day 1, sensitivity to evoked pressure pain was individually calibrated and, on day 2, the individually calibrated painful pressure and a non-painful pressure were delivered during four runs of a functional magnetic resonance imaging (fMRI) pressure pain paradigm. fMRI data (covering the whole brain) from a total of 28 RA patients and 22 HC were included in the analysis (mean age RA patients = 53.64 years; mean age HC = 52.86 years; age range = 23–72 years). The minor difference in the total number of subjects included in this study compared to Sandström et al. (2019) is due to the need to adhere to a specific pipeline tailored to time-resolved fMRI data. All participants gave written informed consent in accordance with the Declaration of Helsinki. The local ethical review board approved the research.

Experimental procedure

The present study forms part of a larger project (referred to as the PARADE study; https://www.clinicaltrials.gov; [identifier NCT01197144, EudraCT 2009-017163-42]). Previously, we have reported differences in spontaneous brain activation patterns (Flodin et al., 2016) and brain activity recorded after painful stimuli delivered to a disease-affected finger joint as well as to the non-affected thumbnail area (Sandström et al., 2019). In this work, we use time-varying functional connectivity (TVC), which allows for a time point-by-time point assessment of changes in brain network activity related to pain. Therefore, the methodological section in this paper is focused on the procedure used for assessing TVC.

Day 1: Individual calibration of pressure pain

One day prior to fMRI scanning, the degree of pain pressures to be used during scanning was subjectively calibrated. Pain sensitivity was assessed by applying pressure to the patient's clinically most affected proximal interphalangeal (PIP) joint (PIP2 n = 21; PIP3 n = 7) of the left hand and to the non-affected, left thumbnail via an automated, pneumatic, computer-controlled stimulator with a 1 cm^2-hard rubber probe (Jensen et al., 2009). Corresponding anatomical sites were used in HC (PIP2 n = 21; PIP3 n = 1). Each participant first received a series of stimuli with a step-wise increase in pressure, then followed by a series of stimuli that had a randomized order of different pressure. The pressure stimuli, in both series, were delivered for a duration of 2.5 s and with 30 s inter-stimulus intervals. After each stimulus, participants were prompted to rate pain intensity on a 0–100 mm visual analog scale (VAS), ranging from "no pain" to "worst imaginable pain." Stimuli in the ascending series were presented in increasing pressure steps of 50 kPa, which led to the identification of each participant's pressure pain threshold (PPT, first VAS rating > 0 mm) and stimulation maximum (SM, first VAS rating > 60 mm). It is within this subjectively calibrated range of PPT and SM that five pressure pain intensities were obtained and delivered, each three times, in a randomized series. A polynomial regression was applied to the 15 VAS ratings from the randomized series and, consequently, used to determine each subjective representation of VAS 50 mm (referred to as P50). Please refer to Jensen et al. (2009) for further details regarding the calibration procedure.

Day 2: Functional magnetic resonance imaging pressure pain paradigm

The subjectively calibrated painful pressure (P50) obtained from day 1 and a standard non-painful pressure (50 kPA) were presented during four pseudo-randomized fMRI runs. Two of the four fMRI runs contained stimuli that were delivered to the most affected joint in patients (equivalent anatomical site in HC), while the remaining two fMRI runs included stimuli applied to the thumbnail. Each run consisted of a total of 30 pressure stimuli events (15 painful and 15 non-painful) presented in a pseudo-randomized fashion. The duration of each stimulus was 2.5 s and all stimuli onsets were jittered over time with a mean interval of 15 s (range 10–20 s) to ensure a fine-grained sampling of the events. The total duration for all runs was 8 min and 15 s. All participants were instructed, prior to scanning, to concentrate on the pressures delivered to joint and thumbnail and to refrain from invoking coping strategies. No pain ratings were collected during the course of the fMRI runs.

Functional magnetic resonance imaging data acquisition and pre-processing

MRI data were acquired on a 3T General Electric 750 MR scanner installed at the MR Research Center at Karolinska Institutet (Stockholm) using a 32-channel head coil. Four task-based fMRI scans, each consisting of 160 volumes, were acquired for each subject using a T2*-weighted single-shot gradient echo planar sequence (TR/TE = 3000/30 ms; 90° flip angle; 96 × 96 matrix size; FOV = 288 × 288 mm; 56 slices; in-plane resolution = 2.5 × 2.5 mm; slice thickness = 3 mm, interleaved slice acquisition). Anatomical MRI data were obtained using a high-resolution T1-weighted image sequence (3D BRAVO; TR/TE = 7908/3.06 ms; 1 × 1 × 1 mm voxel size; 176 slices). Additionally, T2-weighted images were acquired and assessed for clinical abnormalities by a neuroradiologist.

The pre-processing of anatomical and functional data was performed using fMRIPrep (pre-processing pipeline, version 20.1.1, Esteban et al., 2019). A detailed description of all the pre-processing steps can be found in the **Supplementary material**.

Analysis pipeline for time-varying functional connectivity

All TVC analyses reported below (parcellation, denoising, deriving TVC estimates, quantifying network measures of participation coefficient and within-module degree z-score) were carried out using teneto (version 0.5.3), a Python package for temporal network analysis (Thompson et al., 2017a)[1]. Please refer to **Figure 1** for a schematic representation of the TVC analysis steps undertaken in this work. The code used to set up the teneto pipeline and to produce figures is available at https://github.com/silviafan/TVC-RA.

Parcellation and functional magnetic resonance imaging data denoising

The BOLD signal time-series from the pre-processed fMRI data were extracted from brain areas defined using the 7-network (community), 400-node Schaefer parcellation scheme (Yeo et al., 2011; Schaefer et al., 2018). Subsequent to the parcellation step, functional fMRI data underwent denoising, with the following confounds being regressed out: six head motion parameters and their respective derivatives, the first six noise anatomical parameters derived from CompCor (Behzadi et al., 2007), framewise displacement (FD, Power et al., 2014), white matter, and cerebrospinal fluid. Additionally, we employed the criteria that fMRI runs that had a mean FD > 0.5 were to be discarded from the analyses. No fMRI run met this exclusion criteria.

Deriving parameter estimates for time-varying functional connectivity

The time-varying changes in functional connectivity were estimated via the application of the jackknife correlation (JC) method (Richter et al., 2015). When applied to TVC, the JC method calculates the Pearson's correlations between two BOLD time-series x and y over all the individual time points, excluding data at time point t, and then multiplies the resulting correlation value by –1 (Thompson et al., 2018).

$$JC_t = -\left(\frac{\sum_i^T (x_{i-} - \bar{x}_t)(y_{i-} - \bar{y}_t)}{\sum_i^T (x_{i-} - \bar{x}_t)^2 \sum_i^T (y_{i-} - \bar{y}_t)^2}\right) \qquad i \neq t$$

This application of the JC method to compute time-varying functional connectivity was first introduced by Thompson et al. (2017b). Importantly, it has been previously shown that the JC method is more sensitive to quicker temporal changes in covariance compared to other methods (Thompson et al., 2018; Xie et al., 2019). Here, JC values were standardized to have mean of 0 and standard deviation of 1 creating flow TVC estimates (Fransson and Thompson, 2020). Note that the JC method provides time point-by-time point estimates of pairwise functional brain connectivity.

Quantifying time-varying parameters of community integration and segregation

To answer the question of how the degree of integration and segregation of the seven pre-defined communities and six chosen nodes changes over time and is putatively influenced by painful stimulation to the joint across groups and based on the stimulation site, we chose to include network measures that have been previously shown to be informative and relevant for other *qualia* (Cohen and D'Esposito, 2016; Shine et al., 2016), although never before used in the context of chronic pain.

First, we calculated the participation coefficient (PC), a network metrics that quantifies the degree to which specific nodes communicate across communities (Guimerà and Nunes Amaral, 2005). As described in Guimerà and Nunes Amaral (2005), PC is:

$$P_i = 1 - \sum_{s=1}^{N_M} \left(\frac{k_{is}}{k_i}\right)^2$$

Where i = node, s = index of community (N_M), k_{is} = degree of links within each community, k_i = total degree of i. In the computation of PC values, only positive edges were included in the analysis. Next, we computed the within-module degree z-score (z), a network metrics that measures the extent to which specific nodes communicate within their own communities (Guimerà and Nunes Amaral, 2005). As described in Guimerà and Nunes Amaral (2005), z is:

$$z_i = \frac{k_i - \bar{k}_{s_i}}{\sigma_{k_{s_i}}}$$

Where i = node, k_i = degree of links of i to other nodes in its community s_i, $\bar{k}_{s_i}$ = average of k across nodes in community s_i, $\sigma_{k_{s_i}}$ = standard deviation of k in community s_i.

For all analyses, we used the same static parcellation for all time points (Thompson et al., 2020). Taken together, these two measures provide insights into the integration (PC) and segregation (z) of nodes in the whole network.

After computing PC and z for all nodes, integration and segregation were assessed both at community level (i.e., measures per community) and nodal level (i.e., measures per node). The idea was to probe brain network organization at multiple spatial scales (Sporns, 2015), by capturing the temporal dynamics of pain processing in the whole-brain (community level) and at the level of single pain-related brain regions (nodal level).

On the community level, the median PC or z of all nodes within each community was calculated. Note, while the mean of z is always 0 for each community, the median denotes if the majority of edges are skewed below or above the mean, making the different community distributions comparable regarding

1 https://github.com/wiheto/teneto

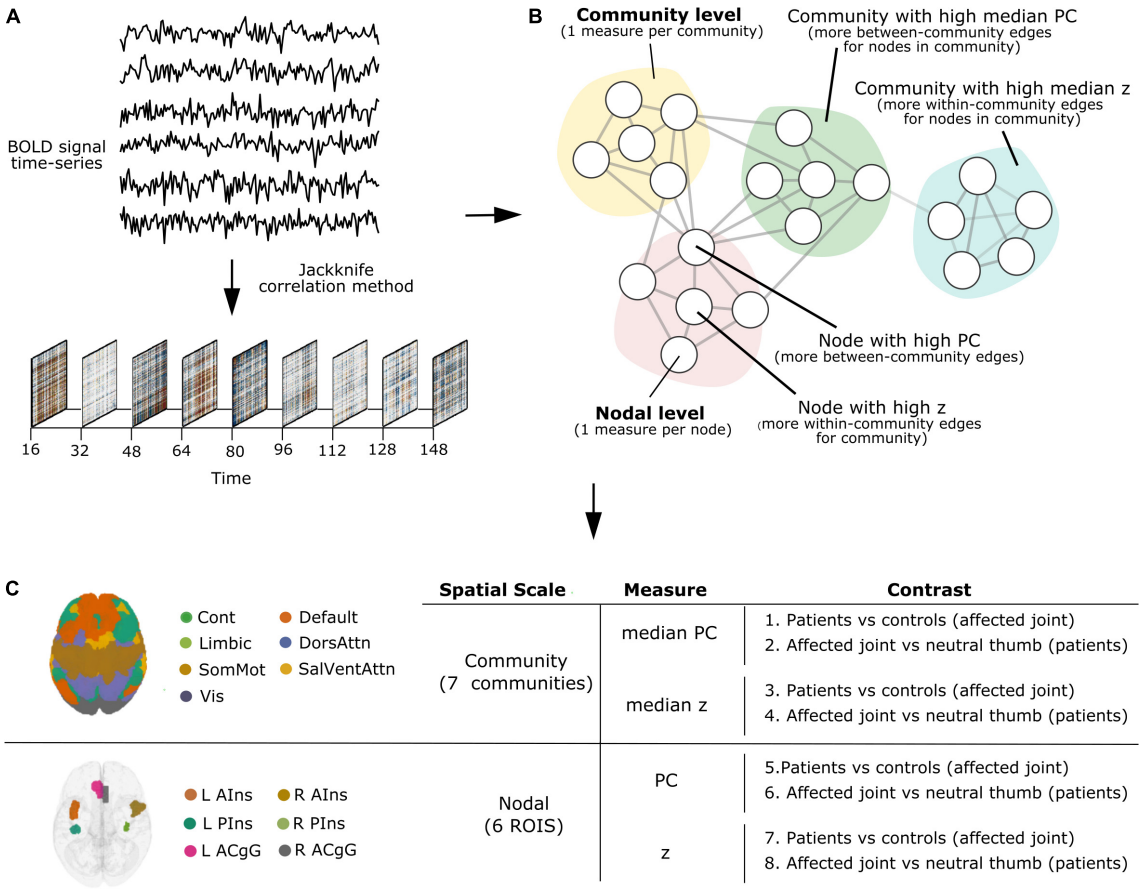

FIGURE 1
A schematic representation of the time-varying functional connectivity (TVC) analysis steps undertaken in this work. **(A)** BOLD signal time-series were extracted from brain regions defined using the 7-network, 400-node Schaefer parcellation scheme (Yeo et al., 2011; Schaefer et al., 2018) and TVC was computed at the level of single time points using the jackknife correlation method (Richter et al., 2015). **(B)** Measures of integration (participation coefficient, PC) and segregation (within-module degree *z*-score, *z*) were quantified and used at the level of single nodes (brain areas, nodal level) and communities (clusters of nodes, community level). **(C)** Analyses were carried out at the community and nodal level, separately. Within each level, we examined how the degree of integration (PC) and segregation (*z*) varies over time and whether this is influenced by painful stimulation to the joint across groups (Contrasts 1, 3, 5, 7) and based on the stimulation site in patients (Contrasts 2, 4, 6, 8).

how the community as a whole is tightly connected. Thus, the median PC or *z* can be interpreted as the degree of *integration* or *segregation* a community as a whole has with respect to the other communities in the whole network. For example, as illustrated in **Figure 1B**, a community with high median PC has more *between-community* edges for nodes in the community (*integration* on the community level), whereas a community with high median *z* has more *within-community* edges for nodes in the community (*segregation* on the community level).

On the nodal level, node selection was informed by overlapping (performed in MRIcron[2]) the brain activation map produced by entering the text query "chronic pain" into NeuroQuery, a recently developed tool for comprehensive meta-analysis of the neuroimaging literature (Dockès et al., 2020), onto the 7-network, 400-node Schaefer parcellation (Yeo et al., 2011; Schaefer et al., 2018). This procedure resulted in the selection of six brain areas (nodes): left anterior insula (L AIns), right anterior insula (R AIns), left posterior insula (L PIns), right posterior insula (R PIns), L anterior cingulate gyrus (L ACgG), and right anterior cingulate gyrus (R ACgG). Please refer to **Figure 2** for a representation of the selected nodes and to **Supplementary Table 1** for their identification by templateflow index (Ciric et al., 2021). Obviously, this approach necessitated some degree of subjectivity in terms of the selection of nodes to include but was, nevertheless, undertaken for the purpose of all results (community and nodal level-related results) to be aligned within the same whole-brain parcellation. The PC or z score for each single node can be defined as the degree of *integration* or *segregation* a node has with respect to the other nodes in the whole network. For example, as illustrated in **Figure 1B**, a node with high PC has more *between-community* edges (*integration*

2 https://www.nitrc.org/projects/mricron

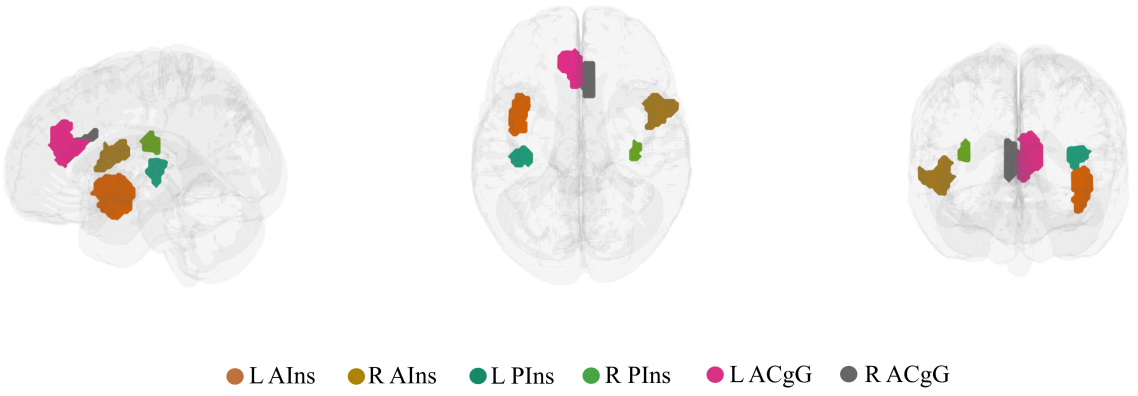

FIGURE 2
The six brain nodes selected to represent key chronic pain brain regions shown in a lateral, superior, and anterior brain view. L AIns, left anterior insula; R AIns, right anterior insula; L PIns, left posterior insula; R PIns, right posterior insula; L ACgG, left anterior cingulate gyrus; R ACgG, right anterior cingulate gyrus.

on the nodal level), whereas a node with high z has more *within-community* edges for the community (*segregation* on the nodal level).

In order to account for the temporal profile of brain connectivity across the two spatial scales (community and nodal), the 160 time point data series were broken down into 6 event-related bins, with bins representing the onset TR when the stimulation was being delivered and until –2 TR pre- and + 3 TR after-stimulus onset, each averaged across participants. This binning partition served as an indicator for the time-varying changes in functional connectivity occurring before, during, and after participants received the painful stimulation.

Statistical analyses

All analyses were carried out using Python version 3.7.2 and were performed: (1) separately for each community and nodal level, (2) only for painful stimuli, (3) by averaging together the two joint or the two thumb runs, respectively, and (4) by focusing only on onset and after-onset time points, each treated separately. Pre-onset time points were not included in the analyses, as the pain pressure task used in the study had not been designed to capture the cerebral processing involved in anticipating pain. However, these pre-onset time points were nonetheless plotted in the graphs, for completeness. Statistical significance was set, conventionally, at $p < 0.05$, false discovery rate (FDR) corrected for multiple comparisons.

Group differences in integration and segregation at nodal and community level for painful stimulation of the joint

A one-way analysis of covariance (ANCOVA) test was performed using the *ols* function in the Python *statsmodels* library (Seabold and Perktold, 2010) to test for differences across groups in the degree of change in integration and segregation over time at the community and nodal level in response to painful stimulation of the affected joint in patients compared to the corresponding site in HC (Contrasts 1, 3, 5, and 7 in **Figure 1C**). In the model, the network metric under investigation (PC, *z*) was used as dependent variable, the group variable was treated as independent variable with two levels (RA, HC), and age was used as a covariate. Despite the unbalanced design, Type II Sum of Squares was used, as proposed by Langsrud (2003).

Differences in integration and segregation at nodal and community level for painful stimulation of the joint compared to thumb in patients

Differences in the degree of change in integration and segregation over time at the community and nodal level in response to painful stimulation of the affected joint compared to the neutral thumb in patients (Contrasts 2, 4, 6, and 8 in **Figure 1C**) were tested by performing a linear mixed-effects model with the *statsmodels* implementation (MixedLM). The variable "site" (joint, thumb) was entered into the model as fixed effect while controlling for age. A random intercept for each subject and, by default, for each site (joint, thumb) were also introduced to account for the variability of subjects and sites (joint, thumb) at baseline. The model was adjusted, also by default, by the Restricted Maximum Likelihood Estimation and the Powell optimization method was used for model fitting.

Brain plots were generated using *netplotbrain* (Thompson and Fanton, 2021[3]).

3 https://github.com/wiheto/netplotbrain

Results

Painful stimulation of the joint induces higher community-wide integration, but no difference in segregation, in patients compared to controls

First, we investigated the degree of change over time in integration (participation coefficient, PC) and segregation (within-module degree *z*-score, *z*) at the community level across groups when pain was delivered to the diseased joint and corresponding site in HC (Contrasts 1 and 3 in Figure 1C). Here, PC was found to be generally higher in patients, compared to HC, in all brain communities and for some time points (Table 1 and Figure 3A). However, groups (patients and HC) did not differ in the degree of community-related segregation (*z*) change over time (Figure 3B and Supplementary Table 2).

No significant group difference in node-related integration or segregation for painful stimulation of the joint

Next, we analyzed the degree of change over time in integration (participation coefficient, PC) and segregation (within-module degree *z*-score, *z*) at the nodal level across groups when pain was delivered to the diseased joint and corresponding site in HC (Contrasts 5 and 7 in Figure 1C). Contrarily to integration at the community level, groups did not differ in node-related integration (Supplementary Figure 1A and Supplementary Table 3) nor segregation (Supplementary Figure 1B and Supplementary Table 4) over time.

No significant difference in integration and segregation at nodal and community level due to the different stimulation site (joint vs. thumb) in patients

Lastly, we examined the degree of change over time in integration (participation coefficient, PC) and segregation (within-module degree *z*-score, *z*) at the community and nodal level in patients when pain was delivered to the diseased joint compared to the neutral thumb (Contrasts 2, 4, 6, and 8). None of the analyses showed any significant degree of change (Supplementary Figures 2, 3 and Supplementary Tables 5–8).

Discussion

The present study capitalized on previously analyzed fMRI data in order to detail the temporal profile of cerebral pain processing in patients with RA, with the final objective to track pain-related patterns of network reconfiguration at the resolution of single data time points.

A major finding of this work is that the participation coefficient was generally higher in RA patients compared to HC during and following pressure pain over the inflamed joint compared to the corresponding site in HC. This result shows that all brain communities integrate to a relatively higher degree in patients than in HC during some, but not all, time points when painful stimulation is delivered to the disease-relevant body site (Figure 3A). Interestingly, our finding of increased community-level integration is in accordance with previous research on pain and cognition, with the latter being a critical component contributing to the multi-dimensionality of pain experience. Regarding pain research, recent work has shown that: (1) in HC, there is elevated integration of brain networks in the presence of more intense pain (Kastrati et al., 2022), (2) a tonic pain model, capable of predicting experimental and clinical sustained low back pain, provides evidence for

TABLE 1 Results from the analysis of covariance (ANCOVA) computed at the community level on participation coefficient (PC) values per time point across groups (patients and controls) when pain was delivered to the diseased joint in patients and corresponding site in controls.

	PC											
	0			+1			+2			+3		
	F	*p*	FDR p	*F*	*p*	FDR p	*F*	*p*	FDR p	*F*	*p*	FDR p
Cont	7.218	0.010	**0.038**	2.997	0.090	0.120	5.157	0.028	**0.043**	1.760	1.191	0.216
Default	0.567	0.455	0.455	5.047	0.029	**0.043**	5.188	0.027	**0.043**	1.084	0.303	0.317
DorsAttn	9.614	0.003	**0.023**	5.246	0.027	**0.043**	6.192	0.016	**0.038**	11.281	0.002	**0.022**
Limbic	1.742	0.194	0.216	6.169	0.017	**0.038**	1.071	0.306	0.317	5.207	0.027	**0.043**
SalVentAttn	8.593	0.005	**0.029**	6.261	0.016	**0.038**	6.627	0.013	**0.038**	6.139	0.017	**0.038**
SomMot	10.007	0.003	**0.023**	6.057	0.018	**0.038**	2.688	0.108	0.131	13.114	0.001	**0.020**
Vis	4.215	0.046	0.064	5.254	0.026	**0.043**	2.756	0.104	0.131	6.545	0.014	**0.038**

Time points are indicated as 0, +1, +2, +3 and represent, respectively, the onset TR (TR = 3 s) of painful stimulation, and +1, +2, and +3 TR after-stimulation. False discovery rate (FDR) corrected p-values, significant at the conventional $p < 0.05$, are presented in bold.

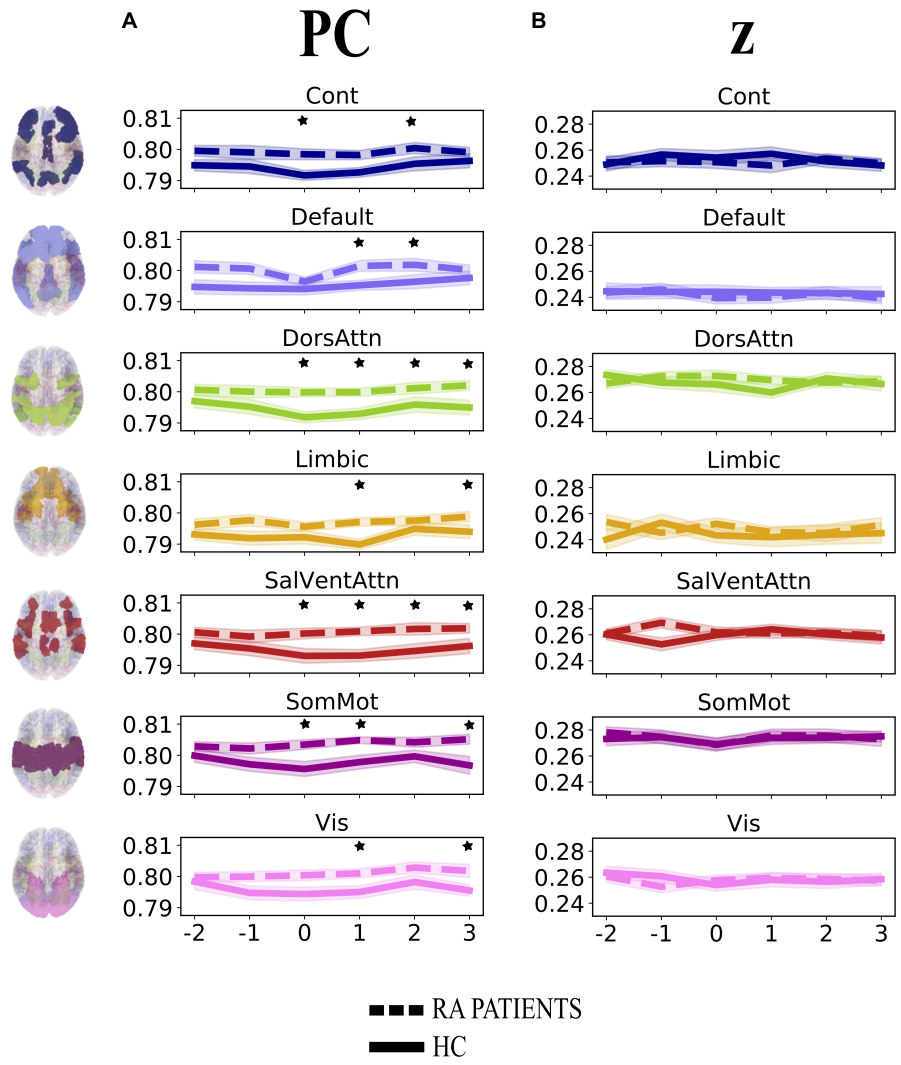

FIGURE 3
Degree of change in community-related integration **(A)** and segregation **(B)** per time point for rheumatoid arthritis (RA) patients and healthy controls (HC), when pain was delivered to the diseased joint and corresponding site in HC. Displayed are the average parameter values (PC, *z*) over trials per time point. Time points are indicated as −2, −1, 0, +1, +2, +3 on the *x*-axis, with 0 representing the onset TR (TR = 3 s) of painful stimulation, −2 and −1 being the two TR pre-stimulation, whereas + 1, +2, and +3 the three TR after-stimulation. The brain plots on the left side of the figure represent each of the seven Yeo communities (Yeo et al., 2011). The shaded areas contouring the lines represent the standard error of the mean. The stars represent time points that differed significantly ($p < 0.05$, FDR corrected) between groups. PC, participation coefficient; *z*, within-module degree *z*-score; RA, rheumatoid arthritis; HC, healthy controls.

the involvement of a number of highly distributed brain networks during a sustained pain state (Lee et al., 2021), and (3) the experience of pain is supported by comprehensive multi-network interactions (Geuter et al., 2020). Regarding the cognitive aspect, several studies have shown an increase in or shift to a state of higher integration between brain networks during the execution of demanding cognitive tasks (Cohen and D'Esposito, 2016; Fransson et al., 2018). That being said, in our work, the observation of an up-ramped degree of integration among the canonical resting-state networks as defined in the Schaefer atlas during and after painful stimulation of the clinically affected area might be responsible for an overly energetically demanding experience for the brain. Indeed, although the brain has long been regarded as a complex system where integration plays a key and decisive role (Tononi, 1998), interactions between communities are costly to maintain, thus occur in alternation with more highly modular periods (Liégeois et al., 2016). Importantly, Shine et al. (2016) have shown that states of integration allow for a more effective and faster processing of information during task execution. However, with reference to our finding and on a speculative note, in the presence of painful information, a sustained state of whole-brain integration, without intermitting segregation, might accelerate the propagation of recursive

noxious information. Consequently, this might lead to the exacerbation of pain experience and, in turn, contribute to pain chronicity in patients. Further, though this state of higher integration in patients compared to HC concerns all brain communities, it distributes differently over time (see **Table 1** and **Figure 3A**). Indeed, the higher integration seen in patients features onset and all after-onset time points in, specifically, DorsAttn and SalVentAttn communities. As for the other tested resting-state networks, group differences were less "durable." A plausible, although speculative, explanation might be that the salience network seems to be relevant in regulating the functional changes of other networks dynamically (Bonnelle et al., 2012), as also pointed out in Borsook et al. (2013), and has been shown to be associated with attention networks, given the dependency between saliency and attention (Menon and Uddin, 2010; Uddin, 2015). Thus, on a speculative level, it might be that the constant high integration of the SalVentAttn and DorsAttn communities is coordinating the functional role of the other communities, thus reducing their integration at times to favor the required high-level attention to salient, painful stimuli. This finding might indicate that the brain of patients enters a state of persistent high integration, not allowing the brain to be in a more modular state at any time. Possibly, this might be a contributing factor to the cognitive fatigue affecting chronic pain patients and, relevant to this work, patients with RA (Nikolaus et al., 2013).

When exploring whether this maladaptive brain network configuration in patients was specific to when pain was delivered to the inflamed joint or also to the non-clinically relevant thumb, our results pointed to the latter. Indeed, there was no difference in community-related integration over time across body sites (**Supplementary Figure 2A**), which might be interpreted as elevated integration not uniquely pertaining to the inflamed area, but also to an area that appears "neutral" when the peripheral nervous system is the focus. Thus, this might be indicative of patients having a more generalized and unspecific cerebral response to pain, unbound to the clinical relevance of the stimulation site. This finding seems to be in conflict, at first, with previous work published from our group, in which it was shown that patients had lower pain-related cerebral activation in response to painful stimulation at the joint compared to the thumb (Sandström et al., 2019). However, it is not surprising that a finding reporting task-evoked BOLD response lacks direct translation into a task-based TVC context. Indeed, although specific to the default mode network and its regions, it has been previously demonstrated that, for example, task-related negative BOLD signal does not affect the temporal profile of task-related FC networks (Razlighi, 2018), thus in accordance with the disagreement in our previous (Sandström et al., 2019) and current results.

Shifting focus from the organization of communities to the role of single nodes in the whole network, all our results indicate that there is no contribution from the six selected network nodes to brain network integration or segregation, neither during pain to joint across groups, nor during pain to joint compared to thumb within patients only (**Supplementary Figures 1**, **3**). This might indicate that the community level may be more informative than the nodal level in terms of revealing potential differences in cerebral pain processing between patients and HC. However, the lack of significant results at the nodal level might be due to the fact that the *robustness* of the measures applied at the nodal level might have been more easily affected by the high number of multiple comparisons. While for PC and z at the community level, we computed the median of all nodes within each community, for PC and z at the nodal level, we considered single nodes among the 400 nodes generated by the Schaefer 400 node x 7 network parcellation. Further, we note that, as also discussed by Kastrati et al. (2022), brain communities were regarded as static clusters of nodes and their integration and segregation profile was investigated over time. Thus, allowing nodes to be dynamically assigned to different communities via community detection might further inform about local reconfigurations and their contribution to the functional architecture of the network in a pain context, as mentioned in Kastrati et al. (2022).

The balance between integration and segregation is crucial for the brain (Shine, 2019). Whereas higher thermal pain has been shown to already disrupt this balance in HC inducing a shift from segregation to integration (Kastrati et al., 2022), in patients with RA, we might speculatively argue that, based on our results, this balance appears to be undergoing a constant perturbation in favor of a permanent high integration state.

With the present study, we were able to track the temporal profile of pain-related network changes in RA patients and HC. From a clinical perspective, this is of great importance for the understanding of the mechanisms involved in the perception of pain and could possibly contribute to the identification of a brain-based biomarker for chronic pain.

Data availability statement

The original contributions presented in this study are included in the article/**Supplementary material**, further inquiries can be directed to the corresponding author.

Ethics statement

The studies involving human participants were reviewed and approved by the regional ethical committee of Stockholm. The patients/participants provided their written informed consent to participate in this study.

Author contributions

SF: conceptualization, methodology, formal analysis, visualization, and writing – original draft and review and editing. RA: data curation, investigation, and writing – review and editing. IE: contribution to formal analysis and writing – review and editing. JL: data curation, funding acquisition, investigation, project administration, resources, and writing – review and editing. EK: conceptualization, data curation, funding acquisition, investigation, project administration, resources, supervision, and writing – review and editing. PF: supervision and writing – review and editing. WT: conceptualization, methodology, supervision, contribution to formal analysis, contribution to visualization, and writing – review and editing. All authors contributed to the article and approved the submitted version.

Funding

The research leading to the results was supported by a grant from AbbVie, the European Union's Horizon 2020 research and innovation programme under the Marie Skłodowska-Curie grant agreement No. 764860, the European Union Seventh Framework Programme (FP7/2007-2013) under grant agreement No. 602919, the Swedish Foundation for Strategic Research, Stockholm County Council (2013-0031, 2015-0073, 2018-0238), the Swedish Research Council (K2013-52X-22199-01-3, 2016-01556), the Swedish Rheumatism Association, Marianne and Marcus Wallenberg Foundation (MMW 2013.0120), and a donation from Leif Lundblad and family.

Acknowledgments

We thank rheumatologists Anna Nordenstedt-Agréus and Birgitta Tengstrand for their invaluable help in patient recruitment, and research nurse Eva Waldheim for her excellent assistance.

Conflict of interest

The authors declare that this study received funding from AbbVie. The funder was not involved in the study design, collection, analysis, interpretation of data, the writing of this article or the decision to submit it for publication.

Publisher's note

All claims expressed in this article are solely those of the authors and do not necessarily represent those of their affiliated organizations, or those of the publisher, the editors and the reviewers. Any product that may be evaluated in this article, or claim that may be made by its manufacturer, is not guaranteed or endorsed by the publisher.

Supplementary material

The Supplementary Material for this article can be found online at: https://www.frontiersin.org/articles/10.3389/fnins.2022.942136/full#supplementary-material

References

Apkarian, A. V., Baliki, M. N., and Geha, P. Y. (2009). Towards a theory of chronic pain. *Prog. Neurobiol.* 87, 81–97. doi: 10.1016/j.pneurobio.2008.09.018

Behzadi, Y., Restom, K., Liau, J., and Liu, T. T. (2007). A component based noise correction method (CompCor) for bold and perfusion based fMRI. *NeuroImage* 37, 90–101. doi: 10.1016/j.neuroimage.2007.04.042

Bonnelle, V., Ham, T. E., Leech, R., Kinnunen, K. M., Mehta, M. A., Greenwood, R. J., et al. (2012). Salience network integrity predicts default mode network function after traumatic brain injury. *Proc. Natl. Acad. Sci.* 109, 4690–4695. doi: 10.1073/pnas.1113455109

Borsook, D., Edwards, R., Elman, I., Becerra, L., and Levine, J. (2013). Pain and analgesia: the value of salience circuits. *Prog. Neurobiol.* 104, 93–105. doi: 10.1016/j.pneurobio.2013.02.003

Ciric, R., Thompson, W. H., Lorenz, R., Goncalves, M., MacNicol, E., Markiewicz, C. J., et al. (2021). TemplateFlow: fAIR-sharing of multi-scale, multi-species brain models. *Cold Spring Harb. Lab.*[Preprint] doi: 10.1101/2021.02.10.430678 .

Cohen, J. R., and D'Esposito, M. (2016). The segregation and integration of distinct brain networks and their relationship to cognition. *J. Neurosci.* 36, 12083–12094. doi: 10.1523/JNEUROSCI.2965-15.2016

Dockès, J., Poldrack, R. A., Primet, R., Gözükan, H., Yarkoni, T., Suchanek, F., et al. (2020). NeuroQuery, comprehensive meta-analysis of human brain mapping. *ELife* 9:e53385. doi: 10.7554/eLife.53385

Esteban, O., Markiewicz, C. J., Blair, R. W., Moodie, C. A., Isik, A. I., Erramuzpe, A., et al. (2019). fMRIPrep: a robust preprocessing pipeline for functional MRI. *Nat. Methods* 16, 111–116. doi: 10.1038/s41592-018-0235-4

Flodin, P., Martinsen, S., Altawil, R., Waldheim, E., Lampa, J., Kosek, E., et al. (2016). Intrinsic brain connectivity in chronic pain: a resting-state fMRI study in patients with rheumatoid arthritis. *Front. Hum. Neurosci.* 10:107. doi: 10.3389/fnhum.2016.00107

Fransson, P., Schiffler, B. C., and Thompson, W. H. (2018). Brain network segregation and integration during an epoch-related working memory fMRI experiment. *NeuroImage* 178, 147–161. doi: 10.1016/j.neuroimage.2018.05.040

Fransson, P., and Thompson, W. H. (2020). Temporal flow of hubs and connectivity in the human brain. *NeuroImage* 223, 117348. doi: 10.1016/j.neuroimage.2020.117348

Geuter, S., Reynolds Losin, E. A., Roy, M., Atlas, L. Y., Schmidt, L., Krishnan, A., et al. (2020). Multiple brain networks mediating stimulus–pain relationships in humans. *Cereb. Cortex* 30, 4204–4219. doi: 10.1093/cercor/bhaa048

Guimerà, R., and Nunes Amaral, L. A. (2005). Functional cartography of complex metabolic networks. *Nature* 433, 895–900. doi: 10.1038/nature03288

Hemington, K. S., Wu, Q., Kucyi, A., Inman, R. D., and Davis, K. D. (2016). Abnormal cross-network functional connectivity in chronic pain and its association with clinical symptoms. *Brain Struct. Funct.* 221, 4203–4219. doi: 10.1007/s00429-015-1161-1

Jensen, K. B., Kosek, E., Petzke, F., Carville, S., Fransson, P., Marcus, H., et al. (2009). Evidence of dysfunctional pain inhibition in Fibromyalgia reflected in rACC during provoked pain. Pain. 144, 95–100. doi: 10.1016/j.pain.2009.03.018

Kaplan, C. M., Schrepf, A., Vatansever, D., Larkin, T. E., Mawla, I., Ichesco, E., et al. (2019). Functional and neurochemical disruptions of brain hub topology in chronic pain. Pain. 160, 973–983. doi: 10.1097/j.pain.0000000000001480

Kastrati, G., Thompson, W. H., Schiffler, B., Fransson, P., and Jensen, K. B. (2022). Brain network segregation and integration during painful thermal stimulation. *Cereb. Cortex* doi: 10.1093/cercor/bhab464 [Epub ahead of print].

Langsrud, Ø (2003). ANOVA for unbalanced data: use Type II instead of Type III sums of squares. *Stat. Comput.* 13, 163–167.

Larkin, T. E., Kaplan, C. M., Schrepf, A., Ichesco, E., Mawla, I., Harte, S. E., et al. (2021). Altered network architecture of functional brain communities in chronic nociplastic pain. *NeuroImage* 226, 117504. doi: 10.1016/j.neuroimage.2020.117504

Lee, J.-J., Kim, H. J., Čeko, M., Park, B., Lee, S. A., Park, H., et al. (2021). A neuroimaging biomarker for sustained experimental and clinical pain. *Nat. Med.* 27, 174–182. doi: 10.1038/s41591-020-1142-7

Liégeois, R., Ziegler, E., Phillips, C., Geurts, P., Gómez, F., Bahri, M. A., et al. (2016). Cerebral functional connectivity periodically (de)synchronizes with anatomical constraints. *Brain Struct. Funct.* 221, 2985–2997. doi: 10.1007/s00429-015-1083-y

Mano, H., Kotecha, G., Leibnitz, K., Matsubara, T., Sprenger, C., Nakae, A., et al. (2018). Classification and characterisation of brain network changes in chronic back pain: a multicenter study. *Wellcome Open Res.* 3:19. doi: 10.12688/wellcomeopenres.14069.2

Menon, V., and Uddin, L. Q. (2010). Saliency, switching, attention and control: a network model of insula function. *Brain Struct. Funct.* 214, 655–667. doi: 10.1007/s00429-010-0262-0

Napadow, V., LaCount, L., Park, K., As-Sanie, S., Clauw, D. J., and Harris, R. E. (2010). Intrinsic brain connectivity in fibromyalgia is associated with chronic pain intensity. *Arthritis Rheum.* 62, 2545–2555. doi: 10.1002/art.27497

Nikolaus, S., Bode, C., Taal, E., and van de Laar, M. A. F. J. (2013). Fatigue and factors related to fatigue in rheumatoid arthritis: a systematic review. *Arthritis Care Res.* 65, 1128–1146. doi: 10.1002/acr.21949

Power, J. D., Mitra, A., Laumann, T. O., Snyder, A. Z., Schlaggar, B. L., and Petersen, S. E. (2014). Methods to detect, characterize, and remove motion artifact in resting state fMRI. *NeuroImage* 84, 320–341. doi: 10.1016/j.neuroimage.2013.08.048

Razlighi, Q. R. (2018). Task-evoked negative BOLD response in the Default Mode Network does not alter its functional connectivity. *Front. Comput. Neurosci.* 12:67. doi: 10.3389/fncom.2018.00067

Richter, C. G., Thompson, W. H., Bosman, C. A., and Fries, P. (2015). A jackknife approach to quantifying single-trial correlation between covariance-based metrics undefined on a single-trial basis. *NeuroImage* 114, 57–70. doi: 10.1016/j.neuroimage.2015.04.040

Sandström, A., Ellerbrock, I., Jensen, K. B., Martinsen, S., Altawil, R., Hakeberg, P., et al. (2019). Altered cerebral pain processing of noxious stimuli from inflamed joints in rheumatoid arthritis: an event-related fMRI study. *Brain Behav. Immun.* 81, 272–279. doi: 10.1016/j.bbi.2019.06.024

Schaefer, A., Kong, R., Gordon, E. M., Laumann, T. O., Zuo, X.-N., Holmes, A. J., et al. (2018). Local-global parcellation of the human cerebral cortex from intrinsic functional connectivity MRI. *Cereb. Cortex* 28, 3095–3114. doi: 10.1093/cercor/bhx179

Seabold, S., and Perktold, J. (2010). "statsmodels: Econometric and statistical modeling with python," in *Proceedings of the 9th Python in science conference* (Austin, TX: SciPy Society). doi: 10.25080/Majora-92bf1922-011

Shine, J. M. (2019). Neuromodulatory influences on integration and segregation in the brain. *Trends Cogn. Sci.* 23, 572–583. doi: 10.1016/j.tics.2019.04.002

Shine, J. M., Bissett, P. G., Bell, P. T., Koyejo, O., Balsters, J. H., Gorgolewski, K. J., et al. (2016). The dynamics of functional brain networks: integrated network states during cognitive task performance. *Neuron* 92, 544–554. doi: 10.1016/j.neuron.2016.09.018

Sporns, O. (2015). Cerebral cartography and connectomics. *Philos. Trans. R. Soc. Lond. B Biol. Sci.* 370:20140173. doi: 10.1098/rstb.2014.0173

Tagliazucchi, E., Balenzuela, P., Fraiman, D., and Chialvo, D. R. (2010). Brain resting state is disrupted in chronic back pain patients. *Neurosci. Lett.* 485, 26–31. doi: 10.1016/j.neulet.2010.08.053

Thompson, W. H., Brantefors, P., and Fransson, P. (2017a). From static to temporal network theory: applications to functional brain connectivity. *Netw. Neurosci.* 1, 69–99. doi: 10.1162/NETN_a_00011

Thompson, W. H., and Fanton, S. (2021). netplotbrain. *Zenodo* [Preprint]. doi: 10.5281/zenodo.4593837

Thompson, W. H., Kastrati, G., Finc, K., Wright, J., Shine, J. M., and Poldrack, R. A. (2020). Time-varying nodal measures with temporal community structure: a cautionary note to avoid misinterpretation. *Hum. Brain Mapp.* 41, 2347–2356. doi: 10.1002/hbm.24950

Thompson, W. H., Richter, C. G., Plavén-Sigray, P., and Fransson, P. (2017b). A simulation and comparison of dynamic functional connectivity methods. *BioRxiv* [Preprint] doi: 10.1101/212241 .

Thompson, W. H., Richter, C. G., Plaven-Sigray, P., and Fransson, P. (2018). Simulations to benchmark time-varying connectivity methods for fMRI. *PLoS Comput. Biol.* 14:e1006196. doi: 10.1371/journal.pcbi.1006196

Tononi, G. (1998). Complexity and coherency: integrating information in the brain. *Trends Cogn. Sci.* 2, 474–484. doi: 10.1016/S1364-6613(98)01259-5

Uddin, L. Q. (2015). Salience processing and insular cortical function and dysfunction. *Nat. Rev. Neurosci.* 16, 55–61. doi: 10.1038/nrn3857

Xie, H., Zheng, C. Y., Handwerker, D. A., Bandettini, P. A., Calhoun, V. D., Mitra, S., et al. (2019). Efficacy of different dynamic functional connectivity methods to capture cognitively relevant information. *NeuroImage* 188, 502–514. doi: 10.1016/j.neuroimage.2018.12.037

Yeo, B. T., Krienen, F. M., Sepulcre, J., Sabuncu, M. R., Lashkari, D., Hollinshead, M., et al. (2011). The organization of the human cerebral cortex estimated by intrinsic functional connectivity. *J. Neurophysiol.* 106, 1125–1165. doi: 10.1152/jn.00338.2011

frontiers | Frontiers in Neuroscience

TYPE Original Research
PUBLISHED 25 August 2022
DOI 10.3389/fnins.2022.971809

OPEN ACCESS

EDITED BY
Roberto Esposito,
ASUR Marche, Italy

REVIEWED BY
Abdul Rauf Anwar,
University of Engineering and Technology, Lahore, Pakistan
Jan Raethjen,
University of Kiel, Germany

*CORRESPONDENCE
Fabrizio Esposito
fabrizio.esposito@unicampania.it

SPECIALTY SECTION
This article was submitted to Brain Imaging Methods, a section of the journal Frontiers in Neuroscience

RECEIVED 17 June 2022
ACCEPTED 08 August 2022
PUBLISHED 25 August 2022

CITATION
Di Nardo F, Manara R, Canna A, Trojsi F, Velletrani G, Sinisi AA, Cirillo M, Tedeschi G and Esposito F (2022) Dynamic spectral signatures of mirror movements in the sensorimotor functional connectivity network of patients with Kallmann syndrome. *Front. Neurosci.* 16:971809. doi: 10.3389/fnins.2022.971809

Dynamic spectral signatures of mirror movements in the sensorimotor functional connectivity network of patients with Kallmann syndrome

Federica Di Nardo[1], Renzo Manara[2], Antonietta Canna[1], Francesca Trojsi[1], Gianluca Velletrani[3], Antonio Agostino Sinisi[1], Mario Cirillo[1], Gioacchino Tedeschi[1] and Fabrizio Esposito[1]*

[1]Department of Advanced Medical and Surgical Sciences, University of Campania "Luigi Vanvitelli," Naples, Italy, [2]Department of Neuroscience, University of Padova, Padova, Italy, [3]Department of Medicine, Surgery and Dentistry, University of Salerno, Salerno, Italy

In Kallmann syndrome (KS), the peculiar phenomenon of bimanual synkinesis or mirror movement (MM) has been associated with a spectral shift, from lower to higher frequencies, of the resting-state fMRI signal of the large-scale sensorimotor brain network (SMN). To possibly determine whether a similar frequency specificity exists across different functional connectivity SMN states, and to capture spontaneous transitions between them, we investigated the dynamic spectral changes of the SMN functional connectivity in KS patients with and without MM symptom. Brain MRI data were acquired at 3 Tesla in 39 KS patients (32 without MM, KSMM-, seven with MM, KSMM+) and 26 age- and sex-matched healthy control (HC) individuals. The imaging protocol included 20-min rs-fMRI scans enabling detailed spectro-temporal analyses of large-scale functional connectivity brain networks. Group independent component analysis was used to extract the SMN. A sliding window approach was used to extract the dynamic spectral power of the SMN functional connectivity within the canonical physiological frequency range of slow rs-fMRI signal fluctuations (0.01–0.25 Hz). K-means clustering was used to determine (and count) the most recurrent dynamic states of the SMN and detect the number of transitions between them. Two most recurrent states were identified, for which the spectral power peaked at a relatively lower (state 1) and higher (state 2) frequency. Compared to KS patients without MM and HC subjects, the SMN of KS patients with MM displayed significantly larger spectral power changes in the slow 3 canonical sub-band (0.073–0.198 Hz) and significantly fewer transitions between state 1 (less recurrent) and state 2 (more recurrent). These findings demonstrate that

the presence of MM in KS patients is associated with reduced spontaneous transitions of the SMN between dynamic functional connectivity states and a higher recurrence and an increased spectral power change of the high-frequency state. These results provide novel information about the large-scale brain functional dynamics that could help to understand the pathologic mechanisms of bimanual synkinesis in KS syndrome and, potentially, other neurological disorders where MM may also occur.

KEYWORDS

Kallmann syndrome, mirror movements, dynamic functional connectivity, sensorimotor network, K-means, connectivity states

Introduction

The occurrence of involuntary hand movements that mirror a voluntary movement of the contralateral hand, a neurological symptom referred to as bimanual synkinesis or mirror movement (MM), is considered physiological only during childhood (up to the age of 10) (Beaulé et al., 2012). However, it could persist during adulthood in congenital conditions like Kallmann syndrome (KS). An imbalance of the developing brain motor circuit has been suggested as a possible cause for reduced suppression of involuntary contralateral hand movements (Mayston et al., 1997; Farmer et al., 2004).

In a previous resting-state fMRI (rs-fMRI) multi-center study on KS (Manara et al., 2018), the presence of the MM symptom was found to be associated with abnormal spectral changes in the static functional connectivity (sFC) of the large-scale sensorimotor network (SMN). More specifically, a relatively lower contribution of the so called "slow-5" frequency band (0.01–0.027 Hz) together with a relatively higher contribution of the so called "slow-3" frequency band (0.073–0.198 Hz), has been reported from the spectral analysis of the spontaneous fluctuations of the SMN time-course, in KS patients with MM (MM+) compared to KS patients without MM (MM−). These effects were further characterized in terms of imbalance between cortical-cortical functional connectivity (more prevalent in the slow five band) and cortical-subcortical functional connectivity (more prevalent in the slow three band) to explain the reduced suppression of involuntary contra-lateral hand movements systematically occurring in MM+ patients when voluntary hand movement is requested.

However, as the human brain is a highly dynamic system, the resting-state functional connectivity has been largely proven to be temporally varying (Chang and Glover, 2010). That is, temporal fluctuations in the functional connectivity of a large-scale functional network, such as the SMN, may also reflect dynamic changes in the corresponding domain-specific functional connectivity with possible non-stationary switching between two or more discrete recurrent patterns or states. This has posed the natural question about whether the previously highlighted spectral signature of the MM symptom in KS patients constitutes an intrinsic stationary feature of the SMN functional connectivity, most likely secondary to abnormal anatomical structures within the motor circuitry, or, rather, is itself subject to dynamic temporal fluctuations between recurrent states, provided that a sufficiently long period of time (e.g., 20 min or more) is used for the observation (Hindriks et al., 2016). In other words, it is not known whether the functional connectivity of SMN can exhibit more than one recurrent (patho)physiological states, whose dynamic features, such as, e.g., the different contributions to the dynamic spectral changes in the canonical frequency bands, appear under- or over-represented in KS subjects manifesting the MM symptom.

As previous results were obtained with a purely static FC analytic approach, i.e., observing rs-fMRI signals from a large-scale network over a typical, yet short, period of 5–10 min, the current study aimed at verifying if a dynamic FC (dFC) analysis, and more specifically a dynamic spectral power analysis of the network-specific amplitude of low-frequency fluctuations, would also disclose similar characteristic dFC features in KS patients with MM.

The most common and straightforward way to investigate dFC is using windowed FC (Hutchinson et al., 2013), which consists of calculating a given FC measure over consecutive and overlapping segments of the rs-fMRI time-course data (e.g., 1–2 min), thus providing a time series of FC values, which can subsequently be used to assess dynamic fluctuations in FC over a substantially longer rs-fMRI session (e.g., 20–30 min). Such dFC analysis would also allow to identify the presence of recurrent spectral patterns for a given large-scale brain network, i.e., two (or more) dFC states with different spectral characteristics of the network time-course of activity, between pairs of which the same network spontaneously fluctuates over time.

To the best of our knowledge, this would be the first rs-fMRI study investigating, with such a spectral dFC approach, the possible spectral dFC correlates of MM in KS patients, thus potentially gathering new insights into the more dynamic

aspects of the cerebral motor circuitry derangement associated with the clinical manifestation of the bimanual synkinesis.

Materials and methods

Subjects and experimental design

Thirty-nine patients with KS (38 male, mean age ± SD 32.53 ± 11.61 and one female, age 13) were enrolled for this study. All patients met the diagnostic criteria for KS, based on clinical findings and smell analysis (hypogonadotropic hypogonadism and hypo/anosmia). The study was approved in accordance with the requirements of the local Ethical Committee at the University Hospital "San Giovanni Di Dio e Ruggi D'Aragona" of Salerno and written informed consent was obtained from patients or their parents. All KS patients underwent a complete physical and neurological examination including the evaluation of handedness and the evaluation of MM according to Woods and Teuber (1978) criteria. In particular MM were scored as follows: "0" absent; "1" barely discernible but repetitive movements; "2" either slight but sustained movement or stronger but briefer repetitive movement; "3" strong and sustained repetitive movement; "4" movement equal to that observed in the intended hand: this phenomenon may be prevalent on the right hand or on the left one. In this way, subjects were divided into two groups: KS patients with MM (KSMM+, mean age ± SD: 34.86 ± 16.94) and KS patients without MM (KSMM–, mean age ± SD: 31.41 ± 10.73). Thus, we have 7 KSMM + and 32 KSMM–. We also scanned 26 healthy age-matched control subjects without MM.

Table 1 reports the full demographical and clinical profile of all KS patients including type of olfactory dysfunction (anosmia/hyposmia), handedness, clinical MRI abnormalities, grade (0–4) of MM separately for right and left hand and with side preference of MM.

TABLE 1 Patients' clinical profile.

Pat.#	Olfactory status	bOb aplasia/ hypoplasia	MM (R)	MM (L)	MM (R + L)	MM (R vs. L)
1	Anosmia	Yes	No MM	No MM	No MM	n.a.
2	Anosmia	Yes	No MM	No MM	No MM	n.a.
3	Anosmia	Yes	No MM	No MM	No MM	n.a.
4	Anosmia	Yes	No MM	No MM	No MM	n.a.
5	Anosmia	Yes	No MM	No MM	No MM	n.a.
6	Anosmia	Yes	No MM	No MM	No MM	n.a.
7	Anosmia	Yes	No MM	No MM	No MM	n.a.
8	Anosmia	Yes	No MM	No MM	No MM	n.a.
9	Anosmia	Yes	No MM	No MM	No MM	n.a.
10	Anosmia	Yes	No MM	No MM	No MM	n.a.
11	Anosmia	Yes	No MM	No MM	No MM	n.a.
12	Anosmia	Yes	No MM	No MM	No MM	n.a.
13	Anosmia	Yes	No MM	No MM	No MM	n.a.
14	Anosmia	Yes	No MM	No MM	No MM	n.a.
15	Anosmia	Yes	No MM	No MM	No MM	n.a.
16	Anosmia	Yes	No MM	No MM	No MM	n.a.
17	Anosmia	Yes	No MM	No MM	No MM	n.a.
18	Anosmia	Yes	No MM	No MM	No MM	n.a.
19	Anosmia	Yes	No MM	No MM	No MM	n.a.
20	Anosmia	Yes	No MM	No MM	No MM	n.a.
21	Anosmia	Yes	No MM	No MM	No MM	n.a.
22	Anosmia	Yes	No MM	No MM	No MM	n.a.
23	Anosmia	Yes	No MM	No MM	No MM	n.a.
24	Anosmia	Yes	No MM	No MM	No MM	n.a.
25	Anosmia	Yes	No MM	No MM	No MM	n.a.
26	Anosmia	Yes	No MM	No MM	No MM	n.a.
27	Anosmia	Yes	No MM	No MM	No MM	n.a.
28	Anosmia	Yes	No MM	No MM	No MM	n.a.
29	Anosmia	Yes	No MM	No MM	No MM	n.a.
30	Anosmia	Yes	No MM	No MM	No MM	n.a.
31	Anosmia	Yes	No MM	No MM	No MM	n.a.
32	Anosmia	Yes	No MM	No MM	No MM	n.a.
33	Anosmia	Yes	4	3	7	Right
34	Anosmia	Yes	2	1	3	Right
35	Anosmia	Yes	2	3	5	Left
36	Anosmia	Yes	2	0	2	Right
37	Anosmia	Yes	3	3	6	No prev.
38	Anosmia	Yes	3	3	6	No prev.
39	Anosmia	Yes	3	2	5	Right

L, left; R, right; MM, grade of mirror movements according to Woods and Teuber criteria; no prev., no R vs. L prevalence; bOBs, bilateral olfactory bulbs.

Magnetic resonance imaging acquisition

MRI image data sets were acquired on a 3T MRI scanner (MAGNETOM Skyra, Siemens, Erlangen Germany) equipped with a 20-channel radiofrequency receive head coil. The imaging protocol consists of a volumetric anatomical scan, followed by resting-state fMRI scan.

The anatomical scans were performed with a 3D T1-weighted magnetization prepared rapid gradient echo sequence (MPRAGE) with TR/TE: 2400/2.25 ms; resolution: 1 mm; matrix size: 256 × 256. Resting-state fMRI scans consisted of 1,800 volumes and 44 slices, performed with a gradient-echo echo planar imaging (GRE-EPI) with a multiband factor of 4 (Feinberg et al., 2010; Moeller et al., 2010; Xu et al., 2013), TR/TE: 662/30 ms, matrix size: 64 × 64; voxel size: 3 × 3 × 3 mm^3, direction of phase encoding acquisition anterior-posterior. The same GRE-EPI series was repeated two

more times with only five dynamic scans and opposite phase encoding directions (anterior-posterior, posterior-anterior) for the purpose to correct GRE-EPI image distortion (Andersson et al., 2003; Smith et al., 2004). Each scanning acquisition was about 25 min long: 20 min for functional imaging and 5 min for anatomical imaging. During the functional scan, subjects were asked to simply stay motionless and awake.

Functional magnetic resonance imaging data preprocessing

Each individual resting-state fMRI time series was first corrected for the different slice scan acquisition times (*via* cubic spline interpolation) and for rigid head motion effects (*via* realignment of all volumes to the first) using BrainVoyager QX (Brain Innovation, Maastricht, Netherlands[1]). Subsequently, the image time series were first exported to NIFTI format for geometrical distortion correction *via* the TOPUP tool of FSL (Andersson et al., 2003; Smith et al., 2004). Then, the subsequent preprocessing steps were performed on distortion-corrected NIFTI images using the Data Processing Assistant for Resting-State fMRI (DPARSF) (Yan and Yu-Feng, 2010),[2] which is based on Statistical Parametric Mapping (SPM)[3] and on the toolbox for Data Processing and Analysis of Brain Imaging (DPABI) (Yan et al., 2016).[4] The alignment of the first volume of each subject resting-state fMRI series to the corresponding anatomical 3D-T1w image was implemented with affine transformation; then, all T1w images were normalized to the MNI space with the non-linear diffeomorphic DARTEL approach (Ashburner, 2007); lastly, the coregistered functional data were normalized to the MNI space with the transformations obtained during the DARTEL procedure.

To reduce the residual effects of head motion, as well as the effects of respiratory and cardiac signals, second-order motion and physiological nuisance correction were performed using a linear regression approach: the regression model included 24 motion-related predictors (Friston et al., 1996), with six head motion parameter time-series, their first-order derivatives and the 12 corresponding squared parameter time-series; the mean time-courses from a white matter mask and a cerebrospinal fluid mask (as obtained from 3D-T1w spatial segmentation) were added as two additional predictors. In order to account for residual motion-related spikes, an additional spike-related regressor was created from the frame wise displacement time-series, i.e., a predictor with a value of 1 at the time points of each detected spike and a value of 0 elsewhere (Lemieux et al., 2007; Satterthwaite et al., 2013). Finally, the image time series were band-pass filtered between 0.01 and 0.5 Hz and spatially smoothed with an isotropic 6-mm full width at half maximum (FWHM) Gaussian kernel.

To minimize the potential effects of head motion and possibly exclude subjects exhibiting excessive amounts of motion, we applied severe inclusion criteria: the six estimated head motion parameters (three translation and three rotation) were considered and subjects exhibiting head translations >3 mm and/or head rotations >3 degrees were excluded from consecutive analyses. Then, the mean frame wise displacement value (FD) was estimated as an additional measure of total instantaneous head motion (Power et al., 2012; Kim et al., 2017) and the percentage of spike-corrupted volumes in each time-series was calculated. Potential spike-corrupted volumes were identified where the FD value exceeded a threshold of 0.5 mm; at this stage, subjects for whom the percentage of corrupted volumes exceeded 50% in the scan were also excluded from the analyses.

Functional magnetic resonance imaging data analysis

Data were decomposed into functional networks using a group-level spatial ICA as implemented in the Group ICA (GICA) of functional MRI Toolbox (GIFT)[5] (Calhoun et al., 2001; Correa et al., 2005). The number of components to be extracted was estimated from the resting-state fMRI data using the minimum description length (MDL) criterion (Li et al., 2007a,b) applied to the concatenated data set of patients and healthy controls, ensuring the same number of components for all the patients and healthy controls. Prior to data reduction, voxel-wise variance normalization was applied to the time course of each voxel (Beckmann and Smith, 2004; Allen et al., 2010). Then, two data reduction steps of Principal Component Analysis (PCA) were performed (subject-specific and group-level) using the expectation maximization algorithm and the independent components were extracted using the Infomax algorithm (Bell and Sejnowski, 1995; Esposito et al., 2002) and repeated 20 times through ICASSO (Himberg et al., 2004); finally, the GICA back reconstruction algorithm (Calhoun et al., 2001; Erhardt et al., 2011) provided participant's spatial maps and their corresponding time courses.

For the dFC analysis, a sliding window approach was performed through custom scripts written in MATLAB R2021a (The MathWorks Inc., Natick, MA, United States[6]) to explore time-varying changes of FC within the individual network components during functional MRI acquisitions. More in details, three hundred and thirty-one tapered sliding windows were obtained by segmenting the time-course of each subject

1 www.brainvoyager.com
2 http://rfmri.org/DPARSF
3 http://www.fil.ion.ucl.ac.uk/spm
4 http://rfmri.org/DPABI
5 https://github.com/trendscenter/gift
6 www.themathworks.com

TABLE 2 Frequency range for the four canonical bands.

Bands	Frequency interval (Hz)
Slow-5	0.01–0.027
Slow-4	0.027–0.073
Slow-3	0.073–0.198
Slow-2	0.198–0.25

into windows 150 volumes (150 TR = 99.3 s) with a step of five volumes (5 TR = 3.31 s). In fact, a window size between 30 s and 1 min was shown to be a reasonable choice for capturing brain dynamics (Shirer et al., 2012; Allen et al., 2014; Damaraju et al., 2014; Rashid et al., 2014; de Lacy et al., 2017). Using the time-series data of all selected independent component pairs within each window, a pairwise covariance matrix was calculated.

Spectral power information was obtained using the time-course of activity corresponding to the selected individual independent component. Following Zuo et al. (2010), we further subdivided the relative contribution of each independent component time-course spectrum to the whole detectable frequency range into four separate bands (**Table 2**). The cross-spectrum was calculated in MATLAB over the entire low-frequency range of interest (0.01–0.25 Hz) *via* the cross-spectrogram function by specifying a Hamming sliding window. As a result, a dynamic spectrum connectivity (DSC) matrix was obtained, representing the changes in the amplitude of the time-course of network activity as a function of time over the entire duration of the scan. For the purposes of this study, only the SMN component was selected and considered. However, as the SMN connectivity may variably include the contribution from the subcortical structures, an additional region of interest (ROI) based analysis of the dynamic functional connectivity was performed on the fMRI signals from the basal ganglia and thalamus. Namely, using the Harvard–Oxford subcortical structural atlas (with 2 mm resolution) distributed with the FMRIB Software Library, we anatomically subdivided the basal ganglia into caudate, putamen and pallidum (De Micco et al., 2019) and downsampled the resulting mask to the size of fMRI data (3 mm).

To assess recurrent dFC patterns over time, a k-means clustering algorithm was performed to the windowed DSC matrix (Allen et al., 2014; Fu et al., 2018, 2019; Espinoza et al., 2019; Schumacher et al., 2019). The k-means clustering was applied twice: first, to find the optimal number of clusters *via* silhouette criterion, and second, to perform clustering analysis with the obtained cluster optimal number (Rousseeuw, 1987; Kim et al., 2017; Fiorenzato et al., 2019). The frequency of each state was estimated for each subject as the proportion of windows assigned to a state (cluster). The number of transitions between different states was also calculated for each subject. Then, a one-way ANOVA analysis of both frequency and transitions was performed considering the group as a between-subject factor with three levels: KSMM+, KSMM- and healthy controls.

Results

No significant differences were found between HC subjects and KS patients and between the two KS subgroups (MM−, MM+) in age and gender. None of the enrolled subjects were excluded from the analysis as all passed the inclusion criteria used for the inter- and intra-voxel residual motion effects.

From the GICA analysis, 13 components were extracted among which the SMN component was selected as the one whose spatial map exhibited highest z values bilaterally in the primary and supplementary motor areas and in the primary and secondary sensory cortices (**Figure 1** and **Table 3**).

The SMN dynamic spectral power data from all subjects and time windows were used in the k-means clustering, resulting in two clusters of most recurrent dFC states: state 1, state 2. For the two states, the mean spectral power (vs. frequency) in the range between 0.01 and 0.25 Hz and the box plot of the mean spectral power in the four canonical frequency bands across all subjects are displayed in **Figure 2**. According to the peak frequency of the mean spectral power of each state, state 1 was descriptively identified as a low-frequency dFC state, whereas state 2 was descriptively identified as a high-frequency dFC state. Indeed, across all subjects, the mean spectral power was significantly higher for state 1 vs. state 2 in the lowest frequency canonical band (slow 5: one-sample paired t-test, $p < 0.0001$) whereas the opposite held true for the other canonical bands (slow 4 and slow 3: one-sample paired t-test, $p < 0.0001$; slow 2: one-sample t-test, $p < 0.01$).

For each canonical frequency band and each experimental group (HC, MM−, MM+), the percent signal change in the mean spectral power associated in average with any transition between two dFC states across two adjacent time windows was estimated. The corresponding boxplots are displayed in **Figure 3**.

The percent spectral power change associated with the transitions from state 1 to state 2 was negative for slow 5 and positive for slow 4, slow 3, and slow 2. The percent spectral power change for slow 3 band was significantly increased in the group of MM + patients (and about double in size) compared to both MM− patients (two-sample t-test, $p = 0.0013$) and HC subjects (two-sample t-test, $p = 0.0015$).

For each subject, both the frequency of occurrence of each state, i.e., independently of the mean spectral power in predefined canonical bands, and the frequency of state transitions between the two states were counted. The box plots of these counts across experimental groups are displayed in the **Figure 4**. While the number (count) of time windows associated with each state did not significantly differ between groups or between states, there was a significant group-by-state

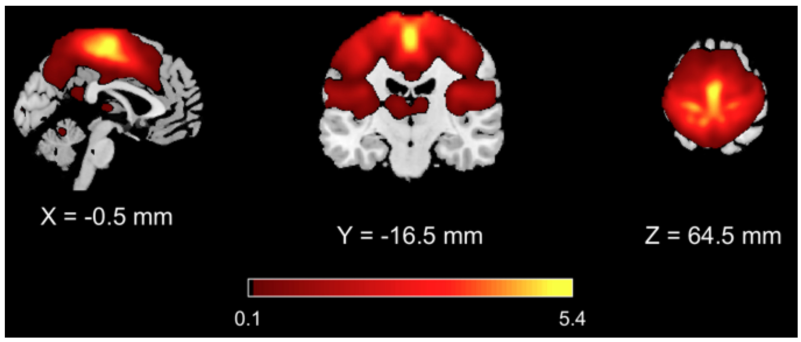

FIGURE 1
Results of GICA analysis. The SMN component was selected as the one with highest z values in the primary and supplementary motor areas and in the primary and secondary sensory areas.

TABLE 3 Coordinates of the three peaks obtained from the sensorimotor network map.

Regions	MNI coordinates (x, y, z)
Supplementary motor area	−1, −20, 67
Left primary motor cortex	−18, −35, 70
Right primary motor cortex	17, −35, 74

interaction (2-way ANOVA, $p = 0.04$). Moreover, even if *post hoc* *t*-test revealed no significant differences in the counts between subgroups (in both states), there was a significant reduction in the number of transitions between states in MM+ patients compared to both HC subjects (two-sample *t*-test: $p = 0.001$) and MM− patients (two-sample *t*-test, $p = 0.013$).

From the basal ganglia and thalamus ROI analysis, for each frequency band, each group (HC, MM−, MM+) and each ROI, the percent signal change in the mean spectral power associated in average with any transition between two dFC states across two adjacent time windows was also estimated but no significant differences were revealed. Finally, for each subject and each ROI, both the frequency of occurrence of each state and the frequency of state transitions between the two states were counted. One-way ANOVA analysis from basal ganglia and thalamus ROI analyses revealed no significant differences in the number of transitions between groups. In each state, there were no significant differences in term of the frequency of the occurrences (count of time windows associated with each state). Moreover, in the same regions, there were no significant group-by-state interactions (2-way ANOVA).

Discussion

This study explored the dynamic spectral changes of the intrinsic functional connectivity of the large-scale sensori-motor brain network in KS patients and HC subjects, demonstrating that KS patients presenting at the clinical examination with the phenomenon of bimanual synkinesis (or MM) may also exhibit different spontaneous fluctuations of the spectral content of SMN component over a 20 min period of observation between two most recurrent oscillatory states.

First, we extracted a common group ICA component for the SMN of the whole group of KS patients and HC subjects with the purpose of extracting the most general spatial pattern characterizing the whole-brain co-activation of the most functionally connected motor regions. Starting from the SMN group component, the subject-specific SMN time-courses of activity were submitted to a sliding-window spectral analysis and a cluster analysis of the spectral power identified two stable and recurrent dFC states: a low-frequency state (state 1) and a high-frequency state (state 2).

Many previous studies have supported the notion that neural oscillations supporting the functional connectivity of the human brain can exhibit frequency-dependent properties, even within the small range of slow rs-fMRI signal fluctuations (Zuo et al., 2010). In general, relatively higher frequency neuronal oscillations (e.g., in the gamma band in the EEG signal) are restricted to a relatively smaller spatial scale, whereas long-range neuronal communications are supported by slower oscillations (e.g., in delta band of the EEG signal) (Buzsáki and Draguhn, 2004). Accordingly, a general theory for brain oscillations, regardless of the scale of spatio-temporal observation, would prescribe that the longer the range of functional connectivity (among remote brain regions), the lower the frequency of the functional connectivity signal emerging from the integration of brain functions, the physiological rationale being that remote regions with different functional specialization most likely oscillate at different frequencies (Wang et al., 2016) and several rs-fMRI studies have shown how the strength of large-scale networks decreases when the frequency increases (Wu et al., 2008; Gohel and Biswal, 2015; Li et al., 2015). Particularly, in the context of large-scale brain functional networks, the functional processes supporting long-range connections among

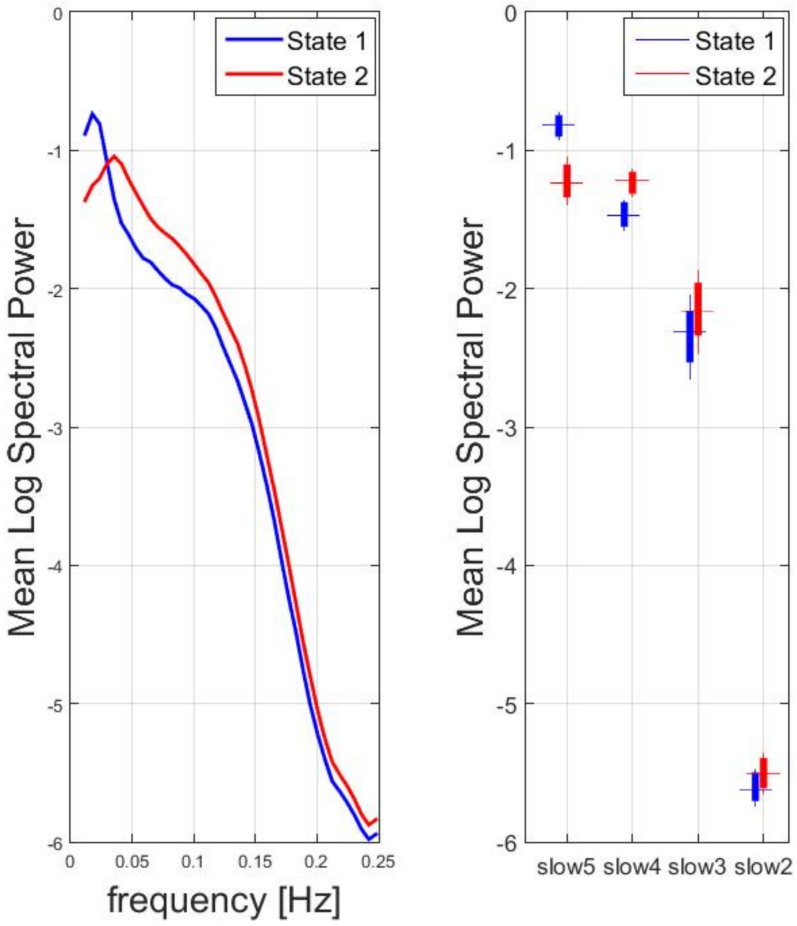

FIGURE 2
Spectral analysis for two clusters of most recurrent dFC states: State 1, State 2. Left: for the two states, the mean logarithm of the spectral power (vs. frequency) in the range between 0.01 and 0.25 Hz was calculated. According to the peak frequency, state 1 was descriptively identified as a low-frequency dFC state, whereas state 2 was descriptively identified as a high-frequency dFC state. Right: Box plot of the mean log spectral power in the four canonical frequency bands across all subjects.

spatially distributed cortical regions normally operate in a lower frequency band compared to those supporting short-range connections within more spatially compact subcortical regions (Buzsáki and Draguhn, 2004). In line with this notion, we had previously observed how slow 5 fluctuations of rs-fMRI signals were more characteristic of a cortical-cortical static functional connectivity, whereas slow 4 and slow 3 were more characteristic of a cortical-subcortical static functional connectivity [see, e.g., Esposito et al. (2013) and Manara et al. (2018)]. Here, for the first time, we were able to demonstrate that at least two distinct (i.e., stable and recurrent) dynamic functional connectivity states may co-exist in the dynamic functional connectivity of the SMN in terms of a different contribution of relatively lower- and higher-frequency oscillatory components. This would imply that (i) there are shorter windows of time (∼1.5 min) where the slower cortical-cortical oscillations would prevail in the SMN functional connectivity against the faster subcortical-cortical oscillations and that (ii) the SMN network would spontaneously (and randomly) fluctuate between such periods, the balance between the occurrences of these two states becoming an interesting new element for the neuroimaging assessment of the motor circuitry functional integrity. In the more specific context of the MM symptom, here we found that, not only the relative spectral change in the switching between these two states was in average significantly increased in the slow 3 band in KS patients with MM (compared to HC subjects and KS patients without MM), but also the number of such transitions was significantly reduced in those patients that therefore appear to persist in the high-frequency dFC state for much longer time than needed or expected. This demonstrates how MM can be seen as a clinical manifestation of a neural deficit in dynamic flexibility of the SMN.

Importantly, the dynamic spectral analysis of the SMN did not show significant differences between KSMM− patients

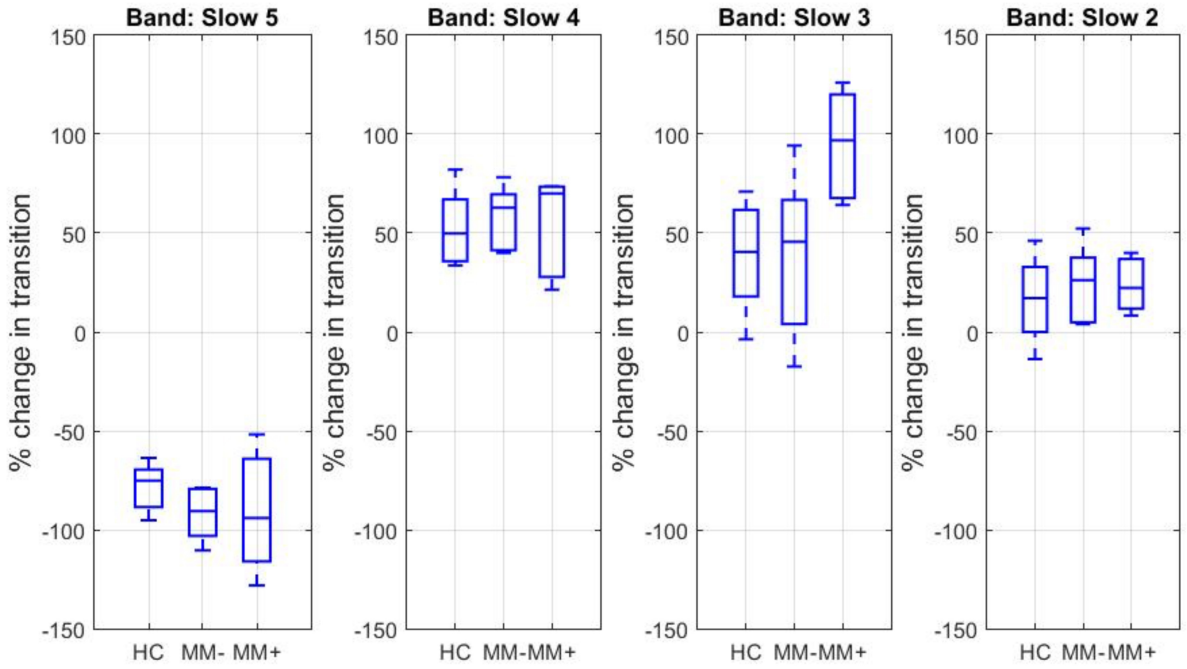

FIGURE 3
Boxplots of the percent signal change in the mean log spectral power associated with transitions between two dFC states for each canonical frequency band and each experimental group.

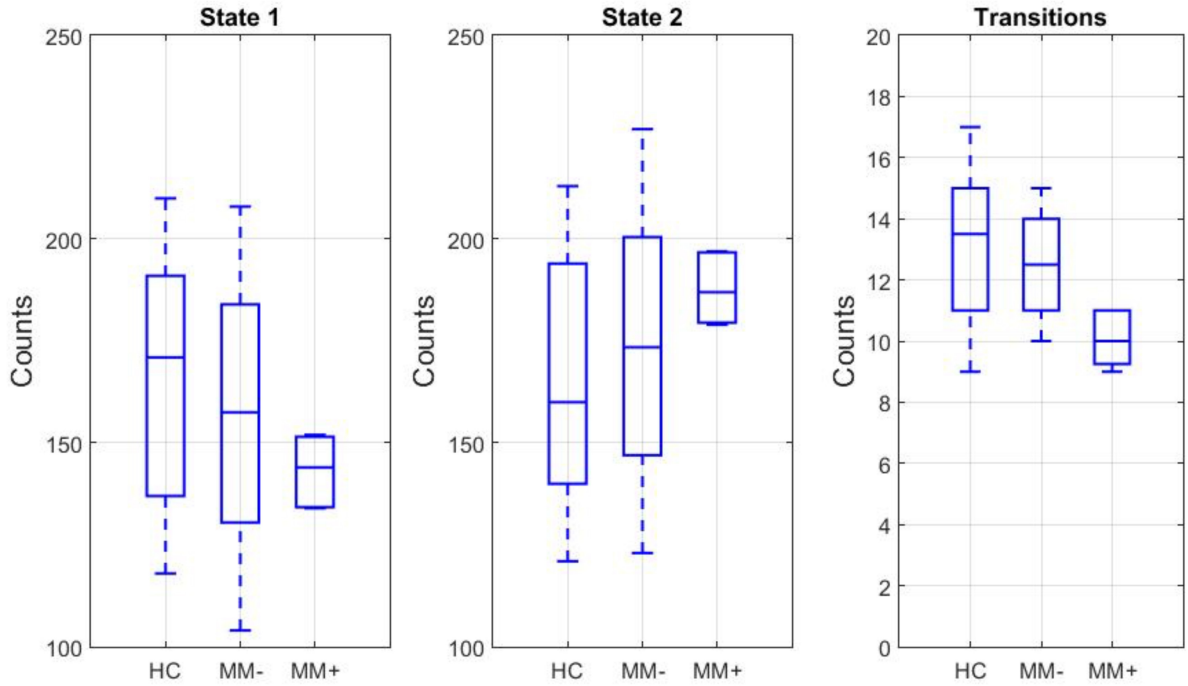

FIGURE 4
Left and middle: box plots of the frequency of occurrence in the state 1 and state 2 for each experimental group. Right: box plot of the frequency of state transitions between the two states.

and controls, indicating that the dynamic spectral shifts observed in the motor circuit of KS MM+ patients may not (primarily) depend on the general KS condition itself or some specific (KS-related) hormone or treatment differences between KS patients and controls. In addition, the absence of regional spectral differences in subcortical ROIs (when taken in isolation from the SMN) may suggest that the dynamic functional changes primarily depend upon on long-range connectivity changes affecting the resting-state cortical activity. More specifically, following up our previous line of interpretation (Manara et al., 2018), we could hypothesize that the spontaneous synchronization of cortical motor areas is abnormally attracted toward a high-frequency state due to an abnormal functioning of the cortical-subcortical loop that controls voluntary movements. On the other hand, the lack of difference between MM+ patients and healthy controls in the functional connectivity of basal ganglia and thalamus was at least unexpected as the role of the interhemispheric control in the case of unilateral movements is well-known. Thus, we cannot exclude that this null finding was due to the lack of statistical power implied by the small size of the MM + group (including only three patients with right unilateral MM and only one patient with left unilateral MM) and anyway future studies (involving a larger sample of MM+ patients) are needed to address the relation between the changes observed here in the SMN functional connectivity and the left-right coupling of the resting-state oscillations across cortical and subcortical homotopic regions.

The analysis of time-varying brain activity and connectivity using rs-fMRI has become an important topic of ongoing neuroscience discussions. Indeed, significant changes in the temporal dynamics of brain network connectivity (both in terms of configuration and synchronization) have been reported in different neurological diseases, thereby some researchers have hypothesized that this type of analysis might eventually provide some important biomarkers of disease [see, e.g., Hutchinson et al. (2013) and Damaraju et al. (2014)].

A crucial point of this study is that KS is a genetic disease in which we can see some functional aspects of a neurological disease, including the presence of MMs, that have originally suggested an involvement of the cerebral motor circuit. However, in KS, structural data from previous neuroimaging studies have provided conflicting results [see, e.g., Krams et al. (1997, 1999), Leinsinger et al. (1997), Koenigkam-Santos et al. (2008)Koenigkam-Santos et al. (2010), and Manara et al. (2015)]. For example, abnormal values of the magnetization transfer ratio at level of the pyramidal decussation were observed in KS patients independently of the presence of MM (Koenigkam-Santos et al., 2010), but diffusion tensor imaging studies did not reveal structural changes of the cortical-spinal tract in KS patients with or without MM (Manara et al., 2014, 2015). At the cortical level, KS patients with MM showed significant cortical thinning in small regions known to be involved in the voluntary hand motor control and bilateral volume decrease of the globus pallidum, compared with KS patients without MM, thus suggesting a complex readjustment of the motor circuitry associated with bimanual synkinesis (Manara et al., 2015). Our results would thus confirm in a newly designed rs-fMRI study on new KS patients, the observations of a previous study (Manara et al., 2018) based a static functional connectivity approach, in which the analysis also revealed a significant group by frequency interaction pointing to a frequency shift in the spectral content in KS patients. However, as the present study was purposefully designed to perform a dynamic functional connectivity analysis, we were here able to pinpoint a more finally detailed aspect of KSMM+ functional connectivity: namely that these patients tend to switch from a lower frequency state of brain connectivity to a higher frequency with significantly greater facility than healthy controls and KSMM− patients and consequently tend to spend more time in this high frequency state.

As mentioned above, a dFC approach similar to the one presented here has been previously employed in other psychiatric and neurological diseases, including Schizophrenia, Parkinson's Disease, Alzheimer's Disease, autism or Huntington disease. In these pathologies, k-means clustering procedures have usually shown transitions among more than two brain networks states and the changes between these transitions were mostly related to cognitive (Rashid et al., 2014; Fiorenzato et al., 2019; Schumacher et al., 2019) or motor (Kim et al., 2017) impairments. On the other hand, most KS patients are cognitively intact and only a small percentage of them develop bimanual synkinesis, which therefore characterize a very rare condition. Consequently, the neural underpinnings of MM phenomenon remain unclear, albeit the dynamic point of view on the functional connectivity addressed here seems promising with respect to the need of better addressing this aspect of the pathology. Of course, larger-sample studies, possibly integrating dFC from other networks or regions remain needed to better elucidate the pathogenic mechanism of MM in KS and in other congenital or acquired conditions, as well as in neurodegenerative diseases.

In conclusion, we have performed, to our knowledge, the first dFC analysis of the SMN, determining two discrete frequency-specific oscillatory states, in KS patients with and without MM. Major limitations should be considered when interpreting the results of this study: First, the relatively low number of KSMM+ patients. We were able to enroll only seven subjects with MM and this number was too small to address the possible correlation between the extent of the mirror movement and the extent of the changes of the network dynamics. Thus, the precise connection of our findings to the mirror movements in KS remains unclear. Fortunately, even with such a low number, significant (albeit few) differences emerged, suggesting that, by increasing the number of the sample, it will be possible to gain more evidence about this phenomenon. Second, as KS is

a disease that mostly affects males, it would be interesting to evaluate what happens to dFC with more female patients at disposal, given that only one was included in our KS sample. Third, little is known, and no data were available, about how the highlighted transient resting-state connectivity states would eventually affect the execution of a motor task. Thus, further work is needed, including the possibility to address this issue by administering motor tasks to the patients. Related to this, an important issue to address would be the choice of window sizes for the sliding-window dFC analysis. Sakoglu et al. (2010) reported that only an ideal window size should be able to estimate dFC variability (capturing the low frequency modes of interest in the rs-fMRI signal) and concurrently detect short-term task-related effects. In this study, functional dynamics were estimated using a validated fixed sliding-window of 150 volumes (about 100s), a measure considered more than reasonable for a 20-min scan, to robustly capture at least two state and the corresponding transition counts. Nonetheless, when attempting to address the influence of the state on the motor response, it is likely that a trade-off existed between the sensitivity for detecting potentially interesting transients in dFC and the signal-to-noise ratio of the task-related FC. Future work should thus evaluate changes across several window lengths that would be then combined in multi-scale approach, e.g., using wavelet transform (Chang and Glover, 2010; Billings et al., 2018). It remains, that the peculiar phenomenon of MM in KS seems to be a good pathological model to investigate spectrally selective variations in long resting-state fMRI sessions and further studies will possibly confirm or better explain the highlighted dynamics behind the pathogenic hypothesis of MM.

Data availability statement

The raw data supporting the conclusions of this article will be made available by the authors, without undue reservation.

Ethics statement

The studies involving human participants were reviewed and approved by Ethical Committee at the University Hospital "San Giovanni Di Dio e Ruggi D'Aragona" of Salerno. The patients/participants provided their written informed consent to participate in this study.

Author contributions

FE, RM, AS, and GV contributed to conception and design of the study. GV organized the database. FD performed the statistical analysis and wrote the first draft of the manuscript. AC and FE wrote sections of the manuscript. All authors contributed to manuscript revision and read and approved the submitted version.

Conflict of interest

The authors declare that the research was conducted in the absence of any commercial or financial relationships that could be construed as a potential conflict of interest.

Publisher's note

All claims expressed in this article are solely those of the authors and do not necessarily represent those of their affiliated organizations, or those of the publisher, the editors and the reviewers. Any product that may be evaluated in this article, or claim that may be made by its manufacturer, is not guaranteed or endorsed by the publisher.

References

Allen, E. A., Damaraju, E., Plis, S. M., Erhardt, E. B., Eichele, T., and Calhoun, V. D. (2014). Tracking whole-brain connectivity dynamics in the resting state. *Cereb. Cortex* 24, 663–676. doi: 10.1093/cercor/bhs352

Allen, E., Erhardt, E., Eichele, T., Mayer, A. R., and Calhoun, V. D. (2010). "Comparison of pre-normalization methods on the accuracy of group ICA results," in *Proceedings of the 16th Annual Meeting of the Organization for Human Brain Mapping* (Barcelona), 6–10.

Andersson, J. L., Skare, S., and Ashburner, J. (2003). How to correct susceptibility distortions in spin-echo echo-planar images: Application to diffusion tensor imaging. *Neuroimage* 20, 870–888. doi: 10.1016/S1053-8119(03)00336-7

Ashburner, J. (2007). A fast diffeomorphic image registration algorithm. *Neuroimage* 38, 95–113. doi: 10.1016/j.neuroimage.2007.07.007

Beaulé, V., Tremblay, S., and Théoret, H. (2012). Interhemispheric control of unilateral movement. *Neural. Plast.* 2012:627816. doi: 10.1155/2012/627816

Beckmann, C. F., and Smith, S. M. (2004). Probabilistic independent component analysis for functional magnetic resonance imaging. *IEEE Trans. Med. Imaging* 23, 137–152. doi: 10.1109/TMI.2003.822821

Bell, A. J., and Sejnowski, T. J. (1995). An information-maximization approach to blind separation and blind deconvolution. *Neural. Comput.* 7, 1129–1159. doi: 10.1162/neco.1995.7.6.1129

Billings, J. C. W., Thompson, G. J., Pan, W. J., Magnuson, M. E., Medda, A., and Keilholz, S. (2018). Disentangling multispectral functional connectivity with wavelets. *Front. Neurosci.* 6:812. doi: 10.3389/fnins.2018.00812

Buzsáki, G., and Draguhn, A. (2004). Neuronal oscillations in cortical networks. *Science* 304, 1926–1929. doi: 10.1126/science.1099745

Calhoun, V. D., Adali, T., Pearlson, G. D., and Pekar, J. J. (2001). A method for making group inferences from functional MRI data using independent component analysis. *Hum. Brain Mapp.* 14, 140–151. doi: 10.1002/hbm.1048

Chang, C., and Glover, G. H. (2010). Time–frequency dynamics of resting-state brain connectivity measured with fMRI. *Neuroimage* 50, 81–98. doi: 10.1016/j.neuroimage.2009.12.011

Correa, N., Adali, T., Li, Y., and Calhoun, V. (2005). "Comparison of blind source separation algorithms for FMRI using a new Matlab toolbox: GIFT," in *Proceedings of the (ICASSP '05). IEEE International Conference on Acoustics, Speech, and Signal Processing, 2005*, Vol. 5 (Philadelphia, PA: IEEE).

Damaraju, E., Allen, E. A., Belger, A., Ford, J. M., McEwen, S., Mathalon, D. H., et al. (2014). Dynamic functional connectivity analysis reveals transient states of dysconnectivity in schizophrenia. *Neuroimage* 5, 298–308. doi: 10.1016/j.nicl.2014.07.003

de Lacy, N., Doherty, D., King, B. H., Rachakonda, S., and Calhoun, V. D. (2017). Disruption to control network function correlates with altered dynamic connectivity in the wider autism spectrum. *Neuroimage Clin.* 15, 513–524. doi: 10.1016/j.nicl.2017.05.024

De Micco, R., Esposito, F., di Nardo, F., Caiazzo, G., Siciliano, M., Russo, A., et al. (2019). Sex-related pattern of intrinsic brain connectivity in drug-naïve Parkinson's disease patients. *Mov. Disord.* 34, 997–1005. doi: 10.1002/mds.27725

Erhardt, E. B., Rachakonda, S., Bedrick, E. J., Allen, E. A., Adali, T., and Calhoun, V. D. (2011). Comparison of multi-subject ICA methods for analysis of fMRI data. *Hum. Brain Mapp.* 32, 2075–2095. doi: 10.1002/hbm.21170

Espinoza, F. A., Liu, J., Ciarochi, J., Turner, J. A., Vergara, V. M., Caprihan, A., et al. (2019). Dynamic functional network connectivity in Huntington's disease and its associations with motor and cognitive measures. *Hum. Brain Mapp.* 40, 1955–1968. doi: 10.1002/hbm.24504

Esposito, F., Formisano, E., Seifritz, E., Goebel, R., Morrone, R., Tedeschi, G., et al. (2002). Spatial independent component analysis of functional MRI time-series: To what extent do results depend on the algorithm used? *Hum. Brain Mapp.* 16, 146–157. doi: 10.1002/hbm.10034

Esposito, F., Tessitore, A., Giordano, A., De Micco, R., Paccone, A., Conforti, R., et al. (2013). Rhythm-specific modulation of the sensorimotor network in drug-naive patients with Parkinson's disease by levodopa. *Brain* 136(Pt 3), 710–725. doi: 10.1093/brain/awt007

Farmer, S. F., Harrison, L. M., Mayston, M. J., Parekh, A., James, L. M., and Stephens, J. A. (2004). Abnormal cortex-muscle interactions in subjects with X-linked Kallmann's syndrome and mirror movements. *Brain* 127(Pt 2), 385–397. doi: 10.1093/brain/awh047

Feinberg, D. A., Moeller, S., Smith, S. M., Auerbach, E., Ramanna, S., Gunther, M., et al. (2010). Multiplexed echo planar imaging for sub-second whole brain FMRI and fast diffusion imaging. *PLoS One* 5:e15710. doi: 10.1371/journal.pone.0015710

Fiorenzato, E., Strafella, A. P., Kim, J., Schifano, R., Weis, L., Antonini, A., et al. (2019). Dynamic functional connectivity changes associated with dementia in Parkinson's disease. *Brain* 142, 2860–2872. doi: 10.1093/brain/awz192

Friston, K. J., Williams, S., Howard, R., Frackowiak, R. S., and Turner, R. (1996). Movement-related effects in fMRI time-series. *Magn. Reson. Med.* 35, 346–355. doi: 10.1002/mrm.1910350312

Fu, Z., Caprihan, A., Chen, J., Du, Y., Adair, J. C., Sui, J., et al. (2019). Altered static and dynamic functional network connectivity in Alzheimer's disease and subcortical ischemic vascular disease: Shared and specific brain connectivity abnormalities. *Hum. Brain Mapp.* 40, 3203–3221. doi: 10.1002/hbm.24591

Fu, Z., Tu, Y., Di, X., Du, Y., Pearlson, G. D., Turner, J. A., et al. (2018). Characterizing dynamic amplitude of low-frequency fluctuation and its relationship with dynamic functional connectivity: An application to schizophrenia. *Neuroimage* 180, 619–631. doi: 10.1016/j.neuroimage.2017.09.035

Gohel, S. R., and Biswal, B. B. (2015). Functional integration between brain regions at rest occurs in multiple-frequency bands. *Brain Connect.* 5, 23–34. doi: 10.1089/brain.2013.0210

Himberg, J., Hyvärinen, A., and Esposito, F. (2004). Validating the independent components of neuroimaging time series via clustering and visualization. *Neuroimage* 22, 1214–1222. doi: 10.1016/j.neuroimage.2004.03.027

Hindriks, R., Adhikari, M. H., Murayama, Y., Ganzetti, M., Mantini, D., Logothetis, N. K., et al. (2016). Can sliding-window correlations reveal dynamic functional connectivity in resting-state fMRI? *Neuroimage* 15, 242–256. doi: 10.1016/j.neuroimage.2015.11.055

Hutchinson, R. M., Womelsdorf, T., Allen, E. A., Bandettini, P. A., Calhoun, V. D., Corbetta, M., et al. (2013). Dynamic functional connectivity: Promise, issues, and interpretations. *Neuroimage* 80, 360–378. doi: 10.1016/j.neuroimage.2013.05.079

Kim, J., Criaud, M., Cho, S. S., Díez-Cirarda, M., Mihaescu, A., Coakeley, S., et al. (2017). Abnormal intrinsic brain functional network dynamics in Parkinson's disease. *Brain* 140, 2955–2967. doi: 10.1093/brain/awx233

Koenigkam-Santos, M., de Castro, M., Versiani, B. R., Diniz, P. R., and Santos, A. C. (2010). Kallmann syndrome and mirror movements: White matter quantitative evaluation with magnetic resonance imaging. *J. Neurol. Sci.* 292, 40–44. doi: 10.1016/j.jns.2010.02.010

Koenigkam-Santos, M., Santos, A. C., Borduqui, T., Versiani, B. R., Hallak, J. E., Crippa, J. A., et al. (2008). Whole-brain voxel-based morphometry in Kallmann syndrome associated with mirror movements. *AJNR Am. J. Neuroradiol.* 29, 1799–1804. doi: 10.3174/ajnr.A1202

Krams, M., Quinton, R., Ashburner, J., Friston, K. J., Frackowiak, R. S., Bouloux, P. M., et al. (1999). Kallmann's syndrome: Mirror movements associated with bilateral corticospinal tract hypertrophy. *Neurology* 52, 816–822. doi: 10.1212/WNL.52.4.816

Krams, M., Quinton, R., Mayston, M. J., Harrison, L. M., Dolan, R. J., Bouloux, P. M., et al. (1997). Mirror movements in X-linked Kallmann's syndrome. II. A PET study. *Brain* 120(Pt 7), 1217–1228. doi: 10.1093/brain/120.7.1217

Leinsinger, G. L., Heiss, D. T., Jassoy, A. G., Pfluger, T., Hahn, K., and Danek, A. (1997). Persistent mirror movements: Functional MR imaging of the hand motor cortex. *Radiology* 203, 545–552. doi: 10.1148/radiology.203.2.9114119

Lemieux, L., Salek-Haddadi, A., Lund, T. E., Laufs, H., and Carmichael, D. (2007). Modelling large motion events in fMRI studies of patients with epilepsy. *Magn. Reson. Imaging* 25, 894–901. doi: 10.1016/j.mri.2007.03.009

Li, J. M., Bentley, W. J., Snyder, A. Z., Raichle, M. E., and Snyder, L. H. (2015). Functional connectivity arises from a slow rhythmic mechanism. *Proc. Natl. Acad. Sci. U.S.A.* 112, E2527–E2535. doi: 10.1073/pnas.1419837112

Li, Y.-O., Adalı, T., and Calhoun, V. D. (2007a). Estimating the number of independent components for functional magnetic resonance imaging data. *Hum. Brain Mapp.* 28, 1251–1266. doi: 10.1002/hbm.20359

Li, Y.-O., Adali, T., and Calhoun, V. D. (2007b). A feature-selective independent component analysis method for functional MRI. *Intl. J. Biomed. Imaging* 2007:15635. doi: 10.1155/2007/15635

Manara, R., Di Nardo, F., Salvalaggio, A., Sinisi, A. A., Bonanni, G., Palumbo, V., et al. (2018). Spectral signatures of mirror movements in the sensori-motor connectivity in kallmann syndrome. *Hum. Brain Mapp.* 39, 42–53. doi: 10.1002/hbm.23806

Manara, R., Salvalaggio, A., Citton, V., Palumbo, V., D'Errico, A., Elefante, A., et al. (2015). Brain anatomical substrates of mirror movements in Kallmann syndrome. *Neuroimage* 1, 52–58. doi: 10.1016/j.neuroimage.2014.09.067

Manara, R., Salvalaggio, A., Favaro, A., Palumbo, V., Citton, V., Elefante, A., et al. (2014). Brain changes in Kallmann syndrome. *AJNR Am. J. Neuroradiol.* 35, 1700–1706. doi: 10.3174/ajnr.A3946

Mayston, M. J., Harrison, L. M., Quinton, R., Stephens, J. A., Krams, M., and Bouloux, P. M. (1997). Mirror movements in X-linked Kallmann's syndrome. I. A neurophysiological study. *Brain* 120, 1199–1216. doi: 10.1093/brain/120.7.1199

Moeller, S., Yacoub, E., Olman, C. A., Auerbach, E., Strupp, J., Harel, N., et al. (2010). Multiband multislice GE-EPI at 7 tesla, with 16-fold acceleration using partial parallel imaging with application to high spatial and temporal whole-brain fMRI. *Magn. Reson. Med.* 63, 1144–1153. doi: 10.1002/mrm.22361

Power, J. D., Barnes, K. A., Snyder, A. Z., Schlaggar, B. L., and Petersen, S. E. (2012). Spurious but systematic correlations in functional connectivity MRI networks arise from subject motion. *Neuroimage* 59, 2142–2154. doi: 10.1016/j.neuroimage.2011.10.018

Rashid, B., Damaraju, E., and Pearlson, G. D. (2014). Dynamic connectivity states estimated from resting fMRI Identify differences among Schizophrenia, bipolar disorder, and healthy control subjects. *Front. Hum. Neurosci.* 8:897. doi: 10.3389/fnhum.2014.00897

Rousseeuw, P. J. (1987). Silhouettes: A graphical aid to the interpretation and validation of cluster analysis. *J. Comput. Appl. Math.* 20, 53–65. doi: 10.1016/0377-0427(87)90125-7

Sakoglu, U., Pearlson, G. D., Kiehl, K. A., Wang, Y. M., Michael, A. M., and Calhoun, V. D. (2010). A method for evaluating dynamic functional network connectivity and task-modulation: Application to schizophrenia. *MAGMA* 23, 351–366. doi: 10.1007/s10334-010-0197-8

Satterthwaite, T. D., Elliott, M. A., Gerraty, R. T., Ruparel, K., Loughead, J., Calkins, M. E., et al. (2013). An improved framework for confound regression and filtering for control of motion artifact in the preprocessing of resting-state functional connectivity data. *Neuroimage* 64, 240–256. doi: 10.1016/j.neuroimage.2012.08.052

Schumacher, J., Peraza, L. R., Firbank, M., Thomas, A. J., Kaiser, M., Gallagher, P., et al. (2019). Dynamic functional connectivity changes in dementia with Lewy bodies and Alzheimer's disease. *Neuroimage Clin.* 22:101812. doi: 10.1016/j.nicl.2019.101812

Shirer, W. R., Ryali, S., Rykhlevskaia, E., Menon, V., and Greicius, M. D. (2012). Decoding subject-driven cognitive states with whole-brain connectivity patterns. *Cereb. Cortex* 22, 158–165. doi: 10.1093/cercor/bhr099

Smith, S. M., Jenkinson, M., Woolrich, M. W., Beckmann, C. F., Behrens, T. E., Johansen-Berg, H., et al. (2004). Advances in functional and structural MR image analysis and implementation as FSL. *Neuroimage* 23 (Suppl 1), S208–S219. doi: 10.1016/j.neuroimage.2004.07.051

Wang, Y. F., Long, Z., Cui, Q., Liu, F., Jing, X. J., Chen, H., et al. (2016). Low frequency steady-state brain responses modulate large scale functional networks in a frequency-specific means. *Hum. Brain Mapp.* 37, 381–394. doi: 10.1002/hbm.23037

Woods, B. T., and Teuber, H. L. (1978). Mirror movements after childhood hemiparesis. *Neurology* 28, 1152–1157. doi: 10.1212/WNL.28.11.1152

Wu, C. W., Gu, H., Lu, H., Stein, E. A., Chen, J. H., and Yang, Y. (2008). Frequency specificity of functional connectivity in brain networks. *Neuroimage* 42, 1047–1055. doi: 10.1016/j.neuroimage.2008.05.035

Xu, J., Moeller, S., Auerbach, E. J., Strupp, J., Smith, S. M., Feinberg, D. A., et al. (2013). Evaluation of slice accelerations using multiband echo planar imaging at 3 T. *Neuroimage* 83, 991–1001. doi: 10.1016/j.neuroimage.2013.07.055

Yan, C. G., and Yu-Feng, Z. (2010). DPARSF: A MATLAB toolbox for pipeline data analysis of resting-state fMRI. *Front. Syst. Neurosci.* 4:13. doi: 10.3389/fnsys.2010.00013

Yan, C. G., Wang, X. D., Zuo, X. N., and Zang, Y. F. (2016). DPABI: Data processing & analysis for (Resting-State) brain imaging. *Neuroinformatics* 14, 339–351. doi: 10.1007/s12021-016-9299-4

Zuo, X. N., Di Martino, A., Kelly, C., Shehzad, Z. E., Gee, D. G., Klein, D. F., et al. (2010). The oscillating brain: Complex and reliable. *Neuroimage* 49, 1432–1445. doi: 10.1016/j.neuroimage.2009.09.037

frontiers | Frontiers in Neuroscience

TYPE Original Research
PUBLISHED 08 September 2022
DOI 10.3389/fnins.2022.972720

OPEN ACCESS

EDITED BY
Filippo Cieri,
Cleveland Clinic, United States

REVIEWED BY
Emanuele Pravatà,
Ente Ospedaliero Cantonale (EOC), Switzerland
Vassiliy Tsytsarev,
University of Maryland, College Park, United States

*CORRESPONDENCE
Simon Skau
simon.skau@gu.se

SPECIALTY SECTION
This article was submitted to Brain Imaging Methods, a section of the journal Frontiers in Neuroscience

RECEIVED 18 June 2022
ACCEPTED 23 August 2022
PUBLISHED 08 September 2022

CITATION
Skau S, Johansson B, Kuhn H-G and Thompson WH (2022) Segregation over time in functional networks in prefrontal cortex for individuals suffering from pathological fatigue after traumatic brain injury. *Front. Neurosci.* 16:972720. doi: 10.3389/fnins.2022.972720

Segregation over time in functional networks in prefrontal cortex for individuals suffering from pathological fatigue after traumatic brain injury

Simon Skau[1,2]*, Birgitta Johansson[1], Hans-Georg Kuhn[1] and William Hedley Thompson[3,4]

[1]Institute of Neuroscience and Physiology, Sahlgrenska Academy, University of Gothenburg, Gothenburg, Sweden, [2]Department of Pedagogical, Curricular and Professional Studies, Faculty of Education, University of Gothenburg, Gothenburg, Sweden, [3]Department of Applied Information Technology, University of Gothenburg, Gothenburg, Sweden, [4]Department of Clinical Neuroscience, Karolinska Institutet, Stockholm, Sweden

Pathological fatigue is present when fatigue is perceived to continually interfere with everyday life. Pathological fatigue has been linked with a dysfunction in the cortico-striatal-thalamic circuits. Previous studies have investigated measures of functional connectivity, such as modularity to quantify levels of segregation. However, previous results have shown both increases and decreases in segregation for pathological fatigue. There are multiple factors why previous studies might have differing results, including: (i) Does the functional connectivity of patients with pathological fatigue display more segregation or integration compared to healthy controls? (ii) Do network properties differ depending on whether patients with pathological fatigue perform a task compared to periods of rest? (iii) Are the brain networks of patients with pathological fatigue and healthy controls differently affected by prolonged cognitive activity? We recruited individuals suffering from pathological fatigue after mild traumatic brain injury (n = 20) and age-matched healthy controls (n = 20) to perform cognitive tasks for 2.5 h. We used functional near-infrared spectroscopy (fNIRS) to assess hemodynamic changes in the frontal cortex. The participants had a resting state session before and after the cognitive test session. Cognitive testing included the Digit Symbol Coding test at the beginning and the end of the procedure to measure processing speed. We conducted an exploratory network analysis on these resting state and Digit Symbol Coding sessions with no *a priori* hypothesis relating to how patients and controls differ in their functional networks since previous research has found results in both directions. Our result showed a Group vs. Time interaction (p = 0.026, η_p^2 = 0.137), with a *post hoc* test revealing that the TBI patients developed higher modularity

toward the end of the cognitive test session. This work helps to identify how functional networks differ under pathological fatigue compared to healthy controls. Further, it shows how the functional networks dynamically change over time as the patient performs tasks over a time scale that affect their fatigue level.

KEYWORDS

connectivity, modularity, fNIRS, pathological fatigue, fatigability, state fatigue

Introduction

Pathological fatigue is when the general tendency of *fatigability* and the *sensation of fatigue* is perceived to interfere with everyday life (Skau et al., 2021). Pathological fatigue is often a consequence of trauma to, or disturbance in, the central nervous system (Johansson and Rönnbäck, 2014; Berginström, 2019). The prevalence of pathological fatigue is estimated to be between 36–77% after stroke, 45–73% after traumatic brain injury (TBI), 38–83% in multiple sclerosis (MS), and 28–58% in Parkinson's disease (Kluger et al., 2013). It is also associated with conditions, such as exhaustion disorder (Sandstrom et al., 2005; Krabbe et al., 2017), infection of the central nervous system (Morris et al., 2015), or hormonal imbalance (Möller et al., 2014), together with additional symptoms such as sensitivity to light and sound and irritability. Individuals suffering from pathological fatigue after mild TBI often report an increased sensation of fatigue after mental activity with an abnormally long recovery time (Johansson and Ronnback, 2017). Studies of pathological fatigue after moderate to severe TBI using functional magnetic resonance imaging (fMRI) indicate a dysfunction within cortico-striatal-thalamic circuits (Kohl et al., 2009; Nordin et al., 2016; Berginstrom et al., 2017; Möller et al., 2017; Wylie et al., 2017).

The interplay between integration and segregation within brain networks is considered a critical property of brain function and cognition (Sporns, 2013). Among the many network measures, modularity is one of the more commonly used when studying fatigue. It is a global measure that quantifies the segregation of the entire network. Based on the co-variation of functional brain activity among different brain regions, groups of nodes get clustered together into communities (note, in network theory, these are called "communities," which is analogous to "brain networks" or "resting-state networks" often used in cognitive neuroscience). Modularity quantifies how tight-knit these communities are compared to chance. Modularity is high if there are fewer between-community connections (see **Figure 1**) which are interpreted as higher segregation between communities. Contrarily, low modularity is indicative of either low segregation or high integration in the network.

Numerous neuroimaging studies on patient populations with fatigue have used functional connectivity measures, but the findings are inconclusive. Some studies have found increased integration or connectivity in pathological fatigue. Messé et al. (2013) investigated network properties for TBI patients, with and without post-concussion symptoms (including fatigue). The group with post-concussion symptoms had lower modularity, i.e., a less segregated functional network. Similarly, higher self-reported fatigue in chronic fatigue patients was associated with a lower degree of connectivity for the medial frontal cortex with the rest of the brain (Gay et al., 2016). On the other hand, Høgestøl et al. (2019) found that connectivity in the default modal network increased for MS patients with high severity of depressive and fatigue symptoms. In contrast, Kim et al. (2015) reported that patients with chronic fatigue syndrome displayed a decrease in global efficiency, a measure for network integration.

In cohorts with healthy adults, previous research has found that inducing fatigue results in an decrease in segregation measured by decreased modularity (Ben Simon et al., 2017) and an increase in path length, another measure of segregation (Sun et al., 2014). Wylie et al. (2020) identified a network made up of the dorsolateral prefrontal cortex (DLPFC), ventromedial PFC (VMPFC), dorsal anterior cingulate cortex (dACC), anterior insula, and the striatum, which showed less connectivity when state fatigue increased after cognitive activity.

In sum, researchers have linked changes in connectivity, through common topographical measures such as modularity, to pathological fatigue and cognitive fatigability in healthy adults. However, whether there is a change in integration or segregation is unclear. Further, we do not know if different factors in design and population impact the varying results. For example, it is unclear if cognitive fatigability (i.e., the decrement in cognitive performance over a consecutive time) affects the modularity of networks differently for healthy adults compared to individuals suffering from pathological fatigue. Moreover, study design aspects, such as the duration of cognitive activity for inducing cognitive fatigue, can vary [e.g., 20 min in Sun et al. (2014), but 2.5 h in Skau et al. (2019)]. Further, some studies above performed their network calculation from

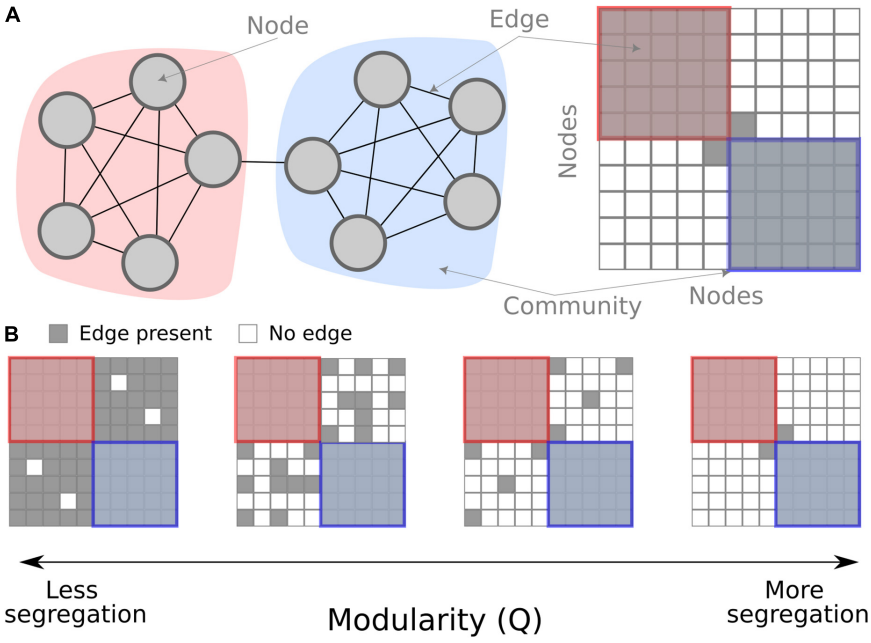

FIGURE 1
Conceptual overview of modularity in a network. **(A)** A schematic network of 10 nodes in two communities (red and blue) connected by binary edges. On the left, the nodes are shown graphically, and on the right, the same schematic network is shown as a connectivity matrix. **(B)** Examples of modularity as a measure. When there are fewer between-community edges, the modularity measure is higher, interpreted as more segregation.

resting-state sessions, while others had participants perform a task. In summary, the following three factors relating to network theory and fatigue are still not fully understood:

1. Do the brain networks of patients with pathological fatigue display more segregation or integration compared to healthy controls?
2. Do network properties differ depending on whether patients with pathological fatigue perform a task compared to periods of rest?
3. Are the brain networks of patients with pathological fatigue and healthy control differently affected by prolonged cognitive activity?

In this study, we provide evidence relating to each of these questions. We use the functional near-infrared spectroscopy (fNIRS) data of pathological fatigue after mild TBI from Skau et al. (2019). fNIRS is an optical imaging technique that applies near-infrared light to measure the change in oxygenated and deoxygenated hemoglobin a couple of centimeters down into the neocortex. Twenty individuals suffering from pathological fatigue after mild TBI and twenty healthy controls performed cognitive tests for about 2.5 h. The test battery consisted of 6 neuropsychological tests done twice, intermediated with a sustained attention task. Throughout the experiment, multiple resting-state sessions were done (see **Figure 2A**).

We conducted an exploratory network analysis with no *a priori* hypothesis related to how patients and controls differ in their functional networks considering previous articles have found results in both directions. We chose modularity to evaluate segregation since modularity is an intuitive, single global measure. Previous studies have used it, and it circumnavigates specific problems relating to network measures over time (see Thompson et al., 2020). We analyze the contrast in modularity before and after performing a long battery of tests in healthy adults and patients. Further, we analyze the first and last resting-state session and the Digit Symbol Coding (DSC) that measures processing speed. This work helps identify how network analyses of pathological fatigue differ from healthy controls and dynamically change over time as the patient performs tasks over a time scale that affects their fatigue.

Materials and methods

Study participants and protocol

Details of the protocol and descriptions of the cognitive and neuropsychological tests included in the test session but not analyzed here are presented in Skau et al. (2019).

Twenty individuals with pathological fatigue after mild TBI (minimum 5 months after injury) were recruited from the

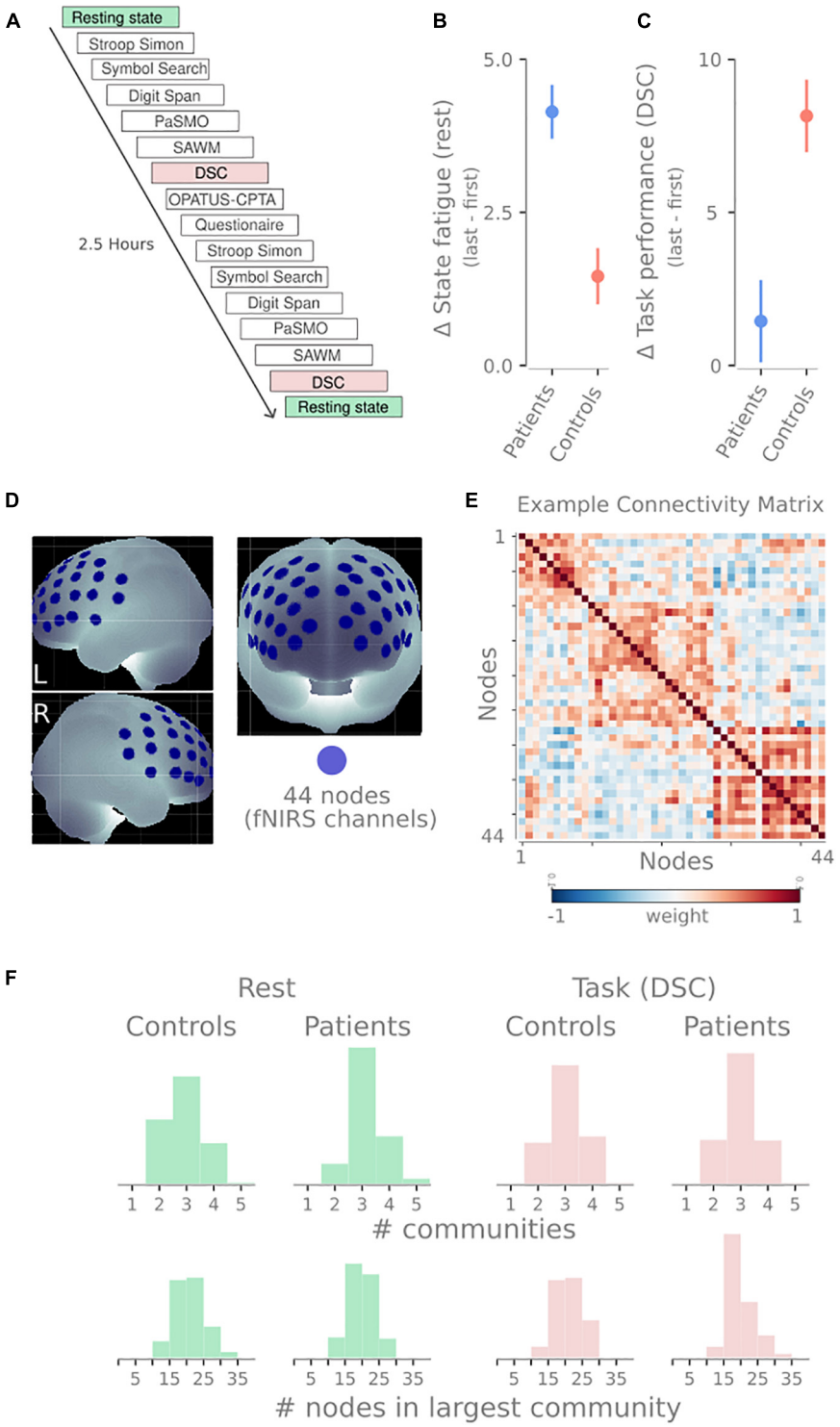

FIGURE 2
Overview of design and methodology. **(A)** Timeline of tasks performed by participants in this study. The blocks analyzed in this manuscript have been highlighted: resting-state sessions (green) and digit symbol coding tasks (DSC, red). **(B)** The difference in self-reported state fatigue following the resting-state session (last–first) for both groups. **(C)** Difference in task performance in the DSC task (last-first). Panels **(C,D)** show data previously reported in Skau et al. (2019). **(D)** The 44 recording sites on the frontal cortex. These 44 recording sites become nodes in the network. **(E)** An example connectivity matrix from one resting-state session showing three communities for the 44 nodes depicted in panel **(B)**. Similar to the connectivity matrix in 1A, but with weighted edges instead of binary edges. **(F)** Descriptive statistics of the community detection properties. Histograms show the number of communities (top) and the number of nodes in the largest community (bottom) for rest (green) and DSC task (red) and both patients and healthy controls.

Department of Neurology, Sahlgrenska University Hospital, Gothenburg. Inclusion criteria were as follows: diagnosed with mild TBI according to the definition proposed by The World Health Organization Collaborating Center for Neurotrauma Task Force (Carroll et al., 2004); scoring above the cut-off score of 10.5 on the Mental Fatigue Scale (MFS) (Johansson and Rönnbäck, 2014); aged 20–65 years and not suffering from any other psychiatric or neurological disorders. All participants recovered well and were independent in their daily living, except for their pathological fatigue. Six individuals received methylphenidate drug treatment but suspended the treatment 1 week before the assessment. As reported in Skau et al. (2019), no significant differences concerning the cognitive test results and ratings on MFS were detected between these six individuals compared to the other individuals with TBI. Twenty-one healthy controls who neither suffered from pathological fatigue (below 10.5 points on MFS) nor had any psychiatric or neurological disorders were recruited from the general community at request. One control subject was excluded due to failure to follow instructions. The Regional Ethical Review Board in Gothenburg approved the study (reference number: 028-16). The participants gave their informed written consent before the assessment and were told they could withdraw at any time.

Experimental design

Each participant was seated in a chair next to a table with a computer screen. All tests were performed sitting in the same location. Depending on the task requirements, different responses from the participants, such as computer input (*via* mouse, tablet, or game controller), pen and paper, or verbal responses, were needed. The fNIRS cap with optodes attached was carefully placed on the participant's head and worn throughout the experimental session. In order to minimize ambient light reaching the optodes at the scalp, the fNIRS cap was covered by another stretchable cap. The experiment consisted of two identical test sessions with six individual tests performed in the same sequence (**Figure 2A**). The two sessions were separated by a sustained-attention test with an 8-min one-back task (OPATUS-CPTA) and completing the MFS (**Figure 2A**). In total, the test procedure took 2 1/2 h. Participants were allowed to take a short break where they could drink water or stand up and stretch their legs between tests while keeping the fNIRS cap on.

Before and after the experimental procedure, participants rated their energy level on a visual analog scale (VAS). The VAS scale was a continuous line (10 cm) between the two end-points: "full of energy" and "totally exhausted, no energy left," and was used to evaluate state fatigue. Mean and SD were 3.13 ± 2.0 and 7.27 ± 1.7 (for the patients) and 2.66 ± 1.5 and 4.12 ± 1.6 (for the controls) for the first and second VAS, respectively (see **Figure 2B**).

There were five separate occasions of 1-min resting-state recordings where participants were asked to focus on a fixation cross. These sessions were positioned: before the first task, after the first Stroop-Simon test, before the second Stroop-Simon test, after the second Stroop-Simon test, and right at the end of the experiment (see **Figure 2A**).

Digit Symbol Coding (DSC) is a subtest within the Processing Speed Index in WAIS-IV (Wechsler, 2010) that was used to measure attention, mental and psychomotor operation speed, and visual discrimination. Participants are asked to perform as many symbols as possible for 2 min. The raw score is the number of correct symbols performed. Mean and SD were 65.6 ± 11.7 and 67.0 ± 15.6 (for the patients) and 72.2 ± 10.9 and 80.4 ± 12.4 (for the controls) for the first and second test, respectively (see **Figure 2C**).

Functional near-infrared spectroscopy data acquisition

The fNIRS measurements were performed using a continuous wave system (NTS) Optical Imaging System, Gowerlabs Ltd., United Kingdom (Everdell et al., 2005), using two wavelengths (780 and 850 nm) to measure changes in the concentration of oxygenated hemoglobin (oxy-Hb), deoxygenated hemoglobin (deoxy-Hb), and their total sum hemoglobin (tot-Hb). The system has 16 dual-wavelength sources and 16 detectors. The array consisted of 44 standard fNIRS channels (i.e., source/detector pairs) with a source-detector distance of 30, plus two short-separation channels with a source-detector distance of 10 mm, as suggested in previous studies (Gagnon et al., 2011; Brigadoi and Cooper, 2015). Short separation channels are only sensitive to hemodynamics in the scalp. Since the regular separation channels measure signals originating in both the brain and the scalp, the use of short-separation channels allowed us to regress the scalp signal from regular-separation signals to improve the brain specificity of the fNIRS measurement (Gagnon et al., 2011; Brigadoi and Cooper, 2015). The placement of the optodes was designed to encompass the frontal cortex, previously reported to be involved in executive function and cognitive control tasks (see **Figure 2D**; Roberts and Hall, 2008). Data were acquired at a sampling frequency of 10 Hz.

Functional near-infrared spectroscopy data analysis

The fNIRS data were preprocessed using MATLAB (2018) and the MATLAB-based fNIRS-processing package *HomER2*

(Huppert et al., 2009). The processing pipeline started with pruning the raw data such that channels were rejected if their mean intensity was below the instrument's noise floor (1e-4 A.U.). The raw data was then converted to optical density. A high band-pass filter of 0.05 was used to correct for drift and a low band-pass 0.5 filter to remove pulse and respiration. The HomER2 functions *hmrMotionArtifactByChannel* and *hmrMotionCorrectSpline* were used to correct for motion artifacts. Optical density was converted to hemoglobin concentration with *hmrOD2Conc* with a default pathlength factor of 6.0 for both wavelengths. Before *hmrBlockAvg* was used, activity from short separation channels was regressed out of the long 44 standard channels. The short channel selected for regression was the one with the highest correlation to the respective long channel.

Functional connectivity and network analysis

To create the networks, we used the 44 fNIRS channels as nodes in the network. To create the edges between the nodes, the preprocessed and denoised time series of each node were correlated with each other using Pearson correlations. This process creates a 44 × 44 symmetrical weighted connectivity matrix for each subject and session, representing the functional connectivity for that session (**Figure 2E**).

Before the community detection, the negative edges were set to 0. The Louvain community detection algorithm was used, as implemented in the *python-louvain* package (V0.15). Through the community detection algorithm, nodes are clustered into non-overlapping communities. The modularity of the network was calculated after the community detection. As there is stochasticity within the Louvain algorithm, it was run 100 times with the modularity calculated each time and the average modularity over all runs was used. The resolution parameter was set to 1, but to demonstrate that this parameter has not induced or influenced the results, **Supplementary Figure 1** shows that this parameter has little effect on the results when jittering between 0.8 and 1.2.

One task or group could have varying community profiles leading to problematic comparisons (e.g., if every node is placed in a singleton community or all nodes belong to the same community). To illustrate that this was not the case, **Figure 2F** shows distributions of the number of communities detected and the size of the largest community. While there is a slight skewness difference between patients and controls at rest regarding the number of communities, they both have the same median (3). None of the distributions display extreme values rendering modularity comparison problematic. We included the number of nodes in the largest community to demonstrate that the community sizes were not the majority of nodes followed by 1–2 singleton communities.

Statistics

We used the open-source program *JASP* version 0.13.1 for statistical analysis (Marsman and Wagenmakers, 2017). We conducted a repeated ANOVA with one between-group variable *Group* (TBI, controls), and two within-group variables *Time* (first, last) and *Activity* (rest, task), with *Age* as a covariate. *Post hoc* *t*-tests were performed with the Holm method used for multiple comparison correction. The datasets generated in the current study are available from the corresponding author on reasonable request.

Pearson's correlations were used to evaluate if the change in state fatigue was linearly associated with the change in task performance and change in rest and task modularity. Delta scores (last–first) were used for the self-reported state fatigue measure (the VAS) and the delta DSC task performance, delta rest modularity, and delta task modularity.

Results

When analyzing the modularity scores, the repeated three-way ANOVA revealed a significant *Group* vs. *Time* interaction [$F(1,34) = 5.399$, $p = 0.026$ $\eta_p^2 = 0.137$]. *Post hoc* test showed higher modularity in TBI last > TBI first with $t(19) = -2.812$, with a Holms corrected p-value of 0.049 and a Cohen's d of −0.653. This result suggests that no matter the activity (rest or task), patients have higher modularity after 2.5 h of cognitive activity (see **Figure 3** and **Supplementary Table 1** for the other *post hoc* results).

Since there was a Group vs. Time interaction, the main effect results of Group and Time need to be interpreted accordingly. There were no main effect differences for Group [$F(1,34) = 0.127$, $p = 0.742$ with a $\eta_p^2 = 0.004$], indicating no overall difference in modularity between patients and control when both time points are pooled together. There were no main effect differences for *Time* [$F(1,34) = 1.054$, $p = 0.312$ with a $\eta_p^2 = 0.03$], indicating that overall (when both groups are pooled together) there was no difference over time, even though the *post hoc* test showed that the TBI group had significantly higher modularity. There were no main effect differences for *Activity* [$F(1,34) = 0.005$, $p = 0.947$ with a $\eta_p^2 = 1.337\text{e-}4$], indicating that overall, for both groups, there was no difference in modularity between rest and task.

Finally, delta VAS (the changes in self-reported state fatigue) correlated negatively with the DSC performance delta score ($r = -0.518$, $p < 0.001$), indicating that the more change in delta VAS, the less change in delta DSC. There was no significant correlation between delta VAS and the delta modularity with $r = 0.201$ and $p = 0.226$ for *rest* and $r = 0.183$ and $p = 0.285$ for *DSC*, indicating no linear correlation between the difference in network measures and behavior.

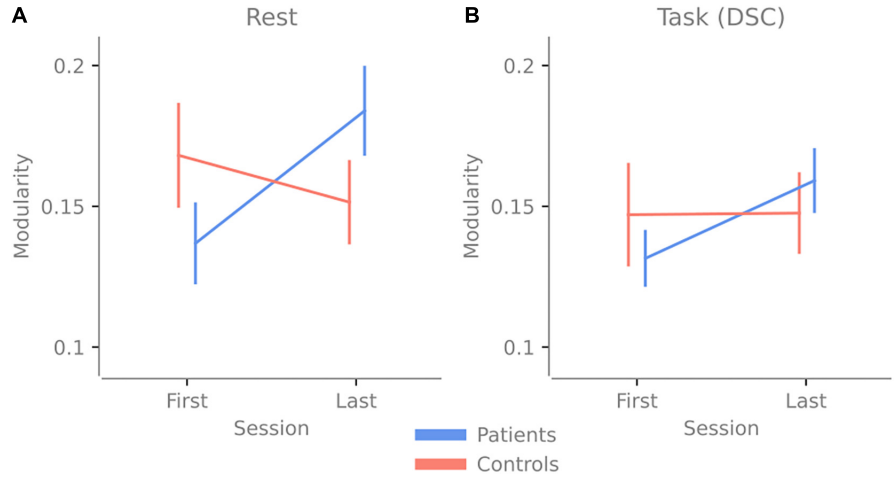

FIGURE 3
Change in modularity over 2.5 h of cognitive activity. Panel **(A)** shows the change in modularity between the first and last resting-state session. **(B)** The change in modularity during the first and last Digit Symbol Coding (DSC) task was done at the experiment's beginning and end. Error bars indicate the standard error of the mean.

Discussion

The debate about fatigue has led to the question whether induced fatigue in healthy individuals (i.e., increased sensation of fatigue after effort) is comparable with pathological fatigue. This scenario would imply that pathological fatigue is only a more intense form of fatigue compared to what healthy individuals experience. It would also suggest a common underlying neural mechanism, as discussed by Wylie et al. (2020). In a second scenario, pathological fatigue would be seen as qualitatively different from induced fatigue in healthy individuals (which is both time-limited and alleviated by rest), having a different underlying pathophysiological mechanism and, consequently, should not be viewed as an extreme on one single fatigue continuum, as discussed by Rönnbäck and Johansson (2022). Under the first assumption, we would expect some common brain network configuration to be impacted, leading to fatigue (e.g., a similar change in network properties). This change would occur regardless of whether the fatigue was induced or pathological.

In the present study, we tried to bring some clarity to this question by evaluating network modularity since it is a common measure of the network topology which has been identified to be associated with both pathological fatigue (Messé et al., 2013) and induced sensation of fatigue by fatigability in healthy adults (Ben Simon et al., 2017). We let healthy adults and individuals suffering from pathological fatigue after mild TBI perform on a 2.5 h long, cognitively intense test battery.

Our results indicate that brain networks of patients with pathological fatigue do not display more segregation or integration compared to healthy controls, nor do we find network properties that differ depending on whether patients with pathological fatigue perform a task compared to periods of rest. When looking over both timepoints, patients and controls have a comparable level of modularity for rest and task, and no significant difference is detected between the groups (see **Figure 3**). These results contradict (Messé et al., 2013), which reported lower modularity for individuals with post-concussion symptoms. On the other hand, the results from Gay et al. (2016) and Høgestøl et al. (2019), that increased fatigue in chronic fatigue and MS patients is associated with less connectivity in the frontal cortex, are in line with our result. However, since we have used previously analyzed data and had no specific hypothesis about how the network properties would vary between conditions, these results should be considered exploratory. Our results highlight features that can guide hypothesis in future confirmatory studies relating to both network analyses using fNIRS and key issues in the experimental design when studying chronic fatigue.

As for our third question: are the brain networks of patients with pathological fatigue and healthy control differently affected by prolonged cognitive activity? The answer is yes; the patients' modularity increased for both rest and task due to the prolonged activity, while the modularity stayed the same for the controls. If we compare this to the behavioral data presented in Skau et al. (2019), both groups reported increased state fatigue, and no group performed worse on the second task—the controls improved their performance. In contrast, patients performed similarly in the first task (see **Figures 2B,C**). Together this means that the prolonged cognitive activity increased state fatigue since both groups reported increased state fatigue (higher values on the VAS post-experiment). However, the controls did not display any change in modularity, whereas

the patients did, suggesting that the fatigue in patients has a different underlying neural or network correlate. This increase in segregation after prolonged mental activity for patients with pathological fatigue could be part of an explanation for the abnormally long recovery time and something future investigation needs to determine.

Changes in modularity could be instantiated in several ways by either within-community edges weakening (splitting the community into two) or by strengthening between-community edges. Further, modularity changes are identified in several related pathological conditions. In their review of the connectivity in stroke patients, Baldassarre et al. (2016) highlight that stroke patients show more network segregation and that the increased cognitive performance after recovery correlated with an increase/restoration of functional connectivity. Similarly, Fleischer and colleagues reviewed the literature on MS that has used the graph theoretical approach for network integration and found that increased modularity was not only typical for MS, but the increase in modularity also negatively correlated with cognitive ability and MS symptom progression (Fleischer et al., 2019). For Parkinson's disease, a recent review found that the global efficiency, another graph theoretical measure, was decreased in patients compared to healthy controls (Tessitore et al., 2019). Community segregation in these patient groups is often pathophysiologically interpreted as a consequence of reorganization or adaptation to the neurological disease or acute/chronic neural inflammation. While all these issues may impact modularity, conversely, pathological fatigue is a very common symptom in these patient groups (stroke, MS, and Parkinson's disease) (Kluger et al., 2013), and research about the overlap between fatigue symptoms and network modularity across different patient groups will be important for our understanding of pathological fatigue.

In a recent paper, Rönnbäck and Johansson (2022) proposed the theory that pathological fatigue after TBI is due to neuro-inflammation in the CNS caused by the trauma. They argue that neuro-inflammation would affect astroglial cells and their ability to fine-tune the extracellular glutamate levels and clearance of excessive glutamate from the extracellular space. The prolonged mental activity would lead to increased excitatory glutamate in the extracellular space, which would cause swelling of astrocytes and shrinkage of the extracellular space. Neural signaling would become less specific, and the shrinking of extracellular space would result in the non-specific activation of adjacent neurons (Rönnbäck and Johansson, 2022). Our results would support such a hypothesis since a latent neuro-inflammatory process could, after prolonged activity, result in diffuse neuronal signaling, causing segregation of functional networks. For controls, assuming the absence of neuro-inflammation, neuronal signaling would not become diffused after prolonged activity; consequently, no functional network segregation would be detected. This interpretation would also support the second scenario mentioned above, that there is no true continuum between the fatigue of healthy adults and the fatigue experienced by individuals suffering from pathological fatigue. However, the leap from cellular events to large-scale network activity is currently not warranted due to a lack of sufficient data. It should be seen as a working hypothesis until more studies become available.

Limitations

Due to the study's design, there was a time difference between the first resting state session and the first DSC, whereas the last resting state session was right after the last DSC. Digitizing the placement of the fNIRS optodes was done, but the measurements were too noisy and were concluded to be unreliable. Therefore, we do not have external measurements confirming the channel localization. However, head size measurements were taken before the experiment. EasyCap sizes 54, 56, and 58 were used to fit the participants' heads as accurately as possible using face and 10/20 head landmarks to get measurements where intended.

Neither coffee intake during the day nor sleep quality of the previous night were controlled for, which might also impact network properties. Although the study was exploratory, the small sample size is a limitation.

Since there was no additional time point after the end of the experiment to evaluate whether the connectivity configurations recovered for the patient group, we cannot rule out that the observed Time vs. Group interaction is not driven by fluctuations unrelated to the effort. Since the recovery time for individuals with pathological fatigue is prolonged, it would be fruitful in future research to investigate several time points after a long and cognitively intense experiment to focus on the recovery of the network properties.

Conclusion

This exploratory analysis suggests increased segregation in the frontal cortex for patients with pathological fatigue after prolonged mental activity but not for healthy controls. Future research should determine if this pattern holds in other patient groups suffering from pathological fatigue, how long and intense the mental activity needs to be to generate segregation in the frontal cortex, and how long the recovery time needs to be to reach the baseline level of modularity.

Data availability statement

The raw data supporting the conclusions of this article will be made available by the authors, without undue reservation.

Ethics statement

The studies involving human participants were reviewed and approved by The Regional Ethical Review Board in Gothenburg. The patients/participants provided their written informed consent to participate in this study.

Author contributions

SS conceived, planned, and carried out the experiments, conceptualization of analysis in this manuscript, statics, and writing—first draft. BJ conceived, planned, and carried out the experiments and writing—review and editing. H-GK wrote—reviewed and edited the manuscript WT contributed to conceptualization of analysis in this manuscript, connectivity analysis, and writing—first draft. All authors contributed to the article and approved the submitted version.

Funding

H-GK was supported by the Swedish Research Council (Vetenskapsraådet 721-2014-2468 and 521-2014-3224), Swedish Childhood Cancer Foundation (Barncancerfonden MT2017-0013), by a grant from the Swedish state under the ALF agreement (ALFGBG-726541) and by the Stena A Olssons Stiftelse för Forskning och Kultur.

Conflict of interest

The authors declare that the research was conducted in the absence of any commercial or financial relationships that could be construed as a potential conflict of interest.

Publisher's note

All claims expressed in this article are solely those of the authors and do not necessarily represent those of their affiliated organizations, or those of the publisher, the editors and the reviewers. Any product that may be evaluated in this article, or claim that may be made by its manufacturer, is not guaranteed or endorsed by the publisher.

Supplementary material

The Supplementary Material for this article can be found online at: https://www.frontiersin.org/articles/10.3389/fnins.2022.972720/full#supplementary-material

References

Baldassarre, A., Ramsey, L. E., Siegel, J. S., Shulman, G. L., and Corbetta, M. (2016). Brain connectivity and neurological disorders after stroke. *Curr. Opin. Neurol.* 29, 706–713.

Ben Simon, E., Maron-Katz, A., Lahav, N., Shamir, R., and Hendler, T. (2017). Tired and misconnected: a breakdown of brain modularity following sleep deprivation. *Hum. Brain Mapp.* 38, 3300–3314. doi: 10.1002/hbm.23596

Berginström, N. (2019). *Fatigue After Traumatic Brain Injury: Exploring Novel Methods for Diagnosis and Treatment*. Ph.D. thesis. Umeå: Umeå University.

Berginstrom, N., Nordström, P., Ekman, U., Eriksson, J., Andersson, M., Nyberg, L., et al. (2017). Using functional magnetic resonance imaging to detect chronic fatigue in patients with previous traumatic brain injury: changes linked to altered striato-thalamic-cortical functioning. *J. Head Trauma Rehabil.* 33, 266–274. doi: 10.1097/HTR.0000000000000340

Brigadoi, S., and Cooper, R. J. (2015). How short is short? Optimum source-detector distance for short-separation channels in functional near-infrared spectroscopy. *Neurophotonics* 2:025005. doi: 10.1117/1.NPh.2.2.025005

Carroll, L. J., Cassidy, J. D., Peloso, P. M., Borg, J., von Holst, H., Holm, L., et al. (2004). Prognosis for mild traumatic brain injury: results of the WHO collaborating centre task force on mild traumatic brain injury. *J. Rehabil. Med.* 84–105.

Everdell, N. L., Gibson, A. P., and Tullis, I. D. C. (2005). A frequency multiplexed near-infrared topography system for imaging functional activation in the brain. *Rev. Sci. Instr.* 76:093705.

Fleischer, V., Radetz, A., Ciolac, D., Muthuraman, M., Gonzalez-Escamilla, G., and Zipp, F. (2019). Graph theoretical framework of brain networks in multiple sclerosis: a review of concepts. *Neuroscience* 403, 35–53. doi: 10.1016/j.neuroscience.2017.10.033

Gagnon, L., Perdue, K., Greve, D. N., Goldenholz, D., Kaskhedikar, G., and Boas, D. A. (2011). Improved recovery of the hemodynamic response in diffuse optical imaging using short optode separations and state-space modeling. *Neuroimage* 56, 1362–1371. doi: 10.1016/j.neuroimage.2011.03.001

Gay, C. W., Robinson, M. E., Lai, S., O'Shea, A., Craggs, J. G., Price, D. D., et al. (2016). Abnormal resting-state functional connectivity in patients with chronic fatigue syndrome: results of seed and data-driven analyses. *Brain Connect.* 6, 48–56. doi: 10.1089/brain.2015.0366

Høgestøl, E. A., Nygaard, G. O., Alnæs, D., Beyer, M. K., Westlye, L. T., and Harbo, H. F. (2019). Symptoms of fatigue and depression is reflected in altered default mode network connectivity in multiple sclerosis. *PLoS One* 14:e0210375. doi: 10.1371/journal.pone.0210375

Huppert, T. J., Diamond, S. G., Franceschini, M. A., and Boas, D. A. (2009). HomER: a review of time-series analysis methods for near-infrared spectroscopy of the brain. *Appl. Opt.* 48, D280–D298. doi: 10.1364/ao.48.00d280

Johansson, B., and Rönnbäck, L. (2014). "Long-lasting mental fatigue after traumatic brain injury – a major problem most often neglected diagnostic criteria, assessment, relation to emotional and cognitive problems, cellular background, and aspects on treatment," in *Traumatic Brain Injury*, ed. Sadaka (Rijeka: InTech).

Johansson, B., and Ronnback, L. (2017). Assessment and treatment of mental fatigue after a traumatic brain injury. *Neuropsychol. Rehabil.* 27, 1047–1055.

Kim, B.-H., Namkoong, K., Kim, J. J., Lee, S., Yoon, K. J., Choi, M., et al. (2015). Altered resting-state functional connectivity in women with chronic fatigue syndrome. *Psychiatry Res.* 234, 292–297.

Kluger, M. B., Krupp, B. L., and Enoka, M. R. (2013). Fatigue and fatigability in neurologic illnesses: proposal for a unified taxonomy. *Neurology* 80, 409–416. doi: 10.1212/WNL.0b013e31827f07be

Kohl, A. D., Wylie, G. R., Genova, H. M., Hillary, F. G., and Deluca, J. (2009). The neural correlates of cognitive fatigue in traumatic brain injury using functional MRI. *Brain Inj.* 23, 420–432.

Krabbe, D., Ellbin, S., Nilsson, M., Jonsdottir, I. H., and Samuelsson, H. (2017). Executive function and attention in patients with stress-related exhaustion: perceived fatigue and effect of distraction. *Stress* 20, 333–340. doi: 10.1080/10253890.2017.1336533

Marsman, M., and Wagenmakers, E.-J. (2017). Bayesian benefits with JASP. *Eur. J. Dev. Psychol.* 14, 545–555.

MATLAB (2018). *MATLAB: The MathWorks*. Natick, MA: The MathWorks.

Messé, A., Caplain, S., Pélégrini-Issac, M., Blancho, S., Lévy, R., Aghakhani, N., et al. (2013). Specific and evolving resting-state network alterations in post-concussion syndrome following mild traumatic brain injury. *PLoS One* 8:e65470. doi: 10.1371/journal.pone.0065470

Möller, M. C., Bartfai, A., Nygren de Boussard, C., Rådestad, A. F., and Calissendorff, J. (2014). High rates of fatigue in newly diagnosed Graves' disease. *Fatigue Biomed. Health Behav.* 2, 153–162.

Möller, M. C., Nordin, L. E., Bartfai, A., Julin, P., and Li, T. Q. (2017). Fatigue and cognitive fatigability in mild traumatic brain injury are correlated with altered neural activity during vigilance test performance. *Front. Neurol.* 8:496. doi: 10.3389/fneur.2017.00496

Morris, G., Berk, M., Walder, K., and Maes, M. (2015). Central pathways causing fatigue in neuro-inflammatory and autoimmune illnesses. *BMC Med.* 13:28. doi: 10.1186/s12916-014-0259-2

Nordin, L. E., Möller, M. C., Julin, P., Bartfai, A., Hashim, F., and Li, T. Q. (2016). Post mTBI fatigue is associated with abnormal brain functional connectivity. *Sci. Rep.* 6:21183. doi: 10.1038/srep21183

Roberts, K. L., and Hall, D. A. (2008). Examining a supramodal network for conflict processing: a systematic review and novel functional magnetic resonance imaging data for related visual and auditory stroop tasks. *J. Cogn. Neurosci.* 20, 1063–1078. doi: 10.1162/jocn.2008.20074

Rönnbäck, L., and Johansson, B. (2022). Long-lasting pathological mental fatigue after brain injury–a dysfunction in glutamate neurotransmission? *Front. Behav. Neurosci.* 15:791984. doi: 10.3389/fnbeh.2021.791984

Sandstrom, A., Rhodin, I. N., Lundberg, M., Olsson, T., and Nyberg, L. (2005). Impaired cognitive performance in patients with chronic burnout syndrome. *Biol. Psychol.* 69, 271–279.

Skau, S., Bunketorp-Käll, L., Kuhn, H. G., and Johansson, B. (2019). Mental fatigue and functional near-infrared spectroscopy (FNIRS) – based assessment of cognitive performance after mild traumatic brain injury. *Front. Hum. Neurosci.* 13:145. doi: 10.3389/fnhum.2019.00145

Skau, S., Sundberg, K., and Kuhn, H.-G. (2021). A proposal for a unifying set of definitions of fatigue. *Front. Psychol.* 12:739764. doi: 10.3389/fpsyg.2021.739764

Sporns, O. (2013). Network attributes for segregation and integration in the human brain. *Curr. Opin. Neurobiol.* 23, 162–171.

Sun, Y., Lim, J., Kwok, K., and Bezerianos, A. (2014). Functional cortical connectivity analysis of mental fatigue unmasks hemispheric asymmetry and changes in small-world networks. *Brain Cogn.* 85, 220–230. doi: 10.1016/j.bandc.2013.12.011

Tessitore, A., Cirillo, M., and De Micco, R. (2019). Functional connectivity signatures of parkinson's disease. *J. Parkinsons Dis.* 9, 637–652.

Thompson, W. H., Kastrati, G., Finc, K., Wright, J., Shine, J. M., and Poldrack, R. A. (2020). Time-varying nodal measures with temporal community structure: A cautionary note to avoid misinterpretation. *Hum. Brain Mapp.* 41, 2347–2356. doi: 10.1002/hbm.24950

Wechsler, D. (2010). *Wechsler Adut Intelligence Scale*, Fourth Edn. Stockholm: Pearson Assessment.

Wylie, G. R., Dobryakova, E., DeLuca, J., Chiaravalloti, N., Essad, K., and Genova, H. (2017). Cognitive fatigue in individuals with traumatic brain injury is associated with caudate activation. *Sci. Rep.* 7:8973.

Wylie, G. R., Yao, B., Genova, H. M., Chen, M. H., and DeLuca, J. (2020). Using functional connectivity changes associated with cognitive fatigue to delineate a fatigue network. *Sci. Rep.* 10:21927. doi: 10.1038/s41598-020-78768-3

frontiers | Frontiers in Neuroimaging

TYPE Original Research
PUBLISHED 04 October 2022
DOI 10.3389/fnimg.2022.971201

OPEN ACCESS

EDITED BY
Filippo Cieri,
Neurological Institute, United States

REVIEWED BY
Carissa Philippi,
University of Missouri–St. Louis, United States
Lena Kaethe Linda Oestreich,
The University of Queensland, Australia
Stefano Ferracuti,
Sapienza University of Rome, Italy
Zonglei Zhen,
Beijing Normal University, China

*CORRESPONDENCE
Corey H. Allen
callen@mrn.org
Kent A. Kiehl
kkiehl@unm.edu

SPECIALTY SECTION
This article was submitted to Brain Imaging Methods, a section of the journal Frontiers in Neuroimaging

RECEIVED 16 June 2022
ACCEPTED 20 September 2022
PUBLISHED 04 October 2022

CITATION
Allen CH, Maurer JM, Edwards BG, Gullapalli AR, Harenski CL, Harenski KA, Calhoun VD and Kiehl KA (2022) Aberrant resting-state functional connectivity in incarcerated women with elevated psychopathic traits. *Front. Neuroimaging* 1:971201. doi: 10.3389/fnimg.2022.971201

Aberrant resting-state functional connectivity in incarcerated women with elevated psychopathic traits

Corey H. Allen[1]*, J. Michael Maurer[1], Bethany G. Edwards[1,2], Aparna R. Gullapalli[1], Carla L. Harenski[1], Keith A. Harenski[1], Vince D. Calhoun[3,4,5] and Kent A. Kiehl[1,2]*

[1]The Mind Research Network, Albuquerque, NM, United States, [2]Department of Psychology, University of New Mexico, Albuquerque, NM, United States, [3]Department of Electrical and Computer Engineering, Georgia Institute of Technology, Atlanta, GA, United States, [4]Tri-Institutional Center for Translational Research in Neuroimaging and Data Science (TReNDS), Georgia Institute of Technology, Georgia State University, Emory University, Atlanta, GA, United States, [5]Department of Computer Science, Georgia State University, Atlanta, GA, United States

Previous work in incarcerated men suggests that individuals scoring high on psychopathy exhibit aberrant resting-state paralimbic functional network connectivity (FNC). However, it is unclear whether similar results extend to women scoring high on psychopathy. This study examined whether psychopathic traits [assessed *via* the Hare Psychopathy Checklist – Revised (PCL-R)] were associated with aberrant inter-network connectivity, intra-network connectivity (i.e., functional coherence within a network), and amplitude of fluctuations across limbic and surrounding paralimbic regions among incarcerated women ($n = 297$). Resting-state networks were identified by applying group Independent Component Analysis to resting-state fMRI scans. We tested the association of psychopathic traits (PCL-R Factor 1 measuring interpersonal/affective psychopathic traits and PCL-R Factor 2 assessing lifestyle/antisocial psychopathic traits) to the three FNC measures. PCL-R Factor 1 scores were associated with increased low-frequency fluctuations in executive control and attentional networks, decreased high-frequency fluctuations in executive control and visual networks, and decreased intra-network FNC in default mode network. PCL-R Factor 2 scores were associated with decreased high-frequency fluctuations and default mode networks, and both increased and decreased intra-network functional connectivity in visual networks. Similar to previous analyses in incarcerated men, our results suggest that psychopathic traits among incarcerated women are associated with aberrant intra-network amplitude fluctuations and connectivity across multiple networks including limbic and surrounding paralimbic regions.

KEYWORDS

psychopathy, functional connectivity, intra-network connectivity, spectra, antisocial

Introduction

Individuals scoring high on psychopathy are characterized by a constellation of traits including impulsivity, poor decision making, callousness, and a lack of empathy (Hare, 2003). An individual with psychopathy is 20–25 times more likely to be arrested than a non-psychopathic individual, and once released, is four to eight times as likely to recidivate violently 1-year post-release (Hemphill et al., 1998; Kiehl and Hoffman, 2011). Relatedly, the social costs due to elevated criminal activity that can be attributed to individuals with psychopathy are estimated to be nearly $460 billion per year (Anderson, 1999; Kiehl and Hoffman, 2011). As such, great efforts have been made to understand the sociological, psychological, and neurobiological origins of the psychopathic phenotype.

Most theories suggest that individuals scoring high on psychopathy exhibit deficits in limbic (e.g., amygdala, cingulate gyrus, and parahippocampal gyrus) and surrounding paralimbic brain regions (e.g., orbitofrontal cortex, insula, and temporal pole) (Kiehl, 2006; Anderson and Kiehl, 2012; though see Blair, 2006). Resting-state functional analyses suggest broadly distributed psychopathy-related aberrations in inter-network functional network connectivity (FNC). These aberrances span across multiple networks but primarily occur in networks associated with executive control, decision making, salience detection, and motor control (Tang et al., 2013; Contreras-Rodríguez et al., 2015; Del Casale et al., 2015; Philippi et al., 2015; Leutgeb et al., 2016; Korponay et al., 2017; Espinoza et al., 2018; Dotterer et al., 2020).

Psychometric analyses generally support dividing psychopathic traits, assessed *via* the Hare Psychopathy Checklist – Revised (PCL-R; Hare, 2003), into two clusters or factors (Harpur et al., 1989; Hare and Neumann, 2010). Factor 1 contains items related to interpersonal and affective traits, while Factor 2 assesses impulsive, life-course developmental, and antisocial traits. Several studies have found interpersonal and affective traits to be associated with localized disruption between the DMN and central executive network (CEN) (Espinoza et al., 2018; Dotterer et al., 2020). Lifestyle/behavioral and antisocial/developmental psychopathic traits, on the other hand, are associated with resting-state correlates ranging from subcortical structures to sensorimotor networks (SEN), DMNs, and visual networks (VIS) (Korponay et al., 2017). Overall, these findings suggest that specific psychopathic traits may associate differentially with resting-state measures.

The bulk of these previous studies have been conducted on entirely male samples, leaving open the question of sex-specific differences in the neurobiological correlates of psychopathy (Verona and Vitale, 2018). Women scoring high on psychopathy are characterized by similar neurobiological deficits as men scoring high on psychopathy (Carré et al., 2013; Cope et al., 2014; Harenski et al., 2014a; Crooks et al., 2019; Maurer et al., 2022), but unique gender differences have also been observed. For example, while men scoring high on psychopathy are characterized by response perseveration deficits, women scoring high on psychopathy are not (Vitale and Newman, 2001b). As such, women scoring high on psychopathy may be characterized by unique FNC patterns compared to men scoring high on psychopathy. Despite advances in our understanding of the relationship between psychopathy and inter-network connectivity of RSNs, research including analyses of amplitude of fluctuations (AFs)—that is, the spectral power of RSN activational profiles—and intra-network connectivity in their relationship to antisocial traits are scant. Furthermore, these studies are largely group comparison based rather dimensionality based (Liu et al., 2014; Xu et al., 2014; Cao et al., 2018). Intra-network high-frequency AFs are believed to contribute to higher-order cognitive processes, and thus, may also differ dimensionally with psychopathic traits (Baria et al., 2011; Craig et al., 2018). These limitations of scope and study obscure functional aberrances associated with psychopathy that may occur on a local RSN specific level rather than an inter-RSN level, as well as potential dimensional correlates associated with psychopathic traits of interest that may be otherwise lost *via* traditional group comparisons.

Here we examine resting-state measures and their relationships to psychopathic traits (assessed *via* the PCL-R) (Hare, 2003) in a large sample of incarcerated women (n = 297). Functional connectivity was assessed using three different measures [static functional network connectivity (sFNC: inter-network connectivity), AFs, and intra-network connectivity], to comprehensively evaluate the functional characteristics of RSNs and their associations with psychopathic traits in women. We hypothesized that the majority of aberrant functional connectivity measures related to psychopathy would occur in limbic and paralimbic regions of the brain (Kiehl, 2006).

Methods

Participants

Participants included 308 adult female offenders recruited from a medium- and maximum-security correctional facility who previously participated as part of NIH-funded research and treatment studies (R01 DA020870, R01 DA026964, and R01 MH085010). While all offenders within the correctional facility were offered the opportunity to participate in the current study, the final sample included participants who completed the relevant clinical assessments and resting-state functional MRI scans and met further inclusion criteria. Inclusion criteria included fluency in English at or above a fourth-grade reading level; estimated IQ over 70 (n = 4 excluded); and no presence of psychotic disorder (schizoaffective disorder, n = 1; delusional

TABLE 1 Participants demographic, PCL-R scores, and disorder rates.

	Mean	*SD*	Min.	Max.	Overall sample (%)
Age (years)	34.6	7.5	21	57	
IQ	94.7	9.9	72	123	
PCL-R total scores	18.8	6.2	2.2	34.0	
Factor 1 scores	4.6	2.7	0	13.0	
Factor 2 scores	12.2	3.8	0	20.0	
Any mood disorder					36.4
Any anxiety disorder					12.5
PTSD					7.1
Any substance use disorder					96.0

Four participants were missing mood disorder data, 10 were missing anxiety disorder data, eight were missing PTSD data, and two were missing substance use disorder data.

disorder, $n = 1$, excluded). An additional $n = 5$ participants were excluded for MRI-related reasons, excessive head motion (i.e., mean framewise displacement values > three standard deviations above the mean or comprising more than 10% of their total volume, $n = 3$; Power et al., 2014), large susceptibility artifacts ($n = 1$), or an incomplete resting-state scan ($n = 1$). In total, 11 (3.57%) participants were excluded from the study, leaving a final sample of 297 adult female offenders.

Participants were between the ages of 21 and 57 (average age = 34.6 years, SD = 7.5 years) at the time of their scan and ∼10% were left-handed. Based on NIH racial and ethnic classification, 78.5% of the sample self-identified as White, 9.1% as Black/African American, 9.1% as American Indian or Alaskan Native, 3.4% as mixed/other, and 56.2% as Hispanic. Participants' demographics and PCL-R scores are shown in Table 1. Participants provided written informed consent in protocols approved by the institutional review board of the University of New Mexico and by the Independent Review (E&I) Services for the Mind Research Network and were paid at a rate commensurate with institution compensation for work assignments at their facility.

Psychopathy scores

Psychopathic traits were assessed using the PCL-R (Hare, 2003), which has been validated for use among women (Vitale and Newman, 2001a; Vitale et al., 2002). The PCL-R consists of 20 items which are scored on a three-point scale, 0 (does not apply), 1 (applies somewhat), and 2 (definitely applies). It is based on participants' clinical interview and extensive file review conducted by trained research staff. The resulting PCL-R total scores range from 0 to 40. Factor analyses of the 20 PCL-R items have consistently revealed two factors: Factor 1 scores correspond to affective/interpersonal characteristics (e.g., manipulativeness, deficient empathy, and a lack of remorse), whereas Factor 2 scores, correspond to impulsive and irresponsible behavior and early and persistent antisocial behavior (Harpur et al., 1989; Hare and Neumann, 2010). While the two-factor model of psychopathy was originally developed and validated in men (Harpur et al., 1989; Hare and Neumann, 2010), research suggests similar validity in women (Kennealy et al., 2007), including participants included in the current sample (Eisenbarth et al., 2018).

Additional psychosocial data

Mood, anxiety, post-traumatic stress, and substance use disorders

Participants were assessed for past or current presence of a mood disorder, including major depressive disorder, dysthymic disorder or persistent depressive disorder, depressive disorder not otherwise specified (NOS), bipolar disorder, mood disorder due to a general medical condition (GMC), and substance-induced mood disorder using the Structured Clinical Interview for DSM-IV-TR Axis I Disorders (SCID-I/P; First et al., 2002) or Structured Clinical Interview for DSM-5–Research Version (SCID-5-RV; First et al., 2015)[1]. Likewise, participants were assessed for lifetime presence of an anxiety disorder (i.e., panic disorder, agoraphobia, social phobia or social anxiety disorder, specific phobia, generalized anxiety disorder, anxiety disorder NOS or otherwise specified, anxiety disorder due to a GMC, and substance-induced anxiety disorder). Finally, participants were also assessed for lifetime posttraumatic stress disorder (PTSD). PTSD assessment procedures differed across SCID versions, and when the SCID-I/P was used, participants completed an initial screening form to determine whether the PTSD interview module would be administered in full. When the SCID-5-RV version was used the PTSD interview module was administered to all participants. Presence of any mood, anxiety, or traumatic disorder was coded dichotomously, and participants meeting past or current diagnostic criteria for any one of these disorders were coded as having the respective disorder (see Table 1).

Alcohol and/or substance-related diagnoses were assigned based on diagnostic criteria for the SCID version administered (either the SCID-I/P or the SCID-5-RV). Participants administered the SCID-I/P were assessed for lifetime alcohol and drug abuse or dependence. A lifetime diagnosis of abuse was defined as scoring at threshold on at least one of four abuse criteria for alcohol and/or seven drug categories (i.e., sedatives-hypnotics-anxiolytics, cannabis, stimulants, opioids, cocaine, hallucinogens/PCP, and other). A lifetime diagnosis of dependence was defined as scoring at threshold in at least three of seven dependence criteria.

1 One participant in the sample was administered the SCID-5-RV, whereas the rest were administered the SCID-I/P.

Alternatively, for participants administered the SCID-5-RV, a lifetime alcohol use disorder was obtained if at least two of 11 alcohol criteria were scored at threshold, and lifetime substance use disorder(s) were obtained if at least two of 11 criteria were scored at threshold for eight categories (i.e., sedative-hypnotics-anxiolytics, cannabis, stimulants, opioids, inhalants, PCP, hallucinogens, and other/unknown; see Table 1).

Imaging parameters

Resting-state functional magnetic resonance images were collected on the grounds of the correctional facility where participants were housed using the Mind Research Network's mobile Siemens 1.5 T Avanto with advanced SQ gradients (max slew rate 200 T/m/s, 346 T/m/s vector summation, rise time 200 us) equipped with a 12-element head coil. The EPI gradient echo pulse sequence (TR = 2,000 ms, TE = 39 ms, flip angle = 75, FOV = 24 x 24 cm, 64 x 64 matrix, 3.75 x 3.75 mm in-plane resolution, 4 mm slice thickness, 1 mm gap, 27 slices) effectively covered the entire brain (150 mm) in 2.0 s. Head motion was minimized using padding and restraint. The participants were asked to lay still, look at the fixation cross and keep eyes open during the 5-min rsfMRI scanning. Compliance with instructions was monitored by eye tracking.

EPI preprocessing

Data were preprocessed using statistical parametric mapping (SPM12) (Friston et al., 1994) (http://www.fil.ion.ucl.ac.uk/spm) including image reorientation, realignment [motion estimation using INRialign (Freire and Mangin, 2001)], and spatial normalization to the Montreal Neurological Institute standard space at a resolution of a 3 x 3 x 3 mm^3. A full width half maximum Gaussian kernel of 6 mm was then used for spatial smoothing. Framewise displacement (FWD) was used to assess motion quality control. For FWD, the translation and rotation parameters were computed as the mean of the sums of the absolute translation and rotation frame displacements, yielding a single FWD value for each participant.

Independent component analysis

Per Espinoza et al. (2018), we applied gICA on the preprocessed rsfMRI data using the GIFT toolbox (http://trendscenter.org/software/gift) (Calhoun et al., 2001). The rsfMRI data was compressed using two stages of principal component analysis (PCA) (Rachakonda et al., 2016). For the first data reduction step, we retained 100 principal components (PCs), and 75 independent components (ICs) for group data reduction, consistent with previously published studies (Kiviniemi et al., 2009; Smith et al., 2009; Ystad et al., 2010; Allen et al., 2011a; Elseoud et al., 2011; Erhardt et al., 2011). High-model order ICA (i.e., 75 components) results in more refined components corresponding to known anatomical and functional segmentations compared to low-model order ICA (i.e., 25 or 50 components) (Allen et al., 2011a; Hu et al., 2020). Individual specific spatial maps and their time-courses were obtained using gICA. Out of the 75 ICs that were estimated, 48 components were identified as components of RSNs by evaluating whether peak activation occurred in gray matter and whether the peak AFs occurred in the low-frequency power portion of the spectra of components (Meda et al., 2008; Robinson et al., 2009; Allen et al., 2011a). The reliability and stability of these extracted networks were evaluated *via* ICASSO (Himberg and Hyvärinen, 2003), a process that iteratively re-runs component estimations with differently bootstrapped datasets. This analysis suggested high stability across the 48 components (*mean stability index* = 0.89), well above the threshold of 0.70 established in the literature (Ma et al., 2011). The other 27 components were excluded, as they appeared to be related to motion artifacts, spatial maps including white matter, the ventricular system, or cerebrospinal fluid, or having irregular time-course spectra power (Allen et al., 2011a,b). Within GIFT, the time-courses of the RSNs underwent despiking and bandpass by filtering with [0.01–0.15] Hz cutoffs.

Functional connectivity measures

In order to assess various types of resting-state functional connectivity measures, we calculated the sFNC between the selected 48 RSNs as pairwise correlations between the RSNs time-courses for each individual (inter-network connectivity), pairwise correlations between individual voxels within the RNSs to the overall RSN's time-course (intra-network connectivity), and the AFs within each RSN.

Statistical analyses

We performed regression analysis to identify associations between individual sFNC values (inter-network connectivity), spatial maps (intra-network connectivity), and AFs with psychopathy measures: PCL-R Factor 1 and Factor 2 as continuous variables (see Supplementary materials for analyses of PCL-R total). The analyses were corrected for "nuisance"

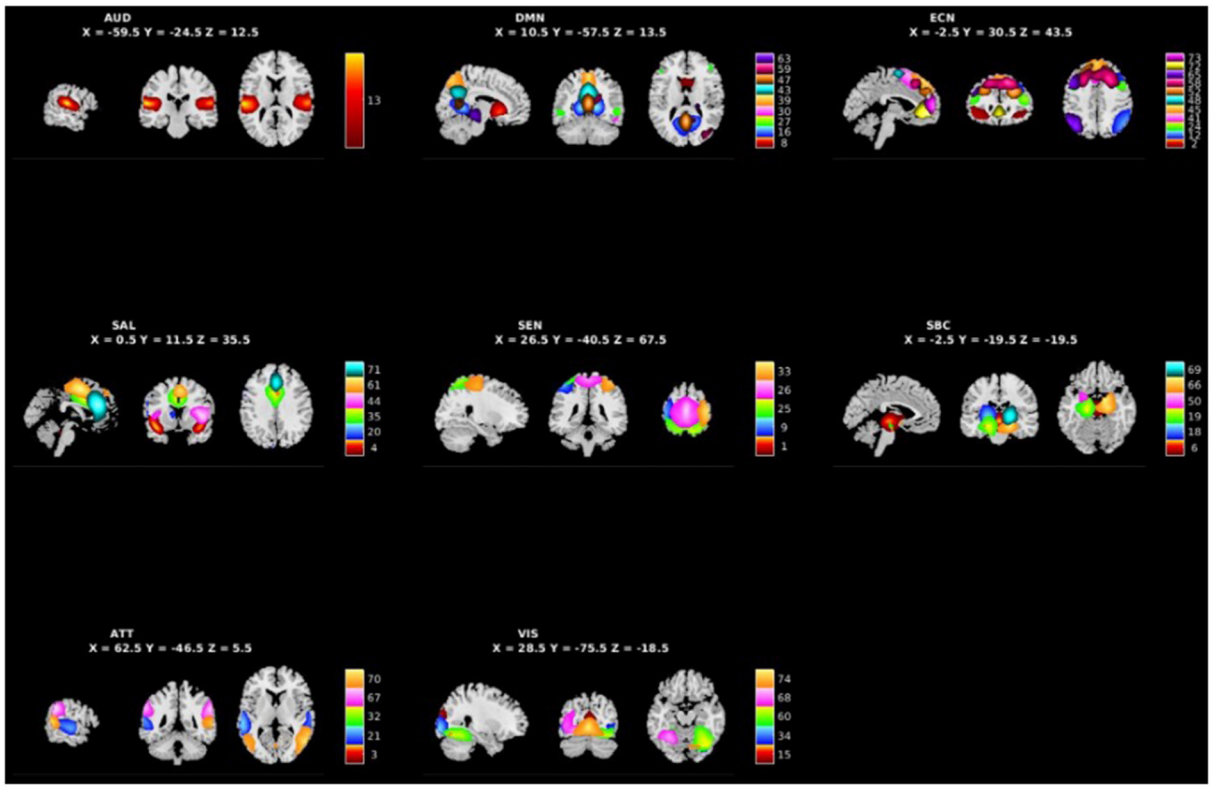

FIGURE 1
Spatial maps of the 48 independent components identified as RSNs categorized by domain [auditory (AUD), default mode network (DMN), executive control (ECN), salience (SAL), sensorimotor (SEN), subcortical (SBC), attentional (ATT), and visual (VIS)] and component number.

covariates (age, IQ[2], FWD[3]). The significance of the univariate psychopathy results for each factor was determined using a false discovery rate (FDR) (Genovese et al., 2002) threshold at $p < 0.05$.

Results

Psychopathic traits

The PCL-R total scores for this sample ranged from 2.2 to 34.0 (mean = 18.8, SD = 6.2, Cronbach's $\alpha = 0.79$; see Table 1). PCL-R Factor 1 scores ranged from 0.0 to 13.0 (mean = 4.6, SD = 2.7; see Table 1), and PCL-R Factor 2 scores ranged from 0.0 to 20.0 (mean = 12.2, SD = 3.8; see Table 1).

2 As estimated by the vocabulary and matrix reasoning subscales of the Wechsler Adult Intelligence Scale; see Ryan and Ward, 1999.

3 Note: The inclusion or exclusion of FWD in analyses did not alter significant findings for any present analyses.

Group independent component analysis and group level inter-network connectivity

Figure 1 shows the spatial maps of the 48 selected RSNs. The 48 RSNs listed in Table 2 were grouped into eight domains: auditory (AUD), default mode network (DMN), executive control (ECN), salience (SAL), sensorimotor (SEN), subcortical (SBC), attentional (ATT), and visual (VIS) based on their peak coordinate, functional properties, the automatic labeling tool in GIFT, and confirmed by visual inspection (see Figure 2 for the estimated inter-network connectivity between domains and RSNs)[4]. Consistent with prior literature, the inter-network

4 While the automatic labels and correlations to networks provided by the GIFT toolbox (http://trendscenter.org/software/gift) (Calhoun et al., 2001) were helpful in the initial network classification and description, these network labels differ from those commonly utilized in relevant literature (i.e., Espinoza et al., 2018). Thus, a combination of the correlational outputs/labeling, the peak coordinates, and functional properties commonly ascribed to the regions were used to name regions and assign those regions to relevant domains. The assignment of regions

TABLE 2 Resting-state networks (RSNs) domain names, IC numbers, and MNI peak coordinates.

RSNs and domain names	IC number	MNI peak (*x*, *y*, *z*)
Auditory (AUD)		
Left superior temporal gyrus	13	(−58, −22, 10)
Default mode network (DMN)		
Anterior cingulate	8	(2, 14, −5)
Posterior cingulate	16	(14, −56, 5)
Right postcentral gyrus	27	(56, −32, 55)
Right inferior temporal gyrus	30	(54, −24, −20)
Precuneus	39	(0, −66, 60)
Precuneus	43	(0, −66, 35)
Posterior cingulate	47	(0, −60, 10)
Right angular gyrus	59	(38, −80, 30)
Right parahippocampal gyrus	63	(22, −28, −10)
Executive control network (ECN)		
Left middle frontal gyrus	2	(−38, 44, −5)
Right inferior parietal lobule	12	(48, −58, 55)
Right inferior frontal gyrus	24	(48, 14, 30)
Superior frontal gyrus	41	(2, 14, 70)
Superior frontal gyrus	45	(0, 44, 55)
Left superior frontal gyrus	48	(−12, −4, 70)
Right superior frontal gyrus	52	(24, 36, 30)
Right middle frontal gyrus	58	(24, 20, 50)
Left superior parietal lobule	65	(−38, −64, 55)
Medial frontal gyrus	72	(0, 52, −5)
Medial frontal gyrus	73	(0, 62, 5)
Salience network (SAL)		
Left superior temporal gyrus	4	(−42, 8, −15)
Left middle frontal gyrus	20	(−42, 52, 10)
Cingulate gyrus	35	(0, 10, 35)
Right inferior frontal gyrus	44	(44, 16, 5)
Medial frontal gyrus	61	(2, 0, 55)
Anterior cingulate	71	(0, 32, 35)
Sensorimotor (SEN)		
Right precentral gyrus	1	(54, −8, 30)
Left precentral gyrus	9	(−48, −36, 60)
Postcentral gyrus	25	(10, −60, 70)
Medial frontal gyrus	26	(0, −22, 70)
Right precentral gyrus	33	(42, −22, 65)
Subcortical (SBC)		
Basal ganglia	6	(0, −22, −5)
Left lentiform nucleus	18	(−18, −10, 0)
Left parahippocampal gyrus	19	(−18, −20, −20)
Left lentiform nucleus	50	(−24, 4, 0)
Right parahippocampal gyrus	66	(18, −4, −15)
Right lentiform nucleus	69	(18, −8, 0)
Attentional (ATT)		
Left superior temporal gyrus	3	(−36, 10, −30)
Left middle temporal gyrus	21	(−60, −30, 0)
Precuneus	32	(4, −82, 45)
Left supramarginal gyrus	67	(−60, −48, 40)
Right middle temporal gyrus	70	(56, −66, 5)
Visual (VIS)		
Cuneus	15	(2, −94, 25)
Right inferior occipital gyrus	34	(32, −94, −10)
Right fusiform gyrus	60	(38, −68, −20)
Left lingual gyrus	68	(−24, −66, −10)
Lingual gyrus	74	(0, −80, −5)

RSN network names were determined by peak MNI coordinates and gICA's component labeling function.

connectivity in Figure 2 suggests largely positive within domain inter-network connectivity within the DMN, ECN, SAL, ATT, and VIS networks (Espinoza et al., 2018; Du et al., 2020). Similar to analyses in clinical populations, Figure 2 also suggests cases of negative inter-network connectivity within SBC networks (Du et al., 2020).

Time-course power spectra

PCL-R factor 1 scores

PCL-R Factor 1 scores were associated with increased AF at low-frequency bands (0–0.05 Hz) in the left middle frontal gyrus (Component 2, ECN), the left superior temporal gyrus (Component 3, ATT), and the right superior frontal gyrus (Component 52, ECN), and decreased AF at high-frequency spectra bands (0.09–0.25 Hz) in the cuneus (Component 15, VIS), left middle frontal gyrus (Component 2, ECN), and the superior frontal gyrus (Component 41, ECN) (see Figures 3, 5, Table 3).

PCL-R factor 2 scores

PCL-R Factor 2 scores were associated with decreased AF at high-frequency bands (0.10–0.25 Hz) in the posterior cingulate cortex (Component 47, DMN) and left middle frontal gyrus (Component 2, ECN) (see Figures 4, 5, Table 3).

to a specific domain was performed independently by three authors and the final domain classification was based upon unanimous agreements.

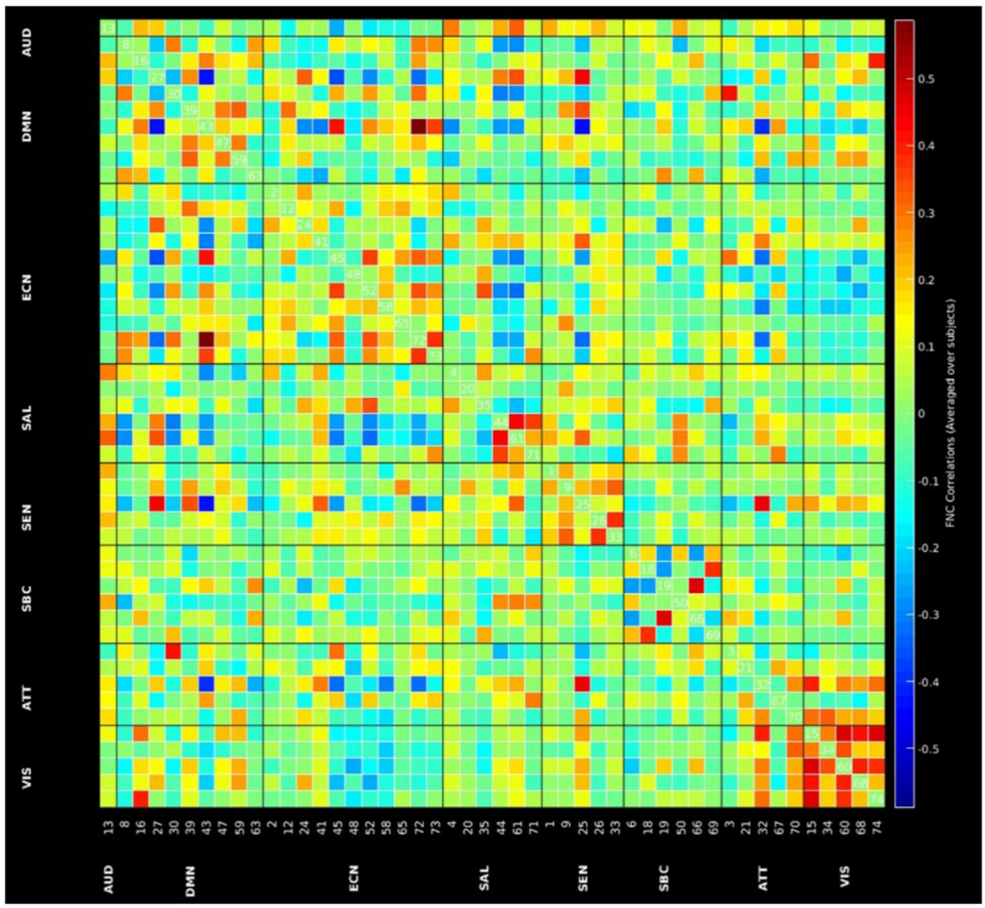

FIGURE 2
Inter-network functional network connectivity matrix of the 48 RSNs.

Component spatial maps

PCL-R factor 1 scores

PCL-R Factor 1 scores were associated with functional connectivity in a network primarily pertaining to the parahippocampal gyrus (Component 63, DMN), such that higher PCL-R Factor 1 scores were associated with decreased intra-network functional connectivity of the left insula and right thalamus within Component 63 (see Figure 6, Table 4).

PCL-R factor 2 scores

PCL-R Factor 2 scores were associated with functional connectivity in the right fusiform gyrus (Component 60, VIS), such that higher PCL-R Factor 2 scores were associated with both increased and decreased intra-network functional connectivity (see Figure 7). PCL-R Factor 2 scores were also associated with functional connectivity in the left lingual gyrus (Component 68, VIS), such that higher PCL-R Factor 2 scores were associated with an increased intra-network functional connectivity (see Figure 7, Table 4).

Functional network connectivity

There were no significant associations between PCL-R scores and sFNC that survived FDR correction while controlling for age, IQ, and FWD.

Discussion

Here we report that psychopathic traits (assessed *via* the PCL-R) were associated with aberrant functional connectivity measures during a resting-state fMRI experimental paradigm in a sample of incarcerated women. Consistent

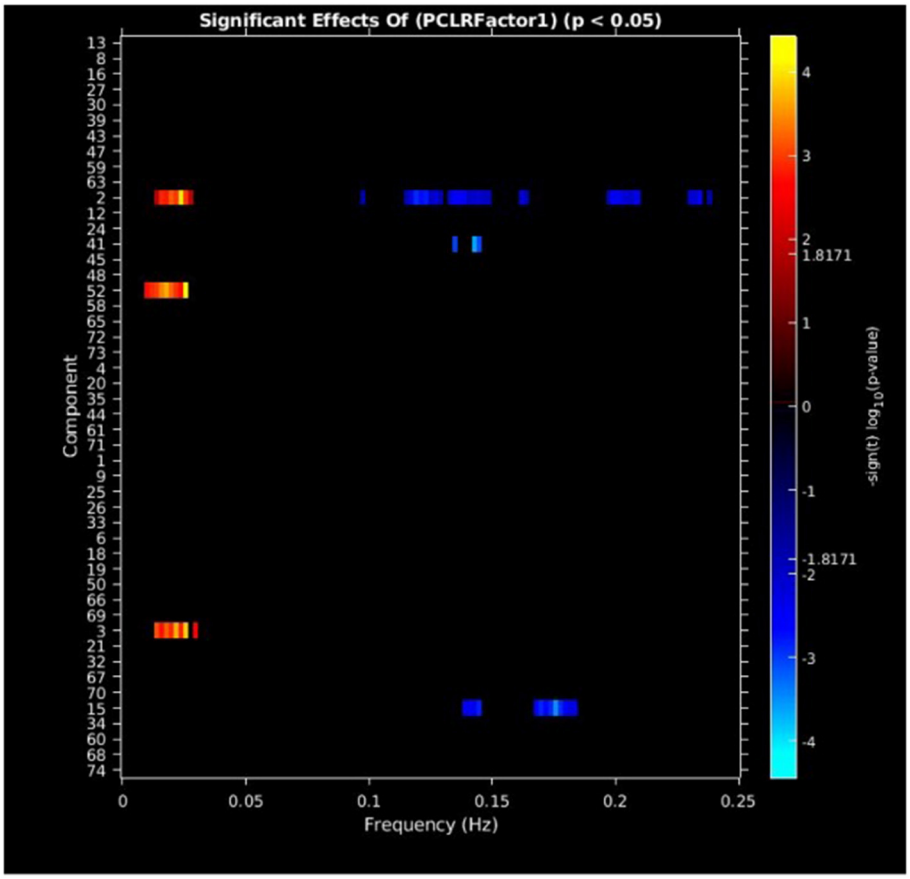

FIGURE 3
Univariate associations between PCL-R Factor 1 score and power spectra of significant components, predominantly occurring in the ECN. Panel depicts the significance and direction of PCL-R Factor 1 scores as a function of frequency for each significant component, displayed as−sign(t) log10(p), FDR corrected $p < 0.05$.

TABLE 3 Effects of psychopathic traits on AFs, FDR corrected.

Measure	RSN	IC, domain	Beta range
PCL-R factor 1			
	Left middle frontal gyrus	2, ECN	−0.0433 to 0.0327
	Left superior temporal gyrus	3, ATT	0.0451 to 0.0543
	Right superior frontal gyrus	52, ECN	0.0468
	Cuneus	15, VIS	−0.0489 to −0.0459
	Superior frontal gyrus	41, ECN	−0.0495 to −0.0443
PCL-R factor 2			
	Posterior cingulate cortex	47, DMN	−0.0459 to −0.0403
	Left middle frontal gyrus	2, ECN	−0.0337 to −0.0317

Table shows all AF effects that survive FDR correction at p < 0.05 level and range of Beta Values per component.

with previous research performed in men and our hypotheses, PCL-R scores were associated with aberrant functional connectivity across multiple domains among incarcerated women.

PCL-R scores were associated with increased amplitude fluctuations (AF) in low-frequency bands and reduced AF in high-frequency bands across regions included within the paralimbic system, including the PCC and superior temporal gyrus, and additional regions, including the superior frontal gyrus, middle frontal gyrus, and cuneus. Compared to low-frequency AFs, high-frequency AFs are believed to contribute to higher-order cognitive processes (Baria et al., 2011; Craig et al., 2018). Reduced high-frequency AFs may relate to some of the previously observed deficits characteristic of women scoring high on psychopathy. For example, successful error-related processing depends on the collaboration of several higher-order brain regions, including the middle/superior frontal gyrus, PCC, and cuneus (Steele et al., 2014). Women scoring high on the PCL-R have been previously characterized by error-related processing deficits, including reduced amplitude of the error-related positivity

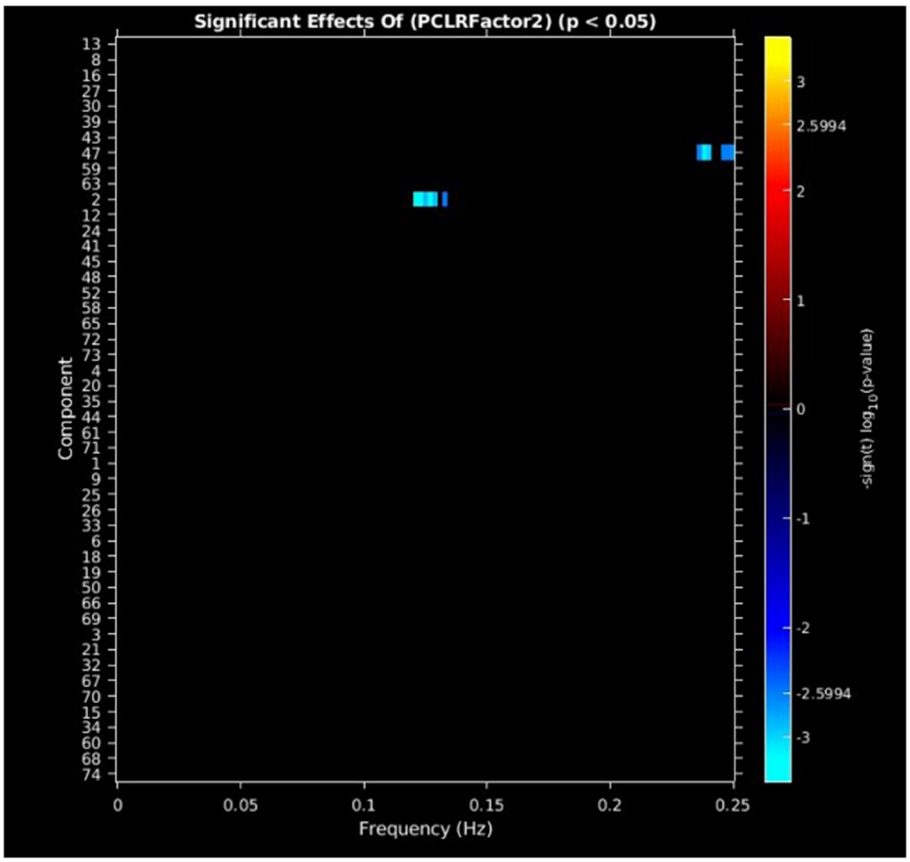

FIGURE 4
Univariate associations between PCL-R Factor 2 score and power spectra of significant components. Panel depicts the significance and direction of PCL-R Factor 2 scores as a function of frequency for the significant component, displayed as−sign(t) log10(p), FDR corrected $p < 0.05$.

event-related potential component (Maurer et al., 2016). Furthermore, women scoring high on psychopathy have been previously characterized by reduced reactivity to emotional facial expressions (Eisenbarth et al., 2013); regions implicated in the current study, including the middle frontal gyrus, have been previously associated with processing of emotional faces (Pessoa et al., 2002; Willis et al., 2010).

We also observed that women scoring high on psychopathy were characterized by aberrant intra-network connectivity within regions of the paralimbic system (e.g., parahippocampal cortex) and additional regions, including the fusiform gyrus and lingual gyrus. Women scoring high on psychopathy were characterized by reduced intra-network functional connectivity within Component 63 (parahippocampal gyrus), Component 60 (right fusiform gyrus), and Component 68 (left lingual gyrus), and increased intra-network functional connectivity in Component 60 (right fusiform gyrus). Reduced intra-network functional connectivity in the fusiform and parahippocampal gyrus is consistent with a previously published study with incarcerated women, observing that women scoring higher on the PCL-R were characterized by reduced hemodynamic activity in the fusiform and parahippocampal gyrus during the processing of moral violations (Harenski et al., 2014b). Our finding of PCL-R Factor 2 relating to increases in intra-network functional connectivity of the fusiform and lingual region is also consistent with previously published studies suggesting relationships between impulsivity and intra-visual network functional connectivity (Davis et al., 2013; Pu et al., 2017).

Published studies investigating resting-state AFs and youth psychopathic traits have reported different findings than those obtained in the current study. For example, Thijssen and Kiehl (2017) observed that youth scoring high on the Psychopathy Checklist: Youth Version (PCL:YV; Forth and Kosson, 2003) were largely characterized by *decreased* AFs in low-frequency bands and *increased* AFs at high-frequency bands. While differences between studies may have been observed, we believe that the results obtained in the current study may relate to specific deficits previously observed in women scoring high on psychopathy. For example, increased low frequency AFs

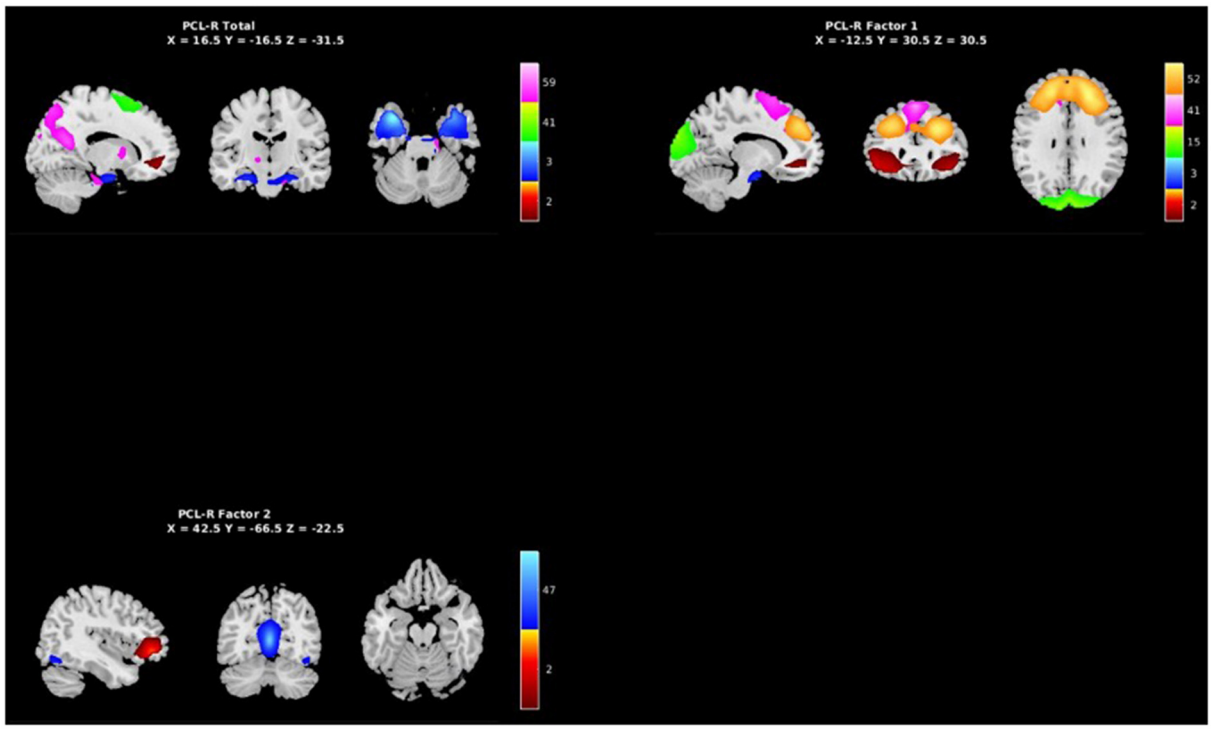

FIGURE 5
Spatial maps of the 7 independent components identified in Table 3 as exhibiting psychopathy related aberrant AFs, grouped by PCL-R Total effects (see Supplementary materials), PCL-R Factor 1 effects, and PCL-R Factor 2 effects.

are believed to relate to improvements within neural efficiency (Biswal et al., 1995). Compared to men scoring high on psychopathy, women scoring high on psychopathy are not characterized by the response perseveration deficits (Vitale and Newman, 2001a). Important to note, response perseveration is associated with dysfunction with several regions implicated in the current study, including the middle frontal gyrus (Yang et al., 2011), superior temporal gyrus (Ersche et al., 2011), and superior frontal gyrus (De Ruiter et al., 2009; Camchong et al., 2011). Therefore, women scoring high on psychopathy may be characterized by increased neural efficiency (observed via higher low-frequency AFs) in several paralimbic brain regions, contributing to improved performance on response perseveration tasks (Vitale et al., 2011). By exhibiting reduced AFs in low-frequency bands, this may relate to youth scoring high on psychopathy exhibiting response preservation deficits (Vitale et al., 2005).

Importantly, and more broadly, our investigation into the relationships between psychopathic traits in women and multiple measurements of rsFNC (inter-network connectivity, intra-network connectivity, and AFs) underscore three points. First, neurobiological aberrances related to psychopathic traits in women may best be accounted for on a local (i.e., intra-network connectivity & AFs) neurobiological level rather than a global level (i.e., inter-network connectivity). Second, while variability in psychopathic traits may be accounted for by the relationships between voxel and RSN time courses (e.g., Thijssen and Kiehl, 2017; Espinoza et al., 2018), additional variability can also be explained by rates and amplitudes of individual RSN activational profiles themselves (i.e., AFs; see Thijssen and Kiehl, 2017). And finally, by exploring both local (i.e., intra-network connectivity and AFs) and global (i.e., inter-network connectivity) rsFNC measures in their relationships to antisocial traits, future research stands to further explore and potentially differentiate how antisocial phenotypes are represented neurobiologically across various demographic groups.

Study limitations

A number of limitations must be considered for the present study. Though all regions identified as being associated with psychopathic traits in the present study were also identified in Espinoza et al. (2018), here we did not find any significant psychopathy related inter-network FNC results. One potential explanation for this result is the size of the sample analyzed. While the present sample is considered large by neuroimaging standards (n = 297), Espinoza et al. (2018)

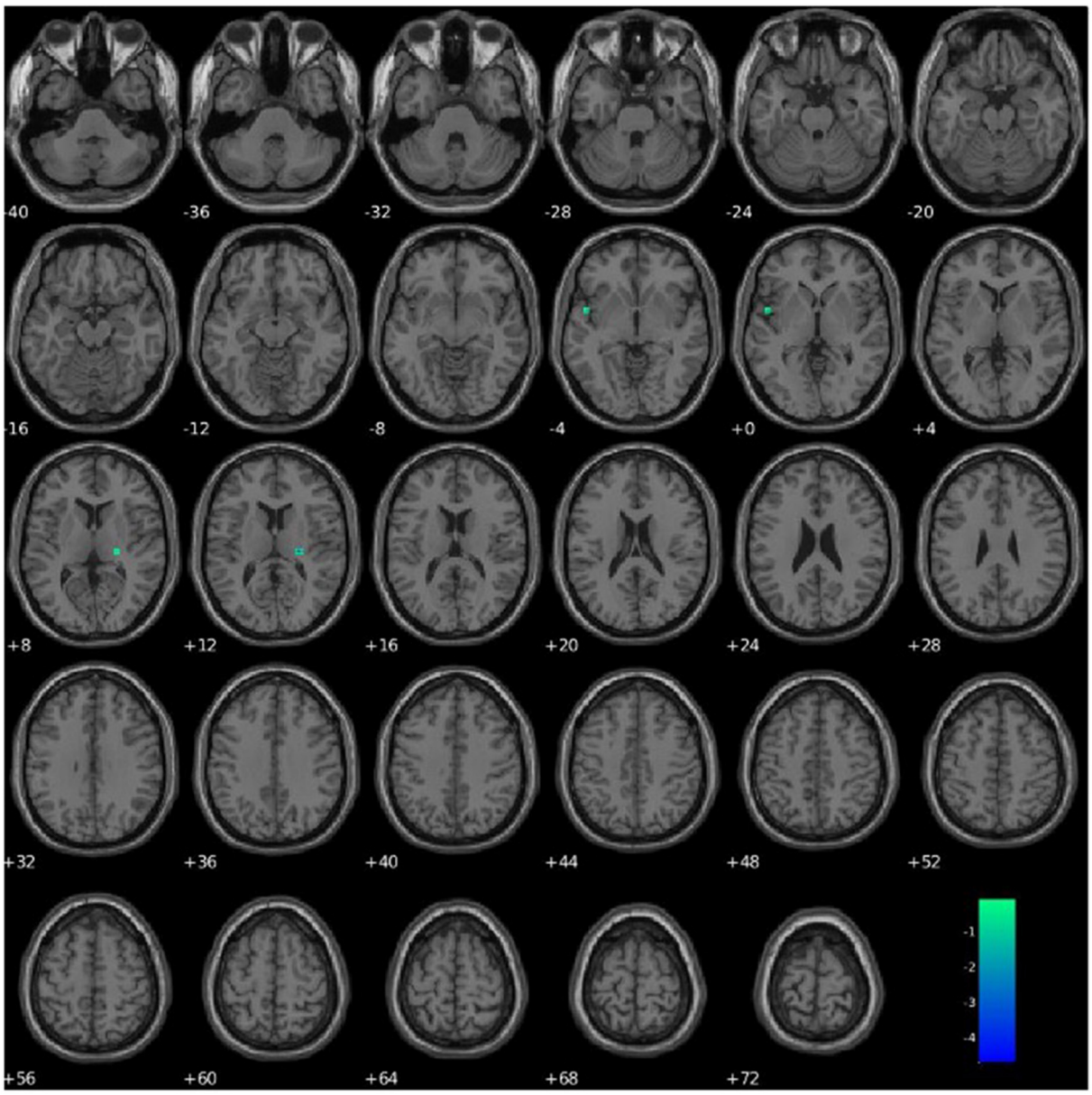

FIGURE 6
Association between PCL-R Factor 1 score and intra-network connectivity within a network primarily pertaining to the parahippocampal gyrus, FDR corrected $p < 0.05$.

TABLE 4 Effects of psychopathic traits on intra-network connectivity, FDR corrected.

Measure	RSN	IC, domain	Average beta
PCL-R factor 1			
	Right parahippocampal gyrus	63, DMN	−0.4143
PCL-R factor 2			
	Right fusiform gyrus	60, VIS	0.2403, −0.2654
	Left lingual gyrus	68, VIS	0.2688

Table shows all clusters that survive FDR correction at $p < 0.05$ level and average Beta effect size per component.

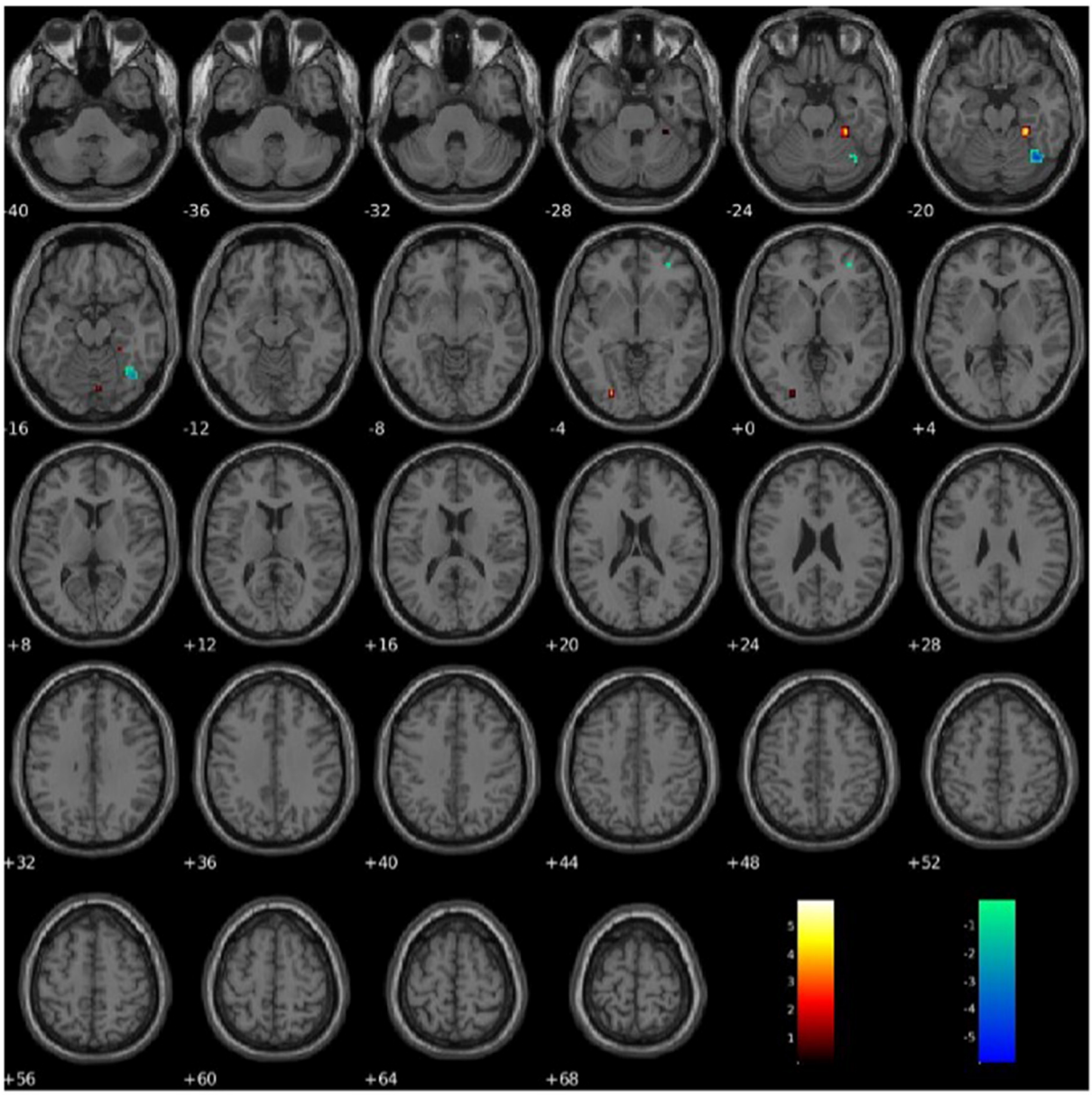

FIGURE 7
Association between PCL-R Factor 2 score and intra-network connectivity within the lingual gyrus and fusiform gyrus, FDR corrected $p < 0.05$.

conducted inter-network connectivity analysis in a sample more than three times as large ($n = 985$). Additionally, because all FNC measures tested in the present analysis were static, there are a number of assumptions being made regarding the relationships between the consistency of network activity across the 5-min resting-state scan. Similarly, because the scans were resting-state rather than task-based, extrapolations of RSN aberrances to specific functional domains are hard to attribute. Finally, while our experimental design utilized 5-min resting-state scans, there is evidence suggesting that longer scans are needed to ensure higher RSN stabilities (e.g., Birn et al., 2013; though see Allen et al., 2011a; Espinoza et al., 2018, 2019; Duda et al., 2022). Thus, more work is needed to probe the relationships between various inter- and intra-network static and dynamic connectivity measures as they relate to psychopathic traits and perhaps longer resting-state and task-based measures in large samples of both men and women.

Conclusion

This study contributes to the current literature by examining whole brain inter- and intra-network connectivity and AFs across RSNs and their relationship to psychopathic traits in women. We showed that psychopathy is associated with increased low-frequency, decreased high-frequency AFs, and both increased and decreased intra-network connectivity across four brain domains (DMN, ECN, VIS, and ATT). Similar to previous analyses in incarcerated men, our results suggest that psychopathic traits among incarcerated women are associated with aberrant intra-network AFs and connectivity across multiple networks associated with executive control, decision making, salience detection, and motor control. Our results showcase aberrant intra-network FNC rather than aberrant inter-network FNC underlying psychopathic traits in women, suggesting the potential for sex-specific neurobiological psychopathy related phenotypes. To our knowledge, this represents the largest study to date on the association of psychopathic traits and intrinsic RSN aberrances in incarcerated women.

Data availability statement

The datasets presented in this article are not readily available because of ethical and privacy restrictions. Requests to access the datasets should be directed to KK, kkiehl@mrn.org.

Ethics statement

The studies involving human participants were reviewed and approved by University of New Mexico IRB and the Independent Review (E&I) Services for the Mind Research Network. The patients/participants provided their written informed consent to participate in this study.

Author contributions

CA performed the statistical analysis and wrote the first draft of the manuscript. JM wrote sections of the manuscript. All authors contributed to the conception, design of the study, manuscript revision, read, and approved the submitted version.

Funding

This material is based upon work supported by the National Institute on Drug Abuse (NIDA; R01 DA020870 and R01 DA026964) and National Institute of Mental Health (NIMH; R01 MH085010).

Conflict of interest

Authors CA, JM, BE, AG, CH, KH, and KK were employed by The Mind Research Network.

The remaining author declares that the research was conducted in the absence of any commercial or financial relationships that could be construed as a potential conflict of interest.

Publisher's note

All claims expressed in this article are solely those of the authors and do not necessarily represent those of their affiliated organizations, or those of the publisher, the editors and the reviewers. Any product that may be evaluated in this article, or claim that may be made by its manufacturer, is not guaranteed or endorsed by the publisher.

Author disclaimer

The contents of this manuscript are solely the responsibility of the authors and do not necessarily represent the views of the National Institute on Drug Abuse nor the National Institute of Mental Health.

Supplementary material

The Supplementary Material for this article can be found online at: https://www.frontiersin.org/articles/10.3389/fnimg.2022.971201/full#supplementary-material

References

Allen, E. A., Erhardt, E. B., Damaraju, E., Gruner, W., Segall, J. M., Silva, R. F., et al. (2011a). A baseline for the multivariate comparison of resting-state networks. *Front. Syst. Neurosci.* 5, 2. doi: 10.3389/fnsys.2011.00002

Allen, E. A., Liu, J., Kiehl, K. A., Gelernter, J., Pearlson, G. D., Perrone-Bizzozero, N. I., et al. (2011b). Components of cross-frequency modulation in health and disease. *Front. Syst. Neurosci.* 5, 59. doi: 10.3389/fnsys.2011.00059

Anderson, D. A. (1999). The aggregate burden of crime. *J. Law Econ.* 42, 611–642. doi: 10.1086/467436

Anderson, N. E., and Kiehl, K. A. (2012). The psychopath magnetized: insights from brain imaging. *Trends Cogn. Sci.* 16, 52–60. doi: 10.1016/j.tics.2011.11.008

Baria, A. T., Baliki, M. N., Parrish, T., and Apkarian, A. V. (2011). Anatomical and functional assemblies of brain BOLD oscillations. *J. Neurosci.* 31, 7910–7919. doi: 10.1523/JNEUROSCI.1296-11.2011

Birn, R. M., Molloy, E. K., Patriat, R., Parker, T., Meier, T. B., Kirk, G. R., et al. (2013). The effect of scan length on the reliability of resting-state fMRI connectivity estimates. *Neuroimage* 83, 550–558. doi: 10.1016/j.neuroimage.2013.05.099

Biswal, B., Zerrin Yetkin, F., Haughton, V. M., and Hyde, J. S. (1995). Functional connectivity in the motor cortex of resting human brain using echo-planar MRI. *Mag. Reson. Med.* 34, 537–541. doi: 10.1002/mrm.1910340409

Blair, R. J. R. (2006). "Subcortical brain systems in psychopathy: the amygdala and associated structures," in *Handbook of Psychopathy*, ed C. J. Patrick (New York, NY: The Guilford Press), 296–312.

Calhoun, V. D., Adali, T., Pearlson, G. D., and Pekar, J. J. (2001). A method for making group inferences from functional MRI data using independent component analysis. *Hum. Brain Mapp.* 14, 140–151. doi: 10.1002/hbm.1048

Camchong, J., MacDonald III, A. W., Nelson, B., Bell, C., Mueller, B. A., et al. (2011). Frontal hyperconnectivity related to discounting and reversal learning in cocaine subjects. *Biol. Psychiatry* 69, 1117–1123. doi: 10.1016/j.biopsych.2011.01.008

Cao, W., Sun, X., Dong, D., Yao, S., and Huang, B. (2018). Sex differences in spontaneous brain activity in adolescents with conduct disorder. *Front. Psychol.* 30, 1598. doi: 10.3389/fpsyg.2018.01598

Carré, J. M., Hyde, L. W., Neumann, C. S., Viding, E., and Hariri, A. R. (2013). The neural signatures of distinct psychopathic traits. *Soc. Neurosci.* 8, 122–135. doi: 10.1080/17470919.2012.703623

Contreras-Rodríguez, O., Pujol, J., Batalla, I., Harrison, B. J., Soriano-Mas, C., Deus, J., et al. (2015). Functional connectivity bias in the prefrontal cortex of psychopaths. *Biol. Psychiatry* 78, 647–655. doi: 10.1016/j.biopsych.2014.03.007

Cope, L. M., Ermer, E., Nyalakanti, P. K., Calhoun, V. D., and Kiehl, K. A. (2014). Paralimbic gray matter reductions in incarcerated adolescent females with psychopathic traits. *J. Abnorm. Child Psychol.* 42, 659–668. doi: 10.1007/s10802-013-9810-4

Craig, M. M., Manktelow, A. E., Sahakian, B. J., Menon, D. K., and Stamatakis, E. A. (2018). Spectral diversity in default mode network connectivity reflects behavioral state. *J. Cogn. Neurosci.* 30, 526–539. doi: 10.1162/jocn_a_01213

Crooks, D., Anderson, N. E., Widdows, M., Petseva, N., Decety, J., Pluto, C., et al. (2019). The relationship between cavum septum pellucidum and psychopathic traits in female offenders. *Behav. Brain Res.* 359, 967–972. doi: 10.1016/j.bbr.2018.06.011

Davis, F. C., Knodt, A. R., Sporns, O., Lahey, B. B., Zald, D. H., Brigidi, B. D., et al. (2013). Impulsivity and the modular organization of resting-state neural networks. *Cereb. Cortex* 23, 1444–1452. doi: 10.1093/cercor/bhs126

De Ruiter, M. B., Veltman, D. J., Goudriaan, A. E., Oosterlaan, J., Sjoerds, Z., and Van Den Brink, W. (2009). Response perseveration and ventral prefrontal sensitivity to reward and punishment in male problem gamblers and smokers. *Neuropsychopharmacology* 34, 1027–1038. doi: 10.1038/npp.2008.175

Del Casale, A., Kotzalidis, G. D., Rapinesi, C., Di Pietro, S., Alessi, M. C., Di Cesare, G., et al. (2015). Functional neuroimaging in psychopathy. *Neuropsychobiology* 72, 97–117. doi: 10.1159/000441189

Dotterer, H. L., Hyde, L. W., Shaw, D. S., Rodgers, E. L., Forbes, E. E., and Beltz, A. M. (2020). Connections that characterize callousness: affective features of psychopathy are associated with personalized patterns of resting-state network connectivity. *NeuroImage Clin.* 28, 102402. doi: 10.1016/j.nicl.2020.102402

Du, Y., Fu, Z., Sui, J., Gao, S., Xing, Y., Lin, D., et al. (2020). NeuroMark: an automated and adaptive ICA based pipeline to identify reproducible fMRI markers of brain disorders. *NeuroImage Clin.* 28, 102375. doi: 10.1016/j.nicl.2020.102375

Duda, M., Iraji, A., Ford, J. M., Lim, K. O., Mathalon, D. H., Mueller, B. A., et al. (2022). Spatially constrained ICA enables robust detection of schizophrenia from very short resting-state fMRI data. *medRxiv [Preprint]*. doi: 10.1101/2022.03.17.22271783

Eisenbarth, H., Angrilli, A., Calogero, A., Harper, J., Olson, L. A., and Bernat, E. (2013). Reduced negative affect response in female psychopaths. *Biol. Psychol.* 94, 310–318. doi: 10.1016/j.biopsycho.2013.07.007

Eisenbarth, H., Krammer, S., Edwards, B. G., Kiehl, K. A., and Neumann, C. S. (2018). Structural analysis of the PCL-R and relationship to BIG FIVE personality traits and parenting characteristics in an Hispanic female offender sample. *Pers. Individ. Differ.* 129, 59–65. doi: 10.1016/j.paid.2018.03.015

Elseoud, A. A., Littow, H., Remes, J., Starck, T., Nikkinen, J., Nissilä, J., et al. (2011). Group-ICA model order highlights patterns of functional brain connectivity. *Front. Syst. Neurosci.* 5, 37. doi: 10.3389/fnsys.2011.00037

Erhardt, E. B., Rachakonda, S., Bedrick, E. J., Allen, E. A., Adali, T., and Calhoun, V. D. (2011). Comparison of multi-subject ICA methods for analysis of fMRI data. *Hum. Brain Mapp.* 32, 2075–2095. doi: 10.1002/hbm.21170

Ersche, K. D., Roiser, J. P., Abbott, S., Craig, K. J., Müller, U., Suckling, J., et al. (2011). Response perseveration in stimulant dependence is associated with striatal dysfunction and can be ameliorated by a D2/3 receptor agonist. *Biol. Psychiatry* 70, 754–762. doi: 10.1016/j.biopsych.2011.06.033

Espinoza, F. A., Anderson, N. E., Vergara, V. M., Harenski, C. L., Decety, J., Rachakonda, S., et al. (2019). Resting-state fMRI dynamic functional network connectivity and associations with psychopathy traits. *NeuroImage Clin.* 24, 101970. doi: 10.1016/j.nicl.2019.101970

Espinoza, F. A., Vergara, V. M., Reyes, D., Anderson, N. E., Harenski, C. L., Decety, J., et al. (2018). Aberrant functional network connectivity in psychopathy from a large (N = 985) forensic sample. *Hum. Brain Mapp.* 39, 2624–2634. doi: 10.1002/hbm.24028

First, M. B., Spitzer, R. L., Gibbon, M., and Williams, J. B. W. (2002). *Structured Clinical Interview for DSM-IV-TR Axis I Disorders, Research Version, Patient Edition.* (SCID-I/P). New York, NY: Biometrics Research, New York State Psychiatric Institute.

First, M. B., Williams, J. B. W., Karg, R. S., and Spitzer, R. L. (2015). *Structured Clinical Interview for DSM-5: Research Version.* Arlington, VA: American Psychiatric Association.

Forth, A. E., and Kosson, D. S. (2003). *Hare Psychopathy Checklist: Youth Version.* Toronto: Multi-Health Systems, 1–52.

Freire, L., and Mangin, J. F. (2001). Motion correction algorithms may create spurious brain activations in the absence of subject motion. *Neuroimage.* 14, 709–722. doi: 10.1006/nimg.2001.0869

Friston, K. J., Holmes, A. P., Worsley, K. J., Poline, J. P., Frith, C. D., and Frackowiak, R. S. (1994). Statistical parametric maps in functional imaging: a general linear approach. *Hum. Brain Mapp.* 2, 189–210. doi: 10.1002/hbm.460020402

Genovese, C. R., Lazar, N. A., and Nichols, T. (2002). Thresholding of statistical maps in functional neuroimaging using the false discovery rate. *NeuroImage* 15, 870–878. doi: 10.1006/nimg.2001.1037

Hare, R. D. (2003). *Manual for the Hare Psychopathy Checklist-Revised.* Toronto, ON: Multi-Health Systems.

Hare, R. D., and Neumann, C. S. (2010). The role of antisociality in the psychopathy construct: comment on Skeem and Cooke. *Psychol Assess.* 22:446–54. doi: 10.1037/a0013635

Harenski, C. L., Edwards, B. G., Harenski, K. A., and Kiehl, K. A. (2014a). Neural correlates of moral and non-moral emotion in female psychopathy. *Front. Hum. Neurosci.* 8, 741. doi: 10.3389/fnhum.2014.00741

Harenski, C. L., Harenski, K. A., and Kiehl, K. A. (2014b). Neural processing of moral violations among incarcerated adolescents with psychopathic traits. *Dev. Cogn. Neurosci.* 10, 181–189. doi: 10.1016/j.dcn.2014.09.002

Harpur, T. J., Hare, R. D., and Hakstian, A. R. (1989). Two-factor conceptualization of psychopathy: construct validity and assessment implications. *Psychol. Assessment A J. Consult. Clin. Psychol.* 1, 6. doi: 10.1037/1040-3590.1.1.6

Hemphill, J. F., Hare, R. D., and Wong, S. (1998). Psychopathy and recidivism: a review. *Legal Criminol. Psychol.* 3, 139–170. doi: 10.1111/j.2044-8333.1998.tb00355.x

Himberg, J., and Hyvärinen, A. (2003). "Icasso: software for investigating the reliability of ICA estimates by clustering and visualization," in *2003 IEEE XIII Workshop on Neural Networks for Signal Processing (IEEE Cat. No. 03TH8718)*, 259–268.

Hu, G., Waters, A. B., Aslan, S., Frederick, B., Cong, F., and Nickerson, L. D. (2020). Snowball ICA: a model order free independent component analysis strategy for functional magnetic resonance imaging data. *Front. Neurosci.* 14, 569657. doi: 10.3389/fnins.2020.569657

Kennealy, P. J., Hicks, B. M., and Patrick, C. J. (2007). Validity of factors of the psychopathy checklist—revised in female prisoners: discriminant relations with antisocial behavior, substance abuse, and personality. *Assessment* 14, 323–340. doi: 10.1177/1073191107305882

Kiehl, K. A. (2006). A cognitive neuroscience perspective on psychopathy: evidence for paralimbic system dysfunction. *Psychiatry Res.* 142, 107–128. doi: 10.1016/j.psychres.2005.09.013

Kiehl, K. A., and Hoffman, M. B. (2011). The criminal psychopath: history, neuroscience, treatment, and economics. *Jurimetrics* 51, 355.

Kiviniemi, V., Starck, T., Remes, J., Long, X., Nikkinen, J., Haapea, M., et al. (2009). Functional segmentation of the brain cortex using high model order group PICA. *Human Brain Mapp.* 30, 3865–3886. doi: 10.1002/hbm.20813

Korponay, C., Pujara, M., Deming, P., Philippi, C., Decety, J., Kosson, D. S., et al. (2017). Impulsive-antisocial psychopathic traits linked to increased volume and functional connectivity within prefrontal cortex. *Soc. Cogn. Affect Neurosci.* 12, 1169–1178. doi: 10.1093/scan/nsx042

Leutgeb, V., Wabnegger, A., Leitner, M., Zussner, T., Scharmüller, W., Klug, D., et al. (2016). Altered cerebellar-amygdala connectivity in violent offenders: a resting-state fMRI study. *Neurosci. Lett.* 610, 160–164. doi: 10.1016/j.neulet.2015.10.063

Liu, H., Liao, J., Jiang, W., and Wang, W. (2014). Changes in low-frequency fluctuations in patients with antisocial personality disorder revealed by resting-state functional MRI. *PLoS ONE* 9, e89790. doi: 10.1371/journal.pone.0089790

Ma, S., Correa, N. M., Li, X. L., Eichele, T., Calhoun, V. D., and Adali, T. (2011). Automatic identification of functional clusters in FMRI data using spatial dependence. *IEEE Trans. Biomed. Eng.* 58, 3406–3417. doi: 10.1109/TBME.2011.2167149

Maurer, J. M., Paul, S., Edwards, B. G., Anderson, N. E., Nyalakanti, P. K., Harenski, C. L., et al. (2022). Reduced structural integrity of the uncinate fasciculus in incarcerated women scoring high on psychopathy. *Brain Imaging Behav.* doi: 10.1007/s11682-022-00684-z. [Epub ahead of print].

Maurer, J. M., Steele, V. R., Cope, L. M., Vincent, G. M., Stephen, J. M., Calhoun, V. D., et al. (2016). Dysfunctional error-related processing in incarcerated youth with elevated psychopathic traits. *Dev. Cogn. Neurosci.* 19, 70–77. doi: 10.1016/j.dcn.2016.02.006

Meda, S. A., Giuliani, N. R., Calhoun, V. D., Jagannathan, K., Schretlen, D. J., Pulver, A., et al. (2008). A large scale (N5400) investigation of gray matter differences in schizophrenia using optimized voxel-based morphometry. *Schizophr. Res.* 101, 95–105. doi: 10.1016/j.schres.2008.02.007

Pessoa, L., McKenna, M., Gutierrez, E., and Ungerleider, L. G. (2002). Neural processing of emotional faces requires attention. *Proc. Natl. Acad. Sci. U.S.A.* 99, 11458–11463. doi: 10.1073/pnas.172403899

Philippi, C. L., Pujara, M. S., Motzkin, J. C., Newman, J., Kiehl, K. A., and Koenigs, M. (2015). Altered resting-state functional connectivity in cortical networks in psychopathy. *J. Neurosci.* 35, 6068–6078. doi: 10.1523/JNEUROSCI.5010-14.2015

Power, J. D., Mitra, A., Laumann, T. O., Snyder, A. Z., Schlaggar, B. L., and Petersen, S. E. (2014). Methods to detect, characterize, and remove motion artifact in resting state fMRI. *Neuroimage* 84, 320–341. doi: 10.1016/j.neuroimage.2013.08.048

Pu, W., Luo, Q., Jiang, Y., Gao, Y., Ming, Q., and Yao, S. (2017). Alterations of brain functional architecture associated with psychopathic traits in male adolescents with conduct disorder. *Sci. Rep.* 7, 1–11. doi: 10.1038/s41598-017-11775-z

Rachakonda, S., Silva, R. F., Liu, J., and Calhoun, V. D. (2016). Memory efficient PCA methods for large group ICA. *Front. Neurosci.* 10, 17. doi: 10.3389/fnins.2016.00017

Robinson, S., Basso, G., Soldati, N., Sailer, U., Jovicich, J., Bruzzone, L., et al. (2009). A resting state network in the motor control circuit of the basal ganglia. *BMC Neurosci.* 10, 137. doi: 10.1186/1471-2202-10-137

Ryan, J. J., and Ward, L. C. (1999). Validity, reliability, and standard errors of measurement for two seven-subtest short forms of the Wechsler Adult Intelligence Scale—III. *Psychol. Assess.* 11, 207. doi: 10.1037/1040-3590.11.2.207

Smith, S. M., Fox, P. T., Miller, K. L., Glahn, D. C., Fox, P. M., Mackay, C. E., et al. (2009). Correspondence of the brain's functional architecture during activation and rest. *PNAS.* 106, 13040–13045. doi: 10.1073/pnas.0905267106

Steele, V. R., Claus, E. D., Aharoni, E., Harenski, C., Calhoun, V. D., Pearlson, G., et al. (2014). A large scale (N = 102) functional neuroimaging study of error processing in a Go/NoGo task. *Behav. Brain Res.* 268, 127–138. doi: 10.1016/j.bbr.2014.04.001

Tang, Y., Jiang, W., Liao, J., Wang, W., and Luo, A. (2013). Identifying individuals with antisocial personality disorder using resting-state FMRI. *PLoS ONE* 8, e60652. doi: 10.1371/journal.pone.0060652

Thijssen, S., and Kiehl, K. A. (2017). Functional connectivity in incarcerated male adolescents with psychopathic traits. *Psychiatry Res. Neuroimaging* 265, 35–44. doi: 10.1016/j.pscychresns.2017.05.005

Verona, E., and Vitale, J. (2018). "Psychopathy in women: assessment, manifestations, and etiology," in *Handbook of Psychopathy*, ed C. J. Patrick (New York, NY: The Guilford Press), 509–528.

Vitale, J. E., Maccoon, D. G., and Newman, J. P. (2011). Emotion facilitation and passive avoidance learning in psychopathic female offenders. *Crim. Justice. Behav.* 38, 641–658. doi: 10.1177/0093854811403590

Vitale, J. E., and Newman, J. P. (2001a). Using the psychopathy checklist—revised with female samples: reliability, validity, and implications for clinical utility. *Clin. Psychol. Sci. Pract.* 8, 117. doi: 10.1093/clipsy.8.1.117

Vitale, J. E., and Newman, J. P. (2001b). Response perseveration in psychopathic women. *J. Abnorm. Psychol.* 110, 644–647. doi: 10.1037//0021-843x.110.4.644

Vitale, J. E., Newman, J. P., Bates, J. E., Goodnight, J., Dodge, K. A., and Pettit, G. S. (2005). Deficient behavioral inhibition and anomalous selective attention in a community sample of adolescents with psychopathic traits and low-anxiety traits. *J. Abnorm. Child Psychol.* 33, 461–470. doi: 10.1007/s10802-005-5727-X

Vitale, J. E., Smith, S. S., Brinkley, C. A., and Newman, J. P. (2002). The reliability and validity of the psychopathy checklist–revised in a sample of female offenders. *Crim. Justice Behav.* 29, 202–231. doi: 10.1177/009385480202900205

Willis, M. L., Palermo, R., Burke, D., McGrillen, K., and Miller, L. (2010). Orbitofrontal cortex lesions result in abnormal social judgements to emotional faces. *Neuropsychologia* 48, 2182–2187. doi: 10.1016/j.neuropsychologia.2010.04.010

Xu, T., Cullen, K. R., Houri, A., Lim, K. O., Schulz, S. C., and Parhi, K. K. (2014). "Classification of borderline personality disorder based on spectral power of resting-state fMRI," in *2014 36th Annual International Conference of the IEEE Engineering in Medicine and Biology Society*. IEEE, 5036–5039.

Yang, Y., Raine, A., Colletti, P., Toga, A. W., and Narr, K. L. (2011). Abnormal structural correlates of response perseveration in individuals with psychopathy. *J Neuropsychiatry Clin. Neurosci.* 23, 107–110. doi: 10.1176/appi.neuropsych.23.1.107

Ystad, M., Eichele, T., Lundervold, A. J., and Lundervold, A. (2010). Subcortical functional connectivity and verbal episodic memory in healthy elderly-a resting state fMRI study. *Neuroimage.* 52, 379–388. doi: 10.1016/j.neuroimage.2010.03.062

frontiers | Frontiers in Neuroscience

TYPE Original Research
PUBLISHED 10 October 2022
DOI 10.3389/fnins.2022.951907

OPEN ACCESS

EDITED BY
Roberto Esposito,
ASUR Marche, Italy

REVIEWED BY
Maya Visser,
Jaume I University, Spain
Martin Fungisai Gerchen,
University of Heidelberg, Germany

*CORRESPONDENCE
Oscar Miranda-Dominguez
miran045@umn.edu

†Deceased

SPECIALTY SECTION
This article was submitted to Brain Imaging Methods, a section of the journal Frontiers in Neuroscience

RECEIVED 24 May 2022
ACCEPTED 20 September 2022
PUBLISHED 10 October 2022

CITATION
Vazquez-Trejo V, Nardos B, Schlaggar BL, Fair DA and Miranda-Dominguez O (2022) Use of connectotyping on task functional MRI data reveals dynamic network level cross talking during task performance.
Front. Neurosci. 16:951907.
doi: 10.3389/fnins.2022.951907

Use of connectotyping on task functional MRI data reveals dynamic network level cross talking during task performance

Valeria Vazquez-Trejo[1,2], Binyam Nardos[3,4†], Bradley L. Schlaggar[5,6,7], Damien A. Fair[8,9,10] and Oscar Miranda-Dominguez[8,9,11*]

[1]Rush Medical College, Chicago, IL, United States, [2]Department of Biology, Portland State University, Portland, OR, United States, [3]Department of Behavioral Neuroscience, Oregon Health and Science University, Portland, OR, United States, [4]Department of Occupational Therapy, Washington University School of Medicine in St. Louis, St. Louis, MO, United States, [5]Kennedy Krieger Institute, Baltimore, MD, United States, [6]Department of Neurology, Johns Hopkins University School of Medicine, Baltimore, MD, United States, [7]Department of Pediatrics, Johns Hopkins University School of Medicine, Baltimore, MD, United States, [8]Department of Pediatrics, Medical School, University of Minnesota, Minneapolis, MN, United States, [9]Masonic Institute for the Developing Brain, University of Minnesota, Minneapolis, MN, United States, [10]Institute of Child Development, College of Education and Human Development, University of Minnesota, Minneapolis, MN, United States, [11]Minnesota Supercomputing Institute, University of Minnesota, Minneapolis, MN, United States

Task-based functional MRI (fMRI) has greatly improved understanding of brain functioning, enabling the identification of brain areas associated with specific cognitive operations. Traditional analyses are limited to associating activation patterns in particular regions with specific cognitive operation, largely ignoring regional cross-talk or dynamic connectivity, which we propose is crucial for characterization of brain function in the context of task fMRI. We use connectotyping, which efficiently models functional brain connectivity to reveal the progression of temporal brain connectivity patterns in task fMRI. Connectotyping was employed on data from twenty-four participants (12 male, mean age 24.8 years, 2.57 std. dev) who performed a widely spaced event-related fMRI word vs. pseudoword decision task, where stimuli were presented every 20 s. After filtering for movement, we ended up with 15 participants that completed each trial and had enough usable data for our analyses. Connectivity matrices were calculated per participant across time for each stimuli type. A Repeated Measures ANOVA applied on the connectotypes was used to characterize differences across time for words and pseudowords. Our group level analyses found significantly different dynamic connectivity patterns during word vs. pseudoword processing between the Fronto-Parietal and Cingulo-Parietal Systems, areas involved in cognitive task control, memory retrieval, and semantic processing. Our findings support the presence

of dynamic changes in functional connectivity during task execution and that such changes can be characterized using connectotyping but not with traditional Pearson's correlations.

KEYWORDS

fMRI, task fMRI, connectotyping, functional connectivity, cognition, dynamic connectivity, widely spaced event-related fMRI, BOLD

Introduction

Task-based functional MRI (fMRI) has had a profound impact on our understanding of brain functioning. Using fMRI, it is possible to design experiments that target specific sensorimotor, perceptual, and/or cognitive operations in efforts to understand the brain's basis of those functions. Complementing neuroscientific findings based on other methods (e.g., single cell or multiunit recording), and lesion cases, task-based fMRI studies have identified functional neuroanatomy underlying various sensorimotor and perceptual systems. Examples include visual (Engel et al., 1994; Sereno et al., 1995; Goebel et al., 1998) and auditory systems (Moerel et al., 2014), as well as systems associated with higher-order cognitive operations such as memory retrieval (Yonelinas and Levy, 2002; Wheeler and Buckner, 2003; Dobbins and Wagner, 2005; Yonelinas et al., 2005; Cabeza et al., 2008; Nelson et al., 2010; Rugg and Vilberg, 2013), semantic processing (Petersen et al., 1988; Fiez, 1997; Thompson-Schill et al., 1997; Friederici et al., 2000; Donaldson et al., 2001; Roskies et al., 2001; Wagner et al., 2001; Badre et al., 2005; Gordon et al., 2014), and cognitive control (Botvinick et al., 2001; Braver and Barch, 2006; Dosenbach et al., 2006, 2007).

The primary measure in fMRI studies is the blood oxygen level dependent (BOLD) signal. Although not a direct measure of neural activity, it has been shown that the measured BOLD signal is correlated with neural activity, particularly with local field potentials (Logothetis et al., 2001; Logothetis, 2003). The BOLD signal, however, is slow compared to neural activity. After an initial stimulus, the BOLD signal peaks typically after 6 s (Vazquez and Noll, 1998), returning to baseline in approximately 20 s –this observed activation trend is known as the hemodynamic response function. The signal delay in returning to baseline needs to be considered in experimental design (Logothetis, 2008). For example, in a typical task experiment, participants are exposed to a given stimulus (cognitive, visual, or auditory) or are asked to perform a task. Given the knowledge of the delayed peak on activation, methods are tuned to look for brain areas that respond specifically to the experimental paradigm once peak response is achieved.

The subsequent development of resting state functional connectivity MRI (rs-fcMRI) was another milestone in neuroimaging. Biswal et al.'s seminal work (Biswal et al., 1995) established that the low frequency (<0.1 Hz) resting BOLD activity in brain regions that are typically coactivated during task-states (or known to be members of a common brain system e.g., left and right primary motor cortex) show a high degree of temporal correlation. This high degree of correlation is hypothesized to be a measure of functional connectivity among the said regions. rs-fcMRI has since become a very convenient technique to characterize brain function. Since it does not require the presence of an overt cognitive task, it can be employed in animals (Miranda-Dominguez et al., 2014b; Stafford et al., 2014), developmental populations (Marek et al., 2019), or in patients that may otherwise be unable to perform intentional cognitive tasks.

There is a growing interest in characterizing dynamic changes in brain connectivity (Chang and Glover, 2010), both at rest and during tasks. Several groups have used different techniques to characterize the cross-talking between brain areas (Friston et al., 1997; Chang and Glover, 2010; Ginestet and Simmons, 2011; Cribben et al., 2012; Lindquist et al., 2014; Billings et al., 2021; Shappell et al., 2021) but there are controversies in the field (Laumann et al., 2016). One of the first methods to estimate dynamics in functional connectivity is the use of "sliding windows" (Sakoğlu et al., 2010), where the BOLD data is split in segments, connectivity is calculated on each segment, then changes in functional connectivity are tracked across time. This has been mostly used in resting state data. Another approach is to assume that functional connectivity is a dynamic process that can be characterized by a multivariate gaussian distribution whose mean and covariance matrix evolves on time and there are efficient algorithms that can estimate those statistical properties (Xu and Lindquist, 2015). Dynamic Causal Modeling (DCM), (Friston et al., 2003, 2019), is another technique that models dynamic changes in functional connectivity. DCM can be applied on resting state and task data. In DCM, the user specifies the brain areas that define "the circuit" involved in a task and then, by using differential equations and non-linear dynamics, a predicted hemodynamic response is modeled and compared against the measured signal within the proposed circuit. An alternative method is to use non-linear dynamics to identify transitions among different states in timeseries (Zhang and Saggar, 2020).

There have also been attempts to characterize dynamic changes in connectivity in task-fMRI experiments. An approach that has been used by some but not all studies, relies on averaging data across participants to increase signal to noise ratio (intrasubject correlation analysis). In this method, dynamic changes in connectivity are estimated after calculating the correlation of each brain area's timeseries against each other across participants and averaging correlations across participants (Hasson et al., 2004; Najafi et al., 2017). There are also methods such as Psychophysiological Interactions (PPI, McLaren et al., 2012) and Rissman connectivity (Rissman et al., 2004) that do not rely on averaging data across participants but need a brain area or areas as seed(s) to estimate changes in connectivity in reference to that seed. The most basic implementation of PPI (McLaren et al., 2012) consists of defining 3 regressors, the timeseries of a) the task, b) the BOLD response of the seed, and c) the product of those 2 signals. The BOLD response of brain areas that can be modeled by the product of the 2 signals considered to be functionally connected to the seed and be involved in the task. The other 2 regressors are used to control for areas that respond to the task but are not connected to the seed and for areas that are in close proximity to the seed but not functionally involved in the task. In Rissman connectivity, the BOLD data is aligned according to the timing of events and, using the Generalized Linear Model framework, beta-weights associated with those events are calculated for every voxel (Rissman et al., 2004). Resulting event-related beta-weights are correlated across voxels to identify connections associated with the task being studied.

One may reasonably hypothesize that there are dynamic functional connectivity changes on the networks supporting any mental process that may occur on the order of seconds during the instantiation, computation, and response frame of a given task. Hence, there is a need for a method able to utilize whole brain connectivity to identify the brain networks that support a task. This could be done by aligning the BOLD data according to the phase of a task, calculating instantaneous connectivity at each phase and tracking changes on time across networks. Unfortunately, one of the main problems in fMRI is that the BOLD signal is highly susceptible to noise and correlations. The traditional method used to characterize whole brain connectivity, may not have the resolving power to unveil dynamic changes in connectivity.

Connectotyping (Miranda-Dominguez et al., 2014a, 2018), a model-based method used to calculate functional connectivity has the potential to address the above limitations. We have shown that connectotyping is able to identify personalized patterns of brain connectivity with an improved signal-to-noise ratio even when using limited amounts of data as demonstrated in a recent study where this approach was used to characterize heritable patterns of brain functional connectivity (Miranda-Dominguez et al., 2018). Connectotyping is based on a linear model that proposes that the activity of a given brain region can be described by the weighted sum of all the other brain regions (**Figure 1**). The coefficients (beta-weights) of the resulting model correspond to a connectivity matrix that is capable of identifying a functional fingerprint in individual participants using a small amount of data (e.g., 5 min of rs-fcMRI), which is the typical amount of movement-free data able to be acquired in most studies.

The aim of this current study is to determine whether connectotyping can be applied to a task fMRI dataset to track changes in network-network functional connectivity *during the progression of a task*. This study relies on the following three assumptions: (1) A given task will activate specific brain areas and networks tuned to respond to the different aspects of the progression of such task. (2) As the task evolves, the balance – or co-activation patterns— among brain areas will change, reflecting dynamical tuning to different aspects of the task. (3) There is a contrast in the task that enables the differentiation of pure activation of brain areas versus task-specific changes in brain connectivity. With connectotyping, the activity of each brain area is modeled as the weighted contribution of all the other brain areas. Therefore, we can use connectotyping to capture instantaneous connectivity maps as the task evolves. Then, dynamic changes in functional connectivity secondary to the evolution of the task can be characterized using statistical testing (repeated measures ANOVA tests).

For this analysis, we first identified a task-fMRI dataset with stimuli presented in a widely spaced manner without

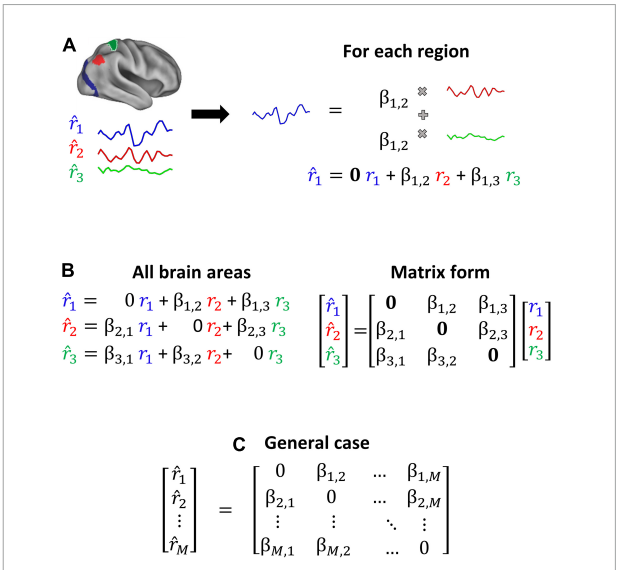

FIGURE 1
Connectotyping. Functional connectivity is calculated as the weighted sum of activity from the remaining brain regions (Miranda-Dominguez et al., 2014a). **(A)** Given 3 brain areas, each timeseries is modeled as the weighted sum of the other timeseries. **(B)** All the equations can be expressed as a matrix and solved using linear algebra. **(C)** This approach can be generalized to *M* brain regions.

the confounding effect of BOLD activity overlap from past stimuli. Again, one of the characteristics of the BOLD signal that must be considered in this context is that it takes about 20 s for the hemodynamic response function to return to baseline following stimulus presentation. However, we avoid overlapping responses by using data from widely spaced event-related fMRI experiment (at least 20 s between individual stimuli) in which subjects were performing a visually presented word vs. pronounceable non-word (hereafter pseudoword or PW) lexical decision task (Nardos, 2015).

Specifically, we hypothesized that connections between networks implicated in cognitive control (Botvinick et al., 2001; Braver and Barch, 2006; Dosenbach et al., 2006, 2007), memory retrieval (Iidaka et al., 2006), and semantic processing (Petersen et al., 1988; Fiez, 1997; Thompson-Schill et al., 1997; Friederici et al., 2000; Donaldson et al., 2001; Roskies et al., 2001; Wagner et al., 2001; Badre et al., 2005) would have dynamic network-network functional connectivity differences as a function of the type of stimulus (word vs. PW) being processed.

In summary, our goal is to track changes in functional connectivity between different functional networks. We hypothesized that the distinction between word and PW relies on the dynamic activation of higher order attention networks and that connectotyping has enough resolving power to characterize such changes and can do so better than using connectivity matrices created *via* Pearson's correlations.

Materials and methods

Participants

The original study sample consisted of 28 participants; after excluding participants who had incomplete or compromised data quality, the current study included 24 individuals. Participants were 24 monolingual (English-speaking), right-handed participants (12 male, mean age 24.8 years, 2.57 std. dev) recruited from neighborhoods surrounding Washington University in St. Louis as well as from the university student body (Nardos, 2015). All participants had no history of psychiatric or neurological illness and scored above the 50th percentile on the Woodcock-Johnson III reading assessment (Woodcock and Johnson, 2002). The Washington University Human Studies Committee approved the study (IRB ID # 201202083) and all participants were reimbursed for their participation.

Task

In a visually presented lexical decision task, individuals identified words vs. PWs while in the MRI scanner *via* button pressing. A set of words (50% animals; 50% artifacts; 3–9 letters; 1–3 syllables) and PWs (5 letters, 1 or 2 syllables) were selected from the English Lexicon Project (Balota et al., 2007; Nardos, 2015). Pseudowords were vetted by an expert, ensuring that words and pseudowords were tightly matched on lexical characteristics like number of letters, number of syllables, bigram frequency, and orthographic neighborhood size (Nardos, 2015). When in the scanner participants had two buttons, one on each hand. Each button corresponded either to words or PWs, participants pressed the buttons with the thumb of either hand to identify the stimuli. Stimuli were presented in a widely spaced manner, i.e., separated by ∼20 s, to avoid hemodynamic response signal overlap across individual stimuli and allow extraction of individual trial BOLD responses (Nardos, 2015). In each trial, a word or PW stimulus was presented for 2.5 s (1 TR or MR frame) with each letter subtending 0.5° of horizontal visual angle, followed by 17.5 s (7TRs or MR frames) of a black fixation screen with a white cross. Participants underwent 10 functional MRI runs each with 24 stimuli (18 PWs and 6 words) per run. Out of 24 trials within a run, 3 of those trials were catch trials, meaning that the intertrial interval after those trials would randomly be 2, 3, or 4 times the duration of the TR (2.5 sec), i.e., 5, 7.5, or 10 s, respectively. Catch trials were run for both words and pseudowords. While there were differences across participants in reaction time, overall accuracy was very high (98%, see (Nardos, 2015) for details).

Data acquisition

Structural and functional MRI data were collected as described in Nardos (2015) from a Siemens 3 Tesla MAGNETOM Trio system (Erlangen, Germany). The scanner included total imaging matrix technology (TIM) and utilized a 12-channel head matrix coil. A high resolution T1-weighted MP-RAGE was acquired (TE = 3.08 ms, TR [partition] = 2.4 s, TI = 1,000 ms, flip angle = 8″, 176 slices with 1 × 1 × 1 mm voxels). To improve atlas alignment a T2-weighted turbo spin echo structural image (TE = 84 ms, TR = 6.8 s, 32 slices with 2 × 1 × 4 mm voxels) matching the acquisition plane of the BOLD images were also collected. Alignment to the anterior commissure-posterior commissure (AC-PC) plane was performed by Siemens pulse sequence protocol. BOLD contrast-sensitive gradient echo echo-planar sequence (TE = 27 ms, flip angle = 90″, in-plane resolution = 4 × 4 mm) was used for functional data collection. Using a TR of 2.5 s, 32 contiguous, 4 mm- thick axial slices whole-brain EPI volumes were collected. Communication with participants was facilitated by MR- compatible headphones which were also used to reduce noise from the scanner. Head movement was minimized by using a molded thermoplastic mask. Stimuli were presented using Psyscope (Cohen et al., 1993) installed on an iMAC computer (Apple, Cupertino, CA) and projected *via* an LCD

projector (Sharp model PG-C20XU) onto an MRI-compatible rear-projection screen combined with a mirror attached to the head coil (CinePlex).

MRI data preprocessing

Data were processed using surface-based registration applying a modified version from the Human Connectome Project pipeline (Glasser et al., 2013) plus in-house denoising methods.[1] Processing includes the use of FSL (Smith et al., 2004; Woolrich et al., 2009; Jenkinson et al., 2012) and FreeSurfer tools (Sereno et al., 1995; Fischl and Dale, 2000; Desikan et al., 2006). Briefly, gradient distortion corrected T1-weighted and T2-weighted volumes were first aligned to the MNI's AC-PC axis and then non-linearly normalized to the MNI atlas. Later, the T1w and T2w volumes were re-registered using boundary-based registration (Greve and Fischl, 2009) to improve alignment. Individual brains were segmented using recon-all from FreeSurfer. Segmentations were improved by using the enhanced white matter-pial surface contrast of the T2-weighted sequence. Additionally, the initial pial and white matter surfaces were used to distinguish an initial cortical ribbon. From these segmentations, a tailored 3D surface was created for each participant and registered to the Conte 69 surface atlas of the Human Connectome Project.

The BOLD data were corrected for field distortions (using FSL's TOPUP) and processed by doing a preliminary 6 degrees of freedom linear registration to the first frame. After this initial alignment, the average frame was calculated and used as a final reference. Next, the BOLD data were registered to this final reference and to the T1-weighted volume, all in one single step, by concatenating all the individual registrations into a single registration. To allow steady state magnetization, the first four volumes of each run were discarded. The cortical ribbon defined by the structural T1-weighted and T2-weighted volumes was used to define a high-resolution mesh used for surface registration of the BOLD data. This cortical ribbon was also used to quantify the partial contribution of each voxel in the BOLD data in surface registration. Timecourses in the cortical mesh were calculated by obtaining the weighted average of the voxels neighboring each vertex within the grid, where the weights are given by the average number of voxels wholly or partially within the cortical ribbon. Voxels with a high coefficient of variation, indicating difficulty with tissue assignment or containing large blood vessels, were excluded. Next, the resulting timecourses in this mesh were downsampled into a standard space of 91, 282 anchor points (grayordinates), which were defined in the brain atlas and mapped uniquely to each participant's brain after smoothing them with a 2 mm full-width-half-max Gaussian filter. Subcortical regions were treated and registered as volumes. Two-thirds of the grayordinates are vertices located in the cortical ribbon while the remaining grayordinates are subcortical voxels. Subsequently, resulting timecourses (surface registration for cortex and volume registration for subcortical gray matter) were detrended. The following steps involved regression of (1) 6 degrees of freedom obtained by rigid-body head motion correction, (2) whole brain signal, (3) ventricular signal averaged from ventricular regions of interest (ROIs), (4) white matter signal averaged from white matter ROIs, (5) first-order derivative terms and the squares for whole brain, ventricular and white matter signals to account for variance between regressors. Finally, timecourses were filtered using a first-order Butterworth band-pass filter with frequency range from 9 to 80 mHz. This filter was applied in the forward and backward direction to remove phase distortions.

Regions of interest and functional networks

Collected BOLD data were parcellated using the Gordon schema that has 333 regions of interest (ROIs) grouped into 12 networks (Gordon et al., 2014). Each grayordinate was assigned to a region and network within this parcelation. The networks, their abbreviation and the number of ROIs included are: Auditory (Aud, $n = 24$), Cingulo-Opercular (CiO, $n = 40$), Cingulo-Parietal (CiP, $n = 5$), Default (Def, $n = 41$), Dorsal Attention (DoA, $n = 32$), Fronto-Parietal (FrP, $n = 24$), Retrosplenial Temporal (ReT, $n = 8$), Somato-sensory hand (Sml, $n = 38$), Somato-sensory mouth (SMm, $n = 8$), Salience (Sal, $n = 4$), Ventral Attention (VeA, $n = 23$), and Visual (Vis, $n = 39$). From the 333 ROIs, 47 ROIs were not assigned to any network. The location of each functional network is shown in **Figure 2**. Per our hypothesis, on this pilot study we excluded primary somatosensory and unimodal networks and included only the Cingulo-Parietal, Default, Dorsal Attention, Fronto-Parietal, Salience, and Ventral Attention, ending up with 129 brain areas from 6 brain networks that were grouped into 36 functional network pairs (CiP-CiP, CiP-Def,. . .). **Table 1** shows all the functional network pairs including the count of unique connectotyping's beta-weights.

Motion censoring

Correction for head motion was completed by calculating six parameters of head movement, movement and rotation along the x, y, and z axes. The absolute sum of movement along these parameters was evaluated after each change of frame and termed "frame displacement" (FD). For our study, we set our FD threshold at 0.3 mm and set the FD of the first frame at zero. This measure was only used as a way to detect motion and was not used for regression (Power et al., 2012; Siegel et al., 2014).

1 https://github.com/DCAN-Labs

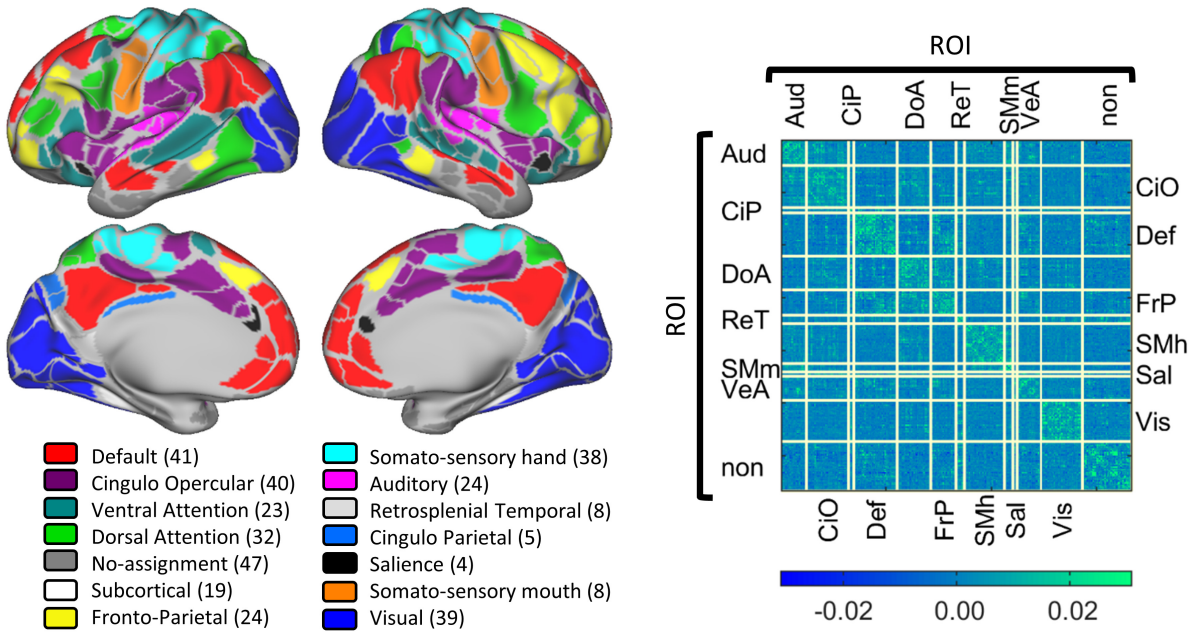

FIGURE 2
Gordon parcelation schema. The **(Left panel)** displays a visual representation of the 13 defined cortical networks in the Gordon Parcelation. Networks are color coded with the number of regions of interest shown in parentheses. The **(Right panel)** shows the average connectivity matrix calculated as the average beta-weights of all the data included in this study. Each row and column correspond to a particular brain region, and each cell is a connection. Connections are grouped by functional network pair.

Grouping data for connectotyping

We calculated instantaneous connectotypes for each participant at each phase (Frame 1–8) of the progression of each task (i.e., for words and PWs) ending up with 16 connectotypes per participant, as shown in **Figure 3**. Each resulting connectotype captures the instantaneous cross-talking among brain areas at each phase of the progression of each task. To do this, for each participant, at each frame and stimulus type, we concatenated the BOLD data from the same frame, relative to the frame at which stimuli was presented for each participant (as shown in **Figure 3A**). We did this because these replica frames correspond to the same point in time in the dynamic evolution of the task. This created a matrix with the dimension 333 by the number of replica frames. The dimension 333 is due to the number or ROIs included in the Gordon parcelation schema (Gordon et al., 2014). Next, we used that stack of replica frames to calculate a connectotype that reflects the crosstalking between ROIs at this phase of the task. This approach was repeated for each phase of the experiment. We only included trials that had a length of 8 TRs for a total of 20 s, with the additional constraint that the preceding trial in the experiment took place at least 20 s prior, ensuring that the timecourse for the current trial under consideration is not adulterated by that previous trial. Frames were excluded if head movement was higher than a given frame displacement (FD) threshold of 0.3 mm (Power et al., 2014). Participants were included only if they had enough data (40 replica frames or more) to calculate personalized connectotypes on each of the 16 conditions. Fifteen participants met this condition. Each connectotype was calculated using 40 "replica" frames to avoid the confounding factor that some connectotypes from specific participants could be calculated with different numbers of frames. For each condition and participant, we calculated connectotypes using 40 frames selected randomly within condition from the surviving frames with head movement lower than the pre-selected threshold. We decided to select frames randomly instead of the ones with the lowest FD to avoid bias and batch effects secondary to head movement. We ended up with 15 participants that successfully completed each trial (word and PW) for 20 s and had at least 40 low head-movement replica frames for each condition (16).

Connectotyping

As described in the original publication (Miranda-Dominguez et al., 2014a), connectotyping mathematically represents a brain region's signal as the weighted sum of the signal from every other brain region using values termed beta-weights (β). Such weights are optimized by regularization and cross-validation. The result is a directional connectivity map

that calculates the interaction between brain regions, allowing the identification of individual connectivity patterns among brain areas and networks. Briefly, in an example application on a hypothetical parcelation schema with only three brain regions, "a," "b," and "c"; this technique models the functional connectivity of region "a" as a weighted sum of regions "b" and "c's" connectivity. The model for the signal resulting from region "a" would be: $\hat{a} = \beta_{a,b}b + \beta_{a,c}c$. This same model is then applied to the remaining brain regions "b" and "c" until the signal for each region in the system is represented by an equation (see a schematic representation of connectotyping in Figure 1).

TABLE 1 List of all 36 functional network pairs tested in the ANOVA with the number of ROI connections between networks listed in the third column. Grouping of connections per functional system pair.

#	Name	Number of connections
1	CiP and CiP	20
2	Def and CiP	205
3	DoA and CiP	160
4	FrP and CiP	120
5	Sal and CiP	20
6	VeA and CiP	115
7	CiP and Def	205
8	Def and Def	1640
9	DoA and Def	1312
10	FrP and Def	984
11	Sal and Def	164
12	VeA and Def	943
13	CiP and DoA	160
14	Def and DoA	1312
15	DoA and DoA	992
16	FrP and DoA	768
17	Sal and DoA	128
18	VeA and DoA	736
19	CiP and FrP	120
20	Def and FrP	984
21	DoA and FrP	768
22	FrP and FrP	552
23	Sal and FrP	96
24	VeA and FrP	552
25	CiP and Sal	20
26	Def and Sal	164
27	DoA and Sal	128
28	FrP and Sal	96
29	Sal and Sal	12
30	VeA and Sal	92
31	CiP and VeA	115
32	Def and VeA	943
33	DoA and VeA	736
34	FrP and VeA	552
35	Sal and VeA	92
36	VeA and VeA	506
	Total	16,512

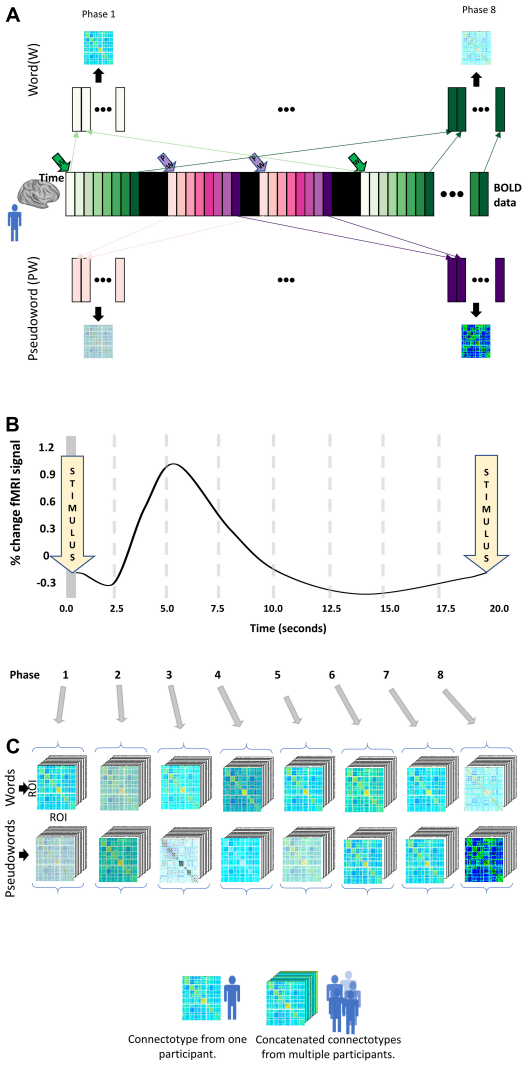

FIGURE 3
Experimental design. The widely spaced design of the word versus pseudoword experiment allows us to characterize dynamic changes in functional connectivity using connectotyping. **(A)** The collected whole-brain BOLD data is represented as the central colored strip. Each bar corresponds to data acquired at each TR and is color-coded according to the stimuli (Green for "Word" and purple for "PW"). A word or pseudoword is displayed for 2.5 s with no new stimuli after 20 s. The bars in black represent "catch" trials. Frames collected at the same time, relative to the exposure to the stimuli, are concatenated to create a stack of frames of size 333 times replica frames. Those frames are used to calculate a connectivity matrix. This approach generates 16 connectivity matrices per participant. **(B)** Temporal evolution of the theoretical hemodynamic response. **(C)** Resulting connectotypes from each participant **(A)** are grouped according to their phase and stacked with the connectotypes of all the participants included in the study.

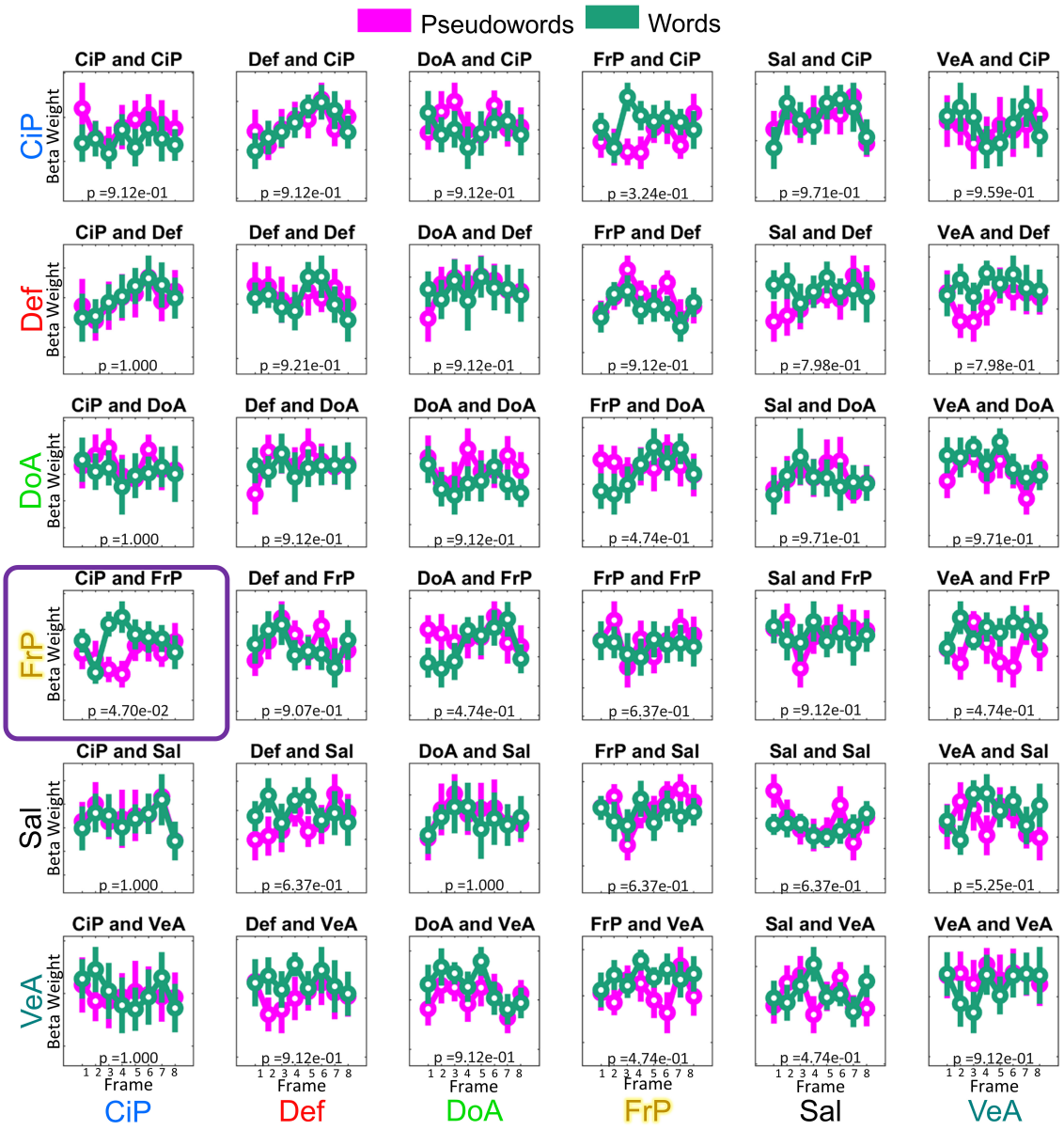

FIGURE 4
Distribution of connectivity values per functional network pair and condition. Beta-weights were calculated for each condition as indicated in our experimental design (**Figure 3**) and grouped by functional network pair. Each boxplot highlights the mean values using a circle and the dispersion is indicated with a bar covering 1.15 times the standard deviation of the connectivity values. Data is color-coded by stimuli: pseudoword (purple) and word (green). *X*-axis indicates the time, in frames (TR of 2.5 s each). In this study we included the following six networks: Cingulo-Parietal (CiP, *n* = 5 Regions of Interest), Default (Def, *n* = 41), Dorsal Attention (DoA, *n* = 32), Fronto-Parietal (FrP, *n* = 24), Salience (Sal, *n* = 4), and Ventral Attention (VeA, *n* = 23).

After applying the connectotyping approach to our filtered and grouped and timely aligned task-fMRI data, we ended up with 15 participants each with 16 connectotypes that characterize the instantaneous connectivity map as each trial evolved (word and PW).

To note, in the original manuscript (Miranda-Dominguez et al., 2014a), which aimed to characterize functional connectivity in resting state data, the first step was to account for the spurious effect of autocorrelations. In contrast, in task-based fMRI, autocorrelations are not spurious; they are

part of the temporal evolution of the task. For this reason, in this study we did not remove autocorrelations from the data.

Additionally, while connectotyping created individualized connectivity patterns, our study performed analyses on concatenated connectotypes from 15 participants resulting in a group level analysis.

Statistical analysis

To identify dynamic changes in functional connectivity, we ran independent repeated measures ANOVA tests for each functional network pair ($N = 36$, as described before) testing for changes in functional connectivity for the interaction of time (frame 1 to 8) and stimulus type, (i.e., word/PW) using the 16 connectotypes from all the surviving participants (**Figure 3**). All statistical analyses were performed in MATLAB. Before statistical testing, connectivity values (i.e., connectotyping beta-weights) were box-cox transformed to normalize distributions (Montgomery, 2005) and the logarithmic base was optimized by gradient descent. In MATLAB, the repeated measures ANOVA tests are performed in two steps. First, a linear mixed effects model is fit to predict outcome values (in this case connectivity values) as a function of the repeated factors time (frames 1 to 8), stimulus type (word and PW) and the interaction between the two of them. Next, the resulting corrected beta-weighted values are grouped according to the factors time, stimulus, and the interaction of time and stimulus type, to characterize statistical differences using regular ANOVA tests (See **Figure 4** for a visualization of the distribution of the marginal means of the data per functional network pairs included in this study). Mauchly's test of sphericity was used to test for differences in variance among the groups being compared, and p-values were adjusted accordingly using the correction factor epsilon. Epsilon-adjusted p-values were corrected for multiple comparisons using the Tukey–Kramer method, and 0.05 was used as threshold for significance (Rudolph et al., 2018; Kovacs-Balint et al., 2019; Miranda-Domínguez et al., 2020).

Methods' recap

We aimed to characterize dynamic changes in functional connectivity in a task fMRI study where participants were asked to identify whether they were exposed to a word or a PW. Stimuli (word of PW) was shown for 2.5 s, and fMRI data was collected every 2.5 s from the beginning of the exposure and for 20 s in total. Trials were repeated several times. Each participant included in the study was exposed to two types of stimuli and we used the same amounts of trials to calculate personalized connectivity maps *via* connectotyping at each time point of each trial. Next, we used series of repeated measures ANOVA tests on group level data to identify changes in functional connectivity for each possible functional network pairs among six networks of interest, the Cingulo-Parietal, Default, Dorsal Attention, Fronto-Parietal, Salience, and Ventral Attention networks from the Gordon parcelation (Gordon et al., 2014). The ANOVA examined differences in functional connectivity for the interaction of time (frames 1–8) and stimulus type, for each network pair. Data are available from the corresponding author upon reasonable request. Code is available in https://fconn-anova.readthedocs.io/en/latest/

Results

Changes in functional connectivity for the interaction of time and stimulus type

The 8(time) × 2(condition) ANOVA showed a significant interaction between the Cingulo-Parietal and Fronto-Parietal Networks ($F = 3.7155$; $p = 0.001$, uncorrected; $p = 0.047$, corrected), as shown in **Figure 5**. *Post-hoc* analysis revealed that differences were driven by changes in connectivity values at frames 3 (paired t-test word vs non-word, $p = 2.65e{-5}$) and 4 (paired t-test word vs non-word, $p = 2.68e{-4}$). To note, we repeated this analysis including the Visual Network and found no significant results. The strongest effect was found for connectivity values between the Cingulo-Parietal and Fronto-Parietal networks ($p = 0.06$, corrected) but none of the functional network pairs including the Visual network showed differences for this interaction, as shown in **Supplementary Figure 1**.

Robustness of results at different motion censoring thresholds

To test the robustness of our analysis using a more stringent threshold, we repeated analyses calculating connectotypes using a FD of 0.25. Only thirteen participants survived filtering at this threshold. While results did not pass corrections for multiple comparisons ($p = 0.508$, corrected) given the reduced sample size, the Cingulo-Parietal and Fronto-Parietal networks also exhibited the same temporal evolution in beta-weights for the interaction of time and stimulus type, as shown in **Supplementary Figure 2A**. In addition, we also recalculated our analysis with an FD of 0.5, allowing data from 17 participants, and found a similar difference in beta-weight response between these two networks. However, when correcting for multiple comparisons, the findings were not significant ($p = 0.941$, corrected) (**Supplementary Figure 2B**). These similarities in observed connectivity between the Cingulo-Parietal and Fronto-Parietal networks at different thresholds displayed a similar trend in temporal connectivity response as the original finding above.

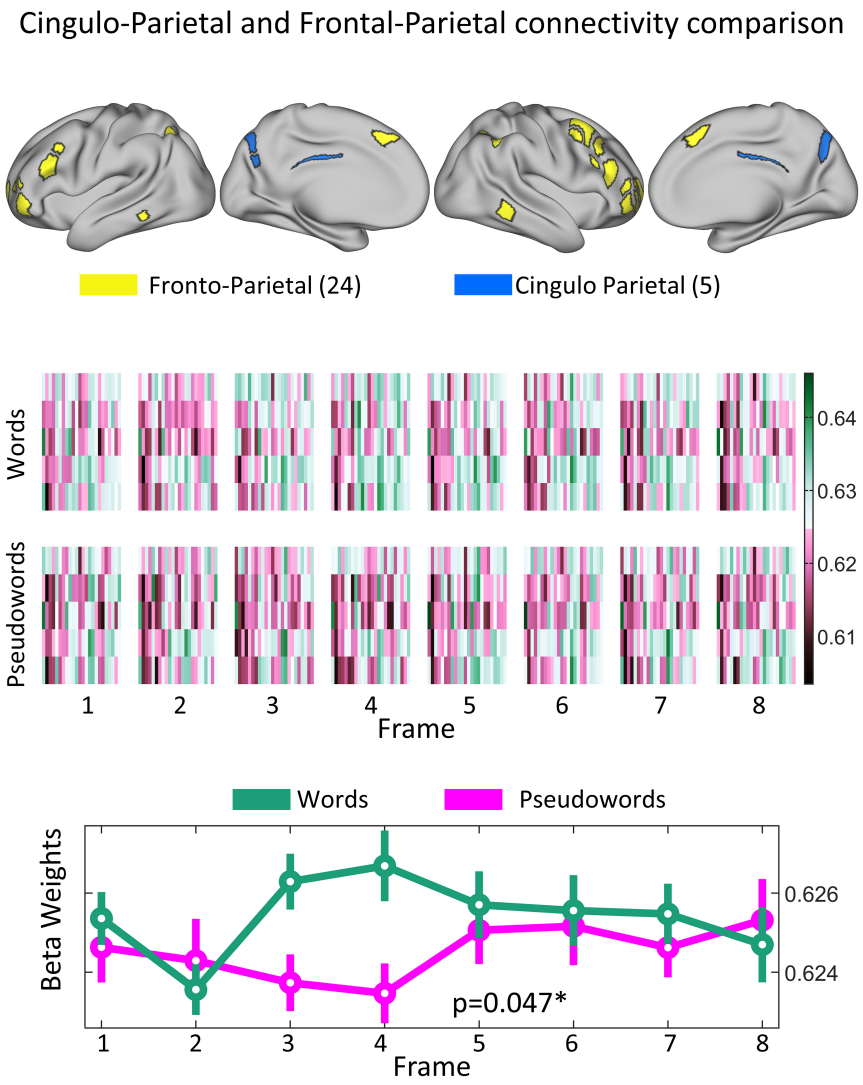

FIGURE 5
Significant difference observed in how the Cingulo–Parietal and Fronto–Parietal networks interact due to both progression of task and stimulus type. **(Top panel)** Shows the topological representation of cortical areas for both the Fronto-Parietal (yellow) and Cingulo Parietal (blue) networks. **(Middle panel)** Shows the mean sub-connectivity matrices between all the Cingulo Parietal and Fronto-Parietal ROIs (5 × 24 matrices) across participants for each stimuli (Word vs. Pseudowords) and each frame. The **(Bottom panel)** shows the distribution of marginal means of connectivity values for each frame and stimuli for connections belonging to the Fronto–Parietal and Cingulo–Parietal networks. Mean values shown as a circle and the dispersion is indicated with a bar covering 1.15 times the standard error of the connectivity values. When testing for how these values changed across frame and stimuli type, this functional system pair was found to be significant with a corrected *p*-value of 0.047.

Characterizing changes in connectivity values in connectivity matrices calculated using pearson-correlations

We repeated all the previous analysis using connectivity matrices calculated *via* Pearson correlations instead of connectotypes using the same frames used to calculate connectotype. No FD threshold led to significant differences in functional connectivity. Figure 6 shows the distribution of marginal means of connectivity values when connectivity matrices were calculated using an FD threshold of 0.3 (i.e., the same threshold used for connectotyping). These data highlight potential improvements in fMRI analyses using connectotyping.

Discussion

Recent advances in rs-fcMRI analysis approaches have led to increased understanding of brain functioning – where experimental designs have been able to identify brain areas

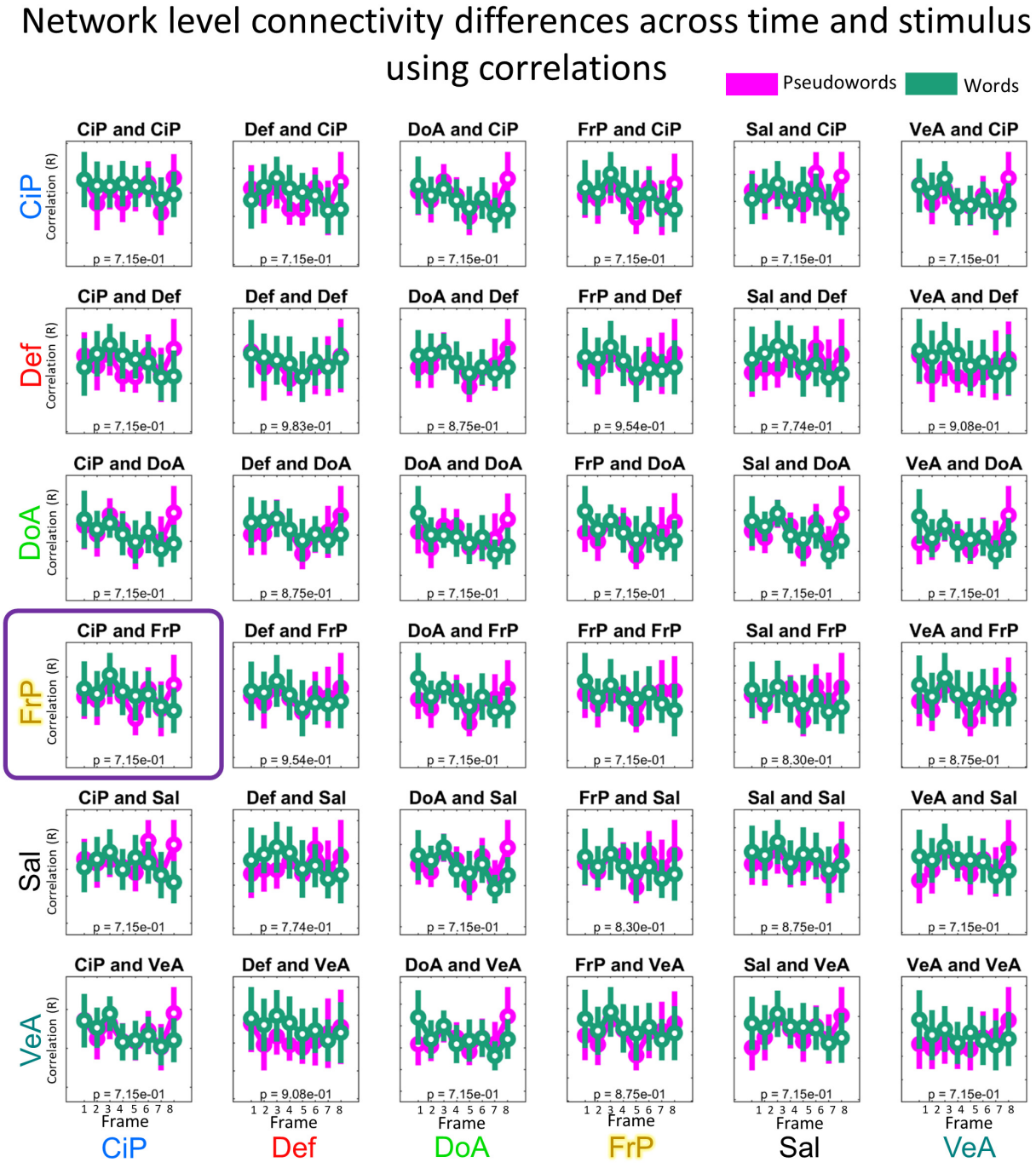

FIGURE 6
Distribution of mean connectivity values calculated using Pearson correlations per functional network pair and condition. Same description as in **Figure 4**.

supporting consciousness (Lloyd, 2002), moral judgment (Greene et al., 2001), as well as heritable patterns of brain connectivity (Miranda-Dominguez et al., 2018). Successful execution of mental tasks might require the collaboration of different brain networks in a timely manner. One approach that has been used to characterize dynamic changes in brain connectivity in task fMRI relies on correlations and averaging signals across participants (Hasson et al., 2004). For example, Najafi and colleagues used this approach to keep track of the changes in connectivity during anxious anticipation and found changes in connectivity between and within the Salience, Executive and Default Mode Networks (Najafi et al., 2017).

Given the noisy nature of functional MRI, some studies average data from multiple participants to improve the signal to noise ratio. While the result is a smoother signal, it comes at the price of blurring individual differences and dynamic changes in functional connectivity. In this study, we aimed to track temporal changes in brain connectivity during task performance using connectotyping, an efficient way to calculate functional connectivity between brain regions. Previously we showed that connectotyping can identify stable fingerprints efficiently (Miranda-Dominguez et al., 2014a, 2018). Connectotyping models how the activity of each brain area can be modeled as the weighted contribution of all the other areas. Resulting beta-weights correspond to a functional connectivity matrix. Changes in functional connectivity at a particular functional network pair for the interaction of time and stimulus might indicate that that specific functional network responds differently to a given stimulus. Here we tested the viability of connectotyping on task data from a lexical decision-based fMRI study that used a widely spaced event-related design (∼20 s trials). The use of this particular dataset, capitalizing on the widely spaced design, allowed for the hemodynamic response function corresponding to a single stimulus to be detected without signal interference from the next or preceding stimulus. Our approach has the potential to reveal how functional connections between ROIs (i.e., here, at the network level) progress during the performance of a task not just at the peak of activation. As hypothesized, application of connectotyping to the word vs PW dataset revealed significant dynamic (i.e., across frames) connectivity differences between the Cingulo-Parietal and Fronto-Parietal networks, as a function of stimulus type (i.e., word vs. PW). Our interpretation of these findings is further elaborated below.

The significantly different dynamic temporal relation occurring as a function of stimulus type between the Cingulo-Parietal and Frontal-Parietal networks suggest that the evolving contributions between the Fronto-Parietal and the Cingulo-Parietal network are distinct in pattern depending on whether participants were viewing something meaningful (i.e., word) vs. meaningless (i.e., PW). It is important to mention that the proposed approach is able to discriminate between areas that respond specifically to the task because (a) the experimental design includes a contrast (Word vs PW) and (b) the repeated measures ANOVA is looking for differences in connectivity for the interaction of time and stimulus type. While there are other functional networks that also display dynamic changes, they are not distinct across stimuli (see for example Default and Cingulo-Parietal networks on **Figure 4**), hence they are not related to this task. Importantly, repeating analysis using connectivity matrices calculated *via* Pearson's correlations, as opposed to connectotyping, did not have the resolving power to identify dynamic changes in brain connectivity.

After further testing and creating connectotypes with both more and less stringent movement thresholds (at 0.25 and 0.5 frame displacement thresholds), this observed Cingulo-Parietal and Frontal-Parietal network pattern of differentiated coactivation persisted, implying the stability of the findings (**Supplementary Figure 2**). Although these additional analyses did not withstand multiple-comparisons correction given the reduced sample size or signal to noise ratio, respectively, the presence of the same pattern of results supports the robustness of our primary finding.

The presence of dynamic connectivity differences between the Cingulo-Parietal and Fronto-Parietal networks support our principal hypothesis that task dependent regional brain communication changes during task progression; a finding that to our knowledge is the first of its kind. Our findings consequently also validate the use of connectotyping as a tool for task fMRI analysis which can provide a novel depiction of brain activity including dynamic temporal changes in functional connectivity. Additionally, we believe our findings are not simply a result of coactivation of networks. The original work by Nardos (2015) on this same dataset reported activation maps for the same contrast (Nardos, 2015). While there is some overlap for the Cingulo-Parietal network, most of the results. Nardos found that, in addition to areas within the Cingulo-Parietal network, areas belonging to the default, motor, ventral attention and Cingulo-Opercular system are behind the discrimination between words and PW (Nardos, 2015). In contrast, we found that dynamic changes in connectivity between the Cingulo-Parietal and Fronto-Parietal networks support discrimination between words and PW. Importantly, the Fronto-Parietal network was not identified as significant by Nardos. Since our findings do not coincide with the activation map, we do not believe that our analyses are a reflection of the activation of these networks.

Although our current approach differs from prior traditional task fMRI analyses, we did expect some overlap with findings from similar studies. Exposure to words vs. PWs resulted in significantly different temporal connectivity patterns between areas known to have a role in cognitive control, semantic processing, and memory retrieval. The Fronto-Parietal network is characterized as a task control network that has a particular role in the adaptive moment-to-moment requirements of a cognitive task such as task instantiation and dynamic feedback or error detection (Dosenbach et al., 2007). Cole et al. published evidence suggesting that the Fronto-Parietal network works as a cognitive hub by communicating with other control and processing networks to allow cognitive adaptation during tasks (Cole et al., 2013). This network also initiates and adjusts cognitive control to produce higher-level cognitive functions (Marek and Dosenbach, 2018). Here, the fact that such an adaptive control network displays distinct relations as a function of stimulus type is consistent

with an expectation that resolution of the identity of a word vs. non-word may have different cognitive control demands.

The regions corresponding to the Cingulo-Parietal network have previously been linked with memory retrieval processes (Power et al., 2011). Parts of the Cingulo-Parietal network are found in the precuneus and near the posterior cingulate, regions that have previously been linked with semantic processing. For instance, the regions have been shown to distinguish between words and PWs in prior work using traditional fMRI analysis (Binder et al., 2009). The same two regions have also previously been associated with supporting word learning in young adults (Nardos, 2015). In addition, there is ample prior work that has associated those same two regions with memory retrieval (Yonelinas and Levy, 2002; Wheeler and Buckner, 2003; Dobbins and Wagner, 2005; Yonelinas et al., 2005; Cabeza et al., 2008; Nelson et al., 2010; Rugg and Vilberg, 2013). In aggregate, the aforementioned findings linking regions in the Cingulo-Parietal network with semantic processing and memory retrieval is consistent with our finding that dynamic functional connectivity between this network and the Fronto-Parietal network supporting adaptive cognitive control is what distinguishes meaningful words from meaningless PWs.

The proposed approach is unique in the fact that it tracks dynamic changes in whole brain functional connectivity contrasting the response to different stimuli at each functional network pair. This method does not require *a priori* knowledge of potential brain areas (seeds) involved in the task. This is made possible because we characterized functional connectivity using connectotyping (Miranda-Dominguez et al., 2014a, 2018), a method with an improved signal-to-noise ratio (compared to traditional correlations) to characterize personalized maps of functional connectivity. In addition, the experimental design includes a contrast (word versus PW) enabling the identification of networks that respond differentially to each stimuli type. This contrast, we believe, makes possible the specificity to identify connections as opposed to merely co-activation. In other approaches, such as PPI, the distinction between co-activation and connectivity is made possible by including a regressor that is the product of the hypothesized hemodynamic response of the task and the timeseries of a seed that is *a priori* known to be involved in the task. It is important to mention that the proposed method is similar to Rissman connectivity (Rissman et al., 2004) in the fact that it aligns data according to their temporal evolution. In Rissman connectivity, the aligned data is used to estimate beta-weights associated with each event for every voxel. Resulting beta-weights are correlated across voxels to identify connections that respond to a given stimulus. Our approach, however, is different since we align whole-brain connectivity matrices and then characterize differences at each network pair for the interaction of time and stimulus type.

Limitations and future work

Because of our stringent motion censoring, our analyses are based on the data of only 15 participants of a narrow age range, which may limit the generalizability of our results. In this exploratory study, due to our limited data and our focus on higher order heteromodal networks, we decided to exclude the primary sensory cortex in our analysis. Studies with a larger number of participants and different tasks might allow the inclusion of more networks and display additional significant interactions among networks. Our additional analysis including the visual network, however, supports our assumption that the visual network might not be involved in this particular paradigm of word discrimination. The usage of a widely spaced dataset was ideal to test the feasibility of using connectotyping to track dynamic changes in functional connectivity. A widely spaced design, however, limits the number of contrasts that can be performed and measured and might lead to fatigue in the participants. Fortunately, participants succeeded in identifying words and PW with an accuracy of 98% suggesting that this slow paradigm did not lead to reduced attention in the participants that could compromise our findings. As we succeed in using a linear model to track dynamic changes, superposition and convolution can be used in event-related experiments where stimuli can be changed at each TR. By applying those validated methods to deconvolve the beta-weights corresponding to each frame and stimulus, the same statistical analysis (i.e., repeated measures ANOVA) can be used to track dynamic changes in functional connectivity. This approach is something we intend to continue exploring using task data from the Adolescent Brain Cognitive Development (ABCD) Study (Casey et al., 2018).

Conclusion

Task execution requires the orchestrated involvement of different brain networks. Here we showed that by calculating connectivity matrices using connectotyping at each time point during the execution of a task, we can identify the changes in brain connectivity that support semantic discrimination in a word versus PW paradigm using fMRI. We showed that connectotyping has a resolving power that cannot be achieved by using traditional correlations. While limited by the constraints of our data and the novelty of our approach, our group level findings serve to expand on the roles and functions of the Cingulo-Parietal and Fronto-Parietal networks as an incentive for others to pursue analyses which account for patterns of dynamic whole-brain connectivity and provide temporal resolution. The application of connectotyping to additional studies exploring other tasks and with differentially spaced study designs will not only further validate the use of this

approach but also has the potential to expand our understanding of brain activity during the performance of a task.

Data availability statement

The original contributions presented in this study are included in the article/**Supplementary material**, further inquiries can be directed to the corresponding author.

Ethics statement

The studies involving human participants were reviewed and approved by the Washington University Human Studies Committee (IRB ID # 201202083). All patients/participants provided their written informed consent to participate in this study.

Author contributions

VV-T, BN, BS, DF, and OM-D contributed to the conception and design of the study. BN performed the data collection. VV-T and BN processed the neuroimaging data. VV-T, BN, and OM-D performed the statistical analysis and wrote the first draft of the manuscript. VV-T, BS, DF, and OM-D read and approved the submitted version. All authors contributed to the manuscript revision.

Funding

This project was funded by the Eunice Kennedy Shriver National Institute of Child Health and Human Development, Grant: NIH R01 HD05707601 (BS), an OHSU Fellowship for Diversity and Inclusion in Research Program (OM-D), a Tartar Trust Award (OM-D), the OHSU Parkinson Center Pilot Grant Program (OM-D), and the Portland State University BUILD EXITO program, Grants: 5TL4GM118965-03, 5TL4GM118965-04, and 5TL4GM118965-05.

Conflict of interest

The authors declare that the research was conducted in the absence of any commercial or financial relationships that could be construed as a potential conflict of interest.

Publisher's note

All claims expressed in this article are solely those of the authors and do not necessarily represent those of their affiliated organizations, or those of the publisher, the editors and the reviewers. Any product that may be evaluated in this article, or claim that may be made by its manufacturer, is not guaranteed or endorsed by the publisher.

Supplementary material

The Supplementary Material for this article can be found online at: https://www.frontiersin.org/articles/10.3389/fnins.2022.951907/full#supplementary-material

SUPPLEMENTARY FIGURE 1
Distribution of mean connectivity values per functional network pair and condition including the visual network. Beta-weights were calculated for each condition as indicated in our experimental design (**Figure 3**) and grouped by functional network pair. Each boxplot highlights the mean values using a circle and the dispersion is indicated with a bar covering 1.15 times the standard deviation of the connectivity values. Data is color-coded by stimuli: pseudoword (purple) and word (green). *X*-axis indicates the time, in frames (TR of 2.5 s each). In this study we included the following networks: Cingulo-Parietal (CiP, $n = 5$ Regions of Interest), Default (Def, $n = 41$), Dorsal Attention (DoA, $n = 32$), Fronto-Parietal (FrP, $n = 24$), Salience (Sal, $n = 4$), and Ventral Attention (VeA, $n = 23$) Visual (Vis, $n = 39$).

SUPPLEMENTARY FIGURE 2
Difference of how the Cingulo-Parietal and Fronto-Parietal networks interact over time at other thresholds of head-movement suggest robust initial finding. The **(A)** shows the change in beta-weights between the Fronto-Parietal and Cingulo-Parietal networks at a movement threshold of 0.25 mm. After correcting for multiple comparisons, this functional system pair was not found to be significant ($p = 0.508$). The **(B)** shows the results from the same analysis as the left information when the movement threshold was set at a higher value of 0.5mm. When this data underwent corrections for multiple comparisons, this functional system pair was not found to be significant ($p = 0.941$).

References

Badre, D., Poldrack, R. A., Paré-Blagoev, E. J., Insler, R. Z., and Wagner, A. D. (2005). Dissociable controlled retrieval and generalized selection mechanisms in ventrolateral prefrontal cortex. *Neuron* 47, 907–918. doi: 10.1016/j.neuron.2005.07.023

Balota, D. A., Yap, M. J., Cortese, M. J., Kessler, B., Loftis, B., Neely, J. H., et al. (2007). The English lexicon project. *Behav. Res. Methods* 39, 445–459. doi: 10.3758/BF03193014

Billings, J., Saggar, M., Hlinka, J., Keilholz, S., and Petri, G. (2021). Simplicial and topological descriptions of human brain dynamics. *Netw. Neurosci.* 5, 549–568. doi: 10.1162/netn_a_00190

Binder, J. R., Desai, R. H., Graves, W. W., and Conant, L. L. (2009). Where is the semantic system? a critical review and meta-analysis of 120 functional neuroimaging studies. *Cereb. Cortex* 19, 2767–2796. doi: 10.1093/cercor/bhp055

Biswal, B., Yetkin, F. Z., Haughton, V. M., and Hyde, J. S. (1995). Functional connectivity in the motor cortex of resting human brain using echo-planar MRI. *Magn. Reson. Med.* 34, 537–541. doi: 10.1002/mrm.1910340409

Botvinick, M. M., Braver, T. S., Barch, D. M., Carter, C. S., and Cohen, J. D. (2001). Conflict Monitoring and Cognitive Control. *Psychol. Rev.* 108, 624–652. doi: 10.1037/0033-295X.108.3.624

Braver, T. S., and Barch, D. M. (2006). Extracting Core Components of Cognitive Control. *Trends Cogn. Sci.* 10, 529–532. doi: 10.1016/j.tics.2006.10.006

Cabeza, R., Ciaramelli, E. I, Olson, R., and Moscovitch, M. (2008). The Parietal Cortex and Episodic Memory: An Attentional Account. *Nat. Rev. Neurosci.* 9, 613–625. doi: 10.1038/nrn2459

Casey, B. J., Cannonier, T., Conley, M. I., Cohen, A. O., Barch, D. M., Heitzeg, M. M., et al. (2018). The Adolescent Brain Cognitive Development (ABCD) Study: Imaging Acquisition across 21 Sites. *Dev. Cogn. Neurosci.* 32, 43–54. doi: 10.1016/j.dcn.2018.03.001

Chang, C., and Glover, G. H. (2010). Time-Frequency Dynamics of Resting-State Brain Connectivity Measured with FMRI. *NeuroImage* 50, 81–98. doi: 10.1016/j.neuroimage.2009.12.011

Cohen, J. D., MacWhinney, B., Flatt, M., and Provost, J. (1993). PsyScope: A New Graphic Interactive Environment for Designing Psychology Experiments. *Behav. Res. Methods Instrum. Comput.* 25, 257–271. doi: 10.3758/BF03204507

Cole, M. W., Reynolds, J. R., Power, J. D., Repovs, G., Anticevic, A., and Braver, T. S. (2013). Multi-Task Connectivity Reveals Flexible Hubs for Adaptive Task Control. *Nat. Neurosci.* 16, 1348–1355. doi: 10.1038/nn.3470

Cribben, I., Haraldsdottir, R., Atlas, L. Y., Wager, T. D., and Lindquist, M. A. (2012). Dynamic Connectivity Regression: Determining State-Related Changes in Brain Connectivity. *NeuroImage* 61, 907–920. doi: 10.1016/j.neuroimage.2012.03.070

Desikan, R. S., Ségonne, F., Fischl, B., Quinn, B. T., Dickerson, B. C., Blacker, D., et al. (2006). An automated labeling system for subdividing the human cerebral cortex on MRI scans into gyral based regions of interest. *NeuroImage* 31, 968–980. doi: 10.1016/j.neuroimage.2006.01.021

Dobbins, I. G., and Wagner, A. D. (2005). Domain-General and Domain-Sensitive Prefrontal Mechanisms for Recollecting Events and Detecting Novelty. *Cereb. Cortex* 15, 1768–1778. doi: 10.1093/cercor/bhi054

Donaldson, D. I., Petersen, S. E., Ollinger, J. M., and Buckner, R. L. (2001). Dissociating State and Item Components of Recognition Memory Using FMRI. *NeuroImage* 13, 129–142. doi: 10.1006/nimg.2000.0664

Dosenbach, N. U. F., Fair, D. A., Miezin, F. M., Cohen, A. L., Wenger, K. K., Dosenbach, R. A. T., et al. (2007). Distinct Brain Networks for Adaptive and Stable Task Control in Humans. *Proc. Natl. Acad. Sci. U.S. A.* 104, 11073–11078. doi: 10.1073/pnas.0704320104

Dosenbach, N. U. F., Visscher, K. M., Palmer, E. D., Miezin, F. M., Wenger, K. K., Kang, H. C., et al. (2006). A Core System for the Implementation of Task Sets. *Neuron* 50, 799–812. doi: 10.1016/j.neuron.2006.04.031

Engel, S. A., Rumelhart, D. E., Wandell, B. A., Lee, A. T., Glover, G. H., Chichilnisky, E., et al. (1994). FMRI of Human Visual Cortex. *Nature* 369:525. doi: 10.1038/369525a0

Fiez, J. A. (1997). Phonology, Semantics, and the Role of the Left Inferior Prefrontal Cortex. *Hum. Brain Mapp.* 5, 79–83. doi: 10.1002/(SICI)1097-0193(1997)5:2<79::AID-HBM1>3.0.CO;2-J

Fischl, B., and Dale, A. M. (2000). Measuring the Thickness of the Human Cerebral Cortex from Magnetic Resonance Images. *Proc. Natl. Acad. Sci. U.S.A.* 97, 11050–11055. doi: 10.1073/pnas.200033797

Friederici, A. D., Opitz, B., and von Cramon, D. Y. (2000). Segregating Semantic and Syntactic Aspects of Processing in the Human Brain: An FMRI Investigation of Different Word Types. *Cereb. Cortex* 10, 698–705. doi: 10.1093/cercor/10.7.698

Friston, K. J., Buechel, C., Fink, G. R., Orris, J. M., Rolls, E., and Dolan, R. J. (1997). Psychophysiological and Modulatory Interactions in Neuroimaging. *NeuroImage* 6, 218–229. doi: 10.1006/nimg.1997.0291

Friston, K. J., Harrison, L., and Penny, W. (2003). Dynamic Causal Modelling. *NeuroImage* 19, 1273–1302. doi: 10.1016/S1053-8119(03)00202-7

Friston, K. J., Preller, K. H., Mathys, C., Cagnan, H., Heinzle, J., Razi, A., et al. (2019). Dynamic Causal Modelling Revisited. *NeuroImage* 199, 730–744. doi: 10.1016/j.neuroimage.2017.02.045

Ginestet, C. E., and Simmons, A. (2011). Statistical Parametric Network Analysis of Functional Connectivity Dynamics during a Working Memory Task. *NeuroImage* 55, 688–704. doi: 10.1016/j.neuroimage.2010.11.030

Glasser, M. F., Sotiropoulos, S. N., Wilson, J. A., Coalson, T. S., Fischl, B., Andersson, J. L., et al. (2013). The Minimal Preprocessing Pipelines for the Human Connectome Project. *NeuroImage* 80, 105–124. doi: 10.1016/j.neuroimage.2013.04.127

Goebel, R., Khorram-Sefat, D., Muckli, L., Hacker, H., and Singer, W. (1998). The Constructive Nature of Vision: Direct Evidence from Functional Magnetic Resonance Imaging Studies of Apparent Motion and Motion Imagery. *Eur. J. Neurosci.* 10, 1563–1573. doi: 10.1046/j.1460-9568.1998.00181.x

Gordon, E. M., Laumann, T. O., Adeyemo, B., Huckins, J. F., Kelley, W. M., and Petersen, S. E. (2014). Generation and Evaluation of a Cortical Area Parcellation from Resting-State Correlations. *Cereb. Cortex* 26, 288–303. doi: 10.1093/cercor/bhu239

Greene, J. D., Sommerville, R. B., Nystrom, L. E., Darley, J. M., and Cohen, J. D. (2001). An FMRI Investigation of Emotional Engagement in Moral Judgment. *Science* 293, 2105–2108. doi: 10.1126/science.1062872

Greve, D. N., and Fischl, B. (2009). Accurate and Robust Brain Image Alignment Using Boundary-Based Registration. *NeuroImage* 48, 63–72. doi: 10.1016/j.neuroimage.2009.06.060

Hasson, U., Nir, Y., Levy, I., Fuhrmann, G., and Malach, R. (2004). Intersubject Synchronization of Cortical Activity During Natural Vision. *Science* 303, 1634–1640. doi: 10.1126/science.1089506

Iidaka, T., Matsumoto, A., and Nogawa, J. (2006). Frontoparietal Network Involved in Successful Retrieval from Episodic Memory . Spatial and Temporal Analyses Using FMRI and ERP. *Cereb. Cortex* 16, 1349–1360. doi: 10.1093/cercor/bhl040

Jenkinson, M., Beckmann, C. F., Behrens, T. E. J., Woolrich, M. W., and Smith, S. M. (2012). FSL. *NeuroImage* 62, 782–790. doi: 10.1016/j.neuroimage.2011.09.015

Kovacs-Balint, Z., Feczko, E., Pincus, M., Earl, E., Miranda-Dominguez, O., Howell, B., et al. (2019). Early Developmental Trajectories of Functional Connectivity Along the Visual Pathways in Rhesus Monkeys. *Cereb. Cortex* 29, 3514–3526. doi: 10.1093/cercor/bhy222

Laumann, T. O., Snyder, A. Z., Mitra, A., Gordon, E. M., Gratton, C., Adeyemo, B., et al. (2016). On the Stability of BOLD FMRI Correlations. *Cereb. Cortex* 27, 4719–4732. doi: 10.1093/cercor/bhw265

Lindquist, M. A., Xu, Y., Nebel, M. B., and Caffo, B. S. (2014). Evaluating Dynamic Bivariate Correlations in Resting-State FMRI: A Comparison Study and a New Approach. *NeuroImage* 101, 531–546. doi: 10.1016/j.neuroimage.2014.06.052

Lloyd, D. (2002). Functional MRI and the Study of Human Consciousness. *J. Cogn. Neurosci.* 14, 818–831. doi: 10.1162/089892902760191027

Logothetis, N. K. (2003). The Underpinnings of the BOLD Functional Magnetic Resonance Imaging Signal. *J. Neurosci.* 23, 3963–3971. doi: 10.1523/JNEUROSCI.23-10-03963.2003

Logothetis, N. K. (2008). What We Can Do and What We Cannot Do with FMRI. *Nature* 453, 869–878. doi: 10.1038/nature06976

Logothetis, N. K., Pauls, J., Augath, M., Trinath, T., and Oeltermann, A. (2001). Neurophysiological Investigation of the Basis of the FMRI Signal. *Nature* 412, 150–157. doi: 10.1038/35084005

Marek, S., and Dosenbach, N. U. F. (2018). The Frontoparietal Network: Function, Electrophysiology, and Importance of Individual Precision Mapping. *Dialogues Clin. Neurosci.* 20, 133–140. doi: 10.31887/DCNS.2018.20.2/smarek

Marek, S., Tervo-Clemmens, B., Nielsen, A. N., Wheelock, M. D., Miller, R. L., Laumann, T. O., et al. (2019). Identifying Reproducible Individual Differences in Childhood Functional Brain Networks: An ABCD Study. *Dev. Cogn. Neurosci.* 40:100706. doi: 10.1016/j.dcn.2019.100706

McLaren, D. G., Ries, M. L., Xu, G., and Johnson, S. C. (2012). A Generalized Form of Context-Dependent Psychophysiological Interactions (GPPI): A Comparison to Standard Approaches. *NeuroImage* 61, 1277–1286. doi: 10.1016/j.neuroimage.2012.03.068

Miranda-Dominguez, O., Feczko, E., Grayson, D. S., Walum, H., Nigg, J. T., and Fair, D. A. (2018). Heritability of the Human Connectome: A Connectotyping Study. *Netw. Neurosci.* 2, 175–199. doi: 10.1162/netn_a_00029

Miranda-Dominguez, O., Mills, B. D., Carpenter, S. D., Grant, K. A., Kroenke, C. D., Nigg, J. T., et al. (2014a). Connectotyping: Model Based Fingerprinting of the Functional Connectome. *PLoS One* 9:e111048. doi: 10.1371/journal.pone.0111048

Miranda-Dominguez, O., Mills, B. D., Grayson, D., Woodall, A., Grant, K. A., Kroenke, C. D., et al. (2014b). Bridging the Gap between the Human and Macaque Connectome: A Quantitative Comparison of Global Interspecies Structure-Function Relationships and Network Topology. *J. Neurosci.* 34, 5552–5563. doi: 10.1523/JNEUROSCI.4229-13.2014

Miranda-Domí,nguez, Ó, Ragothaman, A., Hermosillo, R., Feczko, E., Morris, R., and Carlson-Kuhta, P. (2020). Lateralized Connectivity between Globus

Pallidus and Motor Cortex is Associated with Freezing of Gait in Parkinson's Disease. *Neuroscience* 443, 44–58. doi: 10.1016/j.neuroscience.2020.06.036

Moerel, M., De Martino, F., and Formisano, E. (2014). An Anatomical and Functional Topography of Human Auditory Cortical Areas. *Front. Neurosci.* 8:225. doi: 10.3389/fnins.2014.00225

Montgomery, D. C. (2005). Design and Analysis of Experiments, sixth edition. *J. Qual. Technol.* 37, 175–176. doi: 10.1080/00224065.2005.11980315

Najafi, M., Kinnison, J., and Pessoa, L. (2017). Dynamics of Intersubject Brain Networks during Anxious Anticipation. *Front. Hum. Neurosci.* 11:552. doi: 10.3389/fnhum.2017.00552

Nardos, B. (2015). *Behavioral and fMRI-based characterization of cognitive processes supporting learning and retrieval of memory for words in young adults*. Ph.D. thesis. St. Louis, MI: Washington University, 671.

Nelson, S. M., Dosenbach, N. U. F., Cohen, A. L., Wheeler, M. E., Schlaggar, B. L., and Petersen, S. E. (2010). Role of the Anterior Insula in Task-Level Control and Focal Attention. *Brain Struct. Funct.* 214, 669–680. doi: 10.1007/s00429-010-0260-2

Petersen, S. E., Fox, P. T., Posner, M. I., Mintun, M., and Raichle, M. E. (1988). Positron Emission Tomographic Studies of the Cortical Anatomy of Single-Word Processing. *Nature* 331, 585–589. doi: 10.1038/331585a0

Power, J. D., Barnes, K. A., Snyder, A. Z., Schlaggar, B. L., and Petersen, S. E. (2012). Spurious but Systematic Correlations in Functional Connectivity MRI Networks Arise from Subject Motion. *NeuroImage* 59, 2142–2154. doi: 10.1016/j.neuroimage.2011.10.018

Power, J. D., Cohen, A. L., Nelson, S. M., Wig, G. S., Barnes, K. A., Church, J. A., et al. (2011). Functional Network Organization of the Human Brain. *Neuron* 72, 665–678. doi: 10.1016/j.neuron.2011.09.006

Power, J. D., Mitra, A., Laumann, T. O., Snyder, A. Z., Schlaggar, B. L., and Petersen, S. E. (2014). Methods to Detect, Characterize, and Remove Motion Artifact in Resting State FMRI. *NeuroImage* 84, 320–341. doi: 10.1016/j.neuroimage.2013.08.048

Rissman, J., Gazzaley, A., and D'Esposito, M. (2004). Measuring Functional Connectivity during Distinct Stages of a Cognitive Task. *NeuroImage* 23, 752–763. doi: 10.1016/j.neuroimage.2004.06.035

Roskies, A. L., Fiez, J. A., Balota, D. A., Raichle, M. E., and Petersen, S. E. (2001). Task-Dependent Modulation of Regions in Left Frontal Cortex during Semantic Processing. *J. Cogn. Neurosci.* 13, 829–843. doi: 10.1162/08989290152541485

Rudolph, M. D., Graham, A. M., Feczko, E., Miranda-Dominguez, O., Rasmussen, J. M., Nardos, R., et al. (2018). Maternal IL-6 during Pregnancy Can Be Estimated from Newborn Brain Connectivity and Predicts Future Working Memory in Offspring. *Nat. Neurosci.* 21, 765–772. doi: 10.1038/s41593-018-0128-y

Rugg, M. D., and Vilberg, K. L. (2013). Brain Networks Underlying Episodic Memory Retrieval Michael. *Curr. Opin. Neurobiol.* 23, 255–260. doi: 10.1016/j.conb.2012.11.005

Sakoğlu, Ü, Pearlson, G. D., Kiehl, K. A., Wang, Y. M., Michael, A. M., and Calhoun, V. D. (2010). A Method for Evaluating Dynamic Functional Network Connectivity and Task-Modulation: Application to Schizophrenia. *Magn. Reson. Mater. Physics Biol. Med.* 23, 351–366. doi: 10.1007/s10334-010-0197-8

Sereno, M. I., Dale, A. M., Reppas, J. B., Kwong, K. K., Belliveau, J. W., Brady, T. J., et al. (1995). Borders of Multiple Visual Areas in Humans Revealed by Functional Magnetic Resonance Imaging. *Science* 268, 889–893. doi: 10.1126/science.7754376

Shappell, H. M., Duffy, K. A., Rosch, K. S., Pekar, J. J., Mostofsky, S. H., Lindquist, M. A., et al. (2021). Children with Attention-Deficit/Hyperactivity Disorder Spend More Time in Hyperconnected Network States and Less Time in Segregated Network States as Revealed by Dynamic Connectivity Analysis. *NeuroImage* 229:117753. doi: 10.1016/j.neuroimage.2021.117753

Siegel, J. S., Power, J. D., Vogel, A. C., Church, J. A., Dubis, J. W., Schlaggar, B. L., et al. (2014). Statistical Improvements in Functional Magnetic Resonance Imaging Analyses Produced by Censoring High-Motion Data Points. *Hum. Brain Mapp.* 35, 1981–1996. doi: 10.1002/hbm.22307

Smith, S. M., Jenkinson, M., Woolrich, M. W., Beckmann, C. F., Behrens, T. E. J., Johansen-Berg, H., et al. (2004). Advances in Functional and Structural MR Image Analysis and Implementation as FSL. *NeuroImage* 23, S208—-19. doi: 10.1016/j.neuroimage.2004.07.051

Stafford, J. M., Jarrett, B. R., Miranda-Dominguez, O., Mills, B. D., Cain, N., Mihalas, S., et al. (2014). Large-Scale Topology and the Default Mode Network in the Mouse Connectome. *Proc. Natl. Acad. Sci. U.S.A.* 111, 18745–18750. doi: 10.1073/pnas.1404346111

Thompson-Schill, S. L., D'Esposito, M., Aquirre, G. K., Farah, M. J., and Aguirre, G. K. (1997). Role of Left Inferior Prefrontal Cortex in Retrieval of Semantic Knowledge: A Reevaluation. *Proc. Natl. Acad. Sci. U.S. A.* 94, 14792–14797. doi: 10.1073/pnas.94.26.14792

Vazquez, A. L., and Noll, D. C. (1998). Nonlinear Aspects of the BOLD Response in Functional MRI. *NeuroImage* 7, 108–118. doi: 10.1006/nimg.1997.0316

Wagner, A. D., Paré-Blagoev, E. J., Clark, J., and Poldrack, R. A. (2001). Recovering Meaning: Left Prefrontal Cortex Guides Controlled Semantic Retrieval. *Neuron* 31, 329–338. doi: 10.1016/S0896-6273(01)00359-2

Wheeler, M. E., and Buckner, R. L. (2003). Functional Dissociation among Components of Remembering: Control, Perceived Oldness, and Content. *J. Neurosci.* 23, 3869–3880. doi: 10.1523/JNEUROSCI.23-09-03869.2003

Woodcock, R. W., and Johnson, M. B. (2002). *Woodcock-Johnson-Revised Tests of Achievement*. Itasca, IL: Riverside Publishing.

Woolrich, M. W., Jbabdi, S., Patenaude, B., Chappell, M., Makni, S., Behrens, T., et al. (2009). Bayesian Analysis of Neuroimaging Data in FSL. *NeuroImage* 45, S173–S186. doi: 10.1016/j.neuroimage.2008.10.055

Xu, Y., and Lindquist, M. A. (2015). Dynamic Connectivity Detection: An Algorithm for Determining Functional Connectivity Change Points in FMRI Data. *Front. Neurosci.* 9:285. doi: 10.3389/fnins.2015.00285

Yonelinas, A. P., and Levy, B. J. (2002). Dissociating Familiarity from Recollection in Human Recognition Memory: Different Rates of Forgetting over Short Retention Intervals. *Psychonomic Bull. Rev.* 9, 575–582. doi: 10.3758/BF03196315

Yonelinas, A. P., Otten, L. J., Shaw, R. N., and Rugg, M. D. (2005). Separating the Brain Regions Involved in Recollection and Familiarity in Recognition Memory. *J. Neurosci.* 25, 3002–3008. doi: 10.1523/JNEUROSCI.5295-04.2005

Zhang, M., and Saggar, M. (2020). Complexity of Resting Brain Dynamics Shaped by Multiscale Structural Constraints. *BioRxiv* [Preprint]. doi: 10.1101/2020.05.14.097196

Frontiers in Neuroscience

Provides a holistic understanding of brain function from genes to behavior

Part of the most cited neuroscience journal series which explores the brain - from the new eras of causation and anatomical neurosciences to neuroeconomics and neuroenergetics.

Discover the latest Research Topics

See more →

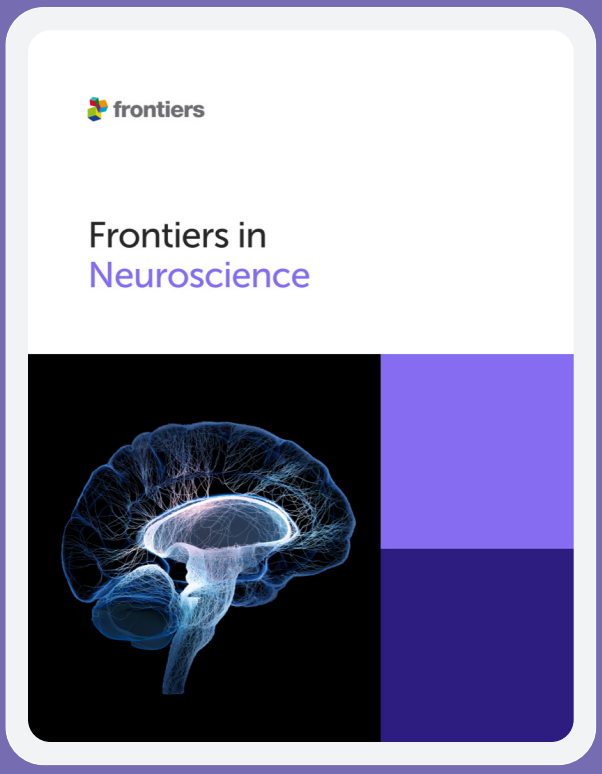

Frontiers

Avenue du Tribunal-Fédéral 34
1005 Lausanne, Switzerland
frontiersin.org

Contact us

+41 (0)21 510 17 00
frontiersin.org/about/contact